PARTS OF THE ORIGINAL DOCUMENT

ARE OF POOR REPRODUCTIVE QUALITY

CERTAINES PARTIES DU DOCUMENT ORIGINAL

SONT DE PIÈTRE QUALITÉ DE REPRODUCTION

Energy, Mines and Resources Canada
Énergie, Mines et Ressources Canada

CANMET
Canada Centre for Mineral and Energy Technology
Centre canadien de la technologie des minéraux et de l'énergie

THE MINERAL CHARACTERISTICS THAT AFFECT METAL RECOVERIES FROM THE Cu, Zn, Pb AND Ag ORES FROM MANITOBA. PART 1.
AN INVESTIGATION OF THE ORE MINERALOGY OF THE TROUT LAKE DEPOSIT WITH A VIEW OF PREDICTING MINERAL LIBERATION AND METAL RECOVERY DURING ORE DRESSING

R.E. Healy
University of Manitoba

W. Petruk
Mineral Processing Laboratory

May 1988

MICROMEDIA

Project: 30.05.02
Mineralogical Evaluation of Process Products

This document is an unedited interim report prepared primarily for discussion and internal working purposes. It does not represent a final expression of the opinion of the Canada Centre for Mineral and Energy Technology (CANMET)

Ce document est un rapport provisoire non révisé et rédigé principalement pour fin de discussion et de documentation interne. Il ne représente nullement l'expression définitive de l'opinion du Centre canadien de la technologie des minéraux et de l'énergie (CANMET)

191 pp

MINERAL SCIENCES LABORATORIES
DIVISION REPORT MSL 88-61(IR)

88-04996/

THE MINERAL CHARACTERISTICS THAT AFFECT METAL RECOVERIES FROM THE Cu, Zn, Pb AND Ag ORES FROM MANITOBA.

PART 1.

AN INVESTIGATION OF THE ORE MINERALOGY OF THE TROUT LAKE DEPOSIT WITH A VIEW TO PREDICTING MINERAL LIBERATION AND METAL RECOVERY DURING ORE DRESSING.

RAYMOND E. HEALY
DEPT. OF GEOLOGICAL SCIENCES
UNIVERSITY OF MANITOBA
WINNIPEG
MANITOBA

Scientific Authority : Dr. W. Petruk, CANMET, Dept. of Energy, Mines and Resources.

Winnipeg, Manitoba

(c) full name of author, 1987

ACKNOWLEDGEMENTS

Initially I would like to thank Dr. D. G. W. Smith for his tuition, his confidence in me, and his recommendation as a referee, without all of which none of the following would have been possible.

Special thanks go to Dr. W. Petruk who has provided essential direction and insight into the study. I am particularly indebted to Dr. Petruk for the many discussions in which he exceeded the call of duty in relating his personal viewpoints and wealth of experience in this field of applied research. The manuscript benefitted enormously from the critical review of, and the large contributions provided by Dr. Petruk.

Prof. A. Turnock is gratefully thanked for his support, enthusiasm and useful suggestions throughout the duration of the project, as well as for critically reviewing the manuscript. Ron Chapman and Lee Groat are acknowledged for their skill and patience in familiarising me with the microprobe and it's myriad idiosyncrasies. Lee Groat and Mati Raudsepp are thanked for their assistance and expertise on the mainframe computer at the U. of M.. The staff members of the Dept. of Geological Sciences at the U. of M. are thanked for ensuring a smooth transition from graduate student to research associate through their encouragement and friendship.

The staff at H.B.M.S. are thanked for their technical assistance, enthusiasm and affability. In particular, I am grateful to Choong Ko for his assistance and geological expertise above and below the ground. Norm McEachern and Dan Wittleton are also gratefully acknowledged for their contributions through technical assistance and fruitful discussion.

Funding for the project was provided by the Federal Government of Canada via the CANADA - MANITOBA MINERAL DEVELOPMENT AGREEMENT.

ABSTRACT

The ore mineralogy of the metamorphosed volcanogenic massive sulphide deposit of Trout Lake, Flin Flon, Manitoba has been investigated under a Canada - Manitoba Mineral Development Agreement contract. Using mineralogical and textural criteria, nine ore types were defined, of which seven approximate to metamorphosed equivalents of the classical ore types recognised from the Kuroko deposits of Japan. These 7 ore types may be considered as a differentiation series from the Zn-rich hangingwall ores to the Cu-rich footwall ores. The remaining 2 ore types are of tectonic origin.

Twenty six ore minerals have been observed and identified. The sulphides are pyrite, chalcopyrite, sphalerite, pyrrhotite, marcasite, galena, arsenopyrite, cubanite, and acanthite; the oxides are magnetite and cassiterite; the Sb-sulfosalts freibergite, gudmundite, pyrargyrite, freieslebenite, boulangerite, costibite, and bournonite; the intermetallic compounds are mercurian electrum and dyscrasite; the tellurides are hessite, rucklidgeite, pilsenite and volynskite; and the selenides are clausthalite and naumannite. The ores are dominated by the textural and spatial distribution of the first three most abundant sulphides pyrite, chalcopyite and sphalerite The principal Cu-mineral is chalcopyrite (pure stoichiometric $CuFeS_2$), whereas the principal Zn-mineral is sphalerite ($\bar{x}$ = 59.8 % Zn, 33.3 % S, 6.6 % Fe, 0.2 % Cd and 0.1 % Cu). Nine Ag-bearing minerals were identified and some Ag occurs in solid solution in galena, probably sphalerite and possibly in chalcopyrite. The principal Ag-bearing minerals freibergite ($\bar{x}$ = 21.7 % Ag) and pyrargyrite occur as fine-grained inclusions in, or intimately associated with galena, and are principally observed in the hangingwall Massive Sphalerite and the Banded Pyrite + Sphalerite ores. The mercurian electrum is the only Au-bearing mineral identified; quantitative microprobe analyses of which yield an average composition of 46.97 % Ag, 41.37 % Au, 10.64 % Hg and 0.73 % Fe (mean total = 99.72 %).

Chemical analyses of the ores identified the existence of two groups of elements that exhibit a high degree of covariance; a Zn-Group : Zn, Cd, Sb, Pb, Ag, Hg, In, Sn and As, and a Cu-Group : Cu, Se, Te, Co and Fe. These two element groups constitute the two principal geochemical associations of the ores, and characterise the ores in terms of their mutual differentiation. Au exhibits no significant covariance with any of the above elements.

Mineral quantity and chord analysis using the MP-SEM-IPS-IAS at CANMET were performed on the ores. Grain size distributions for pyrite, chalcopyrite, sphalerite, freibergite and galena were determined in each ore sample analysed, and average size distributions for each ore type and for the ore as a whole were calculated. From the latter the minimum grinds for sphalerite, chalcopyrite, pyrite, galena and freibergite were interpreted to be +208um, -175um, -95um, -48um and -60um, respectively. Similarly, the optimum grinds for the above minerals were interpreted to be -52um, -52um, -26um, -9.2um and -4.6um, respectively.

Three types of electrum were recognised are (1) inclusions in, and filling fractures in, and grain coatings on, pyrite, (2) anastomosing masses in chalcopyrite and pyrrhotite, and (3) inclusions in galena/freibergite masses. Type 1 and 3 (417 grains of electrum) yield a cumulative grain size curve defined by 80 % -18.5um, whereas electrum of type 2 yields a cumulative grain size curve defined by 80 % -37um. The loss of Au to the tailings is interpreted to be largely attributable to the poor liberation of the fine-grained electrum entrapped in pyrite (type 1). The principal cause of the Ag losses to the tailings is interpreted to be due to the poor liberation of the fine-grained galena + freibergite from pyrite.

Lens No. 2 of the North Zone is the largest and richest of the 6 proven ore lenses, and is characterised by abundant finely interpenetrative intergrowths of chalcopyrite + sphalerite + pyrrhotite ± galena, due to diablastic growth during and after shearing. This shearing accompanied the intrusion of a quartz-diorite sill that is discontinuously interlaced with the lens down dip. If a sphalerite liberation problem is identified as consisting of composite grains of chalcopyrite and sphalerite, and resulting in the high Zn values reporting to the Cu-concentrate, the most probable textural sources are the diablastic-textured chalcopyrite and sphalerite, as well as, but to a much lesser extent, the virtually ubiquitous "chalcopyrite-disease" in sphalerite.

Keywords: Trout Lake ore; volcanogenic base metal ores; copper ore;
zinc ore; ore classification; assays of ore types;
ore petrology; grain size analysis; mineral quantities

RÉSUMÉ

La minéralogie des minerais sulfurés d'origine volcanique et métamorphique du gisement non stratifié de Trout Lake, à Flin Flon, Manitoba, a fait l'objet d'une étude réalisée en sous-traitance dans le cadre de l'Entente Canada-Manitoba sur le développement minéral. On a utilisé des critères minéralogiques et structuraux pour définir neuf espèces minérales dont sept sont, à peu de différences près, les équivalents métamorphiques des espèces classiques établies à partir des gisements de Kuroko, au Japon. Les sept espèces minérales peuvent être utilisées comme série de minerais pour établir des distinctions entre les minerais du toit de faille à haute teneur en zinc et les minerais de la paroi inférieure à teneur élevée en cuivre. Les deux espèces minérales restantes sont d'origine tectonique.

Vingt-six minerais ont été analysés et identifiés. Les minerais sulfurés comprennent la pyrite, la chalcopyrite, la sphalérite, la pyrrhotite, la marcassite, la galène, l'arsénopyrite, la cubane, et l'acanthite; les minerais oxydés comprennent la magnétite et la cassitérite; les sulfosels Sb incluent la freibergite, la gudmundite, la pyrargyrite, la freieslébénite, la boulangérite, la costibite et la bournonite. Au nombre des composés inter-métalliques on retrouve l'or argental et la dyscrasite; les tellurites comprennent l'hessite, la rucklidgéite, la pilsénite et la volynskite; et au nombre des sélénides se trouvent la clausthalite et la naumannite. Les minerais sont dominés par la distribution spatiale et par la texture des trois minerais sulfurés les plus importants et abondants, soit la pyrite, la chalcopyrite et la sphalérite. Le minerai de cuivre principal est la chalcopyrite ($CuFeS_2$ stroichiométrique pur), tandis que le minerai de zinc principal est la sphalérite ($\bar{x}$ = 59,8 % Zn, 33,3 % S, 6,6 % Fe, 0,2 % Cd et 0,1 % Cu). Neuf minerais à teneur en argent ont été identifiés; l'argent est présent dans la galène sous forme de solution solide et peut probablement se retrouver dans la sphalérite et possiblement dans la chalcopyrite. Les principaux minerais à teneur en argent ($\bar{x}$ = 21,7 % Ag), la freibergite et la pyrargyrite sont présents dans la galène sous forme d'inclusions à grains fins ou lui sont étroitement associés. Ils se retrouvent principalement dans les minerais de sphalérite non stratifiés du toit de faille et dans les minerais rubanés de pyrite et de sphalérite. L'or argental est le seul minerai à teneur en Au qui a été identifié. On a effectué des analyses quantitatives au moyen d'une microsonde pour déterminer sa teneur moyenne qui est 46,97 % Ag, 41,37 % Au, 10,64 % Hg et 0,73 % Fe (valeur moyenne = 99,72 %).

Les analyses chimiques des minerais ont permis de déterminer

l'existence de deux groupes d'éléments dont le taux de covariance est élevé; un groupe Zn : Zn, Cd, Sb, Pb, Ag, Hg, In, Sn et As, et un groupe Cu : Cu, Se, Te, Co et Fe. Ces deux groupes d'éléments constituent les deux associations géochimiques principales des minerais et les caractérisent par rapport à leurs différences mutuelles. Au ne démontre aucune covariance importante avec aucun des éléments susmentionnés.

À CANMET, on utilisé les techniques MP-SEM-IPS-IAS pour déterminer la teneur des minerais et en faire l'analyse. On a également déterminé la distribution granulométrique de la pyrite, de la chalcopyrite, de la sphalérite, de la freibergite et de la galène contenue dans chaque échantillon de minerai analysé, et la distribution granulométrique moyenne pour chaque espèce minérale et pour l'ensemble des minerais. Les mailles de broyage les plus fines pour la sphalérite, la chalcopyrite, la pyrite, la galène et la freibergite ont été +208 um, -175 um, -95 um, -48 um et -60 um, respectivement. De même, les minerais susmentionnés ont été broyés à la maille optimale de -52 um, -52 um, -26 um, -9,2 um et -4,6 um, respectivement.

On a déterminé trois espèces d'électrum, soit (1) les inclusions internes, les fractures de remplissage et le revêtement granuleux, dans la pyrite (2) les masses anastomotiques dans la chalcopyrite et la pyrrhotite, et (3) les inclusions dans les masses de galène et de freibergite. La courbe granulométrique cumulative des espèces 1 et 3 (417 grains d'électrum) est de -18,5 um (80 %), tandis que la courbe granulométrique cumulative des électrum de l'espèce 2 est de -37 um (80 %). On croit que les pertes résiduelles de Au sont attribuables à la libération limitée des électrum à grains fins qui sont emprisonnés dans la pyrite (espèce 1). La cause principale des pertes résiduelles de Ag semble être attribuable à la libération limitée de la galène et de la freibergite à grains fins que contient la pyrite.

La stratification lenticulaire n° 2 de la Zone Nord est la plus considérable et la plus riche des stratifications lenticulaires de minerais connues, et est caractérisée par des intercalations fines, abondantes et inter-pénétrantes de chalcopyrite + sphalérite + pyrrhotite + galène résultant de la croissance diablastique pendant et après le cisaillement. Le cisaillement accompagnait l'intrusion d'un seuil de quartz-diorite auquel s'intercalait de façon discontinue le pendage en aval de la stratification lenticulaire. Si un problème sur le plan de la libération de la sphalérite est relié aux grains composites de chalcopyrite et de sphalérite, et résulte dans ces valeurs en zinc élevées par rapport au concentré de cuivre (Cu), les sources texturales les plus probables sont la chalcopyrite et la sphalérite diablastique et texturée, de même que, mais dans une mesure moindre, la "maladie de la chalcopyrite", pratiquement

omniprésente dans la sphalérite.

Mots-clé : minerais en provenance de Trout Lake; minerais de métaux de base d'origine volcanique; minerais de cuivre; minerais de zinc; classification des minerais; titrage des différentes espèces minérales; pétrologie des minerais; analyse granulométrique, teneur en minerais.

CONTENTS

ACKNOWLEDGEMENTS ii

ABSTRACT iii

Chapter page

I. INTRODUCTION 1

II. DISCOVERY, DEVELOPMENT AND PRODUCTION 2

III. GEOLOGY 6

IV. SAMPLING 9

V. METHODS OF INVESTIGATION 12

- MICROPROBE ANALYSIS 12
- CHEMICAL ANALYSES 14
- IMAGE ANALYSIS 16

VI. CLASSIFICATION OF THE ORES : THE ORE TYPES 17

- GENERAL CHARACTERISTICS 17
- DETAILED CHARACTERISTICS 28
  - THE MASSIVE SPHALERITE ORE TYPE 28
  - THE MASSIVE PYRITE ORE TYPE 33
  - THE MASSIVE BANDED PYRITE + SPHALERITE ORE TYPE 36
  - THE MIXED/BANDED CHALCOPYRITE + SPHALERITE ORE TYPE 41
  - MASSIVE CHALCOPYRITE + PYRRHOTITE ORE TYPE 46
  - CHALCOPYRITE STRINGER ORE TYPE 49
  - DISSEMINATED PYRITE + CHALCOPYRITE ORE TYPE 54
  - SHEARED CHALCOPYRITE + SPHALERITE ORE TYPE 59
  - VEIN QUARTZ + CHALCOPYRITE ORE TYPE 64

VII. CHARACTERISTICS OF THE ORE MINERALS 66

- THE COMMON SULPHIDES 66
  - PYRITE (FeS_2) 66
  - MARCASITE (FeS_2) 67
  - PYRRHOTITE ($Fe_{(1-x)}S$) 67
  - CHALCOPYRITE ($CuFeS_2$) 71
  - ARSENOPYRITE (FeAsS) 73
  - CUBANITE ($CuFe_2S_3$) 75
  - GALENA (PbS) 75
  - SPHALERITE (ZnS) 76

ACANTHITE (Ag_2S) 81
THE OXIDES 81
MAGNETITE (Fe_3O_4) 81
CASSITERITE 84
INTERMETALLIC AND ALLOY-LIKE COMPOUNDS 84
MERCURIAN ELECTRUM (Ag,Au,Hg,Fe) 84
DYSCRASITE (Ag_3Sb) 95
THE ANTIMONIAL SULFOSALTS 95
FREIBERGITE ($(Cu,Ag)_{10}(Fe,Zn)_2(Sb,As)_4S_{13}$) 95
GUDMUNDITE (FeSbS) 98
PYRARGYRITE (Ag_3SbS_3) 100
BOULANGERITE ($Pb_5Sb_4S_{11}$) 100
COSTIBITE (CoSbS) 100
FREIESLEBENITE ($Ag_2Sb_2Pb_2S_6$) 101
BOURNONITE (Pb,Cu,Sb,S_3) 105
THE TELLURIDES 105
HESSITE (Ag_2Te) 105
PILSENITE(?) ($(Bi,Pb)_8(Te,Se)_{6.8}$) 107
RUCKLIDGEITE ($(Bi,Pb)_3Te_4$) 109
VOLYNSKITE ($BiAgTe_2$) 111
SELENIDES 113
CLAUSTHALITE-GALENA SOLID SOLUTION (Pb(Se,S)) 113
NAUMANNITE (Ag_2Se) 115
RARE EARTH MINERALS 115
MONAZITE AND BASTNAESITE 115

VIII. MINERAL - METAL BALANCE **118**

CORRELATION ANALYSIS 123
FACTOR ANALYSIS 131
SUMMARY 137

IX. PREDICTION OF MINERAL LIBERATION **140**

X. THE ORE TEXTURES AND METAMORPHISM AT TROUT LAKE **148**

RELICT TEXTURES 149
CHANGES IN THE MINERALOGY DUE TO METAMORPHISM 150
CHANGES IN THE FABRIC DUE TO METAMORPHIC RECRYSTALLISATION 154
CHANGES IN THE FABRIC DUE TO DEFORMATION 156
SULFIDE MOBILISATION 159

XI. DISCUSSION AND CONCLUSIONS **161**

BIBLIOGRAPHY **169**

Appendix page

A. **174**

B. 176
C. 178
D. 179

Chapter I

INTRODUCTION

A mineralogical study was conducted on the ores from the Trout Lake deposit as a project within the CANADA-MANITOBA MINERAL DEVELOPMENT AGREEMENT. This project entitled "The mineralogical characteristics that affect metal recoveries from the Cu, Zn, Pb and Ag ores from Manitoba" was conducted as a contract to Hudson Bay Mining and Smelting Co. Ltd. from CANMET, Dept. of Energy, Mines and Resources, under the supervision and guidance of the CANMET Scientific Authority Dr. W. Petruk. The work was performed by the author at the University of Manitoba as an employee of H.B.M.S. under this contract.

The Trout Lake deposit is a volcanogenic massive sulphide deposit that contains the recoverable metals Cu, Zn, Au, Ag, Pb, Cd, Co and Se. The objective of the project was to establish whether the volcanogenic massive sulphide deposits of Manitoba contain unique mineralogical characteritics, and to determine whether these characteristics can be utilized to modify metallurgical practises, so that recovery could be optimised. The Trout Lake deposit had been selected for study because the copper concentrate commonly contains 5 Wt % zinc, and because approximately 30 % of the gold and of the silver are lost to the tailings.

The study was divided into two parts. Part 1, to define the mineralogical characteristics that could have a bearing on mining and mineral processing, and Part 2, a mineralogical study of the behaviour of the minerals in the concentrator. Part 1 involved collecting a representative suite of samples from the deposit, fitting them into a classification based largely on that developed by the mine geologist, and characterising the ore from each classification. The ore characterisation involved identifying the minerals, determining mineral quantities, determining the average chemical composition, defining the host mineral(s) for each element of interest, determining the size distribution of the minerals in the unbroken ore, and noting mineral textures that might have a bearing on mineral beneficiation. This paper covers Part 1 of the study. It is noteworthy that although this study defines mineralogical characteristics that affect processing, some of these same characteristics also provide fundamental information on ore genesis.

Chapter II

DISCOVERY, DEVELOPMENT AND PRODUCTION

The Trout Lake deposit is located 5 km northeast of Flin Flon (Fig 1). It was discovered by Granges Exploration in the winter of 1976 during a diamond drilling program that was a follow up to both airborne and ground geophysical surveys (Muzylowski, 1979). The mine is a joint venture of Hudson Bay Mining and Smelting Co. Ltd., Granges Exploration, Manitoba Mineral Resources and Outokumpu Oy. The mine was brought into production in 1982 by H.B.M.S. (Duval, 1985), and since then six lenses have been developed. It is presently a 2,000 ton per day operation, is accessed by a decline, and employs a mechanised 'Cut and Fill' mining method.

The ore undergoes primary crushing underground prior to being trucked to the H.B.M.S. mill at Flin Flon. To simplify the accounting with its partners in the Trout Lake Joint Venture, H.B.M.S. treats the ore in a separate circuit. Both the Cu- and the Zn-concentrates are combined with the corresponding concentrates from the main H.B.M.S. circuit and are fed to the Smelter and Zinc Plant, respectively. The tailings are trucked back to the mine for use as backfill. The combined production and ore reserves, and the remaining proven ore reserves as of 1st January 1986 (Ko, 1986) are presented in Table 1, whereas the concentrate and tailings grades and the metal recoveries are presented in Table 2. The grades and tonnages of the six proven ore lenses are presented in Table 3.

FIGURE 1

LOCATION MAP.

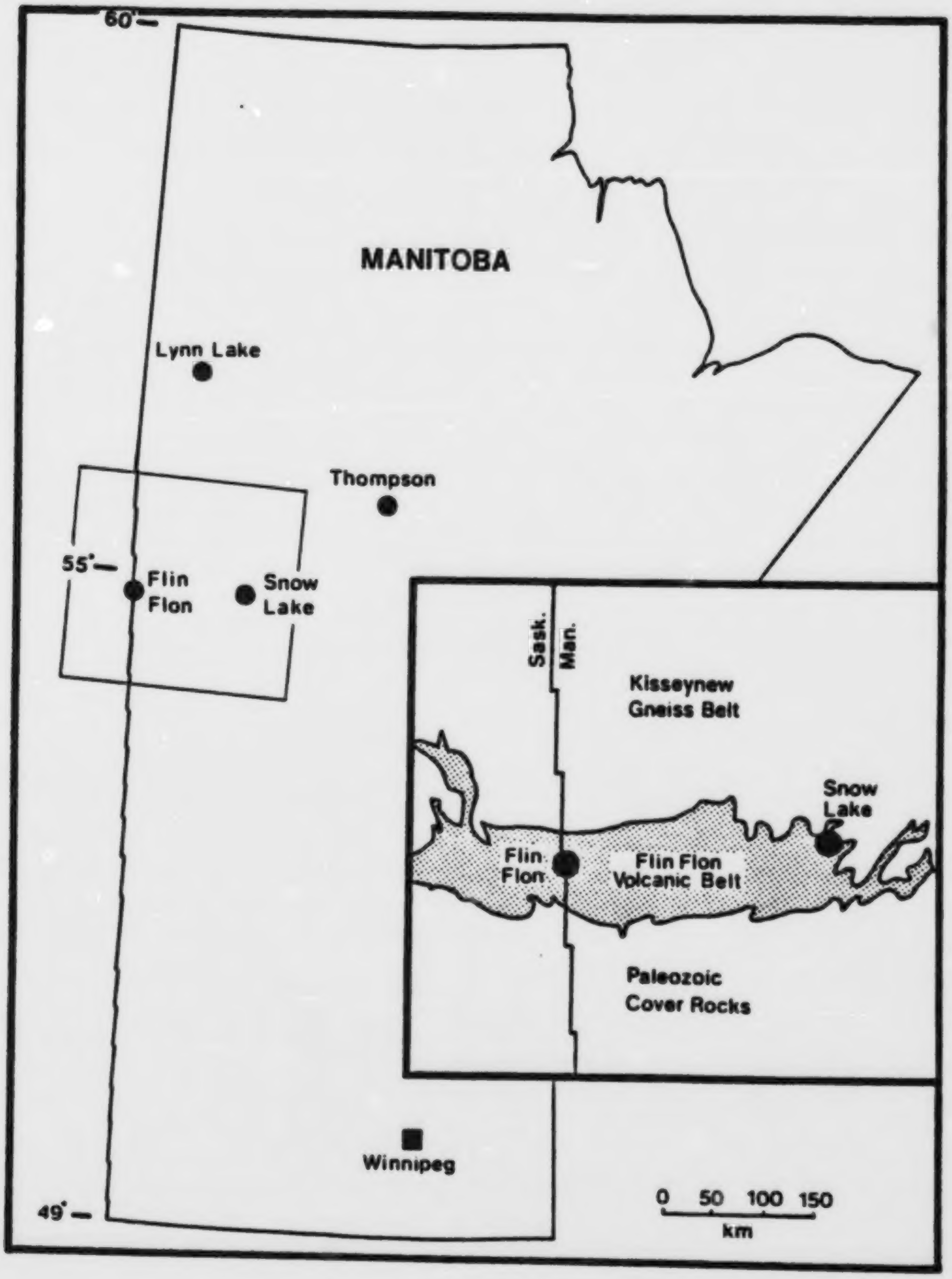
60°
MANITOBA
Lynn Lake
Thompson
55°
Flin Flon
Snow Lake
Sask.
Man.
Kisseynew Gneiss Belt
Snow Lake
Flin Flon
Flin Flon Volcanic Belt
Paleozoic Cover Rocks
Winnipeg
49°
0 50 100 150
km

TABLE 1

1986 TROUT LAKE PRODUCTION AND RESERVES.

	TONS.	Au. (oz/t)	Ag. (oz/t)	Cu. (%)	Zn. (%)
COMBINED PRODUCTION AND RESERVES.	6.31 million	0.050	0.46	2.28	5.6
PROVEN RESERVES.	4.63 million	0.051	0.49	2.32	6.1

Note : data includes 15% dilution and 92.9% mining recovery.

TABLE 2

TROUT LAKE CIRCUIT BALANCE (1984).

	ASSAYS.					
	WT %	Au(oz/t)	Ag(oz/t)	Cu(%)	Zn(%)	Fe(%)
Head	100.00	0.042	0.354	2.45	3.76	19.33
Cu Conc.	9.95	0.256	2.084	22.85	5.12	30.14
Zn Conc.	5.79	0.051	0.949	1.02	50.13	11.41
Tailings	84.29	0.017	0.135	0.14	0.40	18.59
	RECOVERY(%)					
Cu Conc.		59.60	55.13	92.77	13.78	15.52
Zn Conc.		6.87	14.61	2.41	77.25	3.42
Tailings		33.53	30.26	4.82	8.97	81.06

TABLE 3

GRADES AND TONNAGES OF THE SIX PROVEN ORE LENSES.

LENSES	TONNAGE	Au Grade	%	Ag Grade	%	Cu Grade	%	Zn Grade	%
NORTH ZONE									
No. 1 Lens	487,000	0.038	6.	0.38	6.	2.22	8.	4.0	6.
No. 2 Lens	2,213,000	0.069	48.	0.51	39.	2.69	41.	7.4	47.
SOUTH ZONE									
No. 1 Lens	1,098,000	0.050	17.	0.55	21.	2.25	17.	4.2	13.
No. 2 Lens	307,000	0.040	4.	0.59	6.	0.84	2.	6.1	5.
No. 3 Lens	1,591,000	0.038	19.	0.22	12.	2.81	31.	4.2	19.
No. 5 Lens	613,000	0.030	6.	0.74	16.	0.29	1.	6.0	11.

Note : % denotes percentage of the total tonnage of that metal.

Chapter III

GEOLOGY

The Trout Lake deposit is hosted in the Amisk Group Volcanic strata of the Proterozoic Flin Flon greenstone belt (Fig 1). The Flin Flon belt is part of the southern Churchill structural province and was deformed and metamorphosed prior to 1,750 Ma during the Hudsonian Orogeny (Syme et al. 1982). The metamorphic grade of the rocks in the Flin Flon area corresponds to greenschist facies and progressively increases northward where the almandine-amphibolite metamorphic grade has been recognised in the Kisseynew gneisses (Syme et al. 1982).

The Flin Flon belt consists of a sequence of volcanic rocks with associated subordinate sediments, an overlying sequence of terrestrial sediments and a diversity of intrusive rocks. The Amisk Group comprises the lower stratigraphic elements of the Flin Flon belt. This group is dominated by subaqueous and subaerial volcanics of the tholeitic and calc-alkaline affinity, and are interpreted as having been deposited in an island arc setting (Syme et al. 1982). The volcanics consist of massive to pillowed basalt and andesite flows, overlain by pyroclastic andesite breccias and rhyolitic and dacitic quartz-porphyry (Koo and Mossman, 1975). The Amisk Group underwent plutonism, uplift and deformation prior to the deposition of the unconformably overlying fluviatile sedimentary strata of the Missi Group (Syme et al. 1982). The Missi Group constitutes sediments derived from the uplifted and deeply eroded Amisk terrain, including unroofed pre-Missi felsic plutons. Numerous small intrusives are interpreted as being correlative with the Amisk volcanism, whilst the larger intrusive bodies are less clearly syn-volcanic, or are interpreted as being post-volcanic (Price, 1977).

The metamorphic maxima occured during the second of three deformational events associated with the Hudsonian Orogeny (Price, 1977). The earliest deformation event (D1) resulted in east-trending tightly closed folds with steeply dipping axial surfaces and non-penetrative metamorphism. The second deformation event (D2) resulted in north-trending isoclinal folding about steep to vertical dipping axial surfaces (Price, 1977). This folding was associated with penetrative metamorphism (axial foliation) as well as the emplacement of syn-tectonic plutons (Koo, 1973). The latest deformation event (D3) resulted in refolding the rocks about the northeast trending Embury Lake antiform and associated shearing and drag-folding along northwesterly trending faults (Price, 1977, Koo and Mossman, 1975). Post-tectonic magmatism is not evidenced in the Flin Flon area (Price, 1977).

The Trout Lake deposit consists of a series of steeply dipping stacked lenses (6 proven) occurring in two (North and South) zones. The zones strike at 140° azimuth and have a relatively constant dip of 60-70° to the northeast. Each lens consists of two principal types of ore, massive ore occurring in quartz-sericite schists, and disseminated ore occurring in chlorite schists, where the hostrock types represent the metamorphosed equivalents of hydrothermally altered quartz-porphyry fragmental pyroclastics. The lenses generally consist of massive sulphides which are commonly separated by zones of disseminated pyrite and chalcopyrite. The massive ore is interpreted as exhalative mineralisation deposited on the seafloor proximal to a fumarolic vent. The disseminated mineralisation which does not constitute ore, together with the chalcopyrite stringer ore (described later) are interpreted as the metamorphosed equivalent of the feeder pipe stockwork ore (Ko, pers. comm., 1985).

The footwall contact of the stockwork ore is diffuse, whereas the hangingwall contact of the massive ore is sharp. The margins of the lenses commonly display open to tightly closed and isoclinal folding with shearing and dislocations on a mesoscopic scale. The relative distribution of the massive and stockwork mineralisation strongly suggests intense shearing of the highly chloritised footwall rocks, the stringer ore and disseminated mineralisation (Ko, pers. comm., 1985).

The lenses generaly exhibit a zonation from a common graphitic argillite in the hangingwall, to massive sphalerite, to massive pyrite, to massive chalcopyrite + pyrite + sphalerite + pyrrhotite to footwall semi-massive chalcopyrite stringers and disseminated pyrite and chalcopyrite (Fig 2). This zonation is locally reversed or disturbed by folding, as well as by emplacement of quartz-diorite intrusions. Generally coincident with the increases in the Cu / Cu + Zn ratio are increases in the silicate mineral content of the ore and the relative abundance of Au compared to Ag. The fundamental metal zonation can be generalised as coincident high Ag and Pb and low silicate content associated with low Cu / Cu + Zn ratios in the hangingwall, and coincident high Au and high silicate content associated with high Cu / Cu + Zn ratios in the footwall. This zonation is highlighted by the highly differentiated appearance of the ores in terms of the sphalerite and chalcopyrite content, with spectacular semi-massive coarse-grained chalcopyrite stringer ores in the footwall and massive sphalerite ores in the hangingwall. The zonation of the ores is characteristic of many volcanogenic massive sulphides (Sangster, 1972 and Franklin et al. 1980).It can be explained in terms of the chemical evolution of hydrothermal metal-bearing fluids progressively mixing with the seawater, either just below or above and at an increasing distance from the exhalative vent, and with time during the evolution of the hydrothermal cell. High Cu values are associated with the more proximal elements of the hydrothermal cell (stockwork ore and immediate vent area), whereas increasing Zn values are observed upwards and outwards away from the vent towards the margins of the lens.

As each of the lenses possesses a footwall stockwork ore with a highly chloritised alteration zone, each lens is interpreted as being of the proximal type, having formed in the immediate vent area. In addition, as each lens exhibits the gross metal zonation (See above) the lenses are interpreted as representing an entire hydrothermal cycle, possibly fed by one or more hydrothermal cells separated in time and/or space. The consistent occurrence of stockwork ores in the footwall and the gross metal zonation also argues against any form of downslope transportation or reworking of the sulphide mound.

FIGURE 2

GENERALISED ZONATION OF THE PROVEN ORE LENSES.

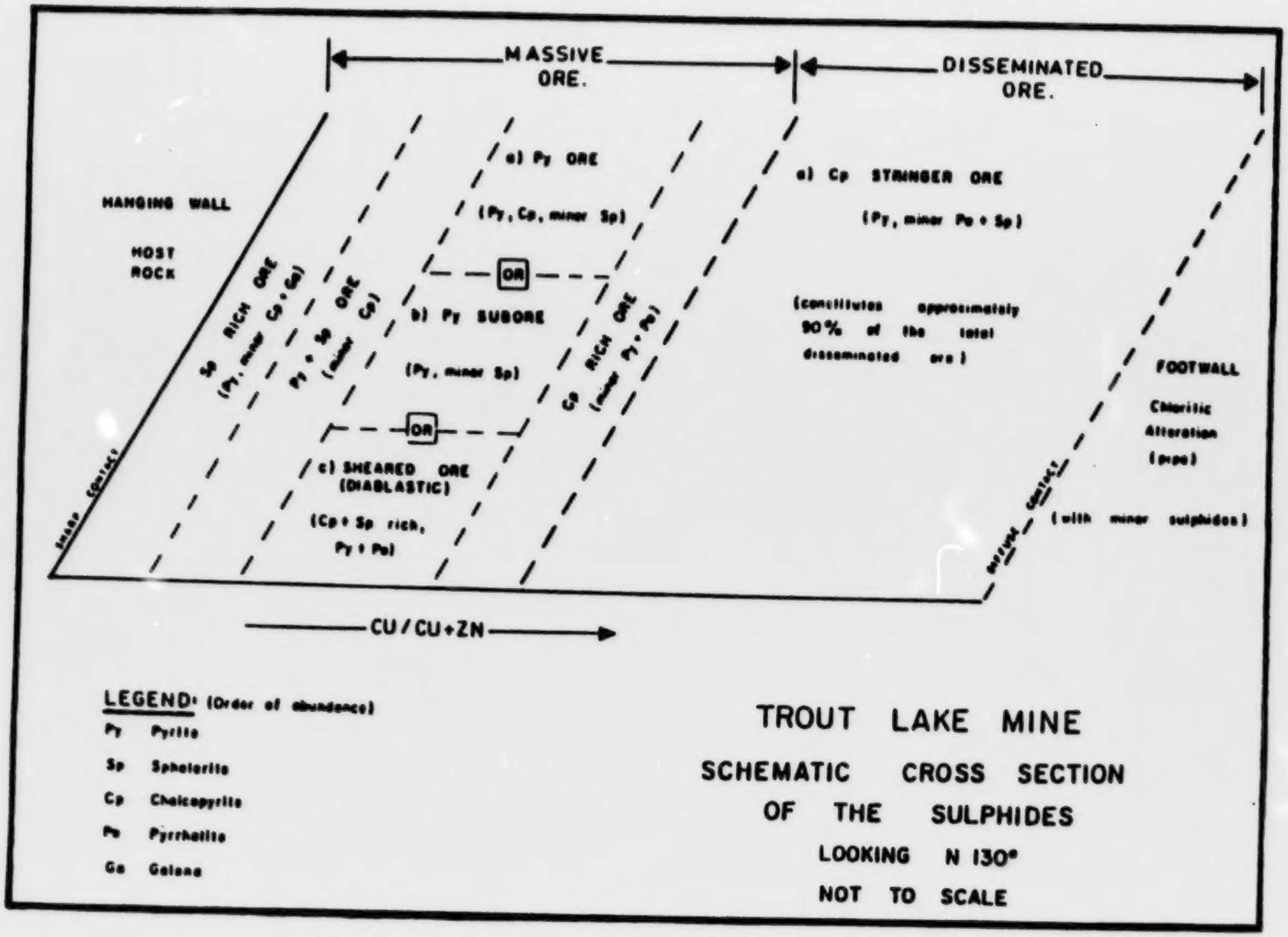
MASSIVE ORE.
DISSEMINATED ORE.
HANGING WALL
HOST ROCK
Sharp contact
Sp RICH ORE (Py, minor Cp + Ga)
Py + Sp ORE (minor Cp)
a) Py ORE
(Py, Cp, minor Sp)
OR
b) Py SUBORE
(Py, minor Sp)
OR
c) SHEARED ORE (DIABLASTIC)
(Cp + Sp rich, Py + Po)
Cp RICH ORE (minor Py + Po)
a) Cp STRINGER ORE
(Py, minor Po + Sp)
(constitutes approximately 90% of the total disseminated ore)
Diffuse contact
FOOTWALL
Chloritic Alteration (pipe)
(with minor sulphides)
CU/CU+ZN
LEGEND: (Order of abundance)
Py Pyrite
Sp Sphalerite
Cp Chalcopyrite
Po Pyrrhotite
Ga Galena
TROUT LAKE MINE
SCHEMATIC CROSS SECTION
OF THE SULPHIDES
LOOKING N 130°
NOT TO SCALE

Chapter IV

SAMPLING

A total of 112 hand-specimen samples were collected during two underground sampling campaigns. Sampling was conducted in such a manner as to obtain the maximum spatial coverage of each lens, as well as to acquire samples that fully encompass the range of ore types at each sample location. Thus, depending on the character of the lens at a selected site, anywhere from 1 to 6 samples were collected with an average of 2.5 samples per site. The spatial coverage was determined by the extent to which each lens could be accessed by drifts, crosscuts and stopes. The spatial coverage of Lens 1 in the North Zone and Lens 2 and 3 of the South Zone is considered to be thorough, whereas Lens 2 of the North Zone and Lens 1 and 5 of the South Zone are poorly covered (Fig 3 and 4).

Samples were also collected at sites where geological, chemical and/or metallurgical data suggested that the mineralogical characteristics of the ore differred significantly from that of their supposed ore type. For example, 4 samples were collected from stope 2451 on the 210 m level of Lens 5 of the South Zone, because of the high Zn values that reported to the tailings when these ores were previously milled.

FIGURE 3

IDEALISED LONGITUDINAL VERTICAL PROJECTION OF THE NORTH ZONE PROVEN ORE LENSES. PORTRAYING THE SAMPLE LOCATIONS AND ORE TYPES.

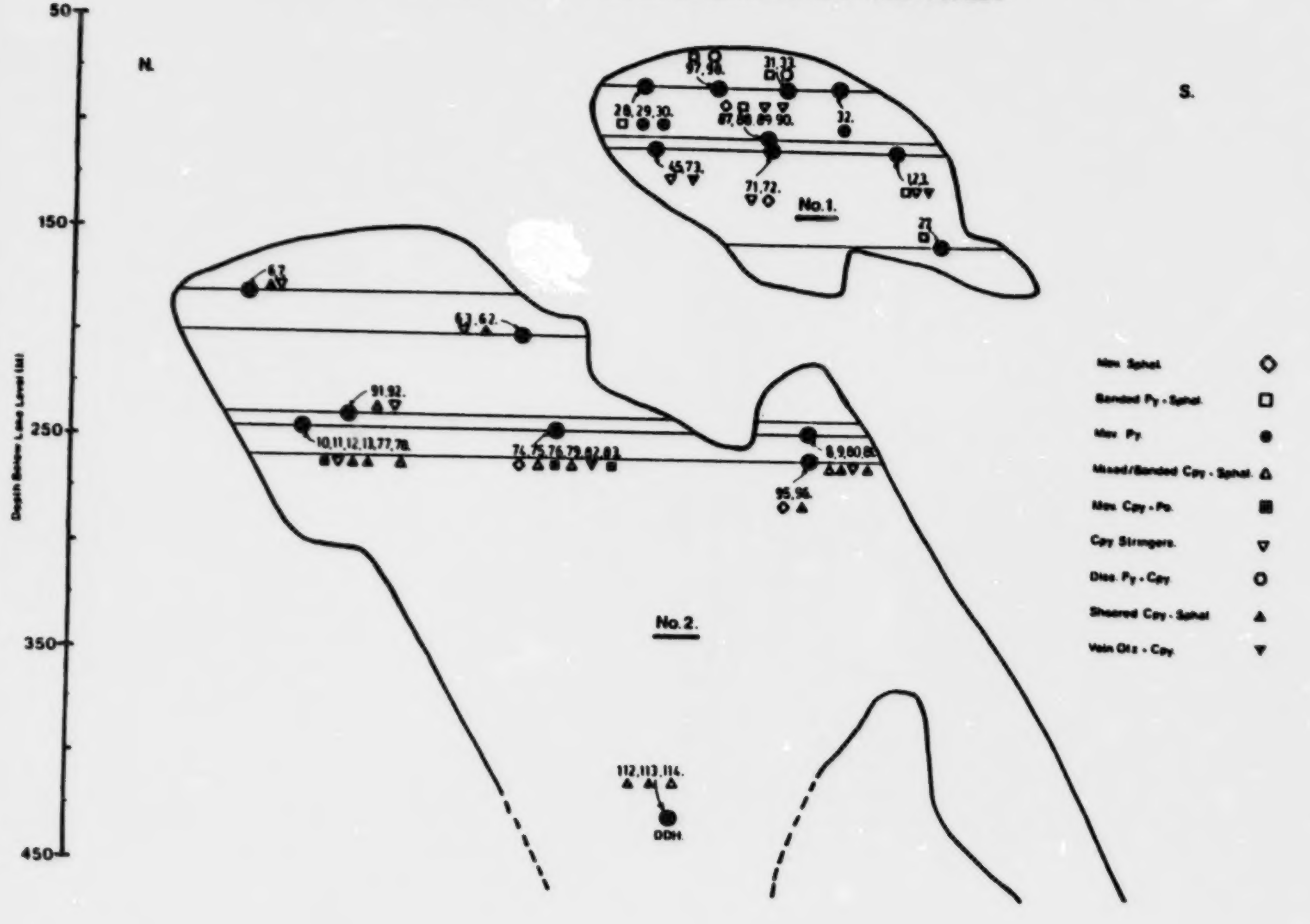

50
150
250
350
450
Depth Below Lake Level (M)
N.
S.
No.1.
No.2.
97,98.
31,33.
28,29,30.
87,88,89,90.
32.
45,73.
71,72.
123.
27.
6,7.
63,62.
91,92.
10,11,12,13,77,78.
74,75,76,79,82,83.
8,9,80,81.
95,96.
112,113,114.
DDH.
Mas. Sphal. ◇
Banded Py - Sphal. □
Mas. Py. ●
Mixed/Banded Cpy - Sphal. △
Mas. Cpy - Po. ■
Cpy Stringers. ▽
Diss. Py - Cpy ○
Sheared Cpy - Sphal ▲
Vein Qtz - Cpy ▼

FIGURE 4

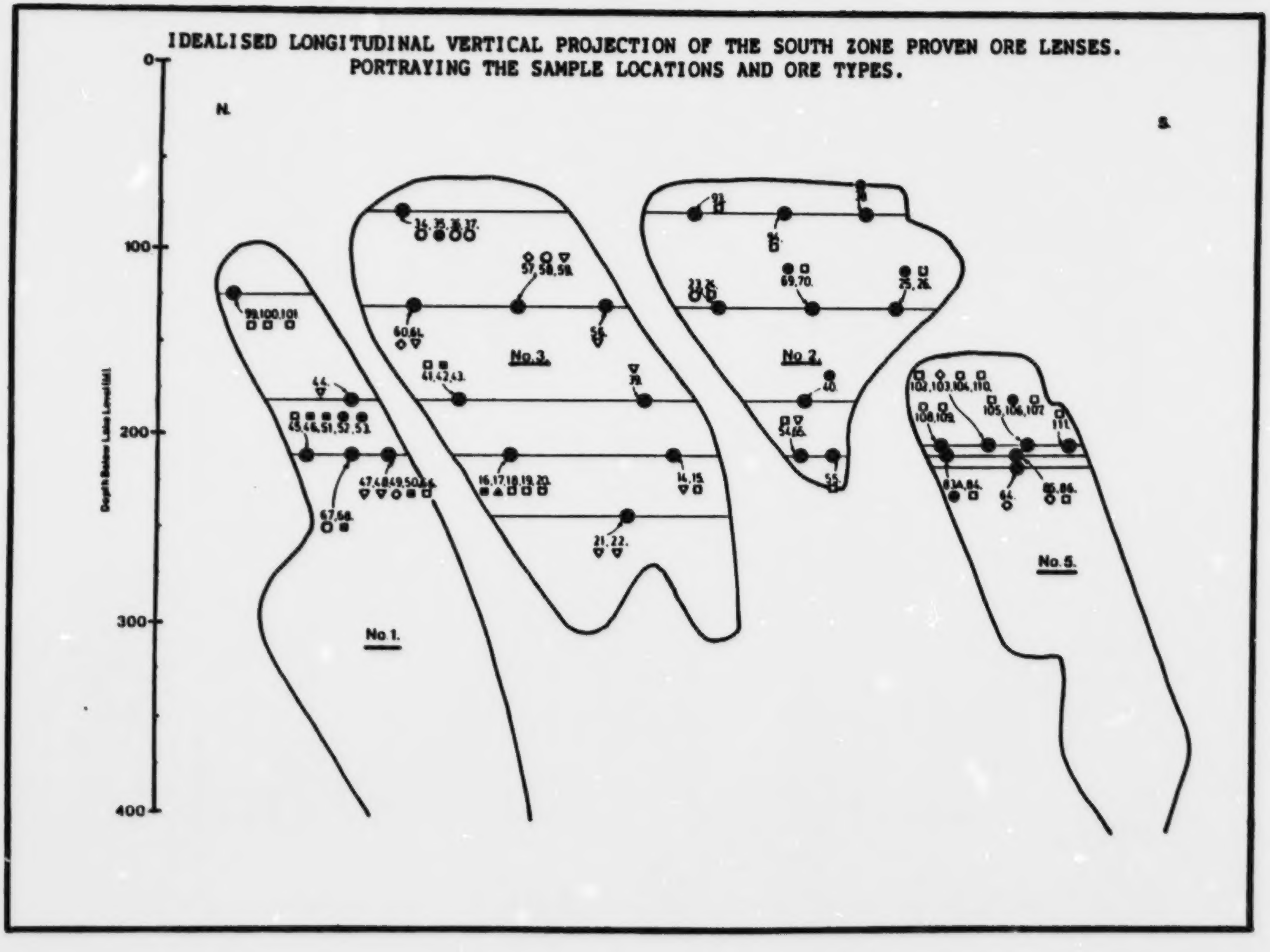

IDEALISED LONGITUDINAL VERTICAL PROJECTION OF THE SOUTH ZONE PROVEN ORE LENSES.
PORTRAYING THE SAMPLE LOCATIONS AND ORE TYPES.

Depth Below Lake Level (M)
0
100
200
300
400
N.
S.
No.1.
No.3.
No.2.
No.5.
99,100,101
44.
45,46,51,52,53.
47,48,49,50,66.
67,68.
34,35,36,37.
57,58,59.
60,61.
56.
41,42,43.
39.
16,17,18,19,20.
14,15.
21,22.
93.
94.
38.
23,24.
69,70.
25,26.
40.
54,65.
55.
102,103,104,110.
108,109.
105,106,107.
111.
83A,84.
64.
85,86.

Chapter V

METHODS OF INVESTIGATION

A total of 118 polished sections and polished thin sections representing 112 samples were viewed under reflected light, using a Reichert Orthoplan research microscope, to classify the samples, to identify the constituent ore minerals, to note specific textures and to select samples for detailed characterisation of each ore type. Each section was thoroughly examined for several hours in an attempt to identify all precious metal-bearing minerals (electrum, freibergite, etc) 0.5um and greater in size. Subsequently the sections were examined with emphasis on textures. The mineral identities were later confirmed by microprobe analysis at the U. of M., and during image analysis using the MP-SEM-IPS Image Analyser at CANMET. A total of 24 ore minerals were identified (See Table 4).

MICROPROBE ANALYSIS

The chemistry of most of the ore minerals (except dyscrasite, costibite, bournonite, volynskite, naumanite and acanthite were determined either quantitatively, semi-quantitatively or qualitatively using the MAC-5 electron microprobe at the U. of M.. The MAC-5 is equipped with an energy dispersive system, which consists of a Kevex Micro-X 7000 analytical spectrometer with a Si(Li) detector and a 1024-multichannel analyser. The majority of the analyses were collected at a 15 kV excitation voltage (Eo), 5 nA specimen current (Sc), a vacuum of approximately 1.1×10^{-4} Torr, and a sample collection time of 200 live seconds. A library of working standard spectra, and several calibration standard (fayalite) spectra were collected and stored at the initiation of the project. Each subsequent analytical run was calibrated in terms of Eo, Sc, peak shape and position by reference to the original fayalite spectra.

Routine data processing involving full Z.A.F. corrections were performed using the Magic 5 program of J.W. Colby. Overlap corrections were applied by stripping off the respective peak of a reference standard spectra that had been scaled to the sample spectra, by normalising on another non-overlapped peak of the overlapping element (Groat et al. 1985). For certain overlapping peak pairs i.e., HgMα-AuMα (electrum), PbMα-BiMα (rucklidgeite and pilsenite) and PbMα-SKα (boulangerite, clausthalite and pilsenite) this was not possible because (1) there was no second peak of the overlapping element (i.e., no SLα) that could be used for normalisation, or (2) the overlapping peak centroids were within approximately 50-100 eV, and could not be resolved satisfactorily without serious degradation of peak shape. The rucklidgeite, pilsenite and electrum were analysed at 20 kV excitation voltage using the Lα and Lβ lines.

TABLE 4

LIST OF ORE MINERALS OBSERVED IN THE TROUT LAKE ORES.

NAME	FORMULA	ABUNDANCE
THE COMMON SULPHIDES.		
Pyrite	FeS_2	Ubiquitous, Major/Minor.
Chalcopyrite	$CuFeS$	Ubiquitous, Major/Minor.
Sphalerite	ZnS	Ubiquitous, Major/Minor.
Pyrrhotite	$Fe(_{1}-x)S$	Common, Major/Trace.
Marcasite	FeS_2	Common, Major/Trace.
Galena	PbS	Common, Major/Trace.
Arsenopyrite	$FeAsS$	Common, Major/Trace.
Cubanite	$CuFe_2S_3$	Occassional, Trace.
Acanthite	Ag_2S	Rare, Trace.
THE OXIDES.		
Magnetite	Fe_3O_4	Occassional, Major/Minor.
Cassiterite	SnO_2	Rare, Trace.
THE INTERMETALLIC AND ALLOY-LIKE COMPOUNDS.		
Mercurian Electrum	Ag,Au,Hg,Fe	Common, Trace.
Dyscrasite	Ag_3Sb	Rare, Trace.
THE ANTIMONIAL SULFOSALTS.		
Freibergite	$(Cu,Ag)_{10}(Fe,Zn)_2(Sb,As)_4S_{13}$	Occassional, Minor/Trace.
Gudmundite	$FeSbS$	Occassional, Trace.
Pyrargyrite	Ag_3SbS_3	Rare, Trace.
Freieslebenite	$Ag_2Sb_2Pb_2S_6$	Rare, Trace.
Boulangerite	$Pb_5Sb_4S_{11}$	Rare, Trace.
Costibite	$CoSbS$	Rare, Trace.
Bournonite	$PbCuSbS_3$	Rare, Trace.
THE TELLURIDES.		
Hessite	Ag_2Te	Rare, Trace.
Rucklidgeite	$(Bi,Pb)_3Te_4$	Rare, Trace.
Pilsenite(?)	$(Bi,Pb)_8(Te,Se)_7$	Rare, Trace.
Volynskite	$BiAgTe_2$	Rare, Trace.
THE SELENIDES.		
Clausthalite	$PbSe$	Occassional, Minor/Trace.
Naumannite	Ag_2Se	Rare, Trace.

Presented in order of decreasing abundance of the mineral groups, and of the minerals in each group.

Microprobe analyses of electrum, volynskite, naumannite and dyscrasite were generated by wavelength dispersive analysis (W.D.A.) on the JEOL 733 at CANMET. These analyses were collected at a 20 kV excitation voltage, a 15 nA probe current (Faraday Cup) and a sample collection time of 60 seconds or less, if acceptable counting statistics (Std Dev. = 0.5) were achieved before the 60 second limit was reached.

CHEMICAL ANALYSES

Twenty seven samples were selected for detailed characterisation of each ore type. They were analysed chemically for Au, Ag, Cu, Zn, Ni, Cd, Co, Mn, Bi, Pb, Fe and S at the H.B.M.S. Assay Laboratory, Flin Flon, and for As, Se, Te, Hg, Sn, Sb and In by Bondar-Clegg, Ottawa. The samples were prepared for chemical analysis at the E.M.R. facility at Logan Ave., Winnipeg. Approximately 400 gm of sample was passed through a jaw crusher, and then through a disc-grinder equipped with standard grade cast iron plates. High quality silica sand was used to clean the surfaces of the plates prior to each sample pass, as well as to evaluate the potential contaminants due to the cast iron plates.

An aqua regia leach of the silica sand, followed by Atomic Absorption indicated significant contaminantion by Cu, Ni, Mn and Fe. The Cu, Ni and Mn are probably due to cross-contamination from the previous sample, and the Fe due to abrasion of the plates with each pass. However, the contamination is considered small enough to be tolerated.

The crushed samples and the CANMET reference ore standard CZN-1 were sealed in labelled vials as unknowns, and submitted to the respective laboratories for analysis. Precision of analysis was tested by duplicate analyses of several submitted samples. Excellent precision was achieved by H.B.M.S., with the exception of Au (See Table 5). The analyses yield a precision of 0.131 ± 0.03 oz/ton Au, which corresponds to an uncertainty of 23 %. This high uncertainty probably reflects the 'particle sparsity' or 'nugget' effect of Au, and the difficulty in acquiring a representative, yet manageable sample aliquot. The duplicate analyses performed by Bondar-Clegg also exhibit relatively good precision.

The accuracy of the analyses was evaluated by including reference ore standard CZN-1 as an unknown, and comparing the measured with the recommended values. Good agreement between the recommended and the measured values was obtained for those elements determined by H.B.M.S. (See Table 5), whereas all 7 elements analysed by Bondar-Clegg (except for Te which has no quoted value) exhibit poor agreement with the recommended or non-certified values. The good agreement of the measured values determined by H.B.M.S. suggests that the reference ore has neither oxidised nor fractionated since its acquisition, and introduces considerable doubt as to the usefulness of the analyses by Bondar-Clegg.

TABLE 5

PRECISION AND ACCURACY TESTS OF THE CHEMICAL ANALYSES.

TEST OF PRECISION BY DUPLICATE ANALYSES.

SAMPLE	Au	Ag	Cu	Zn	Ni	Cd	Co	Mn	Pb	Fe	S	As	Se	Te	Hg	Sn	Sb	In
	ppm		Wt %									ppm						
TI.H.2-91	4.150	44.08	4.7	10.6	0.002	0.025	0.015	0.27	0.002	18.7	16.6							
DUPLICATE	4.802	45.11	4.7	10.6	0.002	0.025	0.015	0.27	0.002	18.7	16.6							
TI.S.1-49													6.			44.	109.	
DUPLICATE													7.			40.	112.	
TI.H.2-96																9.	15.	
DUPLICATE																2.	17.	

TEST OF ACCURACY BASED ON ANALYSES OF REFERENCE ORE STANDARD CZN-1 (SUBMITTED AS AN UNKNOWN).

H.B.M.S. ASSAY LABORATORY.

ELEMENT.	ANALYSIS.	RECOMMENDED/CERTIFIED VALUE.
Au	nd	0.09 ppm (Non-Certified).
Ag	94.84 ppm	93. ppm ± 3 ppm.
Cu	0.15 Wt %	0.144 ± 0.003 Wt %.
Zn	45.2 Wt %	44.74 ± 0.11 Wt %.
Ni	0.001 Wt %	- (Not Quoted).
Cd	0.15 Wt %	0.132 ± 0.002 Wt %.
Co	0.001 Wt %	- (Not Quoted).
Mn	0.21 Wt %	0.219 ± 0.07 Wt %.
Bi	0.004 Wt %	0.003 (Non-Certified).
Pb	7.7 Wt %	7.45 ± 0.05 Wt %.
Fe	11.1 Wt %	10.93 ± 0.06 Wt%.
S	30.0 Wt %	30.2 ± 0.2 Wt %.

BONDAR-CLEGG.

ELEMENT.	ANALYSIS.	RECOMMENDED/CERTIFIED VALUE.
As	268 ppm	260 ± 20 ppm.
Se	1 ppm	5 ppm (Non-Certified).
Te	0.2 ppm	- (Not Quoted).
Hg	46 ppm	43 ± 4 ppm.
Sn	102 ppm	74 ppm (Non-Certified).
Sb	407 ppm	520 ± 30 ppm.
In	71 ppm	86 ppm (Non-Certified).

IMAGE ANALYSIS

The 27 ore samples were analysed by image analysis to determine the quantities and grain size distributions of the constituent ore minerals. The Leitz Tass Plus Image Analyser at the University of Manitoba was proposed initially for this aspect of the work. However, this system is equipped with an optical microscope such that the image produced is based on the reflectance of the ore minerals present. Because of the anisotropic nature of many ore minerals, the reflectance values vary with the orientation of the individual grains, resulting in adjacent or overlapping ranges in the reflectance values for the minerals. In consequence, many of the minerals found in base metal ores cannot be differentiated. Consequently, the MP-SEM-IPS Image Analysis System at CANMET was selected for this work.

MP-SEM-IPS-IAS is an abbreviation for an 'Electron Microprobe' interfaced with a Kontron SEM-IPS Image Analyser and a Tracor Northern EDXA 2000 energy dispersive system, to form an integrated 'Image Analysis System'. The 'front end' or image producing component of this system consists of a JEOL 733 Superprobe with electron beam scanning capabilities, two wavelength dispersive spectrometers and the energy dispersive system. The SEM capabilities of the JEOL permit high resolution backscattered electron (BSE) mages of the sample surface to be generated. The BSE signal discriminates between minerals on the basis of the average atomic number (Z) of the minerals, all of which occur within a narrow range or grey level window (Mainwaring and Petruk, 1984 and Petruk, 1985). Whenever the average atomic number of two or more minerals are so similar that the minerals cannot be differentiated by their grey levels, they are grouped as a 'family' in a single image memory. Each grain in this image memory is then individually and automatically identified by the EDXA.

The 'back end' of the Image Analysis System consists of a Kontron SEM-IPS Image Analyser which collects and processes the image produced by the electron microprobe. The mineral quantities are determined by measuring the relative Area % of each mineral (or mineral group, eg., gangue) within the polished section. The Area % is directly convertible to Volume %, which is in turn recalculated to Weight % mineral by correcting for the mineral densities. From the Wt % values and the composition of the minerals as determined by microprobe analyses, metal and sulfur contents (bulk compositions) of the sample can be calculated.

The grain size distributions of the common sulphides and some minor and trace minerals were determined by chord analysis. The chord analysis scans the image along selected, finitely-spaced lines and measures the intercept lengths for each mineral. These intercept lengths are considered equivalent to the grain diameter (Petruk, 1985). These diameters are classified in the Tyler Mesh Series up to 65 Mesh (208um), to produce a grain size distribution for each of the selected minerals in that sample.

Chapter VI

CLASSIFICATION OF THE ORES : THE ORE TYPES

GENERAL CHARACTERISTICS

The ores were classified into 9 ore types on the basis of the relative abundance and textures of the ore minerals (See Table 6). These ore types correspond closely to ore types recognised by the mine geology staff (Ko, pers. comm., 1985), and seven of them also approximate to metamorphic equivalents of the classical ore types recognised from the Kuroko volcanogenic deposits of Japan (Lambert and Sato, 1974). The other two ore types (the Sheared Chalcopyrite + Sphalerite and the Vein Quartz + Chalcopyrite ore types) are interpreted as having been produced by tectonic forces, and have no equivalent in the definitions for the Kuroko deposits.

In general, all of the seven ore types are represented in each lens, and occur in the following generalised sequence from hangingwall to footwall : Massive Sphalerite; Massive Banded Pyrite + Sphalerite; Massive Pyrite; Mixed/Banded Chalcopyrite + Sphalerite; Massive Chalcopyrite + Pyrrhotite; Chalcopyrite Stringers and Disseminated Pyrite + Chalcopyrite. The lenses in the Trout Lake deposit have an average thickness of 10 metres; the maximum recorded thickness approximates to 25 metres. They are generally vertically stratified comprising all the ore types, although locally the lenses consist of only one ore type. The distribution of the ore types is reflected in the samples that were collected (Figs 3 and 4). However, the relative abundance of the ore types could not be determined within the scope of this work.

Twenty seven samples were selected as typical examples of the nine ore types. They were analysed chemically and with the image analyser to determine the average elemental contents and quantities and size distributions of the ore minerals, respectively, in each ore type. The chemical compositions for each sample are given in Table 7, and the mineral quantities in Table 8. The average chemical composition for each ore type was calculated from Table 7, and the results are given in Table 9. Partial chemical compositions were also calculated from the mineral quantities data (Table 8), using microprobe determined mineral compositions, in order to assess whether the analysed samples were representative (See Table 10). In general good agreement was obtained, particularly in view of the fact that the polished sections represent a very small area of the sample and may over emphasize a particular band within the sample. The material submitted for chemical analysis represents a larger and more homogeneous (finely ground) portion of the sample, and is therefore assumed to be more representative.

The average mineral quantities for each ore type were calculated from Table 8 (See Table 11). However, as noted above, there are differences between the

TABLE 6

LIST OF ORE TYPES DEFINED AT TROUT LAKE.

ORE TYPE.	STRATIGRAPHIC LOCATION.	UNMETAMORPHOSED KUROKO EQUIVALENT (Lambert and Sato, 1974).	PRINCIPAL ORE MINERALS.
Massive Sphalerite.	Hangingwall.	Kuroko (Black) Ore.	Sphal+Py+Cpy+Po+Gal+Aspy+Marc+Freib.
Banded Pyrite + Sphalerite.	Hangingwall.	Kuroko (Black) Ore.	Py+Sphal+Cpy+Po+Aspy+Gal+Marc+Freib.
Massive Pyrite.	Hangingwall/Centre.	Ryukako (Pyrite) Ore.	Py+Sphal+Cpy+Po+Marc+Gal.
Mixed/Banded Chalcopyrite + Sphalerite.	Centre.	Oko (Yellow) Ore.	Cpy+Sphal+Po+Py+Mag.
Massive Chalcopyrite + Pyrrhotite.	Footwall/Centre.	Oko (Yellow) Ore.	Cpy+Po+Py+Sphal+Mag.
Chalcopyrite Stringers.	Footwall.	Keiko (Siliceous) Ore.	Cpy+Po+Py+Sphal+Po+Marc.
Disseminated Pyrite + Chalcopyrite.	Footwall.	Keiko (Siliceous) Ore.	Py+Cpy+Sphal+Po+Marc.
Sheared Chalcopyrite + Sphalerite.	Tectonic Control.	No equivalent.	Cpy+Sphal+Po+py.
Vein Quartz + Chalcopyrite.	Tectonic Control.	No equivalent.	Cpy+Sphal+Py+Po+Marc+Cub.

TABLE 7

THE CHEMICAL ANALYSES OF THE 27 REPRESENTATIVE ORE SAMPLES.

SAMPLE	Au	Ag	Cu	Zn	Ni	Cd	Co	Mn	Pb	Fe	S	As	Se	Te	Hg	Sn	Sb	In
	ppm		wt %									ppm						
MASSIVE SPHALERITE ORE TYPE.																		
TLS.1-49	0.69	27.27	0.11	37.4	0.003	0.077	0.015	0.056	0.031	10.8	24.9	550.	6.	nd	19.	44.	109.	37.
TLS.5-64	2.06	469.9	0.06	38.6	0.001	0.052	0.001	0.038	12.1	10.7	24.3	1400.	nd	nd	49.	47.	38.	61.
TLM.2-74	2.74	21.44	4.4	41.3	0.001	0.093	0.017	0.067	0.035	13.2	29.7	6.	5.	0.2	22.	46.	89.	69.
TLM.2-95	0.52	28.98	2.3	34.3	0.001	0.079	0.005	0.15	0.29	11.6	22.4	3.	62.	1.2	21.	40.	84.	37.
BANDED PYRITE + SPHALERITE ORE TYPE.																		
TLM.2-24	0.86	27.44	2.00	15.0	0.002	0.034	0.007	0.072	0.001	27.9	35.1	165.	80.	1.5	60.	93.	60.	36.
TLM.2-26	0.52	275.8	0.05	30.3	0.003	0.050	0.001	0.027	4.1	14.9	28.8	485.	nd	nd	114.	46.	377.	93.
TLS.2-56	0.86	9.26	0.34	16.1	0.003	0.034	0.003	0.096	0.132	30.8	39.3	500.	15.	0.2	66.	41.	69.	27.
TLS.2-55	13.75	8.06	0.02	18.0	0.002	0.041	0.006	0.096	0.051	26.4	32.0	54000.	13.	nd	65.	39.	162.	28.
MASSIVE PYRITE ORE TYPE.																		
TLM.2-25	0.52	12.52	0.07	6.6	0.002	0.014	0.001	0.020	0.008	39.9	45.0	330.	70.	0.3	44.	34.	56.	27.
TLS.1-52	1.82	5.66	0.46	1.98	0.002	0.005	0.030	0.042	0.008	38.6	36.2	306.	44.	0.2	44.	35.	37.	23.
TLS.5-83A	1.37	112.9	0.04	1.44	0.003	0.001	0.001	0.028	0.85	35.9	37.3	2600.	1.	nd	28.	30.	138.	41.
MIXED/BANDED CHALCOPYRITE + SPHALERITE ORE TYPE.																		
TLM.2-78	3.64	72.03	6.17	25.0	0.002	0.051	0.025	0.078	0.013	23.6	33.7	893.	4.	0.7	43.	42.	98.	46.
TLM.2-91	4.49	44.59	4.7	10.6	0.002	0.026	0.015	0.27	0.002	18.7	16.6	32.	24.	1.0	24.	31.	40.	43.
MASSIVE CHALCOPYRITE + PYRRHOTITE ORE TYPE.																		
TLS.3-42	2.78	28.81	7.99	0.27	0.002	0.001	0.123	0.064	0.004	44.0	28.1	1500.	90.	2.5	62.	42.	40.	25.
TLS.1-50	1.48	44.88	19.74	0.37	0.002	0.001	0.009	0.099	0.005	32.9	28.7	nd	302.	3.5	37.	45.	94.	30.
TLM.2-83	5.83	45.38	8.73	0.54	0.006	0.001	0.027	0.20	0.003	35.1	30.2	175.	94.	5.0	34.	43.	27.	40.
CHALCOPYRITE STRINGER ORE TYPE.																		
TLM.1-2	4.29	68.94	5.3	9.9	0.003	0.026	0.038	0.063	0.029	24.6	28.5	11100.	134.	0.5	67.	36.	92.	63.
TLM.2-11	2.57	28.64	18.81	0.29	0.002	0.001	0.009	0.027	nd	36.3	39.6	2.	209.	3.5	38.	83.	34.	37.
TLS.2-65	0.76	27.78	3.6	0.62	0.002	0.003	0.008	0.042	0.15	17.6	6.2	84.	97.	2.5	17.	6.	18.	12.
TLM.1-71	1.51	28.30	21.89	0.19	0.002	0.001	0.006	0.026	0.004	31.4	31.6	2.	219.	4.5	31.	52.	36.	43.
DISSEMINATED PYRITE + CHALCOPYRITE ORE TYPE.																		
TLS.3-36	0.69	4.63	0.59	9.0	0.002	0.019	0.005	0.035	0.009	7.5	9.8	132.	37.	0.5	14.	nd	30.	11.
TLS.1-67	1.27	8.06	2.04	0.64	0.003	0.002	0.020	0.100	0.015	25.5	21.6	332.	17.	0.8	24.	20.	43.	14.
SHEARED CHALCOPYRITE + SPHALERITE ORE TYPE.																		
TLM.2-12	0.38	11.49	0.71	44.7	0.002	0.126	0.010	0.135	0.010	10.3	27.6	270.	28.	nd	22.	40.	116.	32.
TLM.2-62	6.35	84.89	6.66	25.6	0.001	0.057	0.025	0.069	0.004	19.6	28.2	138.	19.	1.2	37.	50.	78.	82.
TLM.2-63	8.23	132.4	11.02	19.2	0.002	0.042	0.017	0.088	0.010	22.3	27.7	410.	72.	2.5	33.	54.	73.	56.
TLM.2-96	12.52	30.36	3.2	3.3	0.002	0.006	0.003	0.26	0.024	15.7	7.8	30.	18.	0.8	14.	9.	19.	14.
VEIN QUARTZ + CHALCOPYRITE ORE TYPE.																		
TLM.1-3	6.17	13.21	3.2	0.43	0.003	0.001	0.001	0.014	0.005	5.6	3.9	19.	16.	1.5	7.	nd	2.	nd

TABLE 8

MINERAL QUANTITIES (BY Wt %) OF THE 27 REPRESENTATIVE ORE SAMPLES.

SAMPLE ID.	PYRITE	CHALCOPYRITE	SPHALERITE	PYRRHOTITE	GALENA	FREIBERGITE	ARSENOPYRITE	GANGUE
MASSIVE SPHALERITE.								
TLS.1-49.	3.55	0.96	82.72	3.28	0.02	0.01	0.02	9.42
TLS.5-64.	3.60	0.05	70.59	1.79	12.45	0.01	0.02	11.50
TLM.2-74.	0.00	13.27	70.65	4.74	0.02	0.00	0.00	11.32
TLM.2-99.	0.00	1.06	61.53	1.10	0.84	0.01	0.00	35.47
BANDED PYRITE + SPHALERITE.								
TLS.2-24.	40.80	4.30	26.43	0.09	0.00	0.00	0.00	28.37
TLS.2-26.	22.80	0.07	64.77	0.01	5.09	0.09	0.30	6.87
TLS.2-54.	66.78	0.12	19.46	0.01	0.02	0.00	0.07	13.54
TLS.3-55.	48.26	0.04	18.92	0.00	0.02	0.00	20.10	12.66
MASSIVE PYRITE.								
TLS.3-25.	86.17	0.05	2.15	0.01	0.00	0.00	0.00	11.63
TLS.1-52.	73.96	0.57	0.02	0.03	0.00	0.00	0.00	25.42
TLS.5-83A.	60.90	0.00	2.19	0.00	3.81	0.10	0.16	32.84
MIXED/BANDED CHALCOPYRITE + SPHALERITE.								
TLM.2-78.	24.34	24.64	27.24	6.94	0.00	0.00	0.03	16.09
TLM.2-91.	8.03	15.06	7.57	0.04	0.00	0.00	0.00	69.31
MASSIVE CHALCOPYRITE + PYRRHOTITE.								
TLS.3-42.	51.76	16.09	0.31	12.06	0.00	0.00	0.00	19.78
TLS.1-50.	0.08	61.37	0.30	27.73	0.00	0.00	0.00	10.48
TLM.2-83(#2).	9.27	28.51	1.42	27.88	0.00	0.00	0.00	32.93
CHALCOPYRITE STRINGERS.								
TLM.1-2.	18.82	33.82	22.65	0.20	0.00	0.00	0.21	24.31
TLM.2-11.	0.12	25.68	0.22	23.84	0.00	0.00	0.00	50.14
TLS.2-65.	1.72	10.92	0.34	1.08	0.15	0.00	0.00	85.79
TLM.1-71.	23.59	55.65	0.16	0.43	0.00	0.00	0.00	20.17
TLM.1-89.	7.86	38.50	0.56	0.96	0.00	0.00	0.00	52.50
DISSEMINATED PYRITE + CHALCOPYRITE.								
TLS.2-36(#2).	28.67	1.60	0.98	0.04	0.02	0.00	0.02	68.66
TLS.1-67.	39.79	1.78	0.19	0.02	0.02	0.00	0.00	58.22
SHEARED CHALCOPYRITE + SPHALERITE.								
TLM.2-12.	0.00	4.92	67.87	9.45	0.00	0.00	0.00	17.76
TLM.2-62.	3.61	14.76	36.15	4.17	0.00	0.00	0.00	41.31
TLM.2-63.	1.32	35.88	35.17	10.83	0.00	0.00	0.00	16.79
TLM.2-96.	11.50	17.79	7.69	19.37	0.00	0.00	0.00	43.62
VEIN QUARTZ + CHALCOPYRITE.								
TLM.1-3.	3.28	68.08	1.05	0.90	0.00	0.00	0.00	26.69

TABLE 9

AVERAGE CHEMICAL COMPOSITIONS OF EACH ORE TYPE.

AVERAGE CHEMICAL COMPOSITION OF EACH ORE TYPE.

ORE TYPE	Au	Ag	Cu	Zn	Ni	Cd	Co	Mn	Pb	Fe	S	As	Se	Te	Hg	Sn	Sb	In
	ppm		Wt %									ppm						
Msv Sp.	1.51	131.	1.72	37.9	0.002	0.075	0.009	0.076	3.11	11.6	25.3	490.	18.	0.4	27.	44.	148.	43.
Banded Py+Sp.	4.01	80.	0.60	19.9	0.002	0.040	0.004	0.073	1.071	25.0	33.8	13940.	27.	0.4	76.	45.	167.	35.
Msv Py.	1.02	44.	0.19	3.34	0.002	0.007	0.013	0.030	0.289	38.1	39.5	1080.	38.	0.2	39.	10.	76.	22.
Mix/Ban Cp+Sp.	4.05	58.	5.43	17.8	0.002	0.038	0.020	0.174	0.007	21.1	25.1	460.	14.	0.8	26.	37.	69.	45.
Msv Cp+Po.	3.36	39.	12.18	0.39	0.003	0.001	0.053	0.121	0.004	37.3	29.0	560.	162.	3.7	44.	43.	60.	32.
Cp Stringers.	2.26	38.	12.4	2.75	0.001	0.007	0.015	0.039	0.046	27.5	24.0	2800.	155.	2.7	38.	38.	69.	39.
Diss Py+Cp.	1.27	8.1	2.04	0.64	0.003	0.002	0.020	0.100	0.015	25.5	21.6	332.	17.	0.5	26.	20.	63.	16.
Sheared Cp+Sp.	6.86	65.	5.24	23.2	0.002	0.058	0.014	0.138	0.012	17.0	22.8	210.	34.	1.1	27.	38.	71.	38.
Vein Qtz+Cp.	6.17	13.2	3.2	0.43	0.003	0.001	0.001	0.014	0.005	5.6	3.9	19.	16.	1.5	7.	nd	2	nd

Note : Composition of Diss. Py + Cpy Ore Type based on TLS.1-67 only, because the chemical composition of TLS.2-26(82) is inconsistent with the mineral quantity analysis and the defined ore type.

TABLE 10

PARTIAL CHEMICAL COMPOSITIONS OF THE ORE SAMPLES, CALCULATED FROM THE MINERALOGICAL COMPOSITIONS.

SAMPLE ID.	S	Fe	Cu	Zn	Pb
MASSIVE SPHALERITE.					
TLS.1-49.	30.90	9.66	0.33	49.63	0.02
TLS.5-64.	27.76	7.64	0.02	42.35	10.70
TLN.2-74.	29.87	11.90	4.51	42.39	0.02
TLN.2-95.	21.14	5.30	0.36	36.92	0.72
MASSIVE BANDED PYRITE + SPHALERITE.					
TLS.2-24.	37.12	25.20	1.46	15.86	0.00
TLS.2-26.	34.65	14.82	0.02	38.86	4.38
TLS.2-54.	43.19	31.46	0.04	11.66	0.02
TLS.2-55.	37.22	30.09	0.01	11.35	0.02
MASSIVE PYRITE.					
TLS.2-25.	48.13	38.96	0.02	1.29	0.00
TLS.1-52.	40.89	33.47	0.19	0.01	0.00
TLS.5-83A.	34.78	27.61	0.00	1.31	3.28
MIXED/BANDED CHALCOPYRITE + SPHALERITE.					
TLN.2-78.	33.78	24.60	8.38	16.34	0.00
TLN.2-91.	11.01	10.03	5.12	4.54	0.00
MASSIVE CHALCOPYRITE + PYRRHOTITE.					
TLS.3-42.	39.01	35.53	5.47	0.19	0.00
TLS.1-50.	32.71	35.73	20.87	0.19	0.00
TLN.2-83(#2).	26.70	29.84	9.69	0.85	0.00
CHALCOPYRITE STRINGER.					
TLN.1-2.	29.75	20.66	11.50	13.59	0.00
TLN.2-11.	18.67	21.76	8.11	0.13	0.00
TLS.2-65.	5.33	4.83	3.71	0.20	0.13
TLN.1-71.	32.68	28.14	18.92	0.10	0.00
TLN.1-89.	18.37	16.10	13.09	0.34	0.00
DISSEMINATED PYRITE + CHALCOPYRITE.					
TLS.3-36(#2).	16.67	13.49	0.54	0.59	0.03
TLS.1-67.	22.58	18.48	0.61	0.11	0.02
SHEARED CHALCOPYRITE + SPHALERITE.					
TLN.2-12.	27.90	11.95	1.67	40.72	0.00
TLN.2-62.	20.65	11.15	5.02	21.69	0.00
TLN.2-63.	29.23	20.67	12.20	21.10	0.00
TLN.2-96.	22.85	22.86	6.05	4.61	0.00
VEIN QUARTZ + CHALCOPYRITE.					
TLN.1-3.	26.34	23.20	23.15	0.63	0.00

compositions determined by chemical assay and image analysis. It is assumed that the best or most representative mineral content is one derived from a combination of the chemical composition and the image analysis data. The average mineral quantities were therefore recalculated using both the average chemical composition and the mineral quantities as follows. The sphalerite, chalcopyrite, galena, arsenopyrite, electrum and gangue (by difference) were calculated from the average chemical composition using 60 Wt % Zn for sphalerite, 34 Wt % Cu for chalcopyrite, 86.7 Wt % Pb for galena, 43 Wt % As for arsenopyrite and 41 Wt % Au for electrum. The average gangue content was determined from the chemical composition (by difference), and the pyrite + marcasite + magnetite content was adjusted to normalise the total to 100 %. A close correlation was obtained between the analysed pyrite and gangue contents reported in Table 11, and the calculated values from chemical analyses. This suggests that the calculated values for the pyrite and gangue are realistic. The results are therefore given as 'interpreted mineralogical compositions' of each ore type in the Trout Lake deposit (See Table 12). The Table contains check marks (i.e., 'X') to indicate all trace minerals that were observed during petrological and other studies. This table is therefore considered to provide the best and most complete mineralogical compositions of the ore types.

Ternary diagrams for Sphalerite - Chalcopyrite - Pyrrhotite + Pyrite (the latter includes marcasite and magnetite) and Zn - Cu - Fe were constructed from the data in Tables 12 and 9. These diagrams portray the mineralogical and chemical compositions and inter-relationships of each ore type, respectively (Figs 5 and 6). Comparing the two diagrams, it is apparent that the Sphalerite - Chalcopyrite - Pyrrhotite + Pyrite diagram which is based on mineralogy, provides superior discrimination between the ore types, than the Zn - Cu - Fe diagram. This is primarily due to the multiphase host mineralogy of Fe, occurring in a large number of minerals including chalcopyrite and sphalerite, and thereby lacking selectivity.

TABLE 11

AVERAGE MINERAL QUANTITIES FOR EACH ORE TYPE.

ORE TYPE.	PY.	CPY.	SPHAL.	PO.	GAL.	FREIB.	ASPY.	GANG.
MASSIVE SPHALERITE.	1.86	3.84	71.63	2.75	3.53	0.01	0.00	16.39
BANDED PYRITE + SPHALERITE.	46.68	1.13	32.39	0.02	1.28	0.02	5.12	13.36
MASSIVE PYRITE.	73.67	0.21	1.45	0.01	1.27	0.03	0.08	23.30
MIXED/BANDED CHALCOPYRITE + SPHALERITE.	13.62	20.93	18.83	7.71	0.00	0.00	0.02	38.89
MASSIVE CHALCOPYRITE + PYRRHOTITE.	21.21	34.33	0.66	21.31	0.00	0.00	0.00	22.46
CHALCOPYRITE STRINGERS.	11.25	34.22	5.19	5.01	0.00	0.00	0.00	44.33
DISSEMINATED PYRITE + CHALCOPYRITE.	34.37	1.73	0.58	0.03	0.02	0.00	0.02	63.25
SHEARED CHALCOPYRITE + SPHALERITE.	3.94	18.49	37.20	10.97	0.00	0.00	0.00	29.39
VEIN QUARTZ + CHALCOPYRITE.	3.28	68.08	1.05	0.90	0.00	0.00	0.00	26.69

TABLE 12

INTERPRETED MINERALOGICAL COMPOSITIONS OF THE ORE TYPES.

MINERAL.	Massive Sphal.	Banded Py+Sphal.	Massive Py.	Massive/ Banded Cpy+Sphal.	Massive Cpy+Po.	Cpy Stringers.	Disseminated Py+Cpy.	Sheared Cpy+Sphal.	Vein Qtz+Cpy.
Gangue	20.16	18.11	18.42	30.30	20.92	32.96	61.94	31.52	86.64
Pyrite	5.10	42.46	74.88	16.30	21.31	20.35	30.46	3.33	2.14
Pyrrhotite	2.70	0.02	0.01	7.70	21.30	5.00	0.03	11.00	0.90
Sphalerite	63.20	33.17	5.57	29.60	0.70	4.60	0.50	38.70	0.72
Chalcopyrite	5.10	1.77	0.56	16.00	35.70	36.50	3.90	15.40	9.60
Galena	3.60	1.28	0.34	0.01	0.00	0.03	0.01	0.01	0.00
Arsenopyrite	0.09	3.24	0.28	0.00	0.07	0.56	0.05	0.04	0.00
Electrum	0.00036	0.00090	0.00131	0.00097	0.00080	0.00056	0.00024	0.00165	0.0160
Cubanite				x	x	x	x		x
Freibergite	x	x	x						
Gudmundite	x	x						x	
Pyrargyrite	x	x							
Dyscrasite	x								
Boulangerite		x							
Freieslebenite		x							
Costibite								x	
Clausthalite	x			x		x			
Hessite						x		x	
Rucklidgeite						x			
Pilsenite						x			

NOTE 1 : Pyrite data includes contributions from the minor marcasite and magnetite in the ore.

NOTE 2 : Bournonite, Volynskite, Naumannite and Acanthite were observed in the mill products only, and are thus omitted.

NOTE 3 : Distribution and abundance of Monesite and Parisite not recorded, though they are relatively more abundant in the Cu-rich footwall area.

FIGURE 5

SPHALERITE - CHALCOPYRITE - PYRRHOTITE + PYRITE TERNARY DIAGRAM.

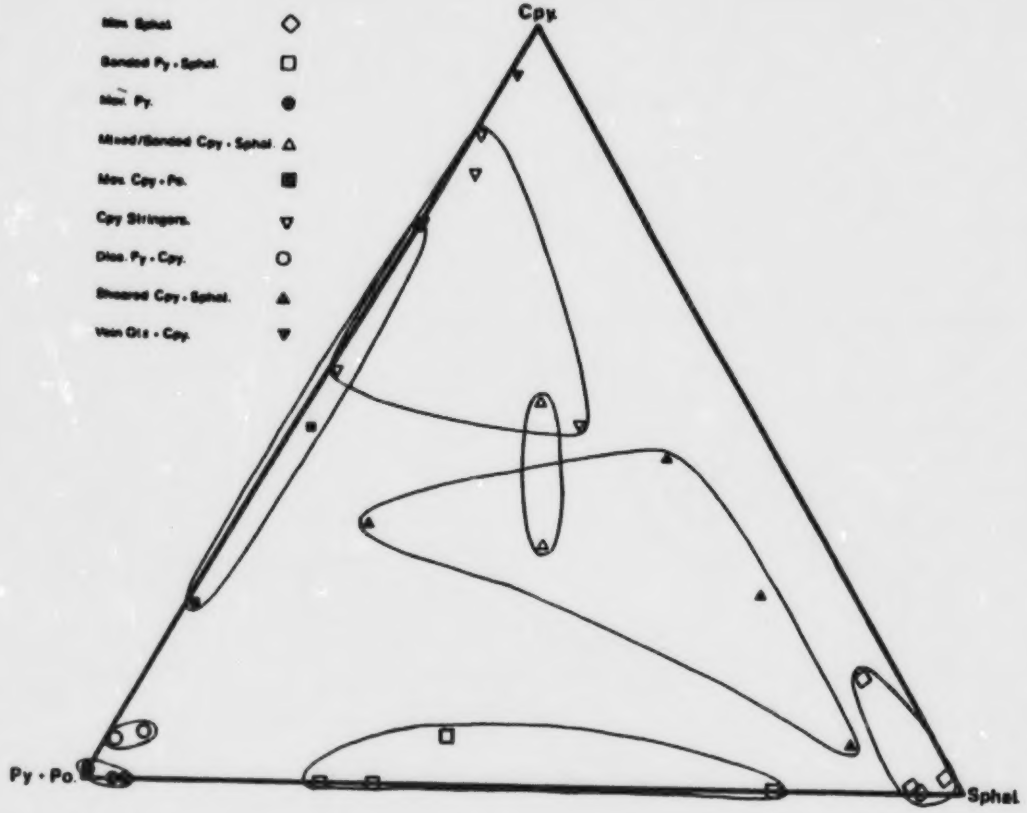

FIGURE 6

Zn - Cu - Fe TERNARY DIAGRAM.

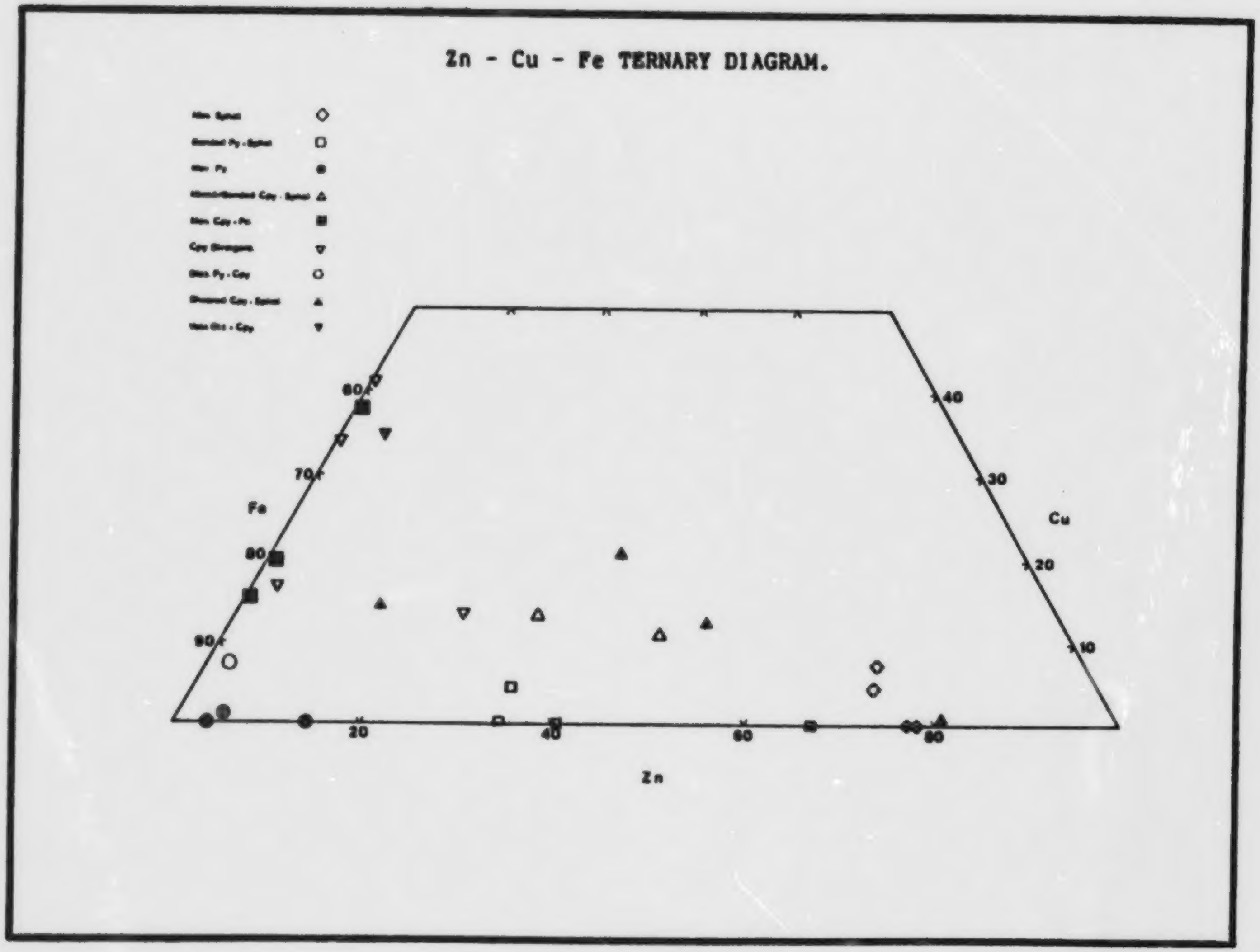

DETAILED CHARACTERISTICS

THE MASSIVE SPHALERITE ORE TYPE

The massive sphalerite ore type occurs in the immediate hangingwall of the ore lenses. Ten samples corresponding to this ore type were collected from the ore lenses 1N, 2N, 1S, 3S and 5S. The average chemical analysis of 4 representative samples of this ore type is 37.9 Wt % Zn, 1.72 Wt % Cu, 3.11 Wt % Pb, 131 ppm Ag and 1.5 ppm Au (See Table 9). The average mineralogical analysis for the same samples is 63.2 Wt % sphalerite, 5.2 Wt % pyrite (includes trace magnetite and marcasite), 5.1 Wt % chalcopyrite, 3.6 Wt % galena and trace amounts of freibergite, pyrargyrite and electrum (See Table 12). It is interpreted that the gold occurs only in electrum, and the silver in freibergite, pyrargyrite, sphalerite and galena. This ore type plots near the sphalerite apex of the Sphalerite - Chalcopyrite - Pyrrhotite + Pyrite ternary diagram and the Zn apex of the Zn - Cu - Fe ternary diagram.

The ore consists of semi-massive to massive sphalerite. The massive sphalerite envelopes the gangue, pyrite and other minor to trace minerals (Plate 1a). Size analysis data shows that 55 % of the mineral occurs in grains that are larger than 208 um (Fig 7). The gangue is foliated and consists of lenses, rafts and pods of carbonate (calcite), quartz, chlorite, sericite and biotite. The foliation is commonly defined by schistose flakes of chlorite, sericite and/or biotite disseminated throughout the ore.

The pyrite occurs as small disseminated grains and porphyroblasts (discrete or separate, euhedral, medium- to coarse-grained pyrite grains) in sphalerite (Plate 1a). The disseminations are concentrated in zones which form diffuse thin laminae. It is inferred that the thin laminae follow the primary banding of the ore. The porphyroblasts have been corroded and rounded by the surrounding sphalerite and this leads to the development of 'Atoll texture' (Plate 1b), where the pyrite is replaced by sphalerite, and more rarely galena and pyrrhotite. The pyrite is occassionally fractured and invaded by sphalerite, and some is replaced by fine-grained marcasite.

The chalcopyrite occurs as blebs and rods along crystallographically oriented planes in sphalerite, and as interstitial fillings between sphalerite grains (Plate 1c). The blebs and rods will be referred to in this report as "chalcopyrite-disease". Commonly a gradation is discernible from the "chalcopyrite-disease" to abundant interstitial blebs and films which coalesce to form masses of chalcopyrite (See Plate 1d). The cumulative size distribution curve for chalcopyrite shows a change in slope at 13um. It is interpreted from this size distribution data that most of the chalcopyrite smaller than 13um occurs as "chalcopyrite-disease", whereas the remainder is interstitial fillings between sphalerite grains. It follows from this interpretation that about 40 % of the chalcopyrite in the Massive Sphalerite ore type occurs as "chalcopyrite-disease". Some of the interstitial chalcopyrite occurs as elongate masses which parallel the preferred orientation of the "chalcopyrite-disease" within the foliated and twinned sphalerite. Both features define a foliation in the sphalerite which is parallel to the schistosity defined in the gangue minerals, and to an inferred primary banding of the ore.

Galena occurs as disseminated blebs (<10um) and grains in sphalerite, and as interstitial fillings between sphalerite grains (Plate 1e). The cumulative size distribution curve for galena shows three slopes. It is interpreted that the slope for galena below 10um represents blebs in sphalerite, the 10 to 37um slope represents grains in sphalerite, and the third slope which parallels the chalcopyrite size distribution curve in that region, represents galena in the interstices between sphalerite. This analysis suggests that 25 % of the galena occurs as blebs, 50 % as galena grains, and 25 % as interstitial galena. The galena, like chalcopyrite defines a foliation by occurring along sphalerite-sphalerite, sphalerite-pyrite and sphalerite-gangue grain boundaries, which are themselves parallel to the schistosity. Freibergite, gudmundite and pyrargyrite occur as inclusions in galena; the freibergite as fine-grained (<30um) rounded inclusions forming marginally within galena; gudmundite as subhedral bladed inclusions; and the pyrargyrite as anhedral, fine-grained (<20um) inclusions associated with pyrrhotite.

Pyrrhotite occurs as masses and rounded inclusions in chalcopyrite; as parts of composite grains and blebs of chalcopyrite + galena + pyrrhotite; and as oriented blebs and rods in sphalerite, reminiscent of the "chalcopyrite-disease". Chalcopyrite and pyrrhotite exhibit straight to curved contacts with sphalerite, though carious to myrmekitic interpenetrative contacts are occassionally developed due to recrystallisation during and after shearing (Plate 1f for an example of carious to myrmekitic textures).

Arsenopyrite occurs as diffuse laminations of disseminated small euhedral to subhedral fractured grains. It is interpreted that the various laminations in sphalerite represent primary banding inherited from the initial ore-forming process (Plate 1g).

One grain of electrum was observed in sample TLS.1-52. The grain measured 15 x 15um and occurred as a rounded inclusion in an unfractured pyrite porphyroblast.

FIGURE 7.

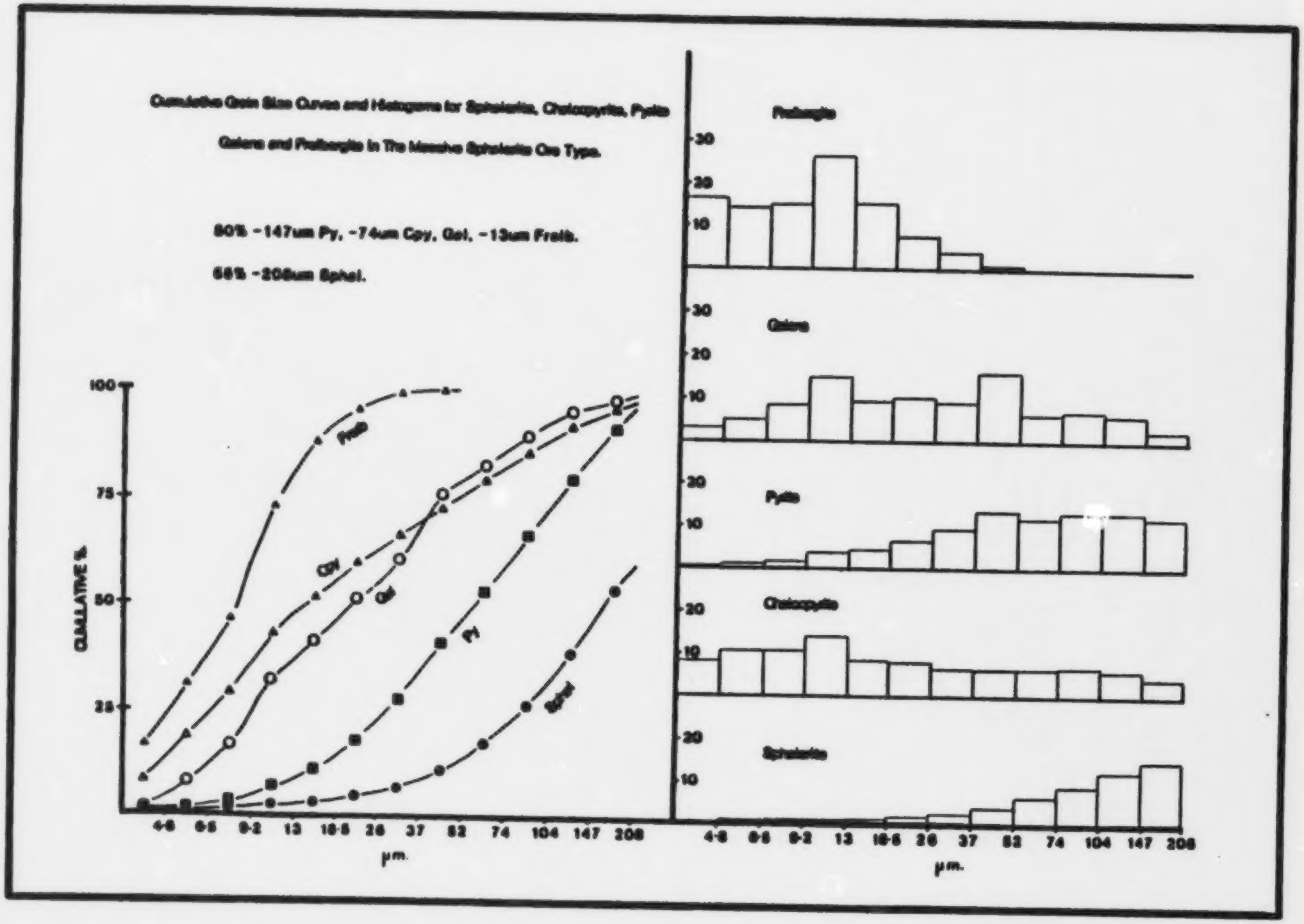

Cumulative Grain Size Curves and Histograms for Sphalerite, Chalcopyrite, Pyrite Galena and Freibergite In The Massive Sphalerite Ore Type.

80% -147um Py, -74um Cpy, Gal, -13um Freib.

68% -208um Sphal.

PLATE 1.

PLATE 1.

PHOTOGRAPH A.

SAMPLE TLS.5-111 : A Massive Sphalerite (Sp) ore with disseminated pyrite (Py) grains and foliaceous gangue grains. Plane polarised light. Bar scale = 325 µm.

PHOTOGRAPH B.

SAMPLE TLS.2-55 : Pyrite (Py) euhedra that have well developed atoll texture, disseminated in a matrix of sphalerite (Sp). Note the arsenopyrite (Asp) porphyroclasts with fractures, pits and reticulate replacements of sphalerite. Plane polarised light. Bar scale = 160 µm.

PHOTOGRAPH C.

SAMPLE TLN.2-114 : Sphalerite (Sp) with interstitial chalcopyrite (Cp) and exquisitely formed chalcopyrite disease. Chalcopyrite blebs are alligned along the straight to slightly curved twin lamellae in the sphalerite. Plane polarised light, with the Illuminator Field Diaphragm virtually closed. Bar scale = 325 µm.

PHOTOGRAPH D.

SAMPLE TLN.2-74 : Interstitial blebs, films and wedges of chalcopyrite (Cp) and lesser pyrrhotite (Po) coalescing between and partially enveloping sphalerite (Sp) grains. Note the well developed chalcopyrite-disease, and the smooth, straight to curved sphalerite-chalcopyrite contacts. Plane polarised light. Bar scale = 160 µm.

PHOTOGRAPH E.

SAMPLE TLS.5-64 : A massive sphalerite (Sp) ore with an interstitial mass of galena (gal) which contains inclusions of gudmundite (Gud) and freibergite (Fr). Note the fine-grained rounded inclusions of freibergite form on the margin of the galena. Plane polarised light. Bar scale = 160 µm.

PHOTOGRAPH F.

SAMPLE TLN.2-12 : Carious blebs of chalcopyrite (Cp) in massive sphalerite (Sp). Note the WNW trending foliation in these blebs, interpreted as a shear plane. Plane polarised light. Bar scale = 160 µm.

PHOTOGRAPH G.

SAMPLE TLS.2-26 : A diffuse lamination consisting of clusters of fine-grained, euhedral, rhombic arsenopyrite (Asp) grains in a sphalerite (Sp) matrix. Note the disseminated anhedral galena (Gal), and the corroded pyrite (Py) grains. Plane polarised light. Bar scale = 160 µm.

PHOTOGRAPH H.

SAMPLE TLS.2-69 : A Massive Pyrite (Py) ore with interstitial sphalerite (Sp), chalcopyrite (Cp) and gangue (black). Plane polarised light. Bar scale = 325 µm.

PLATE 1.

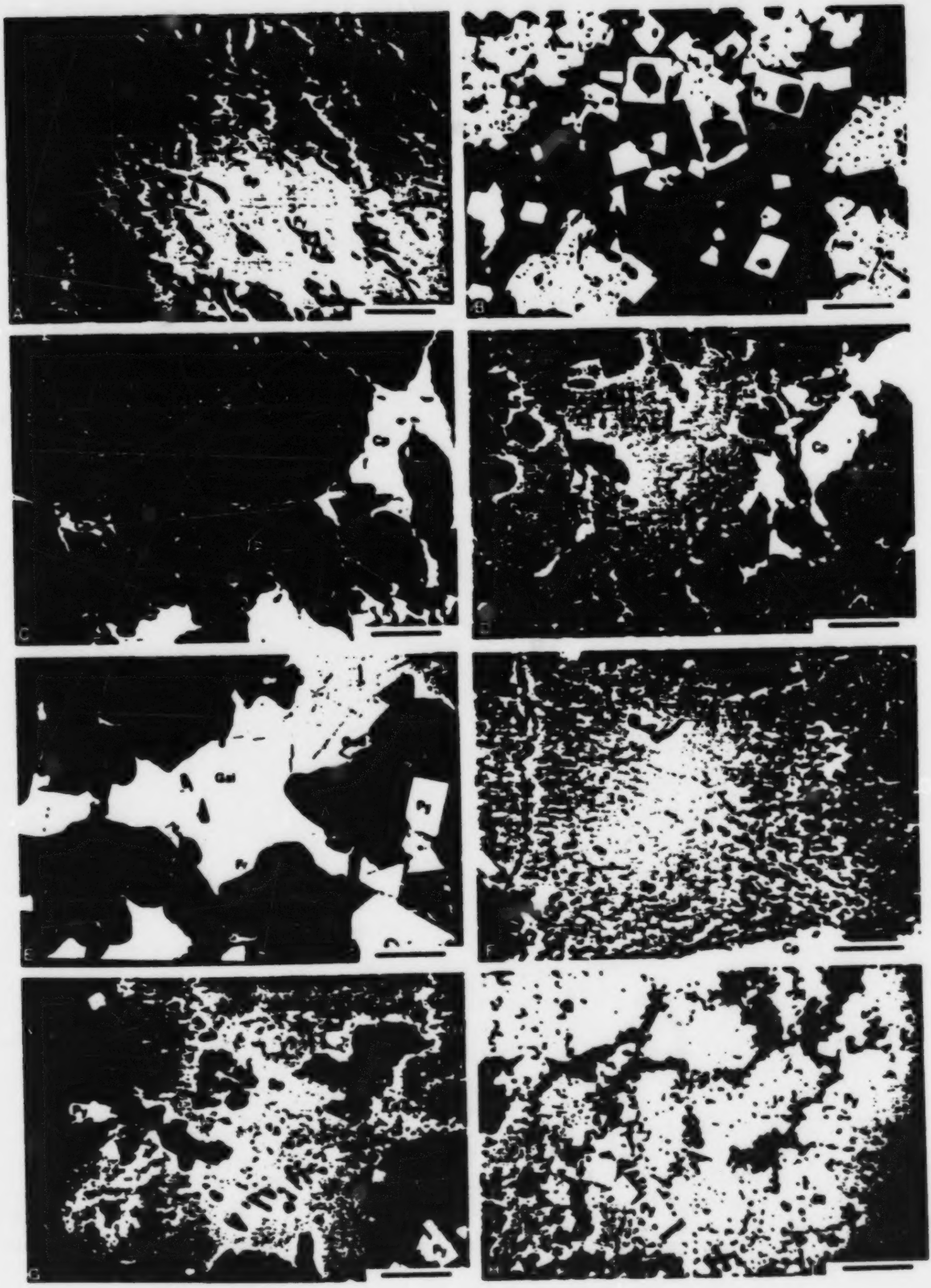
A
B
C
D
Gal
E
F
G
H

THE MASSIVE PYRITE ORE TYPE

The massive pyrite ore type generally occurs in the hangingwall to central parts of the ore lenses. Eleven samples corresponding to this ore type were collected for study from lenses 1N, 1S, 2S, 3S and 5S (Figs 3 and 4). This ore type has an average grade of 3.34 Wt % Zn, 0.19 Wt % Cu, 0.29 Wt % Pb, 44 ppm Ag and 1.24 ppm Au (See Table 9). It contains 74.9 Wt % pyrite (includes trace magentite + marcasite), 5.6 Wt % sphalerite and 0.6 Wt % chalcopyrite, 0.34 Wt % galena, 0.25 Wt % arsenopyrite, 0.01 Wt % pyrrhotite and trace amounts of freibergite and electrum. The gold is interpreted to occur in electrum and much of the silver is in freibergite. This ore type plots near the pyrite + pyrrhotite apex on the Sphalerite - Chalcopyrite - Pyrrhotite Pyrite ternary diagram, and the Fe apex of the Zn - Cu - Fe ternary diagram.

Petrographic studies show that the ore consists of semi-massive to massive pyrite with interstitial sphalerite, chalcopyrite, and lesser galena, freibergite and pyrrhotite (Plate 1h). The pyrite occurs as polygonal masses that are composed of individual pyrite grains, and as porphyroblasts that are up to 500 um in diameter. Commonly the pyrite has been granulated and fractured and the cleavages and fractures are infilled with interstitial minerals, particularly chalcopyrite. Furthermore, minor amounts of marcasite occur along grain boundaries of the fractured pyrite. In addition, the pyrite is occassionally smeared out to produce schistose pyrite and/or web-like to dendritic fringes on pyrite, or remobilised into veinlets. These textures suggest locally intense deformation. Image analysis studies show that most of the pyrite grains range from 10 to 208 um in diameter; 98 Wt % are smaller than 208 um; the mean size is about 45 um; and the median size is between 52 and 74 um in diameter (See Fig 7). The size analysis was performed in such a manner that the size is the uninterrupted length on the pyrite surface between grain boundaries, fractures and inclusions. This size analysis is therefore, the size of the solid portions of pyrite. Large pyrite porphyroblasts would likely be measured as smaller grains because of fractures and inclusions in the porphyroblasts.

The sphalerite, chalcopyrite and lesser galena, pyrrhotite and freibergite occur as (1) interstitial fillings in massive pyrite (Plate 2a), (2) as replacements of pyrite along fractures and cleavages (Plate 2b), (3) as replacements of individual grains in the massive pyrite, and (4) as rounded inclusions in pyrite (Plate 2c). The replacement of pyrite grains by sphalerite produces an intricate network of sphalerite in pyrite (Plate 2d). This network will be referred to in this report as 'dendritic-like replacements'. It is interpreted that the rounded inclusions in pyrite, shown in Plate 2c, represent grains that were entrapped during recrystallisation of pyrite. Size analysis of the chalcopyrite and sphalerite, determined with the image analyser provide the general size distributions for interstitial minerals in this ore. The median size for both minerals is between 9.2 and 13 um. The chalcopyrite, however, has a larger -4.6 um fraction, which probably reflects the veinlets in pyrite, whereas the sphalerite has more +18.5 um grains, because it contains proportionally less of these veinlets and a greater predominance of interstitial fillings. Magnetite occurs as subhedral to anhedral equant grains that are commonly fractured, embayed and invaded dominantly by chalcopyrite and sphalerite.

Electrum was observed in 3 of the 10 samples studied with the petrographic microscope. It is associated with sphalerite and chalcopyrite, and occurs as fracture-fillings in, inclusions in, and in the interstitial spaces between, pyrite grains.

Abundant interstitial masses of tetrahedrite + galena + sphalerite arsenopyrite + chalcopyrite were observed in Sample TLS.2-40(#2) (Plate 2e), which is transitional between the Massive Pyrite and the Banded Pyrite + Sphalerite ore types.

FIGURE 8.

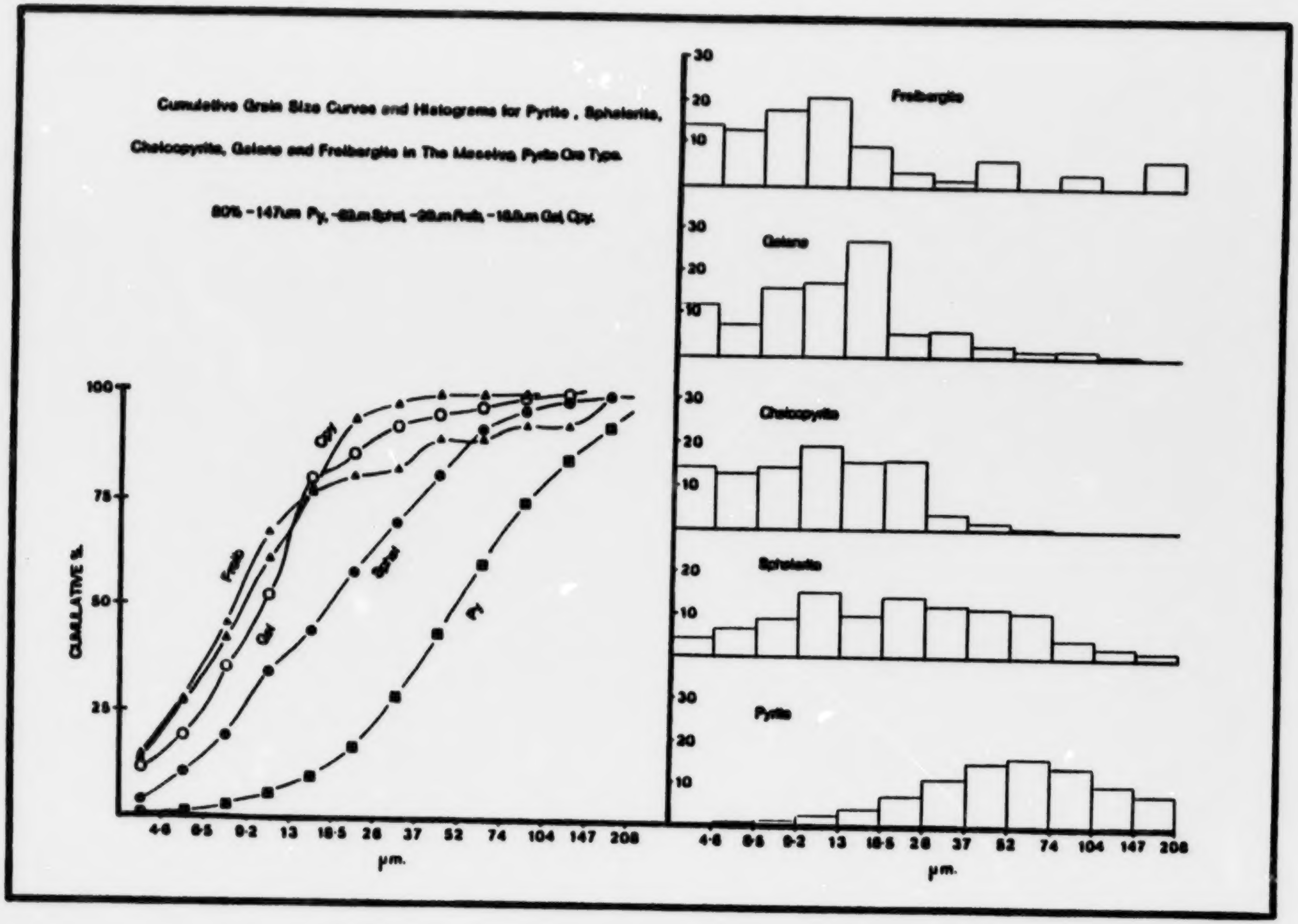

Cumulative Grain Size Curves and Histograms for Pyrite, Sphalerite, Chalcopyrite, Galena and Freibergite in The Massive Pyrite Ore Type.

80% -147um Py, -52um Sphal, -26um Freib, -18.5um Gal, Cpy.

THE MASSIVE BANDED PYRITE ± SPHALERITE ORE TYPE

The Massive Pyrite + Sphalerite ore type occupies the intermediate range between the Massive Pyrite and the Massive Sphalerite ore type in terms of composition, texture and stratigraphic location. It occurs in the hangingwall to central parts of the lenses. This ore type contains an average composition of 19.9 Wt % Zn, 0.6 Wt % Cu, 1.07 Wt % Pb, 80 ppm Ag and 4.0 ppm Au (See Table 7). It is composed of approximately 51 Wt % pyrite (includes trace magnetite and marcasite), 27 Wt % sphalerite, 1.4 Wt % chalcopyrite, 1 Wt % galena, minor to trace freibergite, and trace amounts of gudmundite, pyrargyrite, electrum, dyscrasite, freieslebenite and boulangerite (See Table 12). This ore type plots as a thin band on or adjacent to the sphalerite - pyrrhotite + pyrite join of the Sphalerite - Chalcopyrite - Pyrrhotite + Pyrite ternary diagram, and similarly on the Zn - Fe join of the Zn - Cu - Fe ternary diagram. The ore consists of finely (<1mm) to coarsely (<1cm) banded pyrite and sphalerite laminae (Plate 2f). Banding may also be manifest as laminae of gangue superimposed on the pyrite-sphalerite banding. The gangue, however, is generally distributed diffusely, or as pods and rafts in the ore.

The pyrite laminae consist essentially of pyrite and gangue in a matrix of sphalerite. The pyrite occurs as annealed masses, porphyroblasts, and as diffusely laminated disseminations in sphalerite. The annealed masses display the same features as in the Massive Pyrite ore type (previous section), and contain sphalerite, chalcopyrite, galena and pyrrhotite in the interstices. These laminae commonly contain fractured pyrite that is invaded and/or replaced along fractures and cleavages by sphalerite, chalcopyrite, galena, pyrrhotite and marcasite. Dendritic replacements of pyrite by sphalerite, galena and chalcopyrite are also common. Similarly, individual pyrite grains in sphalerite have features that are common in the Massive Sphalerite ore type. In particular, the pyrite is generally unfractured, while 'Atoll-texture' is commonly developed in pyrite grains, where the pyrite cores have been replaced by sphalerite and associated lesser minerals.

The sphalerite occurs as massive sphalerite in the sphalerite laminae, and as the predominant interstitial mineral in the pyritic laminae. The median grain size of the sphalerite is between 74 and 104 um. The sphalerite contains negligible to abundant "chalcopyrite-disease". The sphalerite laminae contain chalcopyrite, galena and/or pyrrhotite as interstitial fillings between the sphalerite grains. The chalcopyrite and galena grain size distributions yield a median sze of between 9.2 and 13 um for both minerals, and reflects the predominance of "chalcopyrite-disease" and fine-grained blebs and wedges of chalcopyrite and galena.

The galena tends to be preferentially concentrated in the pyritic laminae forming interstitial masses that envelope, invade, cement and/or corrode the pyrite grains (Plate 2g). Less commonly the galena occurs associated with freibergite in foliated scaley masses of marcasite that are interpreted to have formed in shear zones (Plate 2h). Freibergite, gudmundite, pyrargyrite, freieslebenite, boulangerite and dyscrasite occur exclusively associated with galena, either as fine-grained inclusions (Plate 3a), or in the case of freibergite only, as discrete grains adjacent to or intimately associated with the galena (Plate 3b). The grain size distributions for freibergite indicates a strong break of slope at approximately 30 um, with a median size of between

37 and 52 um. The -40 um material probably corresponds to the fine-grained inclusions in galena, whereas the +30 um material corresponds to the coarser-grained inclusions in galena, and the discrete interstitial grains. Thus, approximately 50 % of the freibergite occurs as fine-grained rounded inclusions in galena.

Both arsenopyrite and magnetite occur as porphyroblasts, and exhibit a mineral banding that is superimposed on the pyrite - sphalerite banding. The arsenopyrite occurs as unfractured, fine-grained disseminations defining thin laminations within the sphalerite laminae, and as diffuse laminae of commonly fractured grains within the massive pyritic laminae (Plate 3c). The magnetite commonly occurs as fractured and corroded equant grains that are enveloped and invaded by sphalerite and chalcopyrite (Plate 3d), and which also contains rounded inclusions of pyrite, chalcopyrite and sphalerite.

Electrum was observed in 7 of the 24 samples of this ore type, and occurs as inclusions in pyrite, along grain boundaries and in fractures in pyrite. It also occurs as inclusions in interstitial freibergite and galena in pyrite.

FIGURE 9.

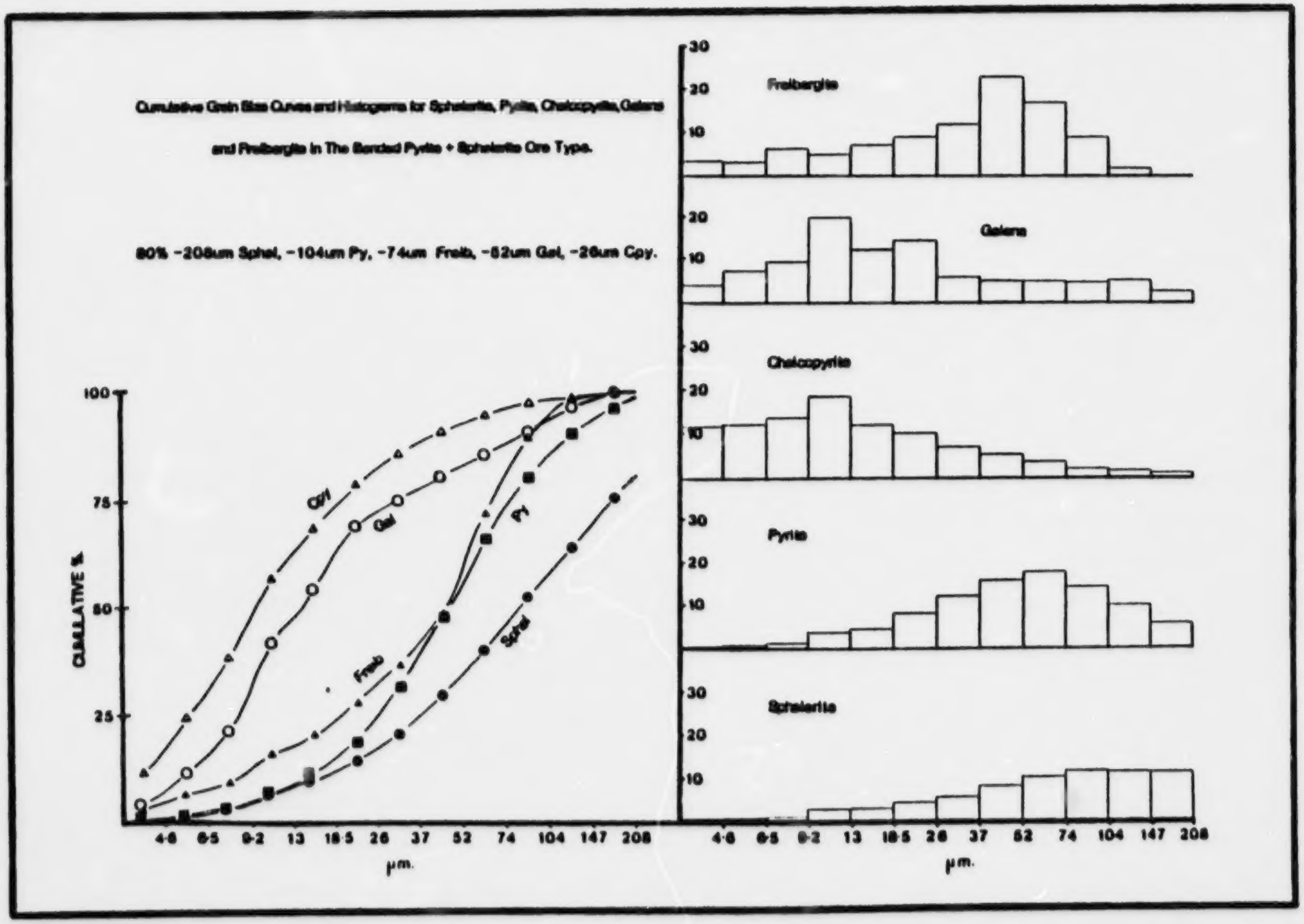

Cumulative Grain Size Curves and Histograms for Sphalerite, Pyrite, Chalcopyrite,Galena and Freibergite In The Banded Pyrite + Sphalerite Ore Type.

80% -208um Sphal, -104um Py, -74um Freib, -52um Gal, -26um Cpy.

PLATE 2.

PLATE 2.

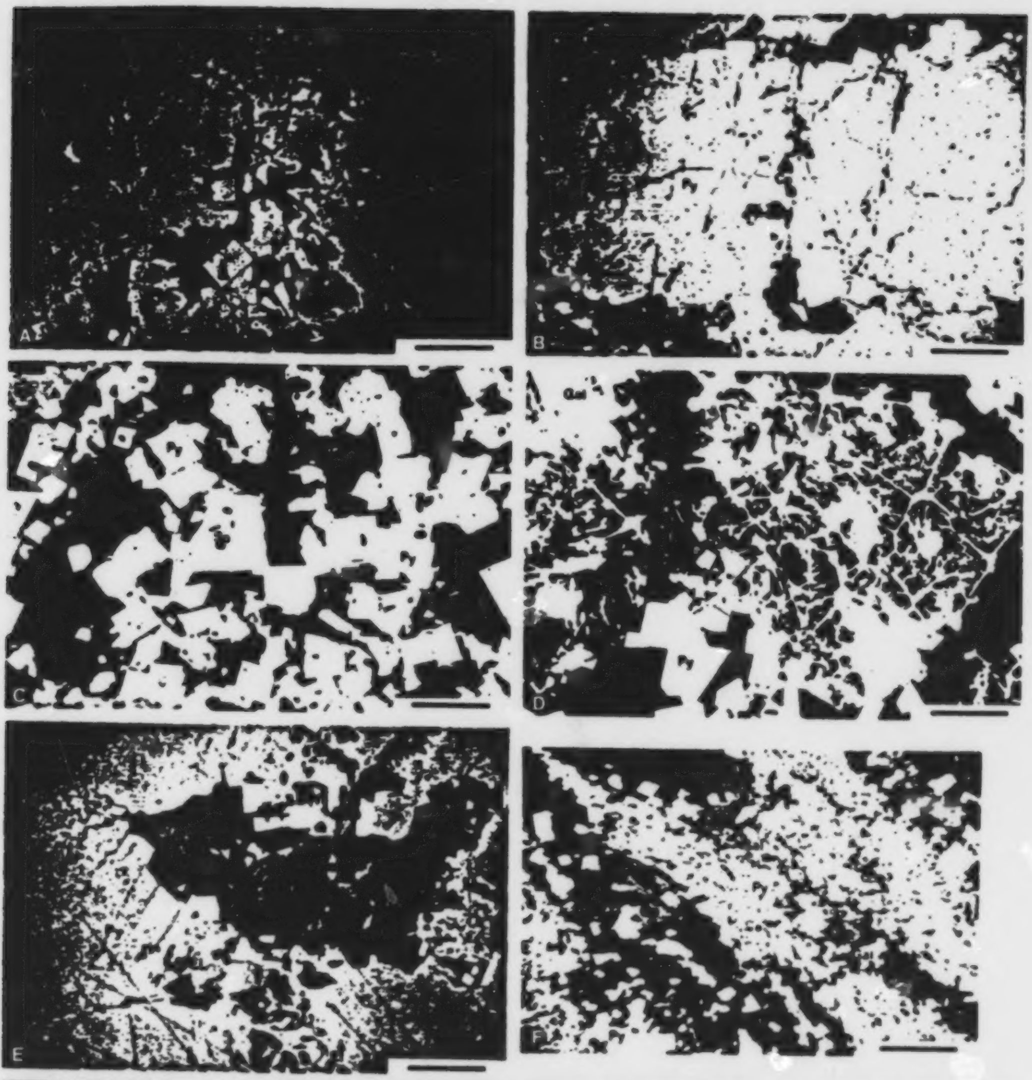

THE MIXED/BANDED CHALCOPYRITE + SPHALERITE ORE TYPE

The Mixed/Banded Chalcopyrite + Sphalerite ore type was found to occur across virtually the entire width of the massive exhalative ore (i.e., excluding the stockwork ore) in lens 2N, and all 5 samples of this ore type were collected from lens 2N. The apparently exclusive occurrence of this ore type in lens 2N is significant because this lens exhibits (1) pronounced disturbance of the generalised Cu / Cu + Zn distribution, (2) loss of the stratigraphic control on the ore type location within the lens, and (3) extensive intrusion by the quartz diorite dyke. The average chemical composition of 2 representative samples is 17.8 Wt % Zn, 5.43 Wt % Cu, 0.01 Wt % Pb, 58 ppm Ag and 4.05 ppm Au. The average mineralogical composition for the same samples is 29.6 Wt % sphalerite, 16.0 Wt % chalcopyrite, 0.01 Wt % galena (includes clausthalite), 16.3 Wt % pyrite (includes minor magnetite), 7.7 Wt % pyrrhotite, and trace amounts of arsenopyrite and electrum. The sphalerite is interpreted to be the main host of the Ag in this ore type, whereas Au is hosted in electrum. This ore type plots in the centre of the Sphalerite - Chalcopyrite - Pyrrhotite + Pyrite ternary diagram, and centrally towards the Fe - Zn join of the Zn - Cu - Fe ternary diagram.

The ore consists of massive to semi-massive sulphides with pods, bands or rafts of gangue, or with diffusely distributed gangue. The sphalerite, chalcopyrite and pyrrhotite envelope and occur interstitially to the gangue and pyrite, and can be considered as forming the matrix (Plate 3e).

The pyrite varies from fine-grained to less commonly coarse-grained, granulated, fractured and rounded grains. The grains are invariably enveloped invaded and replaced by the matrix sulphides, commonly as a texture that can be described as 'rounded islands of pyrite in a sea of chalcopyrite, sphalerite and pyrrhotite' (Plate 3f). Chalcopyrite and sphalerite also occur as dendritic-replacements in pyrite, whereas magnetite forms reticulate-textured fringes and zones in the pyrite (Plate 3g, and MAGNETITE). The grain size distribution of pyrite, is 80 % -26 um, and the median size is between 13.0 and 18.5 um; this is the finest grained pyrite of all the ore types. The break of slope at 26 um is interpreted to reflect the granulated, fractured and corroded pyrite comprising the -26 um material, and which forms 75 % of the pyrite. The remaining 25 % corresponds to relatively undeformed +26 um pyrite.

The sulphide matrix consists essentially of sphalerite and chalcopyrite with lesser pyrrhotite, where the latter generally forms granular masses and disseminated grains in the chalcopyrite. The chalcopyrite also occurs as well developed "chalcopyrite-disease" in sphalerite. The contacts of these three matrix minerals are generally straight to curved, though mutually carious to myrmekitic contacts are developed along localised zones, which are interpreted to be shear planes (Plate 1f for example of carious to myrmekitic contacts. The sphalerite and chalcopyrite grain size distributions yield a median size of between 104 and 147 um and 52 and 74 um, respectively.

Minor magnetite occurs commonly as disseminated, medium-grained, fractured and corroded grains, or as clusters of grains enveloped in matrix chalcopyrite and/or sphalerite. Arsenopyrite occurs as rare disseminated subhedral grains enveloped in the sphalerite and/or chalcopyrite. Clausthalite (identified on the basis of its higher reflectance relative to galena) was observed as rare interstitial films in fractured pyrite.

Electrum was observed in 3 of the 5 samples, and in all cases occurred spatially associated with pyrite. The electrum occurred along fractures and embayments in pyrite, as partial grain coatings on pyrite, as interstitial films between pyrite grains, and as inclusions in pyrite. The occurrence of electrum as interstitial films between pyrite grains typifies the 99 grains of electrum observed in sample TLN.2-8, which was collected from the ore contact with the quartz-diorite intrusion.

FIGURE 10.

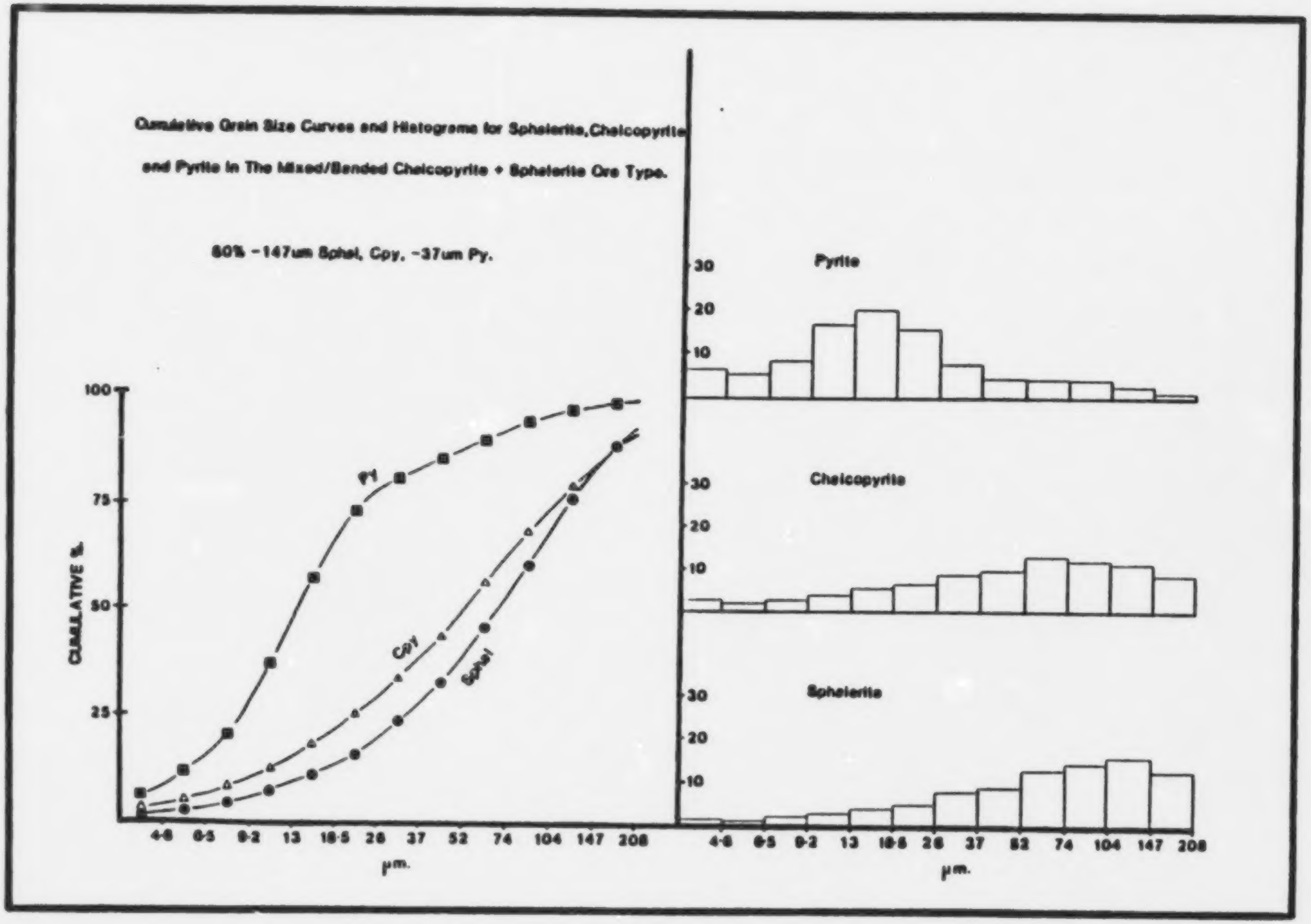

Cumulative Grain Size Curves and Histograms for Sphalerite,Chalcopyrite and Pyrite in The Mixed/Banded Chalcopyrite + Sphalerite Ore Type.

80% -147um Sphal, Cpy, -37um Py.

PLATE 3.

PLATE 3.

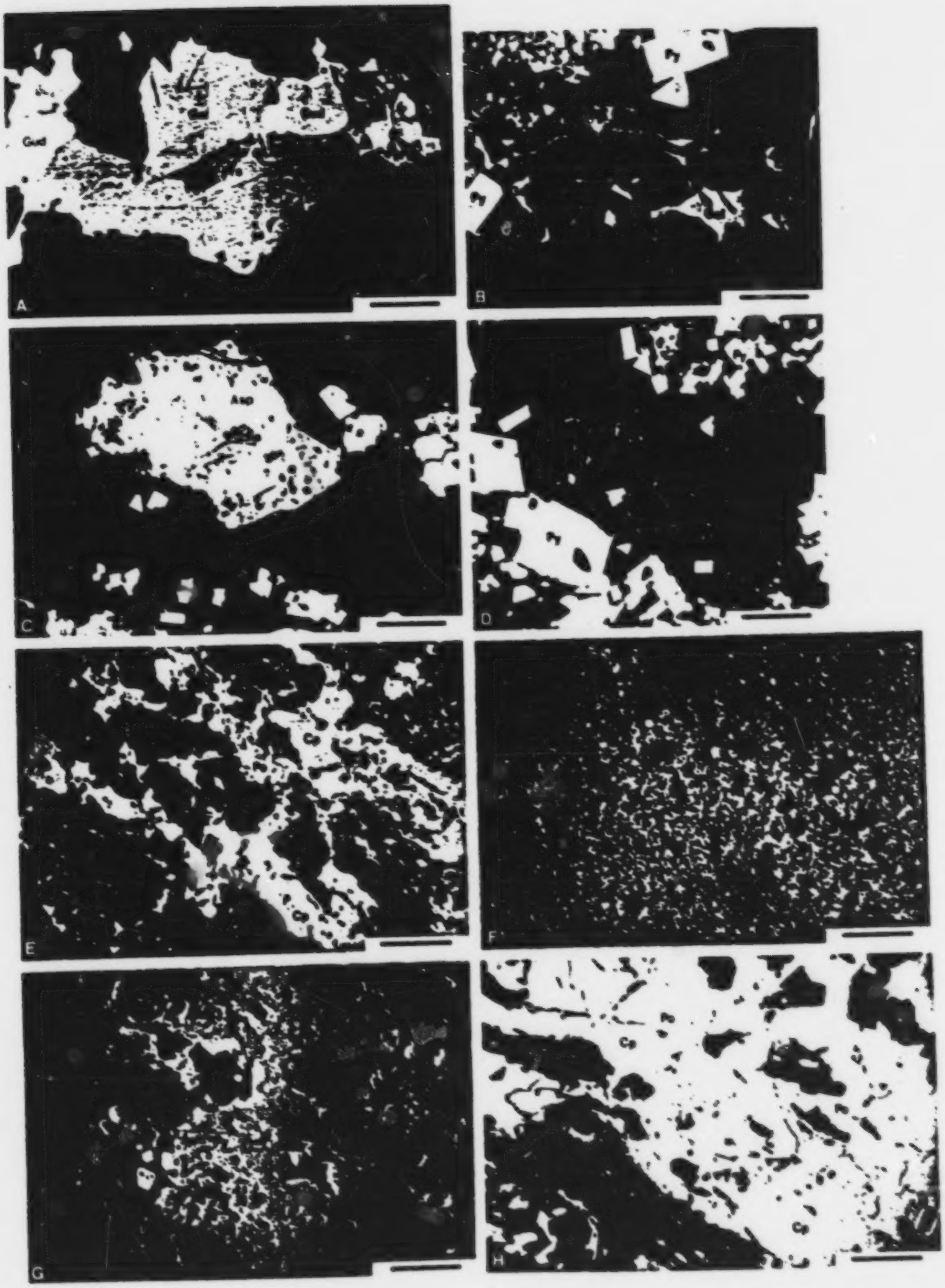
Gud
A
B
Ano
C
D
Co
E
F
G
Co
H

MASSIVE CHALCOPYRITE ± PYRRHOTITE ORE TYPE

The Massive Chalcopyrite - Pyrrhotite ore type occurs at the centre through to the base of the massive ore (exhaled ore), and stratigraphically immediately above the Chalcopyrite Stringer ore type (stockwork ore). Nine samples of this ore type were collected from lenses 2N, 1S and 3S. The average chemical composition of 3 representative samples of this ore type is 0.39 Wt % Zn, 12.15 Wt % Cu, 0.004 Wt % Pb, 39 ppm Ag and 3.36 ppm Au. The average mineralogical composition for these same samples is 0.7 Wt % sphalerite, 35.7 Wt % chalcopyrite, 21.3 Wt % pyrite (includes trace magnetite and marcasite), 21.3 Wt % pyrrhotite, minor to trace magnetite and marcasite, and trace cubanite and electrum. It is interpreted that electrum hosts the Au, whereas the host of the Ag is problematical, as only minor sphalerite and no galena, Sb-sulfosalts or hessite were observed. The electrum can only accomodate 10 % of the Ag in the ore, whereas the Cu - Ag correlation coefficient indicates that chalcopyrite is an improbable host of the Ag (See **METAL-MINERAL BALANCE**). This ore type plots on the centre portion of the chalcopyrite - pyrrhotite + pyrite join of the Sphalerite - Chalcopyrite - Pyrrhotite + Pyrite ternary diagram, and similarly towards the Fe apex on the Fe - Cu join of the Zn - Cu - Fe ternary diagram.

The ore consists of massive to semi-massive sulphides that are mineralogically banded in terms of chalcopyrite - pyrrhotite, and as chalcopyrite - sphalerite, magnetite and/or pyrite (Plate 3h). The sulphide banding is commonly very coarse (<2cm). The gangue varies from unfoliated quartzose pods and laminae to foliated chloritic schist laminae and rafts. The ore is very heterogeneous in terms of the relative abundance of pyrite, magnetite and sphalerite (i.e., pyrite varies from approximately 30 Vol % to <0.05 Vol %).

The pyrite is typically deformed, occurring as anhedral, fractured, granulated and/or rounded coarse-grained porphyroblasts, as rounded, corroded, embayed and fractured medium-grained disseminations, as ruptured annealed masses, as well as fine-grained disseminations, particularly within the rafts of gangue. Chalcopyrite, pyrrhotite and/or sphalerite typically envelope, invade and replace the pyrite, locally leading to rounded islands of fine-grained relict pyrite enveloped in chalcopyrite, pyrrhotite and/or sphalerite (Plate 4a). Rare pyrite grains exhibit radial replacement by chalcopyrite + pyrrhotite, as well as circular cross-sections, suggesting relict primary spheroidal pyrite (Plate 4b). The pyrite commonly exhibits zones and fringes of fine-grained reticulate-textured magnetite, and more rarely clouded patches of submicroscopic flecks of marcasite (Plate 4c). The grain size distribution of pyrite yields a median size of between 52 and 74 um.

The chalcopyrite with subordinate pyrrhotite and minor sphalerite contents, envelope and occur interstitially to the gangue and the pyrite. It can, therefore be considered as forming a sulphide matrix. This matrix is generally coarse-grained and banded, with laminae of granular to foliated masses of pyrrhotite enveloped by chalcopyrite. The sphalerite occurs as disseminated grains, pods and diffuse to discrete laminae of massive sphalerite with intense "chalcopyrite-disease", and with chalcopyrite forming in the interstices between the sphalerite grains. The mutual contacts of chalcopyrite, pyrrhotite and sphalerite are generally straight, though less commonly and/or locally, carious and more rarely myrmekitic with the development of diablastic texture. The chalcopyrite commonly contains slightly bent exsolution lamellae of cubanite. The grain size distribution for chalcopyrite and sphalerite yield median sizes of between 74 and 104 um and 18.5 and 26 um, respectively.

Magnetite occurs as disseminations and as diffuse laminae of corroded, embayed and/or fractured porphyroblasts, as well as pods and laminae of annealed polygonal magnetite grains (Plate 4d). The magnetite commonly contains rounded inclusions of chalcopyrite and pyrite. Magnetite commonly envelopes and invades fractured pyrite. Chalcopyrite and lesser pyrrhotite are commonly observed invading and replacing magnetite.

Electrum was observed in 5 of the 9 samples of this ore type, and occurred within fractures in, or along the grain margins of pyrite, and was associated with interstitial chalcopyrite, sphalerite and/or pyrrhotite.

FIGURE 11.

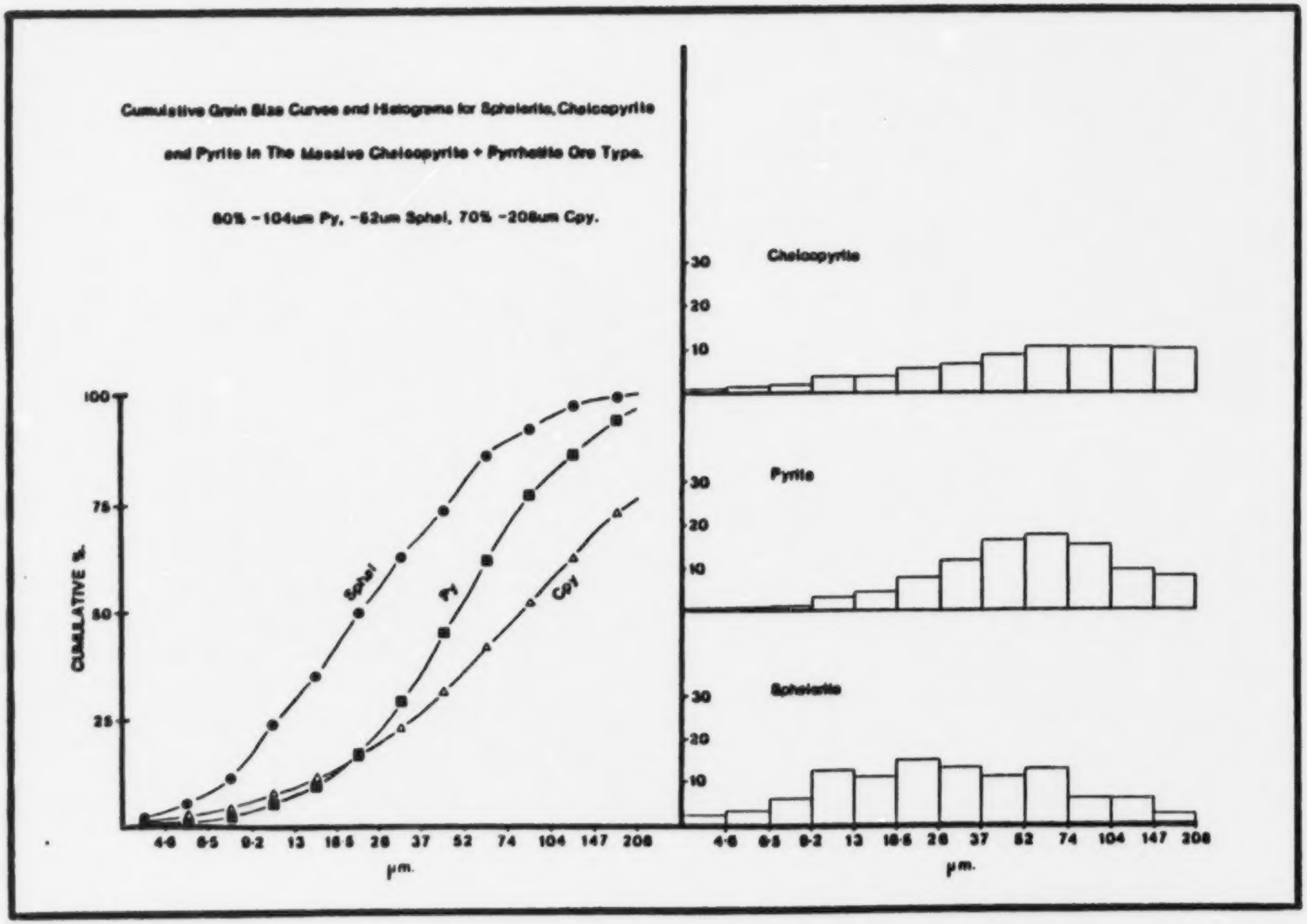

Cumulative Grain Size Curves and Histograms for Sphalerite, Chalcopyrite and Pyrite in The Massive Chalcopyrite + Pyrrhotite Ore Type.

80% −104um Py, −52um Sphal, 70% −208um Cpy.

CHALCOPYRITE STRINGER ORE TYPE

The Chalcopyrite Stringer ore type underlies, with a sharp contact, the massive ore (exhalative ore) and togethar with the Disseminated Pyrite + Chalcopyrite ore type (next section) constitutes the footwall stockwork mineralisation. The Chalcopyrite Stringer ore grades into the Disseminated Pyrite + Chalcopyrite ore type downwards and towards the margins of the lenses. Eighteen samples corresponding to this this ore type were collected from lenses 1N, 2N, 1S, 2S and 3S. The average chemical composition of 4 representative samples is 2.75 Wt % Zn, 12.4 Wt % Cu, 0.05 Wt % Pb, 38 ppm Ag and 2.26 ppm Au. The average mineralogical composition of the same samples is 4.60 Wt % sphalerite, 36.5 Wt % chalcopyrite, 0.05 Wt % galena + clausthalite, 20.35 Wt % pyrite (includes trace marcasite and magnetite), 5.0 Wt % pyrrhotite, major to trace marcasite, and trace amounts of cubanite, electrum, hessite, pilsenite and rucklidgeite. The electrum is interpreted to be the host of the Au, whereas at least part of the Ag is carried in hessite, electrum and galena (including clausthalite). This ore type plots towards the chalcopyrite apex of the Sphalerite - Chalcopyrite - Pyrrhotite + Pyrite ternary diagram, and towards the Fe apex on the Fe - Cu join of the Zn - Cu - Fe ternary diagram.

The ore consists of semi-massive to disseminated sulphides in the gangue. The sulphide matrix is composed of coarse-grained chalcopyrite with lesser pyrrhotite and sphalerite, all of which envelope the pyrite and gangue (See Plate 4e). The gangue is generally highly foliated, consisting of chloritic-schist laminae, which are generally interstratified with laminae of the massive sulphides. These chloritic-schist laminae are commonly folded, sheared and dislocated to form rafts in a 'sea of sulphides'. The stratification is interpreted as being formed by metamorphic segregation under conditions of intense shearing within a highly chloritised 'plastic' zone, rather than representing primary mineral banding. The gangue also occurs as discrete grains distributed diffusely throughout the sulphide matrix, and swirling around pyrite porphyroblasts.

The pyrite occurs as (1) anhedral, granulated, fractured porphyroclasts with variably developed deformation cleavage; as (2) large, granulated and disrupted annealed masses of fine- to medium-grained pyrite; and as (3) disseminated corroded and rounded grains in the chalcopyrite matrix. The grain size distribution of pyrite yields a median size of between 37 and 52 um. The pyrite contains fine-grained reticulate-textured magnetite, and contains anhedral inclusions of pyrrhotite, marcasite and sphalerite. The marcasite commonly occurs as fine-grained flecks associated with pyrrhotite in pyrite, as disseminated bladed subhedral grains, and rarely as abundant (≤10 Vol %) fresh bladed grains and interlocking aggregates replacing pyrite (Plate 4g). Rare lobes with concentric rings of 'sooty-textured' marcasite replace pyrrhotite in contact with pyrite in a texture called 'birds eye texture' (Plate 4h).

Chalcopyrite is the dominant sulphide and it envelopes and invades the gangue and the pyrite. The mineral occurs as coarse-grained, anhedral grains and commonly contains barely discernible spindle-shaped inversion twins, rare exsolution lamellae of cubanite, and poorly formed sphalerite stars (Plate 5a). These three textures suggest the existence of a high temperature chalcopyrite phase which re-equilibrated on cooling (Ramdohr, 1980, pp. 526). Pyrrhotite occurs as fine-grained rounded disseminations and granular masses in the chalcopyrite, whereas sphalerite occurs as rounded inclusions and rarely as coarse-grained, anhedral grains enveloped and embayed by the chalcopyrite, and displays a well developed "chalcopyrite-disease". Sphalerite and/or lesser pyrrhotite also occur as trails (parallel to the foliation) of carious blebs and myrmekitic masses in the chalcopyrite, and is interpreted as collection crystallisation during and after shearing, and termed diablastic growth (Ramdohr, 1980). Chalcopyrite, pyrrhotite and sphalerite commonly occur invading, cementing or replacing pyrite along grain boundaries, fractures and cleavages. The grain size distribution of chalcopyrite and sphalerite yield median sizes of between 104 and 147 um and between 9.2 and 13.0 um, respectively. This reflects the general occurrence of sphalerite as inclusions in the chalcopyrite.

Galena and clausthalite occur as fine-grained trace phases, generally as inclusions in pyrite or as anhedral grains in the chalcopyrite + pyrrhotite matrix. In TLS.2-65 the galena is associated with sphalerite forming intergrown masses that envelope and corrode pyrrhotite and chalcopyrite. Abundant fine-grained rucklidgeite, clausthalite and lesser electrum were observed in sample TLS.3-14, and with chalcopyrite and/or pyrrhotite infilling and replacing deformed pyrite along fractures and grain boundaries, as interstitial wedges and films, and also as rounded and lenticular (commonly composite) inclusions in the pyrite (Plate 5b and 5c).

Hessite was observed as a rare inclusion in galena, whereas in sample TLS.1-47 it was associated with trace pilsenite, both occurring as fine-grained, anhedral, tabular inclusions in chalcopyrite (Plate 5d).

Electrum was observed in 6 of the 18 samples. It occurs as two distinct textural types; (1) electrum forming inclusions and fracture-fillings in pyrite, and commonly associated with chalcopyrite, sphalerite and pyrrhotite as well as trace tellurides and selenides, and (2) large (≤2mm) anastomosing masses crystallising along the sulphide-chloritic schist contacts and enveloping and corroding chalcopyrite, and lesser pyrrhotite, sphalerite and/or pyrite (Plate 5e).

FIGURE 12.

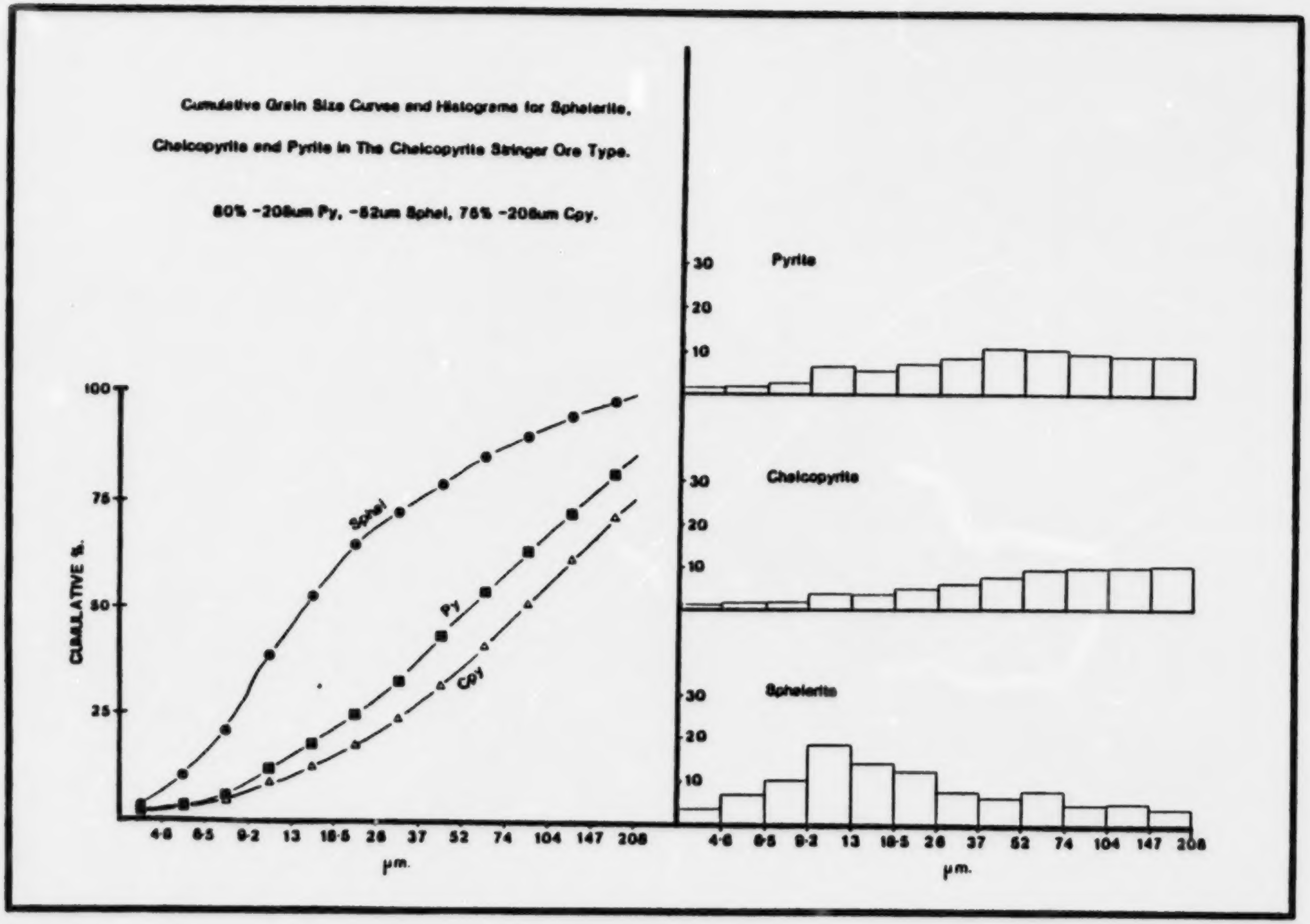

Cumulative Grain Size Curves and Histograms for Sphalerite, Chalcopyrite and Pyrite in The Chalcopyrite Stringer Ore Type.

80% -208um Py, -52um Sphal, 75% -208um Cpy.

PLATE 4.

PLATE 4.

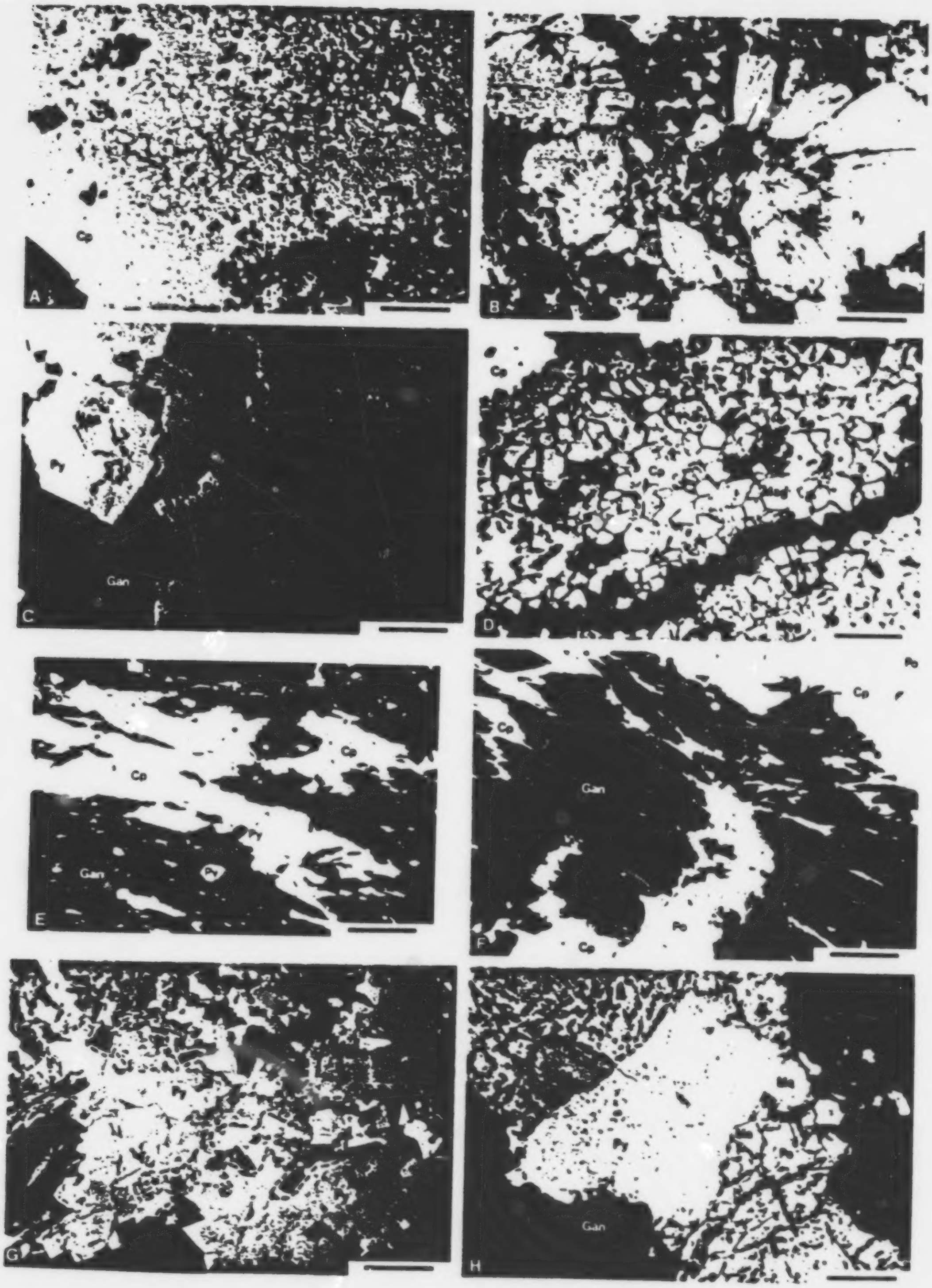
Cp
A
Py
B
Py
Gan
C
Cp
Cp
D
Po
Cp
Cp
Gan
Py
E
Po
Cp
Cp
Gan
Po
Cp
F
G
Gan
H

DISSEMINATED PYRITE ± CHALCOPYRITE ORE TYPE

The Disseminated Pyrite + Chalcopyrite ore type occurs in the footwall stockwork minerlisation, forming a diffuse envelope around the Chalcopyrite Stringer ore type. It grades into barren wallrock downwards and towards the margins of the ore lenses. Eight samples corresponding to this ore type were collected from lenses 1N, 1S, 2S and 3S. The chemical composition of this ore type, based on only one sample (TLS.1-67) is 0.64 Wt % Zn, 2.04 Wt % Cu, 0.02 Wt % Pb, 8.1 ppm Ag and 1.3 ppm Au. The average mineralogical composition is based on two samples, including TLS.1-67, and is 0.58 Wt % sphalerite, 3.9 Wt % chalcopyrite, 0.01 Wt % galena and clausthalite, 38.46 Wt % pyrite (including magnetite and marcasite), 0.03 Wt % pyrrhotite, and trace amounts of cubanite and electrum. This ore type does not consistently attain ore grade, though it is at least partly included in the mining width of the lenses. It plots adjacent to the pyrrhotite + pyrite apex of the Sphalerite - Chalcopyrite - Pyrrhotite + Pyrite ternary diagram, and similarly adjacent to the Fe apex of the Zn - Cu - Fe ternary diagram.

The ore consists of disseminated to locally semi-massive pyrite in a gangue matrix of chlorite, carbonate, quartz and sericite (Plate 5f). The pyrite occurs as (1) euhedral to anhedral, fine- to coarse-grained porphyroblasts, (2) as anneled polygonal masses, and (3) as disseminated, fine-grained, anhedral grains. Annealed masses of pyrite exhibit 120° triple junctions between equant grains, in relatively undeformed samples. The fine-grained, anhedral disseminations of pyrite in the gangue exhibit feather-like to dendritic habit, streaked to anastomosing forms, and also occur as veinlets. The pyrite typically exhibits development of cleavage and fractures, marginal granulation, and disruption of annealed masses. Rare occurrences of radially-textured anisotropy in pyrite suggests primary medium-grained spheroidal textured pyrite (Plate 5g). Rare pyrite porphyroblasts exhibit radial pitting, fractures and replacement by chalcopyrite, pyrrhotite and sphalerite along radial features that are interpreted as inherited from primary spheroidal pyrite. The grain size distribution of pyrite yields a median size of between 52 and 74 um. Chalcopyrite, sphalerite and pyrrhotite occur interstitially to the pyrite and the gangue, and are observed invading and replacing pyrite along fractures, and rounding and corroding the pyrite along grain boundaries. Advanced stages of this replacement result in rounded islands of relict pyrite enveloped in chalcopyrite, and dendritic-textured chalcopyrite and sphalerite in pyrite (Plate 5h). The sphalerite typically contains fine-grained blebs of chalcopyrite in the form of weakly developed "chalcopyrite disease". Chalcopyrite, sphalerite and pyrrhotite are all found as fine-grained, rounded inclusions in pyrite. The grain size distributions of chalcopyrite and sphalerite yield median sizes of between 52 and 74 um and between 74 and 104 um, respectively.

Fine-grained flecks to medium-grained subhedral to anhedral grains of marcasite are observed replacing pyrite along fractures and as fringes on pyrite grains, particularly in what are interpreted to be shear zones. Marcasite is observed as subhedral grains disseminated in the gangue, and rarely enveloping and replacing pyrite porphyroclasts. Rare fractured, medium- to fine-grained magnetite grains with rims and cross-cutting veinlets of pyrite, were observed. Galena and clausthalite occur as rare interstitial, fine-grained films and wedges in the annealed pyrite masses. Electrum was observed in 3 of the 8 samples, and typically occurred associated with chalcopyrite and pyrrhotite along the grain boundaries of, within fractures in, or as fine-grained (≤2um) inclusions in, pyrite.

FIGURE 13.

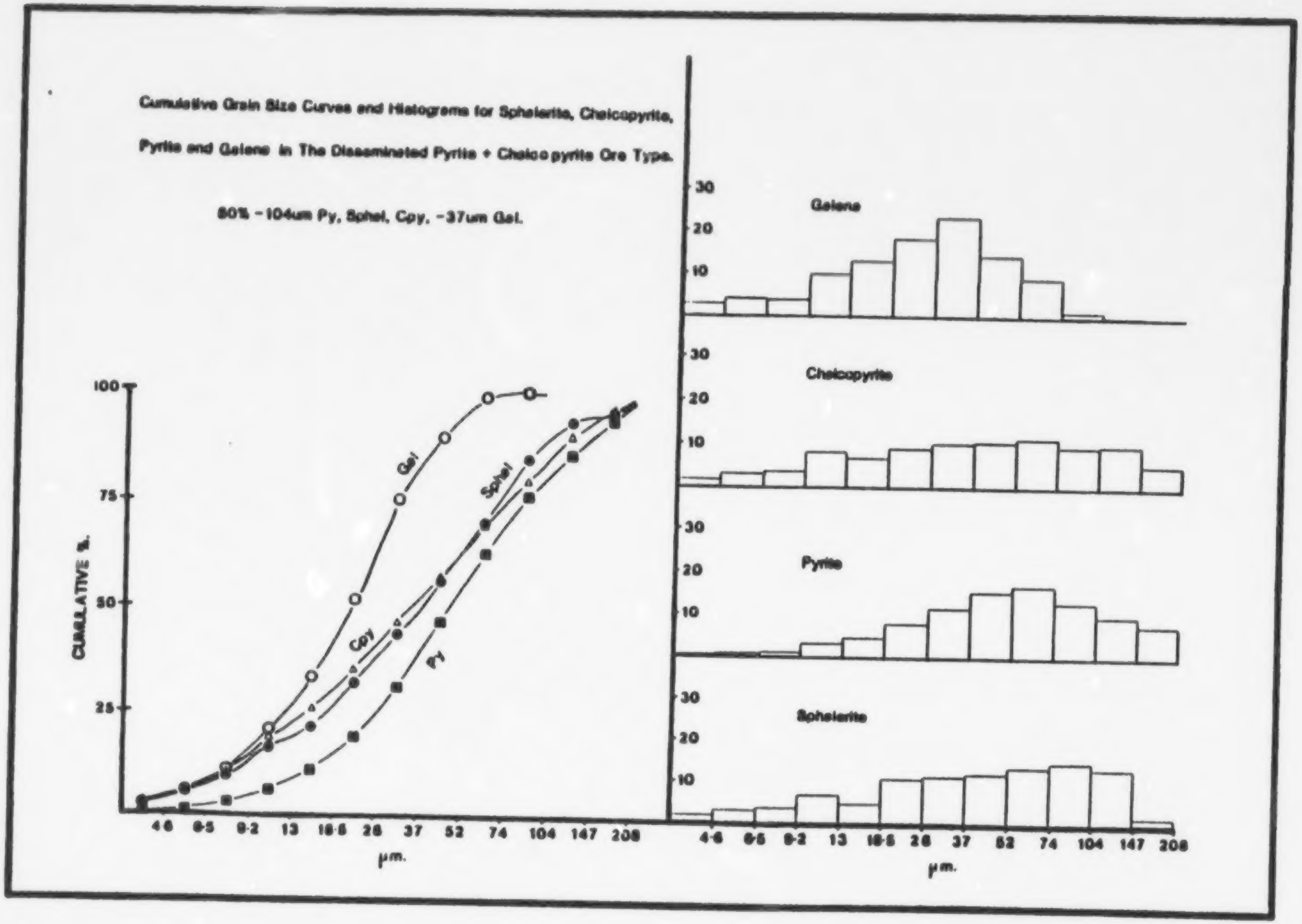

Cumulative Grain Size Curves and Histograms for Sphalerite, Chalcopyrite, Pyrite and Galena in The Disseminated Pyrite + Chalcopyrite Ore Type.

80% -104um Py, Sphal, Cpy, -37um Gal.

PLATE 5.

PLATE 5.

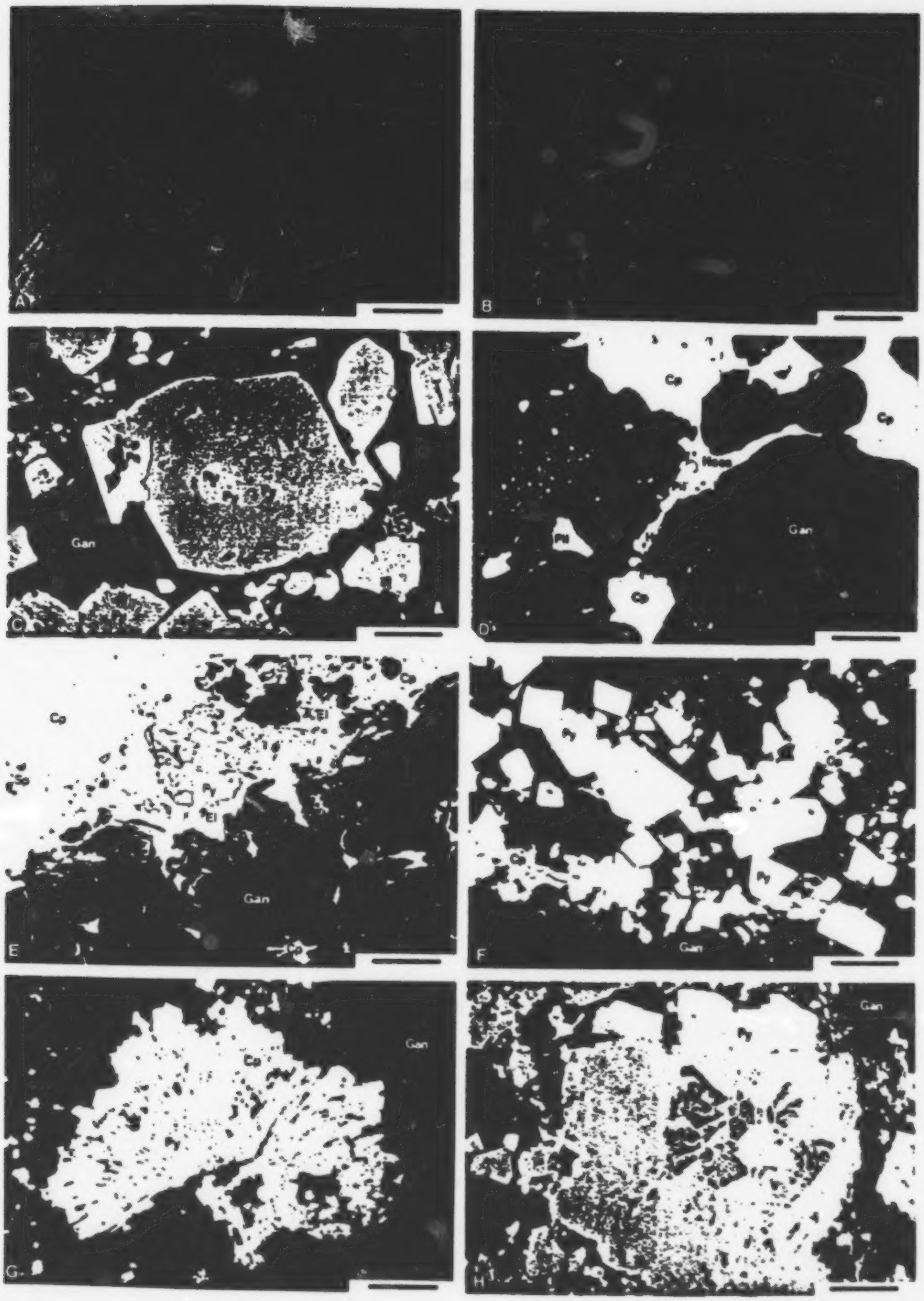
A
B
Gan
C
Cp
Cp
Hem
Py
Gan
Cp
D
Cp
El
Py
El
Gan
Cp
E
Py
Cp
Cp
Py
Gan
F
Gan
Cp
G
Gan
Py
H

SHEARED CHALCOPYRITE + SPHALERITE ORE TYPE

The Sheared Chalcopyrite + Sphalerite ore type occurs with negligible stratigraphic control. The sole stratigraphic control is that sufficient (>5 %) of both sphalerite and chalcopyrite must be present in the ore to warrant it's definition due to the intricate intergrowth of the valuable minerals chalcopyrite and sphalerite, and thus tends to restrict the occurrence of the ore type to the central portions of the massive ore lenses. Ten samples of the Sheared Chalcopyrite + Sphalerite ore type were collected; 1 from lens 3S and 9 from lens 2N. The average chemical composition of 4 representative samples is 23.2 Wt % Zn, 5.24 Wt % Cu, 0.01 Wt % Pb, 65 ppm Ag and 6.86 ppm Au. The average mineralogical composition of the same samples is 38.7 Wt % sphalerite, 15.4 Wt % chalcopyrite, 0.01 Wt % galena, 11.0 Wt % pyrrhotite, 3.33 Wt % pyrite (includes trace magnetite), and trace amounts of arsenopyrite, cubanite, magnetite, hessite, gudmundite and electrum. It is interpreted that electrum is the host of the Au, whereas sphalerite, hessite, galena and electrum probably host the bulk of the Ag. This ore type plots in a broad field extending from adjacent to the sphalerite apex to the central portions of the Sphalerite - Chalcopyrite - Pyrrhotite + Pyrite ternary diagram (Fig 5),and in a wide field close to the Fe - Zn join of the Zn - Cu - Fe ternary diagram (Fig 6).

This ore type is defined as a chalcopyrite - sphalerite ore that contains more than 5 % of each mineral, and where bulk of the chalcopyrite and sphalerite in the ore occur as an intricately intergrown and interpenetrating, fine-grained matrix. This texture is interpreted as a deformational texture, which is produced by collection crystallisation during and after shearing, and termed diablastic growth. The gangue in this ore type is commonly schistose- to augen-textured with sericite and/or chlorite forming in the vortices of compression around the augens ('eyes'). The textures of these ores are characterstic of the penetrative deformation that is developed by internal rotational movements, and is termed 'Durchbewegung' (Vokes, 1969). Two such deformational textures that are commonly observed are the total disaggregation of primary banding, and the intense deformation and ultimate breakdown of pyrite. Since this ore type is deformational it lacks strong stratigraphic control, though it tends to be restricted in occurrence to the central portions of the ore lenses, where there is sufficient concentrations (>5%) of both sphalerite and chalcopyrite to warrant it's definition.

The Sheared Chalcopyrite + Sphalerite ore type consists of chalcopyrite, sphalerite and pyrrhotite which form a highly foliated sulphide matrix and exhibit various degrees of deformation and intensity of the characteristic diablastic texture (Plate 6a). Commonly the chalcopyrite (with exsolution lammellae of cubanite), sphalerite (with "chalcopyrite-disease") and/or pyrrhotite occur as medium-grained masses with mutually carious to myrmekitic interpenetrative contacts (Plate 6b and 6c) and well developed zones of diablastic texture. The matrix, therefore commonly consists of fine-grained myrmekitic chalcopyrite, sphalerite and pyrrhotite, with medium-grained masses forming in the pressure shadows at the terminations of the augens in intensely deformed samples (Plate 6d). The matrix sulphides commonly invade the fractured augens of rolled and folded gangue, as well as the cleavages of micaceous minerals (Plate 6e). The grain size distributions of the chalcopyrite and the sphalerite yield median sizes of between 37 and 52 um, and between 52 and 74 um, respectively.

The pyrite varies from not observed to a major constituent, occurring as anhedral, fine-grained disseminations and coarse-grained porphyroblasts The mineral is granulated and fractured, and is invaded, replaced and cemented by the matrix sulphides. A deformation cleavage is often highlighted by the invading matrix sulphides, particularly in the rare examples of 'blow apart' textured pyrite (Plate 6f), whereas 'atoll' texture is rare. Rounded islands of fine-grained relict pyrite and skeletal pyrite enveloped in a chalcopyrite matrix are common. Pyrite commonly contains reticulate-textured fringes and zones of magnetite. The pyrite in samples of less intense deformation tend to deform by rounding to produce 'pyrite pebbles', rather than by deforming brittley (Plate 6g). Rare carious contacts with sphalerite, as well as pyrite injected into fractures and the bent cleavage traces of micaceous minerals suggests that the pyrite has been locally mobilised. The pyrite is interpreted as having partly broken down during the formation of pyrrhotite. The pyrite grain size distribution yields a median size of between 52 and 74 um. Rare, anhedral, disseminated grains of arsenopyrite are observed enveloped in the sulphide matrix.

The galena commonly occurs associated with chalcopyrite, sphalerite and/or pyrrhotite invading deformed pyrite. In sample TLN.2-9 the galena occurs as carious blebs in the diablastic matrix of chalcopyrite, sphalerite and pyrrhotite, and also associated with chalcopyrite and inclusions of hessite forming veinlets and disseminations in the gangue rafts (Plate 6h). Gudmundite inclusions in granular masses of pyrrhotite were observed hosted in a rim of massive sphalerite adjacent to a large quartz vein.

Electrum was observed in 6 of the 10 samples. It occurs with chalcopyrite and/or sphalerite infilling and replacing pyrite along fractures and cleavages. However, in sample TLN.2-9 the electrum (14 grains observed) exhibited no spatial relationship with the pyrite, but instead occurred in the matrix chalcopyrite and/or pyrrhotite. This sample contains trace pyrite, all of which was hosted in rafts of gangue. The general decrease in the pyrite content and increase in the pyrrhotite content with increased deformation in these ores, suggests that the pyrrhotite forms, at least in part, by the breakdown of pyrite and results in the release of trace Au present in solid solution in the pyrite, with the resultant crystallisation of electrum.

FIGURE 14.

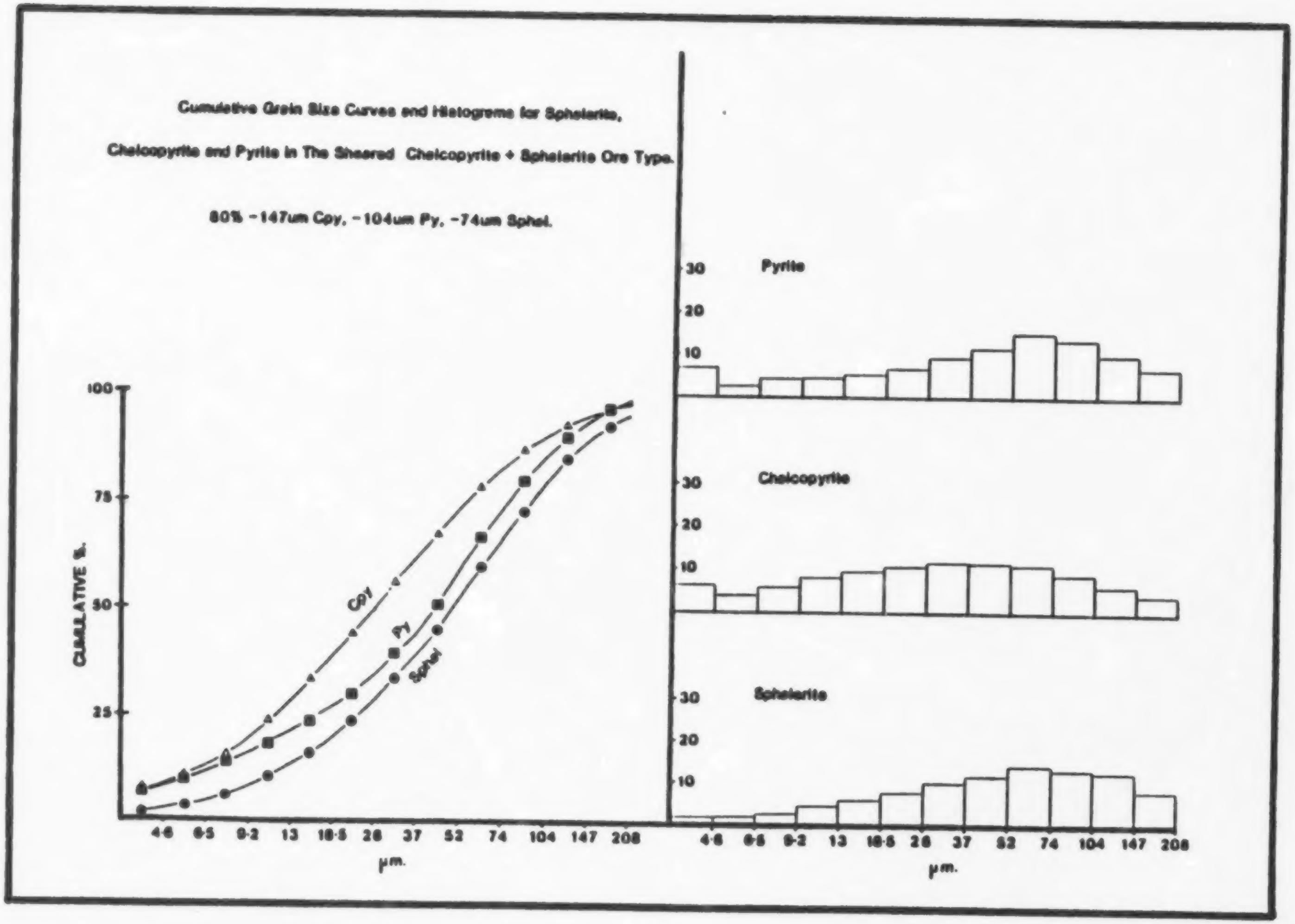

Cumulative Grain Size Curves and Histograms for Sphalerite, Chalcopyrite and Pyrite in The Sheared Chalcopyrite + Sphalerite Ore Type.

80% -147um Cpy, -104um Py, -74um Sphal.

PLATE 6.

PLATE 6.

PHOTOGRAPH A.

SAMPLE TLN.2-12 : Diablastic-textured chalcopyrite (Cp), sphalerite (Sp) and pyrrhotite (Po), showing myrmekitic intergrowths of the sphalerite with chalcopyrite, and where the pyrrhotite is essentially found as inclusions in the chalcopyrite. Plane polarised light. Bar scale = 40 µm.

PHOTOGRAPH B.

SAMPLE TLN.2-63 : Diablastic-textured ore consisting of augen-textured gangue (Gan) rafts, and oriented grains of sphalerite (Sp) with carious contacts with chalcopyrite (Cp) and lesser pyrrhotite (Po). Interpreted as the product of a sphalerite ore with abundant interstitial films and grains of chalcopyrite, which having being sheared and 'streaked out', underwent collection crystallisation to produce these carious contacts. Plane polarised light. Bar scale = 325 µm.

PHOTOGRAPH C.

SAMPLE TLN.2-12 : Disrupted and fractured gangue (Gan) rafts within a diablastic-textured chalcopyrite (Cp), sphalerite (Sp) and pyrrhotite (Po) matrix, which swirls around the augens in a truely 'tectonised' or 'Durchbewegung' style of deformation. Plane polarised light. Bar scale = 325 µm.

PHOTOGRAPH D.

SAMPLE TLN.2-12 : Augen-textured rafts of gangue (Gan) 'floating in a sea' of diablastic-textured chalcopyrite (Cp), sphalerite (Sp) and pyrrhotite (Po). Note the coarse-grained chalcopyrite and sphalerite in the pressure shadows at the terminations of the gangue rafts. Plane polarised light. Bar scale = 325 µm.

PHOTOGRAPH E.

SAMPLE TLN.2-113. Diablastic-textured sphalerite (Sp), chalcopyrite (Cp) and pyrrhotite (Po) bearing ore from the 425m drillhole intersection of Lens 2 of the North Zone. Note the sphalerite and chalcopyrite invading the gangue rafts at the top of the photograph. Plane polarised light. Bar scale = 160 µm.

PHOTOGRAPH F.

SAMPLE TLN.2-114 : A matrix of sphalerite (Sp) and chalcopyrite (Cp) containing a 'Blow apart' textured pyrite (Py) porphyroclast (1.25 mm in diameter) cemented by chalcopyrite and trace pyrrhotite (Po). Note there is negligible replacement of the pyrite along the dilated fracture surfaces. Plane polarised light. Bar scale = 160 µm.

PHOTOGRAPH G.

SAMPLE TLN.2-63 : Rounded pyrite (Py) porphyroclasts in a matrix of diablastic-textured sphalerite (Sp), chalcopyrite (Cp) and pyrrhotite (Po), which are characterised by the carious and myrmekitic texture. Plane polarised light. Bar scale = 325 µm.

PHOTOGRAPH H.

SAMPLE TLN.2-9 : A Sheared Chalcopyrite + Sphalerite ore with masses of fine-grained galena (Gal) and hessite (Hess - outlined by dashed line) hosted in chalcopyrite (Cp), which is invading ruptured and fractured gangue (Gan) rafts. Plane polarised light. Bar scale = 40 µm.

PLATE 6.

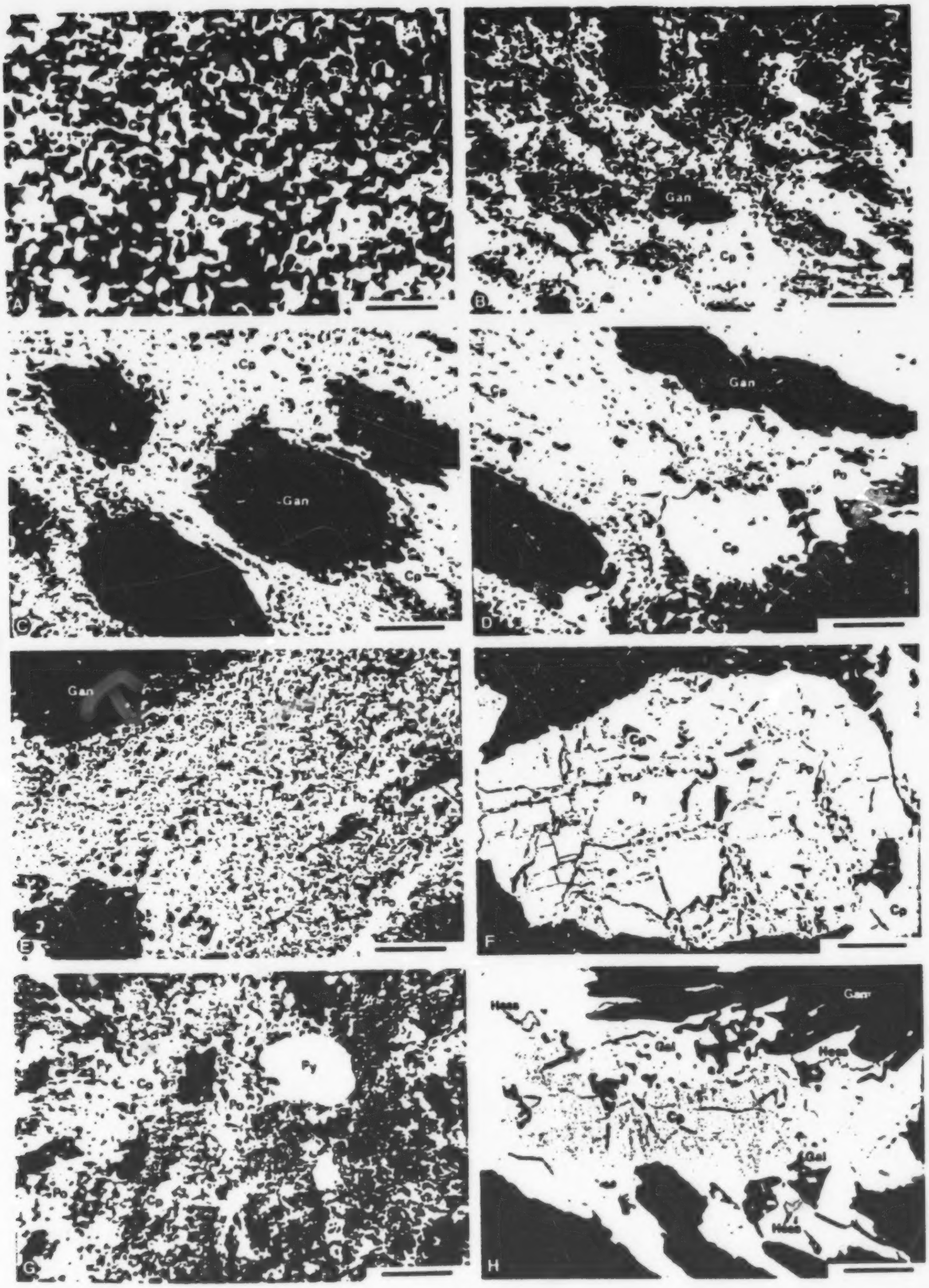
A
Cp
Cp
B
Po
Cp
Gan
Cp
C
Cp
Po
Gan
Cp
D
Gan
Cp
Po
Po
Cp
E
Gan
Cp
Po
F
Py
Cp
Py
Py
Cp
G
Py
Cp
Py
Po
Po
Cp
H
Hess
Gan
Gal
Hess
Cp
Gal
Hess

VEIN QUARTZ ± CHALCOPYRITE ORE TYPE

The Vein Quartz + Chalcopyrite ore type exhibits no stratigraphic control, and is tectonic in origin. This ore type was defined because of the common occurrence of mineralised quartz veins within the ore lenses. These veins exhibit a textural uniqueness of some of the sulphides, and have the potential for concentration of precious metal phases. It is noteworthy that similar quartz veins were observed in the Flin Flon deposit, and are interpreted as resulting from hydrothermal remobilisation during metamorphism (Koo, 1973).

The chemical composition of this ore type based on sample TLN.1-3 is 0.43 Wt % Zn, 3.20 Wt % Cu, 0.005 Wt % Pb, 13 ppm Ag and 6.16 ppm Au. The mineralogical composition of the same sample is 0.72 Wt % sphalerite, 9.4 Wt % chalcopyrite, 2.14 Wt % pyrite (includes trace marcasite), 2.14 Wt % pyrrhotite, and trace cubanite and galena. Electrum is interpreted to be the host of the Au, whereas sphalerite, galena and electrum host at least the bulk of the Ag. This ore type plots adjacent to the chalcopyrite apex of the Sphalerite - Chalcopyrite - Pyrrhotite + Pyrite ternary diagram, and centrally on the Fe - Cu join of the Zn - Cu - Fe ternary diagram.

The gangue consists predominantly of coarse-grained, quartz with pronounced wavey extinction, and lesser calcite, sericite, chlorite and trace tourmaline. The sulphides, consisting predominantly of chalcopyrite, occupy the interstitial spaces between the quartz grains.

The chalcopyrite is the dominant sulphide and is coarse-grained with spindle-shaped inversion twins. The chalcopyrite also contains abundant sphalerite stars, typically 20um in diameter, though occassionally as large as 90um in diameter (Plate 7a). The sphalerite stars are concentrated along twin planes, and along grain boundaries of the chalcopyrite. Rare exsolution lamellae of cubanite up to 5 mm in length and 50 um in width occur in the chalcopyrite (Plate 5a). These three textures suggest that a high temperature chalcopyrite crystallised during the metamorphic maxima and equilibrated on cooling. The sphalerite also occurs as minor medium-grained, anhedral grains with intense "chalcopyrite disease", and is enveloped and severely embayed by the matrix chalcopyrite. The grain size distributions for chalcopyrite and sphalerite yield median sizes greater than 208 um, and between 52 and 74 um, respectively.

Pyrite occurs as a minor constituent, but as large (≤5mm) granulated and fractured annealed polygonal masses that are invaded and replaced by chalcopyrite and lesser sphalerite. Minor anhedral inclusions of pyrrhotite are typically associated with marcasite, where the latter occurs as rare subhedral, bladed grains replacing the pyrite masses. In TLN.1-3 the pyrite exhibits clouded texture with fine-grained, comb-textured flecks of marcasite forming by replacement along the pyrite grain boundaries. Galena occurs as rare, disseminated, anhedral grains in chalcopyrite. No precious metal-bearing minerals or sulfosalts were observed.

FIGURE 15.

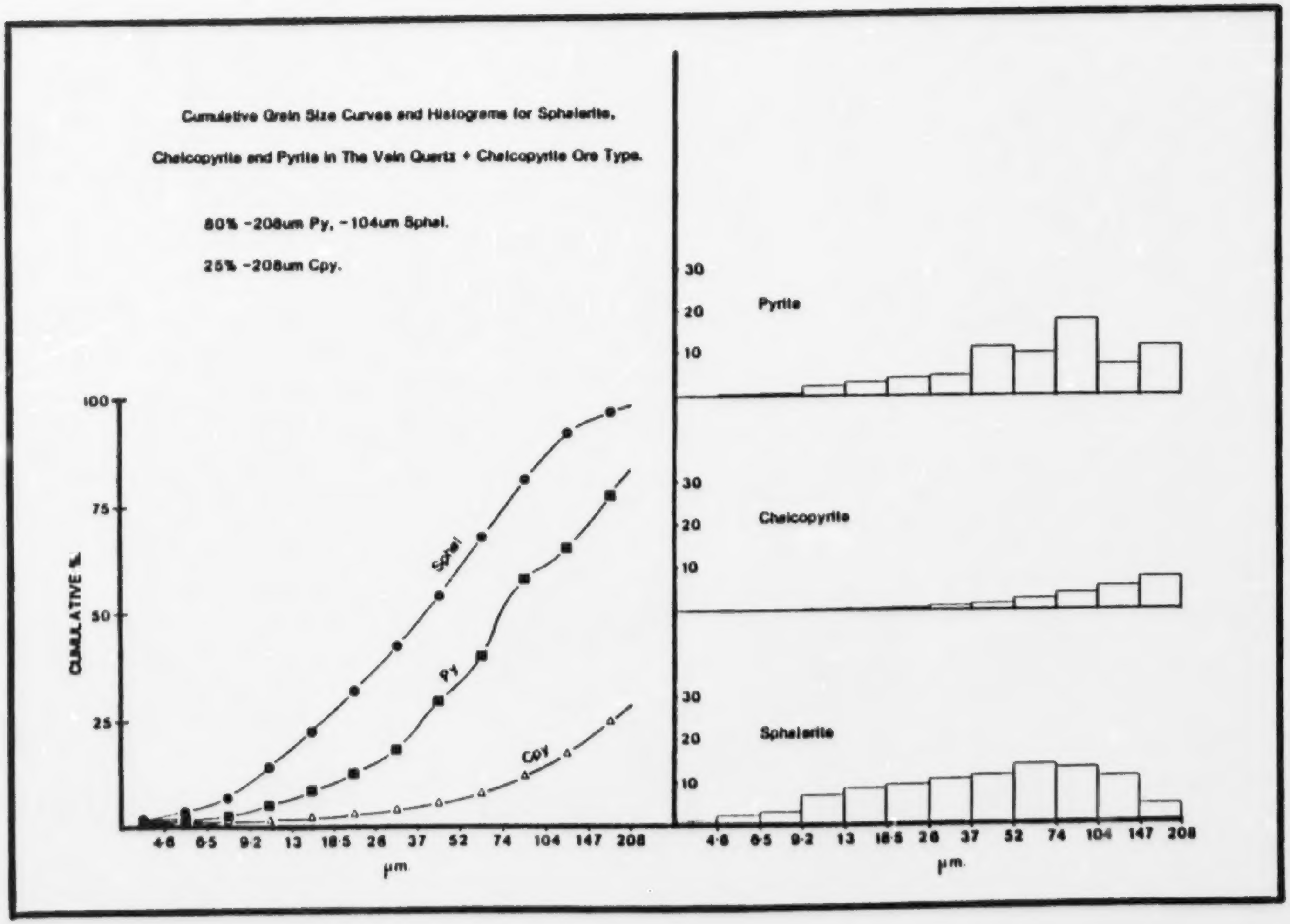

Cumulative Grain Size Curves and Histograms for Sphalerite, Chalcopyrite and Pyrite in The Vein Quartz + Chalcopyrite Ore Type.

80% -208um Py, -104um Sphal.

25% -208um Cpy.

Chapter VII

CHARACTERISTICS OF THE ORE MINERALS

Twenty six ore minerals were observed in the ores, and these are listed in Table 4. The minerals are classified into mineral groups, and listed in order of decreasing abundance of the groups and of the minerals in each group. These are discussed in detail in this chapter. In addition, the occurrence and composition of two Rare Earth minerals is discussed.

THE COMMON SULPHIDES

PYRITE (FeS_2)

Pyrite is the most abundant mineral in the ore (See Table 11), and was observed in each ore type. It exhibits five principal textural styles; (1) annealed, medium-grained, polygonal masses (Plate 4g and 7b), (2) disseminated porphyroblasts and metacrysts (Plate 7c), (3) granulated, rounded, fractured, anhedral porphyroclasts (fractured porphyroblasts) with variably developed deformation cleavage (Plate 2b), (4) streaked, smeared, schistose, deformed pyrite (Plate 7d), and (5) remobilised pyrite in veinlets and cleavages of gangue minerals (Plate 7e). These textures demonstrate that the pyrite has been recrystallised during the metamorphism, has been sheared and fractured by tectonism, and has been replaced by other minerals. The grain size distribution of the pyrite in all the ore types yields the median size of between 52 and 74 um.

The matrix sulphides sphalerite, chalcopyrite, pyrrhotite, galena and/or freibergite occur interstitially to the pyrite, and invade fractures and cleavages and may cement or replace the pyrite. The dominant replacement textures of pyrite are (1) corrosion, embayment and development of atoll texture, where sphalerite is the dominant matrix sulphide (Plate 1b), (2) fine-grained, dendritic replacement by sphalerite, chalcopyrite and/or galena in the Massive Pyrite and the Banded Pyrite Sphalerite ore types (Plate 2d), (3) replacement by chalcopyrite, pyrrhotite and/or sphalerite along grain boundaries, fractures and cleavages (Plate 2b), (4) envelopment and corrosion to form rounded, fine-grained, relict islands of pyrite in matrix chalcopyrite and/or pyrrhotite (Plate 4a), and (5) replacement by marcasite in a variety of textures (See MARCASITE).

Quantitative microprobe analyses revealed that the pyrite contains no detectable trace elements, nor variation in stoicheometry.

MARCASITE (FeS_2)

Marcasite is generally a trace constituent, though it has been observed as a major constituent, reaching 15 Vol % in sample TLN.1-2, a Chalcopyrite Stringer ore. Marcasite always occurs as a replacement of pyrite and is generally more abundant where the pyrite has undergone intense deformation, particularly along shear zones. The dominant textures of marcasite are (1) fine-grained flecks and bladed inclusions in pyrite and as fringes on pyrite (Plate 7f), (2) clouded or sooty-textured pyrite (sub-microscopic marcasite), occassionally with comb-textured marcasite forming on the pyrite grain boundaries (Plate 4c), (3) fine- to medium-grained subhedral grains and interlocking aggregates with simple, and rarely repeated lamellar twinning (Plate 4g), and (4) foliated, scaley masses of marcasite associated with intergrown galena, freibergite and pyrrhotite, enveloping and replacing deformed and fractured pyrite (Plate 2h).

PYRRHOTITE ($Fe_{(1-x)}S$)

Pyrrhotite is an abundant ore mineral, and is a major constituent in some ore types, particularly the Massive Chalcopyrite + Pyrrhotite ore type. The mineral is commonly associated with chalcopyrite and tends to be concentrated in the Massive Chalcopyrite + Pyrrhotite, the Sheared Chalcopyrite + Sphalerite and the Chalcopyrite Stringer ores. The pyrrhotite content of the Sheared Chalcopyrite Sphalerite ores tends to increase with the apparent intensity of deformation, and with a decrease in the pyrite content. This suggests that the pyrrhotite formed by the breakdown of pyrite during and after the deformation that followed the porphyroblastic growth of pyrite.

Pyrrhotite is invariably anhedral, and commonly occurs as an interstitial mineral. The dominant textural styles of pyrrhotite are (1) inclusions, interstitial material, and fracture-fillings cementing or replacing pyrite (Plate 6f), (2) disseminated rounded grains and granular to gneissic-textured masses in chalcopyrite (Plate 3h), (3) oriented blebs and rods, and disseminated grains in sphalerite (Plate 7g), (4) carious blebs and myrmekitic intergrowths with chalcopyrite and/or sphalerite characteristic of diablastic texture eg., in the Sheared Chalcopyrite Sphalerite ores, and (5) as inclusions in interstitial galena (Plate 7h).

Four microprobe analyses are presented below. The analyses yield an average unit formula of $Fe_{6.8}S_{8.0}$, which corresponds to monoclinic pyrrhotite and/or hexagonal pyrrhotite of the 1C or MC type (Craig and Scott, 1976). Monoclinic pyrrhotite, unlike hexagonal pyrrhotite, is strongly ferromagnetic, and this is in agreement with the strong magnetic response of all magnetite-free, pyrrhotite-rich polished sections. In the absence of an x-ray diffraction study or etching, the presence of hexagonal pyrrhotite remains unproven.

TABLE 13

Representative Microprobe Analyses of Pyrrhotite.

Wt %.	1	2	3	4	Uncertainty.
S.	39.34	40.33	40.15	40.30	± 0.2
Fe.	59.69	59.29	59.54	59.30	± 0.5
Total.	99.03	99.62	99.69	99.60	
At %.					
S.	53.45	54.23	54.01	54.21	
Fe.	46.55	45.77	45.99	45.79	
Number of Atoms.					
S.	1.00	1.00	1.00	1.00	
Fe.	0.87	0.84	0.85	0.85	

* Uncertainty quoted at 95% confidence limits.
* Unit formula calculated on the basis of 1 sulfur atom.
* A pyrite standard was employed for both Fe and S.

PLATE 7.

PLATE 7.

PHOTOGRAPH A.

SAMPLE TLN.1-3 : A large well-formed sphalerite (Sp) star exsolved in a matrix of coarse-grained chalcopyrite (Cp). Plane polarised light. Bar Scale = 160 µm.

PHOTOGRAPH B.

SAMPLE TLN.1-12 : An identical view as Plate 4g, except plane polarised light was used in this photograph. Note the 120° triple junctions in the annealed polygonal pyrite in the areas indicated by A and B. Note the areas of pitting, due to plucking of marcasite (Ma). Plane polarised light. Bar scale = 160 µm.

PHOTOGRAPH C.

SAMPLE TLS.5-105 : A cluster of pyrite (Py) euhedra in a matrix of sphalerite (Sp).and carbonate gangue (Gan). Plane polarised light. Bar scale = 160 µm.

PHOTOGRAPH D.

SAMPLE TLN.1-29 : Highly deformed and sheared pyrite (Py) developed locally as swirled patches of 'schistose' pyrite. Plane polarised light. Bar scale = 325 µm.

PHOTOGRAPH E.

SAMPLE TLN.1-98 : Pyrite (Py) invading and replacing calcite (Calc) along grain boundaries, cleavages and twin planes. Sphalerite (Sp) also seen invading and corroding calcite and other gangue phases. Plane polarised light. Bar scale = 160 µm.

PHOTOGRAPH F.

SAMPLE TLS.3-36(#2) : A large pyrite (Py) porphyroclast enveloped by a granular mass of marcasite (Ma). Note the fracture at the bottom left corner of pyrite porphyroclast, which contains fine-grained chalcopyrite and electrum. Plane polarised light. Bar scale = 325 µm.

PHOTOGRAPH G.

SAMPLE TLN.1-27 : A matrix of massive sphalerite (Sp) containing oriented blebs and rods of pyrrhotite (Po). Note the rounded and corroded disseminations of pyrite (Py). Plane polarised light. Bar scale = 160 µm.

PHOTOGRAPH H.

SAMPLE TLS.5-84 : A massive sphalerite (Sp) ore containing bent and foliated rafts and grains of gangue (Gan) with galena (Gal) preferrentially forming along the gangue-sphalerite contacts. Note that the galena contains inclusions of pyrrhotite (Po), and that the pyrite (Py) is fractured and corroded. Plane polarsied light. Bar scale = 160 µm.

PLATE 7.

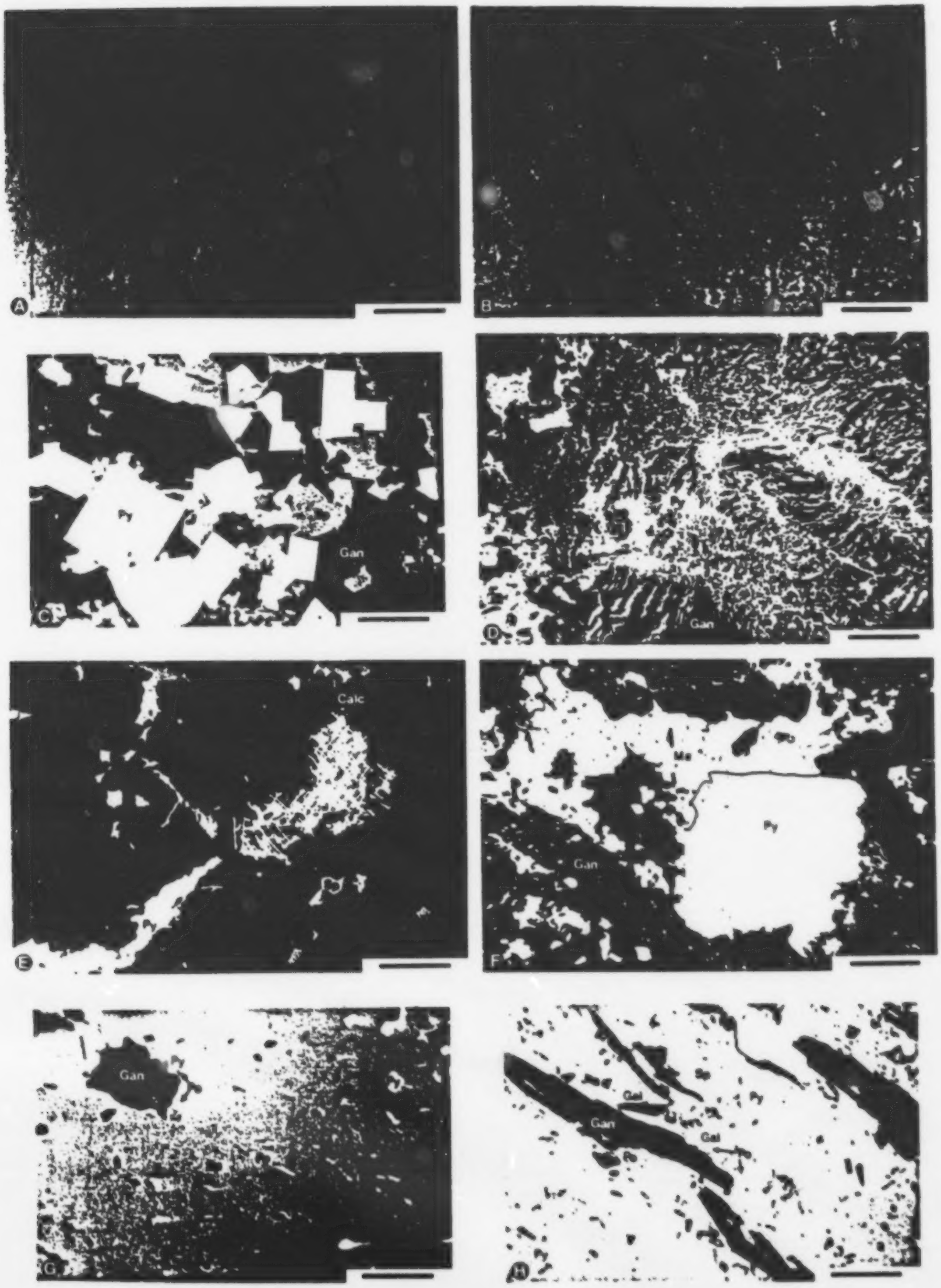
A
B
C
Gan
D
Gan
E
Calc
F
Mc
Py
Gan
G
Gan
H
Gal
Gan
Gal
Py

CHALCOPYRITE ($CuFeS_2$)

Chalcopyrite is the main Cu-bearing mineral in the ore, with cubanite, freibergite and bournonite constituting the remaining, yet relatively insignificant, Cu-bearing minerals. The chalcopyrite and hence Cu, tends to be concentrated in the footwall massive exhalative ores, and particularly in the highly differentiated and spectacular Chalcopyrite Stringer ores.

Chalcopyrite is invariably anhedral, and commonly occurs as an interstitial mineral. It is variably coarse-grained (up to 1 cm in the Vein Quartz + Chalcopyrite ore type) to fine-grained, with the grain size decreasing with the relative abundance; the chalcopyrite occupies smaller and more restricted interstitial spaces between the phases with higher crystallinity. Both chalcopyrite and sphalerite constitute the dominant matrix sulphides in the ore. However, because of the lower crystallinity of chalcopyrite and the interpreted later crystallisation of chalcopyrite in the paragenesis, it displays a diversity of textural styles. These are (1) massive coarse-grained matrix chalcopyrite with granuloblastic- to gneissic-textured masses and disseminations of pyrrhotite, and with cubanite lamellae and/or sphalerite stars, particularly in the Massive Chalcopyrite + Pyrrhotite, Chalcopyrite Stringer and the Vein Quartz + Chalcopyrite ore types (Plate 3h), (2) massive chalcopyrite enveloping, invading and/or replacing all other major constituents, including the gangue and excluding galena (Plate 4f), (3) chalcopyrite associated with other matrix sulphides invading and cementing or replacing fractured pyrite (Plate 6f), (4) irregular interstitial material between sphalerite grains (Plate 1d), (5) crystallographically oriented blebs and rods of chalcopyrite in sphalerite termed "chalcopyrite-disease" (Plate 1c), (6) fine-grained, dendritic replacements of pyrite (Plate 5h), and (7) myrmekitic intergrowths of chalcopyrite with sphalerite and/or pyrrhotite, characteristic of diablastic texture, especially in the Sheared Chalcopyrite + Sphalerite ores (Plate 6a). It is interpreted from the size analysis data that the chalcopyrite occurring as inclusions in pyrite, as interstitial blebs, wedges and films between pyrite grains, as fracture-fillings in pyrite, and as "chalcopyrite-disease" in, carious blebs in, and interstitial material between sphalerite dominate the - 18.5 um fraction. This fraction corresponds to approximately 20 % of the chalcopyrite in the ore. The remaining 80 % + 18.5 um fraction corresponds to the massive matrix chalcopyrite with a median grain size between 74 and 104 um. The cumulative grain size curves for chalcopyrite in each ore type are presented in Figure 16.

Quantitative microprobe analyses of the chalcopyrite revealed no detectable trace elements, nor variation in stoicheometry.

FIGURE 16.

Cumulative Grain Size Curves for Chalcopyrite and Sphalerite in each of the 9 Ore Types.

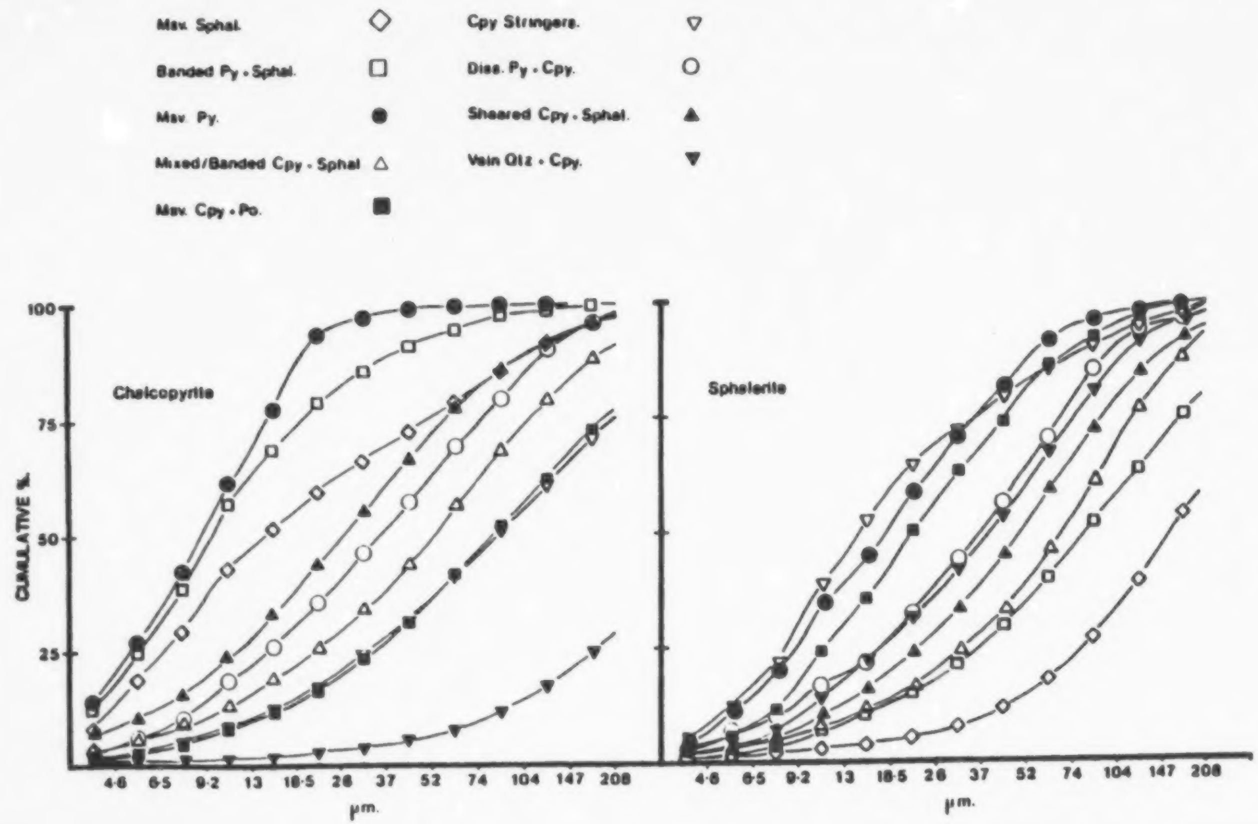

ARSENOPYRITE (FeAsS)

The arsenopyrite constitutes a minor to trace mineral, and only assumes the abundance of a major constituent in the hangingwall Massive Sphalerite and the Banded Pyrite + Sphalerite ore types (See Table 11). The arsenopyrite tends to be distributed along discrete to diffuse laminae within the pyrite- and/or sphalerite-rich bands of these ore types and is suggestive of primary mineral banding. Arsenopyrite is generally not spatially associated with freibergite, which is also abundant in these ore types. However, in one sample of Massive Pyrite ore, euhedral, medium-grained arsenopyrite occurs enveloped in Ag-poor freibergite (approximately 13 to 15 % Ag, i.e., tetrahedrite) , and where the latter contained networked blebs of chalcopyrite, interpreted to be an exsolution texture (Plate 2e).

Arsenopyrite is generally medium- to fine-grained, though less commonly grains measuring up to 500 um have been observed. It also varies from euhedral, rhombic porphyroblasts and smaller metacrysts to fractured and granulated, anhedral grains, as well as granular masses disseminated within annealed polygonal pyrite masses/bands. The dominant textures exhibited by arsenopyrite are (1) thin laminae of disseminated, medium- to fine-grained, euhedral (i.e., characteristically rhombic) grains in sphalerite (Plate 1g), (2) laminae of fractured coarse-grained, subhedral to anhedral porphyroblasts that are invaded by, and contain reticulate replacements of sphalerite (Plata 1b), and (3) medium- to fine-grained granular masses in massive polygonal pyrite.

Arsenopyrite was found to contain no detectable trace elements (Sb and Co were specifically sought for), but did display minor variation in stoichiometry. Occassionally minor detected Zn was observed, but this was interpreted as contamination from common reticulate replacements of arsenopyrite by sphalerite. Six microprobe analyses are presented below.

The variation in stoichiometry relates to the diadochic substitution of S for As, and results in a slightly As-deficient mean composition (i.e., $Fe_{0.98},As_{0.96},S_{1.06}$). The slight cation deficiency (As + S = 2.02, Fe = 0.98) reflects the minor inaccuracy in the calibration procedure for the microprobe.

TABLE 14

Representative Microprobe Analyses of Arsenopyrite.

Wt %	1	2	3	4	5	6	Uncertainty.
S	22.39	21.12	22.32	20.65	19.91	21.68	± 0.2
Fe	35.42	33.76	34.27	33.64	33.57	33.64	± 0.5
As	43.15	45.30	43.70	46.19	44.95	45.34	± 1.1
Zn	-----	-----	-----	-----	-----	1.08	± 0.4
Total.	100.96	100.18	100.28	100.48	98.43	101.75	

Number of atoms.						
S	1.10	1.06	1.10	1.04	1.02	1.07
Fe.	1.00	0.97	0.97	0.97	0.99	0.95
As.	0.90	0.97	0.93	0.99	0.99	0.96
Zn	____	____	____	____	____	0.03

* Uncertainty quoted at the 95% confidence limits.
* Unit formula calculated on the basis of 3 atoms.
* An arsenopyrite standard was employed for S, Fe and As, whereas a sphalerite standard was employed for Zn.

CUBANITE ($CuFe_2S_3$)

Cubanite is a trace constituent of the ores. The mineral tends to be concentrated with chalcopyrite in the footwall massive exhalative ores, the Chalcopyrite Stringer and the Vein Quartz + Chalcopyrite ore types. Cubanite occurs in two textures, and these are (1) thin lamellae in massive chalcopyrite, and measuring up to 5mm x 50um, as well as exhibiting composite or finely-lamellar habit (Plate 5a), and (2) rare fine-grained flame-textured inclusions in chalcopyrite that is replacing pyrite. The lamellae are interpreted to have exsolved from a high temperature chalcopyrite which contained an appreciable dissolved cubanite component, and which unmixed on cooling.

The cubanite was found to contain neither detectable trace elements, nor deviations in stoichiometry.

GALENA (PbS)

Galena is generally a trace constituent of the ores, though occassionally it is a minor and rarely a major constituent (See Table 11). The mineral tends to be concentrated in the hangingwall Massive Sphalerite ore type, and particularly in the Banded Pyrite + Sphalerite ore type. The relationship of galena with sphalerite-rich ores can be described as permissive; galena occurs as a major constituent exclusively, but infrequently in sphalerite-rich ores. The occurrence of the antimonial-sulfosalts freibergite, pyrargyrite, gudmundite, boulangerite, freieslebenite, bournonite, as well as dyscrasite, as inclusions in interstitial galena is the most pronounced association of the ores. Except for rare grains of gudmundite these sulfosalts and the dyscrasite occur exclusively as inclusions in galena, or also in the case of freibergite only, intimately associated with galena.

Galena is a common constituent of the ores, occurring invariably as an anhedral, interstitial mineral with the lowest crystallinity of the common sulphides (Vokes, 1969). It is generally fine-grained, though more rarely coarse-grained (≤1mm), with the grain size generally increasing with the relative abundance of the galena. Because of galena's low crystallinity, it occurs in a variety of textures. These are (1) interstitial films, wedges and masses in massive pyrite (Plate 2g and 8a), (2) irregular interstitial material between grains of massive sphalerite (Plate 1e), (3) invading, cementing and/or replacing fractured pyrite (Plate 2a), (4) dendritic replacements of pyrite (Plate 8b and 8c), (5) fine-grained inclusions in pyrite, (6) associated with freibergite, pyrrhotite and scaley masses of marcasite that envelope pyrite (Plate 2h), (7) disseminated grains in chalcopyrite + pyrrhotite matrix, (8) carious blebs to myrmekitic intergrowths with sphalerite and pyrrhotite in highly sheared Banded Pyrite + Sphalerite ores (Plate 8d and 8e), and (9) carious blebs in diablastic-textured chalcopyrite, pyrrhotite and sphalerite in the Sheared Chalcopyrite + Sphalerite ores (Plate 8f). Size analysis data of the galena from 4 ore types yields a cumulative grain size curve defined by 80 % - 52 um, with a somewhat bimodal distribution. This reflects (1) the inclusions in pyrite, interstitial blebs and films between pyrites and/or sphalerites, and the fracture-fillings of galena in pyrite, and (2) the coarser-grained masses that are interstitial to and envelope pyrite and sphalerite, particularly in the Banded Pyrite + Sphalerite and the Massive Sphalerite ore types.

The vast majority of qualitative microprobe analyses of galena, performed on the MAC V, failed to reveal the presence of any trace elements, namely Ag, Bi, Fe, Se and Te. However, analyses of rare graphic-textured galena in Fe-poor sphalerite, and of grains of galena with a slightly blue-white colour (when a daylight filter is interposed) and high reflectivity, indicated the presence of compositions across a wide range of the clausthalite-galena (PbSe-PbS) solid solution. In addition, Ag, Fe and Te were detected in these blue-white coloured galenas, and all (rare) occurrences of galena with this characteristic colour were assumed to lie intermediate within the clausthalite-galena solid solution. These rare and optically and/or texturally distinct varieties are treated separately under the CLAUSTHALITE-GALENA SOLID SOLUTION section, whereas this section only considers the trace element-free, stoichiometric, common variety of galena, at least as determined by the MAC V microprobe. However, wavelength dispersive microprobe analyses of the Ag content of the galenas were generated on the JEOL 733 at CANMET. These analyses indicated an average of 250 ppm Ag in galena, with a maximum value of 1,200 ppm Ag. Because of a poor background correction the analyses generated depressed Ag values, and are therefore considered minimum values.

SPHALERITE (ZnS)

Sphalerite is ubiquitous, and was observed in all the samples examined, generally occurring as a major, and more rarely as a minor or trace constituent. Sphalerite and hence Zn, Cd and possibly Hg tend to be concentrated in the hangingwall massive exhalative ores, specifically in the Massive Sphalerite and the Banded Pyrite + Sphalerite ore types. Galena and a host of antimonial sulfosalts, and hence Pb, Sb and Ag only occur in significant concentrations within these ore types.

The sphalerite is generally anhedral, and occurs typically as an interstitial or matrix mineral. It varies from coarse-grained (≤3mm) to fine-grained, with the grain size generally increasing with the relative abundance of the sphalerite. The dominant textures of sphalerite are (1) as massive coarse-grained matrix sphalerite that is interstitial to both the gangue and the pyrite, particularly in the Massive Sphalerite and Banded Pyrite + Sphalerite ore types (Plate 1a), (2) massive coarse-grained sphalerite with interstitial blebs, films, wedges and irregular masses of chalcopyrite and/or galena in the Massive Sphalerite and the Banded Pyrite + Sphalerite ore types (Plate 1d), (3) generally abundant to occassionally absent "chalcopyrite-disease" (Plate 1c), (4) embayments and development of atoll-textured pyrite by matrix sphalerite (Plate 1b), (5) sphalerite invading and replacing pyrite along fractures and deformation cleavages (Plate 8g), (6) fine-grained inclusions (Plate 8h) and dendritic replacements in pyrite (Plate 2d), and (7) fine-grained carious blebs and myrmekitic intergrowths with chalcopyrite and pyrrhotite in the Sheared Chalcopyrite + Sphalerite ore type (Plate 6a).

The coarse-grained sphalerite of the Massive Sphalerite and Banded Pyrite + Sphalerite ore types particularly, commonly display straight to curved repeated lamellar twinning in unetched, but poorly polished sections with high relief (Plate 1c). These twins are interpreted to be the product of either the initial sphalerite growth and/or more probably twin gliding in response to stress. Fine-grained (approximately 10 to 15um) oriented blebs and rods of chalcopyrite ("chalcopyrite-disease") are observed lying on these twin planes, where the latter are descernible. The "chalcopyrite-disease" is the most common and distinctive textural characteristic of the sphalerite, and its abundance generally increases with the degree of deformation and abundance of matrix chalcopyrite. It is typically most abundant in the Sheared Chalcopyrite + Sphalerite ore type. Traditionally interpreted as the product of exsolution, "chalcopyrite-disease" has recently been interpreted as the product of sphalerite replacement by Cu-rich fluids (Eldridge et al. 1983). The presence of composite blebs of chalcopyrite + galena, chalcopyrite + pyrrhotite and occassionally abundant rods and blebs of pyrrhotite as well as the common peripheral nature of the "chalcopyrite-disease", also suggest that it is not an exsolution texture.

Sphalerite was found to contain several minor and trace elements, namely Fe, Cd and Cu. Mn, In and Ag were sought for, but not detected, while the presence of Hg (inferred from concentrate assays) was obscured by the overlap of the large SKα peak into the R.O.I. of the HgMα. However, the Hg and Zn content of the 1983 Zn-concentrates were 112 ppm and 47.6 Wt %, respectively. Assuming sphalerite to be the sole Zn- and Hg-bearing phase, the calculated Hg content of sphalerite is 0.014 Wt %. This level of concentration is well below the detection limits of the E.D.S. at 15 kV. The approximate detection limit of Hg using the HgMα line is 0.1 Wt %. Six microprobe analyses are presented in Table 8, whereas a complete table of analyses is given in Appendix A.

The six microprobe analyses above are considered representative of the total of 59 analyses collected from 18 samples, and which yield a mean analysis of 33.25 % S, 59.76 % Zn, 6.57 % Fe, 0.16 % Cd and 0.06 % Cu (mean total = 99.84 %). This corresponds to the unit formula $(Zn_{0.882}, Fe_{0.114}, Cd_{0.002}, Cu_{0.001}) S_{1.000}$; stoichiometric Fe-rich sphalerite $(Zn, Fe, Cd, Cu)_{0.999} S_{1.000}$. Cu was detected in 5 of the 59 analyses. It is interpreted as contamination by blebs of chalcopyrite ("chalcopyrite-disease") beneath the surface and hence not visible at the point of analysis, rather than Cu in solid solution. Cd was detected in 34 of the 59 analyses at concentration levels which approximate to the detection limits and yield analytical uncertainties of the order of ± 100% of the determined value. The analyses for Cd are included for completeness only, and cannot be considered as being quantitative. However, assuming that sphalerite is the sole Zn-bearing mineral, the assays of 0.11 % Cd and 47.6 % Zn in the 1983 Zn-concentrates, yields a calculated 0.14 % Cd content in the sphalerite. Thus, the concentrate assays and the microprobe analyses suggest that sphalerite is the sole host of the Cd, and that the concentration level in sphalerite approximates to 0.15 % Cd.

The Fe-content of the sphalerite varies from 1.72 to 8.28 %, which yields an average composition of 6.57 % Fe, but includes 3 analyses of Fe-poor sphalerite that are optically and texturally distinct from all other

TABLE 15

Representative Microprobe Analyses of Sphalerite.

Wt %	1	2	3	4	5	6	7	Uncertainty.
S	33.10	34.08	32.24	33.00	33.27	33.35	33.44	± 0.2
Fe	5.39	8.24	4.85	2.30	6.42	1.72	7.76	± 0.2
Zn	60.26	58.34	61.59	63.58	60.21	65.61	58.67	± 1.2
Cd	-----	0.14	0.12	0.41	-----	0.39	-----	± 0.2
Cu	0.85	-----	-----	-----	-----	-----	-----	± 0.3
Total	99.60	100.80	98.81	99.28	99.91	101.07	99.87	

Number of atoms.

S	1.00	1.00	1.00	1.00	1.00	1.00	1.00
Fe	0.09	0.14	0.09	0.04	0.11	0.03	0.13
Zn	0.89	0.84	0.94	0.95	0.89	0.97	0.86
Cd	-----	0.001	0.001	0.004	-----	0.003	-----
Cu	0.013	-----	-----	-----	-----	-----	-----

* Uncertainty quoted at the 95% confidence limits.

* Unit formula calculated on the basis of 1 sulfur atom.

* A sphalerite standard was employed for Zn and S, whereas a pyrite, chalcopyrite and a Cd-metal standard were employed for Fe, Cu and Cd, respectively.

PLATE 8.

PLATE 8.

PHOTOGRAPH A.

SAMPLE TLS.5-84 : A lamination of annealed pyrite (Py) with interstitial galena (Gal), sphalerite (Sp) and freibergite (Fr). Note the rounded and apparently corroded margins of the pyrite in contact with the galena. Plane polarised light. Bar scale = 160 µm.

PHOTOGRAPH B.

SAMPLE TLS.5-111 : Dendritic galena (Gal) and lesser freibergite (Fr) replacing pyrite (Py) porphyroclast along a zone of shearing. Note the interstitial freibergite filling a large fracture in the pyrite at the upper centre of the photograph. Plane polarised light. Bar scale = 160 µm.

PHOTOGRAPH C.

SAMPLE TLS.5-111 : Dendritic galena (Gal) and lesser sphalerite (Sp) replacing a pyrite (Py) porphyroclast within a zone of shearing. Plane polarised light. Bar scale = 160 µm.

PHOTOGRAPH D.

SAMPLE TLS.1-115 : A highly sheared Banded Pyrite + Sphalerite ore with deformed, fractured and highly corroded pyrite (Py) porphyroclasts in a matrix of sphalerite (Sp). The sphalerite contains abundant carious blebs and myrmekitic masses of galena (Gal) and pyrrhotite (Po), and bot galena and pyrrhotite infill fractures and embayments in the pyrite. Plane polarised light. Bar scale = 160 µm.

PHOTOGRAPH E.

SAMPLE TLS.1-115 : A highly sheared Banded Pyrite + Sphalerite ore with deformed, fractured and highly corroded pyrite (Py) porphyroclasts in a matrix of sphalerite (Sp), as shown in Plate 8d. The sphalerite contains abundant carious blebs and myrmekitic masses of galena (Gal) and pyrrhotite (Po). Both galena and pyrrhotite infill fractures and embayments in the pyrite, form grain coatings on the pyrite, and cement the pyrite grains togethar. Plane polarised light. Bar scale = 160 µm.

PHOTOGRAPH F.

SAMPLE TLN.2-9 : A Sheared Chalcopyrite + Sphalerite ore with carious blebs of galena (Gal - outlined by dashed line) and sphalerite (Sp) in coarse-grained matrix chalcopyrite. Plane polarised light. Bar scale = 40 µm.

PHOTOGRAPH G.

SAMPLE TLS.5-84 : Galena (Gal) and sphalerite (Sp) and trace freibergite envelope, invade and replace a deformed pyrite (Py) porphyroclast along grain boundaries, fractures and cleavages. Plane polarised light. Bar scale = 160 µm.

PHOTOGRAPH H

SAMPLE TLS.3-35(#2) : Entrapped, fine-grained, rounded inclusions of sphalerite (Sp) in pyrite (Py). Plane polarised light. Bar scale = 160 µm.

PLATE 8.

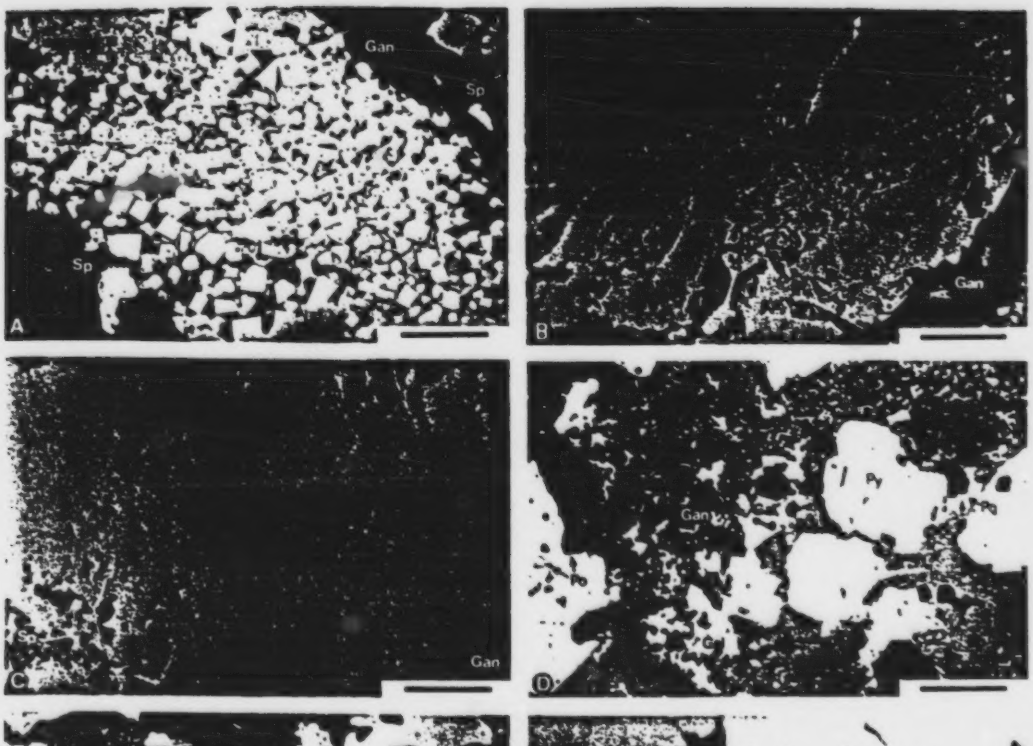
Gan
Sp
Sp
A
Gan
B
Sp
Gan
C
Py
Gan
D
Py
E
F
Sp
Sp
Gan
G
Gan
H

sphalerites. These 3 analyses were collected from an orange-coloured (when viewed under transmitted light) sphalerite with graphic-textured clausthalite-galena solid solution that was only observed in sample TLN.1-87 (Plate 9a). The Fe-poor sphalerite is observed as having crystallised interstitiallly to the red-coloured common variety of sphalerite, as well as invading and corroding the latter along twin planes. Excluding these three analyses, the Fe-content of the red-coloured sphalerite varies from 3.75 to 8.28 %, with an average composition of 33.26 % S, 59.53 % Zn, 6.82 % Fe, 0.15 % Cd and 0.06 % Cu.

ACANTHITE (Ag_2S)

Acanthite constitutes a trace mineral, having been observed in only one polished section. It was detected during image analysis of the Zn-rougher concentrate (#22), using the EDX-assisted routine for the identification of minor minerals. Because it was not observed in an ore sample, it cannot be ascribed to any ore type.

The acanthite occurred as a mass (approximately 50 um in diamter) that enveloped and rounded several enclosed grains of sphalerite and pyrite. Associated with the acanthite were 3 grains (≤5um) of silver amalgam (?). Qualitative microprobe analyses of the amalgam failed to detect Au, and indicated approximately 30 Wt % Hg, suggesting the amalgam possibly constitutes a distinct phase relative to the common mercurian electrum. Semi-quantitative microprobe analyses of the acanthite indicated stoichiometric proportions of Ag (2) and S (1), and failed to detect any minor or trace elements. The acanthite and silver amalgam (?) may constitute additional trace Ag-bearing minerals in the ore, or possibly precipitates formed in the pulp during the processing of the ore, and which therefore suggests dissolution, at least in part, of one or more Ag-bearing minerals (Petruk, pers. comm., 1986).

THE OXIDES

MAGNETITE (Fe_3O_4)

Magnetite is observed in the occassional sample, but where present, it generally constitutes a major to less commonly a trace constituent. The magnetite is observed in many of the more differentiated ore types including the footwall Chalcopyrite Stringer and the hangingwall Banded Pyrite + Sphalerite ore types, and does not exhibit any distinct mineralogical association. It occurs as disseminated grains, in clusters and in laminae within the massive ore and the gangue (Plate 9g), and whose distribution is suggestive of primary mineral banding. It is interpreted that the magnetite is not a product of the original ore deposition, but is a metamorphic product, whose distribution is controlled by the mineralogical and hence chemical banding of the ores.

The magnetite typically occurs as dodecahedral porphyroblasts (Plate 9b), which are generally medium- to fine-grained to less commonly coarse-grained

(≤2mm). The porphyroblasts generally contain inclusions of pyrite, chalcopyrite and sphalerite, and are observed occassionally enveloping and invading fractured pyrite (Plate 9c). The magnetite is thereby interpreted to postdate the porphyroblastic growth of pyrite, and its subsequent deformation. However, in sample TLS.1-53 severe deformation has resulted in the mobilisation of pyrite into veinlets that rim and crosscut the fractured magnetite (Plate 9d). In addition, fringes and zones of fine-grained, reticulate-textured magnetite in pyrite are common in many of the ore types (Plates 3g, 4c, 9e and 9f). This texture is interpreted as the product of incomplete replacement of magnetite by pyrite, or their simultaneous growth during periods of higher oxygen activity.

Ten microprobe analyses of magnetite revealed no detectable trace elements, and only slight apparent variation in stoichiometry. Three microprobe analyses encompassing the full range in composition are presented below. The 10 analyses yield an average composition of 72.15 % Fe and 27.85 % O, which compares favourably with the ideal composition of 72.36 % Fe and 27.64 % O for pure end-member magnetite.

TABLE 16

Representative Microprobe Analyses of Magnetite.

Wt %.	1	2	3	Uncertainty.
Fe.	72.35	71.60	72.59	± 0.6
O.	27.65	28.40	27.41	
At %.				
Fe.	42.84	41.94	43.13	
O.	57.16	58.06	56.87	

* Unceratinty quoted at the 95% confidence limits.

* Oxygen is not amenable to electron microprobe anaysis and is calculated by difference from 100% (not by stoichiometry).

CASSITERITE

Cassiterite is a trace constituent of the ores, that was identified during image analysis of the mill products. Because it was not detected in any of the ore samples, it cannot be ascribed to any of the ore types. It occurs in the mill products as ≤25 um grains with an approximate mean grain size of 10 to 15 um. It generally occurs locked with chalcopyrite or sphalerite, and was observed with greater frequency in the Cu-circuit. Qualitative microprobe analysis of the cassiterite indicated pure (minor element-free) SnO_2.

INTERMETALLIC AND ALLOY-LIKE COMPOUNDS

MERCURIAN ELECTRUM (Ag,Au,Hg,Fe)

Electrum was observed in 37 of the 112 samples which were petrographically examined. The mineral was found in all the ore types, except the Vein Quartz - Chalcopyrite ore type. The mineral quantities derived from chemical assays indicate that the Massive Pyrite, Disseminated Pyrite - Chalcopyrite and the Massive Sphalerite ore types contain the lowest amounts, and the Sheared Chalcopyrite Sphalerite, the Vein Quartz + Chalcopyrite and the Banded Chalcopyrite Sphalerite contain the highest amounts of electrum. However, since only three samples of the Vein Quartz + Chalcopyrite were examined it is likely that the mineral is present in the amounts indicated by the chemical assays. The electrum is invariably a trace constituent, but in sample TLN.1-89, a Chalcopyrite Stringer ore, 'visible' electrum consisting of a 2 mm long anastomosing mass that contributed to a calculated 0.2 Area % of the polished section, was observed (Plate 5e). A second polished section of this same sample, constituting a plane separated from that of the first by 4 to 8mm down the fold plunge and along the foliation, contained several larger masses of electrum.

The electrum was recognised as occurring in three textural types: (1) fine-grained electrum occurring as inclusions in, as fracture-fillings in, and as films on, pyrite grains, (2) large (≤ 2mm) masses and associated disseminations in massive chalcopyrite (Plate 5e), and (3) fine-grained inclusions in galena/freibergite interstitial masses in pyrite (Plate 9h). Electrum of type 1 consists of (A) fine-grained discrete inclusions or part of composite inclusions composed of other minerals, particularly chalcopyrite and/or pyrrhotite, in pyrite (Plate 10a), (B) fracture-fillings in pyrite, generally associated with chalcopyrite, sphalerite and/or pyrrhotite, which cement or corrode the fractured pyrite host (Plate 10b and 10c), and (C) as films on the margins of, and as interstitial films and wedges between pyrite grains, and generally associated with sphalerite and/or chalcopyrite (Plate 10c and 10d). The volumetrically insignificant type 3 electrum is probably an extension of type 1, where the electrum is associated with and occurs as inclusions in galena and freibergite that occurs as interstitial masses in, and cements fractured pyrite (Plates 2e, 11a and 11b). Type 2 was observed in 2 samples; TLN.1-89 and TLN.2-11. This electrum consists of anastomosing masses and lesser disseminations that are distributed along the chalcopyrite - chlorite schist contact (Plates 5e, 10e, 10f, 10g and 10h), and which envelopes and corrodes the chalcopyrite and coexisting sulphides (Plate 11c).

Type 1 electrum is found in all but one (See above) ore type, and is by far the most common type. Type 2 occurs only in the Chalcopyrite Stringer ores, and despite being relatively rare, it undoubtedly constitutes the most volumetrically significant type. Type 3 is both relatively rare and volumetrically insignificant, and is restricted to the Massive Pyrite and the Banded Pyrite + Sphalerite Ore Types.

A total of 85 wavelength dispersive electron microprobe analyses of the electrum were generated using the JEOL 733 Superprobe at CANMET. These analyses revealed the presence of the Ag, Au, Hg and Fe in varying proportions. Six analyses are presented below, and cover the entire range in elemental concentrations observed, whereas a complete table of the analyses is presented in Appendix B.

The 85 analyses yield an average composition of 46.97 % Ag, 41.37 % Au, 10.64 % Hg and 0.73 % Fe, with a mean total of 99.72 %. The Ag varies from 17.23 to 68.70 % Ag, the Au from 1.62 to 79.86 % Au, the Hg from 1.29 to 30.87 % Hg, and the Fe from undetected ($\leq$ 0.05) to 3.49 % Fe. The Fe content is anomalous in that it is not known to occur in native metals and alloys, as determined by microprobe analyses (Cabri, pers. comm., 1986). The Fe content is attributable to the following possible causes: (1) Fe in solid solution in electrum, (2) contamination of the analyses by primary excitation or secondary fluorescence of FeKα in adjacent Fe-bearing minerals eg., pyrite, (3) residual discrete submicroscopic 'islands' of pyrite or chalcopyrite enveloped in the electrum and thus included in the analytical volume, and (4) micron-sized particles of pyrite embedded in the 'soft' electrum during polishing, as indicated by a 'pock-marked' surface as seen by B.S.E. imagery. Higher and more erratic concentrations of Fe were detected in type 1 electrum, suggesting point 2 above. However, electrum that is replacing pyrite is likely to contain higher concentrations of Fe than type 2 electrum which is replacing chalcopyrite. Two analytical methods are available to determine the cause of the anomalous Fe content, and these are (1) wavelength dispersive electron microprobe analyses, and observing the relationship between the Fe content and any detected S content, which is not visible on the energy dispersive spectrum, and (2) Auger electron spectroscopy to determine the nature of the bonding of the Fe i.e., pure metallic or partly covalent as in pyrite. If the Fe is determined not to be in solid solution in the electrum, then many of the present analyses will be rejected, as the Fe content is sufficiently large (> 0.5 Wt % Fe) to degrade the quality of the analysis.

A review of the literature, has indicated that most analyses of naturally occurring alloys of these three elements are resolved into the binary systems Ag-Hg (eg., silver amalgam), Au-Hg (eg., gold amalgam) and Au-Ag (eg., electrum). However, Scott (1977), Nazmova and Spiridnov (1979), Basu et al. (1981), Nysten (1986) and other workers have reported naturally occurring alloys of Ag and Au with major concentrations of Hg. These 'ternary amalgams' correspond to the α-phase binary solid solutions of the Au-Hg and Ag-Hg systems extrapolated into the Ag-Au-Hg ternary system. Nysten (1986) refers to these amalgams as gold silver amalgams. Amalgam is defined as "the naturally occurring alloy of silver with mercury" or "a general term for alloys of mercury with one or more well known metals", whereas electrum is defined as "the naturally occurring alloy of gold with silver" (Bates and Jackson, 1980). As mercury is the subordinate major element, and the minimum silver content is

TABLE 17

Six Representative Microprobe Analyses of Electrum.

WT %.	1	2	3	4	5	6	Std. Dev.
Ag.	68.70	17.34	66.28	27.85	37.47	43.03	± 0.5 - 0.6
Au.	8.04	79.86	1.62	67.18	54.52	43.96	± 0.5 - 5.8
Hg.	22.71	2.68	30.87	1.29	4.92	11.80	± 0.5 - 3.8
Fe.	0.01	0.55	1.59	2.20	3.49	0.30	± 0.8 - >>
Total.	99.43	100.40	100.34	98.49	100.37	99.06	

* Standard deviation quoted at the 95% confidence limits.

* Operating Conditions :

Excitation voltage : 20 kV.

Sample Current : 15 nA on the Faraday Cup.

Count Time : 60 secs or until 0.5 % standard deviation on the standard or unknown is reached.

Ag : AgLα analytical line; PET crystal; Ag-Au alloy (71.6 Wt % Ag, 28.4 Wt % Au) standard.

Au : AuMα analytical line; PET crystal; Ag-Au alloy (50.1 Wt % Ag, 49.9 Wt % Au) standard.

Hg : HgLα analytical line; LIF crystal; Temagamite (Pd_3HgTe_3) standard.

Fe : FeKα analytical line; LIF crystal; Pyrite standard.

17.34 %, the term mercurian electrum was employed in his report in preference to gold silver amalgam, etc..

The analyses are plotted on a Ag-Au-Hg ternary compositional diagram, which portrays the composition of several known alloys of the separate binary systems (Fig 17). The three binary systems Ag-Hg, Au-Hg and Au-Ag form the joins between the apices, which themselves represent the three native metals. The Au-Ag join is considered to be a complete solid solution (Craig and Scott, 1976), whereas the Ag-Hg and Au-Hg joins represent apparenlty discontinuous solid solutions with the discrete stoichiometric compositions of individual mineral species eg., moschellandsbergite (Ag_2Hg_3). The present analyses form an extremely large field adjacent to the Ag-Au join, which exhibits a general increase in the Hg with increasing Ag and decreasing Au. The analyses confirm the presence of a large field of solid solution within the ternary system, which corresponds to the cubic α-phase solid solution of Basu et al. (1981). These authors, in the absence of experimental work on the Ag-Au-Hg ternary system, combined the three binary systems (i.e., Ag-Au, Ag-Hg and Au-Hg) to determine the stability field for the cubic α-phase. These same authors, presuming no other ternary solid phase, constructed a schematic 450° C isothermal section of the ternary system, which defines the extrapolated stability field of the α-phase. It can also be inferred that the α-phase solid solution field exists, though it becomes more restricted with increasing temperature of the system, at least up to 900° C. In addition, extensive liquid fields exist down to and below 421° C, at the Hg-rich apex of the ternary diagram. Below this temperature, the Hg-rich apex of the ternary diagram is uncertain, because it is not known whether the stoichiometric phases eg., β-phase observed in the appropriate binary systems extend into the ternary field, and if so whether the stability fields are unchanged (Basu et al. 1981).

The analyses were also plotted on the schematic 450° C isothermal section of the Ag-Au-Hg ternary system (Fig 18), a geologically reasonable temperature for the greenschist facies metamorphic grade at Trout Lake. All the analyses plot within the α-phase solid solution field and span virtually the entire range of known compositions of this phase (Nysten, 1986). In fact, analyses from type 2 electrum in Sample TLN.1-89 span the entire compositional range exhibited at Trout Lake, except for the extreme Ag- and Hg-rich end of the field. The most Ag- and Hg-rich composition was encountered in type 1 electrum, which formed an inhomogenous inclusion in pyrite within a Massive Sphalerite ore, eg., TLS.1-52.

The analyses of type 2 electrum from Sample TLN.1-89 highlight the extreme compositional inhomogeneity of the electrum (See Appendix 3). High resolution, high contrast B.S.E. imagery (on the JEOL 733) was employed to select analytical points on composite grains of distinctly different compositions. This procedure secured analyses of the extreme compositions. This would not have been possible without the B.S.E. imagery, and lead in the past to analyses with more medium range compositions, because of contributions from several adjacent grains, due to poor analytical site selection while using the MAC V at the U. of M.. The inhomogeneity of the electrum is clearly discernible in the B.S.E. photograph of a portion of the large anastomosing mass in Sample TLN.1-89 (Plate 10f). The mass consists of complexly intergrown grains of distinctly different compositions. Each grain appears relatively homogenous and unzoned, though the numerous grey levels exhibited by different grains indicates a large number of distinct compositions are present. Such inhomogeneity suggests (1) unmixing and breakdown of the α-phase solid solution on cooling, leading to the crystallisation of numerous low temperature phases, or (2) variations in the activities of Ag, Au and Hg in the pore fluids, leading to nonequilibrium conditions during metamorphism. The fact that all the compositions observed lie within the extrapolated α-phase stability field, that complete solid solution is observed in the Ag-Au binary system, and that up to 20 and 50 Wt % Hg is completely soluble in the Au-Hg and the Ag-Hg binary systems, respectively, points to nonequilibrium conditions. In addition, textural evidence suggests sequential crystallisation of increasingly Ag- and Hg-rich compositions. Within the mass of type 2 electrum in Sample TLN.1-89, high Au compositions occur as discrete grains ($\leq$10um) enveloped in more medium-ranged compositions, which are themselves infilled by Ag- and Hg-rich compositions, which tend to fill the interstices between the former grains. This observation is in good agreement with the progressively increasing Hg content, with decreasing temperature, of analyses of amalgams as reported by Ozerova et al. (In Basu et al. 1981). Mercury being a highly mobile element is likely to be available in the metamorphic pore fluids during late crystallisation and retrogressive metamorphism.

As mentioned earlier, the analyses of type 2 electrum yield compositions which span virtually the entire composition field of Trout Lake electrums. This suggests that the electrum of all three types was deposited by a single mechanism. Boyle (1979) postulates that pyrite at high temperature contains Au and Ag in solid solution, and that on cooling the Au and Ag, which now distort the lattice, migrate by solid state diffusion to sites of low chemical potential, such as fractures and grain boundaries. This process however cannot explain the distribution and localised abundance of the electrum of type 2, nor the high Hg content of the electrum.

A process combining solid state diffusion of the type discussed and fluid state mobilisation is proposed. Au and Ag liberated by the breakdown of pyrite are taken up into the migrating pore fluids, as is the Hg liberated during the metamorphic recrystallisation of sphalerite. Jonasson and Sangster (1975) determined that the Hg content of canadian sphalerites decrease with the age of the hostrocks, possibly suggesting that Hg is liberated during metamorphism. Once in solution migration occurs to areas of low stress and strain rates eg., nose of a minor overturned fold, which is the site of the 2mm long mass of electrum in TLN.1-89, or to areas where solid state diffusion of Au and Ag is proceeding in pyrite, with resulting nucleation.

PLATE 9.

PLATE 9.

PHOTOGRAPH A.

SAMPLE TLN.1-87 : Graphic-textured clausthalite-galena (Cl) solid solution in Fe-poor sphalerite (outlined by a solid line), which envelopes, invades and corrodes the Fe-rich common variety sphalerite (Sp). Plane polarised light. Bar scale = 160 µm.

PHOTOGRAPH B.

SAMPLE TLS.3-16 : Coarse-grained, fractured and corroded magnetite (Mag) porphyroclasts containing abundant inclusions of pyrite (Py) and chalcopyrite (Cp). Note the fine-grained swirls (Sw) of gangue forming in the vortices of compression around the magnetite porphyroclasts. The chalcopyrite matrix also contains minor rounded pyrite disseminations and carious blebs of sphalerite (Sp). Plane polarised light. Bar scale = 325 µm.

PHOTOGRAPH C.

SAMPLE TLS.3-42 : Anhedral, fractured magnetite (Mag) porphyroclasts enveloping and invading (indicated by arrow) deformed pyrite (Py) along fractures and cleavages. Chalcopyrite (Cp) and lesser pyrrhotite (Po) and sphalerite (Sp) form the interstitial matrix around the magnetite, and invade and corrode fractures in both magnetite and pyrite. Plane polarised light. Bar scale = 160 µm.

PHOTOGRAPH D.

SAMPLE TLS.1-53 : Anhedral to subhedral magnetite (Mag) porphyroblasts enveloping rare pyrite (Py) grains and being enveloped, invaded and corroded by a thin film of pyrite. Plane polarised light. Bar scale = 160 µm.

PHOTOGRAPH E.

SAMPLE TLS.3-46 : A granular mass of pyrite (py) with zones and fringes of reticulate-textured magnetite (Mag), in a matrix of coarse-grained chalcopyrite (Cp), pyrrhotite (Po) and minor sphalerite (Sp). Plane polarised light. Bar scale = 160 µm.

PHOTOGRAPH F.

SAMPLE TLS.3-46 : A zone of reticulate-textured magnetite (Mag) in pyrite (Py). The matrix consists predominantly of pyrrhotite (Po) and chalcopyrite. Plane polarised light. Bar scale = 40 µm.

PHOTOGRAPH G.

SAMPLE TLN.1-114 : A disrupted pod of annealed magnetite (Mag) in a matrix of carbonate gangue (Gan) and sphalerite (Sp). Note the preserved 120° triple junctions and the relatively equigranular and mosaic texture of the polygonal mass. Plane polarised light. Bar scale = 160 µm.

PHOTOGRAPH H.

SAMPLE TLS.2-40(#2) : Detail of the area indicated by the upper arrow in Plate 2e. The freibergite (Fr) contains networked and interconnecting blebs of exsolved chalcopyrite (Cp), inclusions of sphalerite (Sp) and fine-grained disseminations of type 3 electrum (El). Plane polarised light. Bar scale = 40 µm.

PLATE 9.

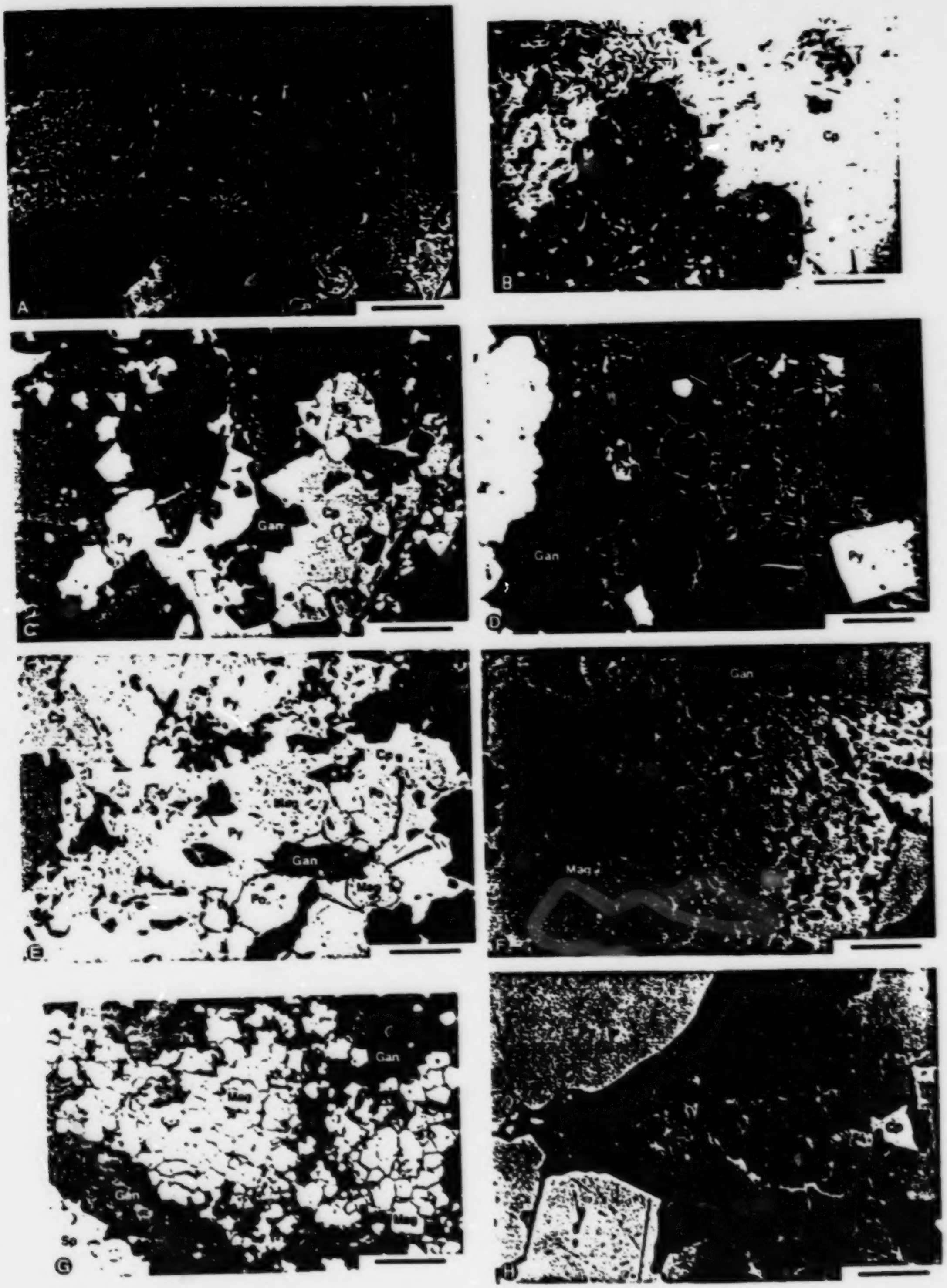

A
Cp
Po Py
Cp
B
Gan
Cp
Py
C
Gan
Py
D
Cp
Mag
Py
Py
Gan
Po
Mag
E
Gan
Mag
Mag
F
Gan
Mag
Gan
Mag
Sp
G
Cp
H

PLATE 10.

PLATE 10.

PHOTOGRAPH A.

SAMPLE TLN.2-8 : A composite, fine-grained inclusion of type 1 electrum (El) and chalcopyrite (Cp) in pyrite (Py). Plane polarised light. Bar scale = 40 µm.

PHOTOGRAPH B

SAMPLE TLN.2-8 : A fine-grained inclusion of type 1 electrum (El) forming in a fracture in pyrite (Py). Note the rounded inclusion of chalcopyrite (Cp). Plane polarised light. Bar scale = 40 µm.

PHOTOGRAPH C.

SAMPLE TLN.2-8 : Type 1 electrum (El) forming grain coatings on and fracture-fillings in pyrite (Py). Sphalerite (Sp) and chalcopyrite (Cp) are the dominant matrix sulfides, and are interstitial to the pyrite. Plane polarised light. Bar scale = 40 µm.

PHOTOGRAPH D.

SAMPLE TLN.2-8 : Type 1 electrum (El) forming grain coatings on pyrite (Py). Electrum is associated with interstitial sphalerite (Sp) and lesser chalcopyrite (Cp). Note the pyrite grains are well rounded. Plane polarised light. Bar scale = 40 µm.

PHOTOGRAPH E.

SAMPLE TLN.1-89 : Low magnification BSE photograph of the anastomosing mass of type 2 electrum shown in Plate 5e. The electrum (El - white) crystallised along the chalcopyrite - schist contact within the nose of a fold, a zone of low stress and strain rates. Note the carious texture of the sphalerite (Sp - light grey) and pyrrhotite (Po - dark grey) in the matrix chalcopyrite (Cp - medium grey). BSE. Bar scale = 250 µm.

PHOTOGRAPH F.

SAMPLE TLN.1-89 : High magnification BSE photograph of the area indicated by the arrow in Plate 10e, and showing electrum (El - white to grey) and gangue (Gan - black). The high contrast image demonstrates the existence of chemically homogeneous grains with complex grain relationships forming the anastomosing mass. BSE. Bar scale = 30 µm.

PHOTOGRAPH G.

SAMPLE TLN.2-11 : A similar, but smaller anastomosing mass of type 2 electrum (El) also having crystallised on the chalcopyrite - schist contact. BSE. Bar scale = 50 µm.

PHOTOGRAPH H.

SAMPLE TLN.2-11 : Detail of Plate 10g. Note the tarnishing (T) of the chalcopyrite (Cp) due to the decomposition of the adjacent electrum (El). BSE. Bar scale = 25 µm.

PLATE 10.

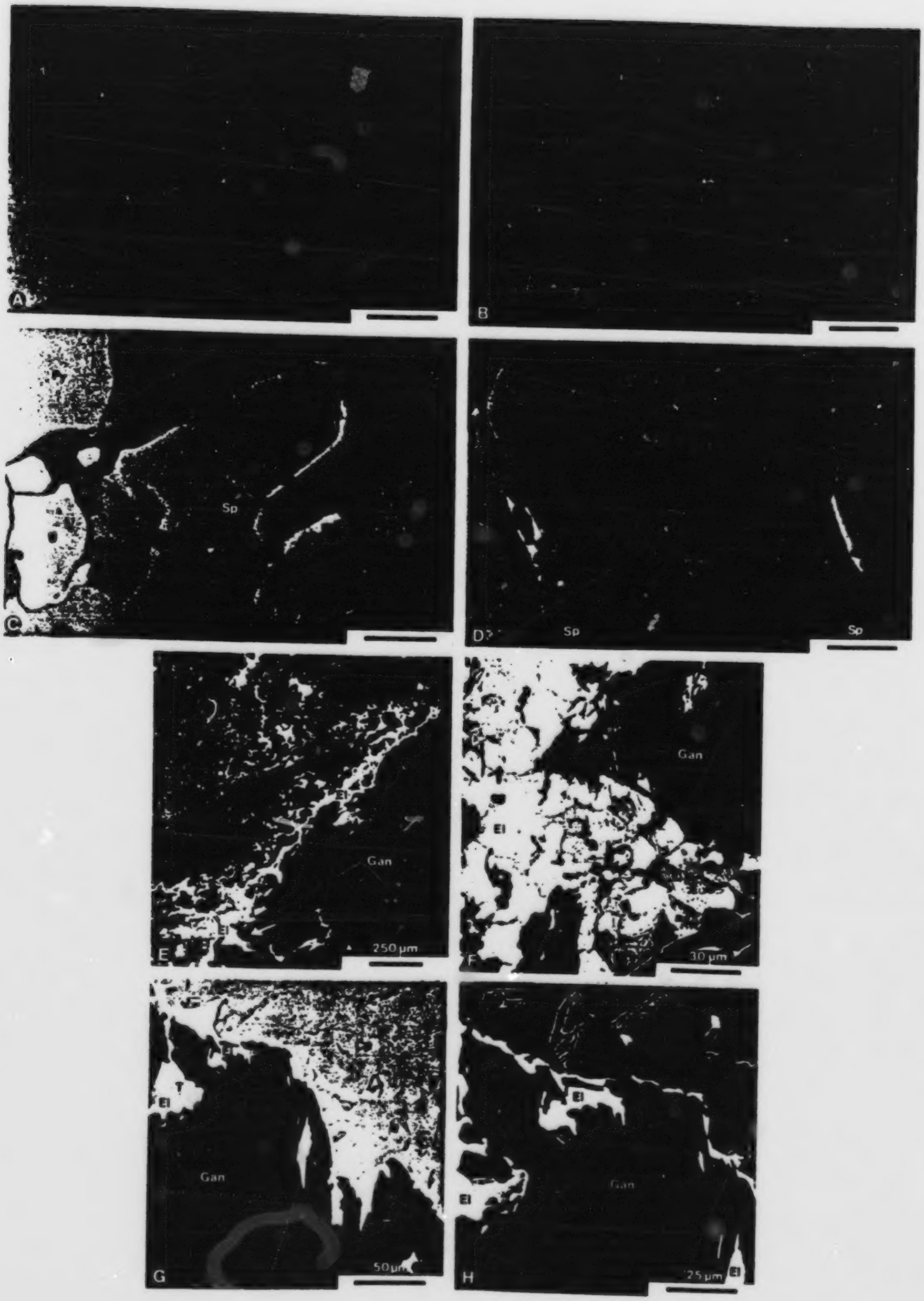
A
B
C
Sp
D?
Sp
Sp
E
El
Gan
El
250 µm
F
Gan
El
30 µm
G
El
T
El
Gan
50 µm
H
El
El
Gan
25 µm
El

FIGURE 17

Ag–Au–Hg Ternary Compositional Diagram (by Wt%)
Portraying the Composition of the Trout Lake Mercurian Electrum.

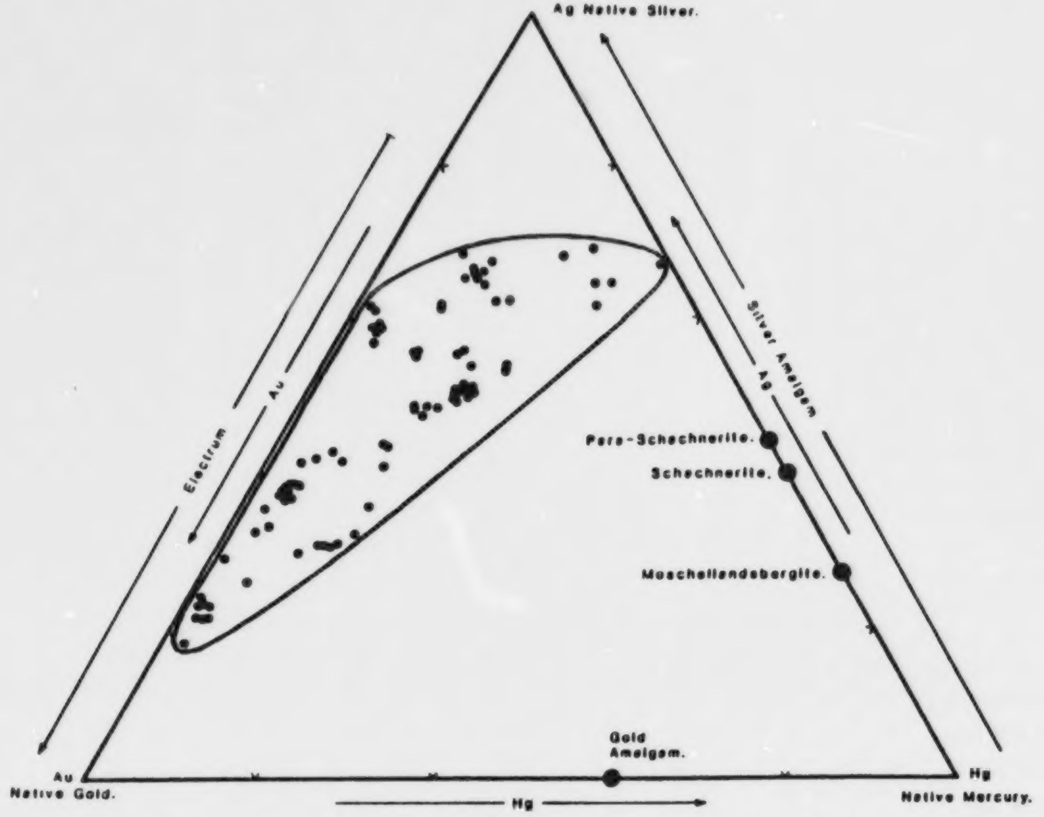

FIGURE 18

Schematic 450°C Isothermal Section of the Ag-Au-Hg Ternary System (by Wt%)
Portraying the Composition of the Trout Lake Mercurian Electrum.

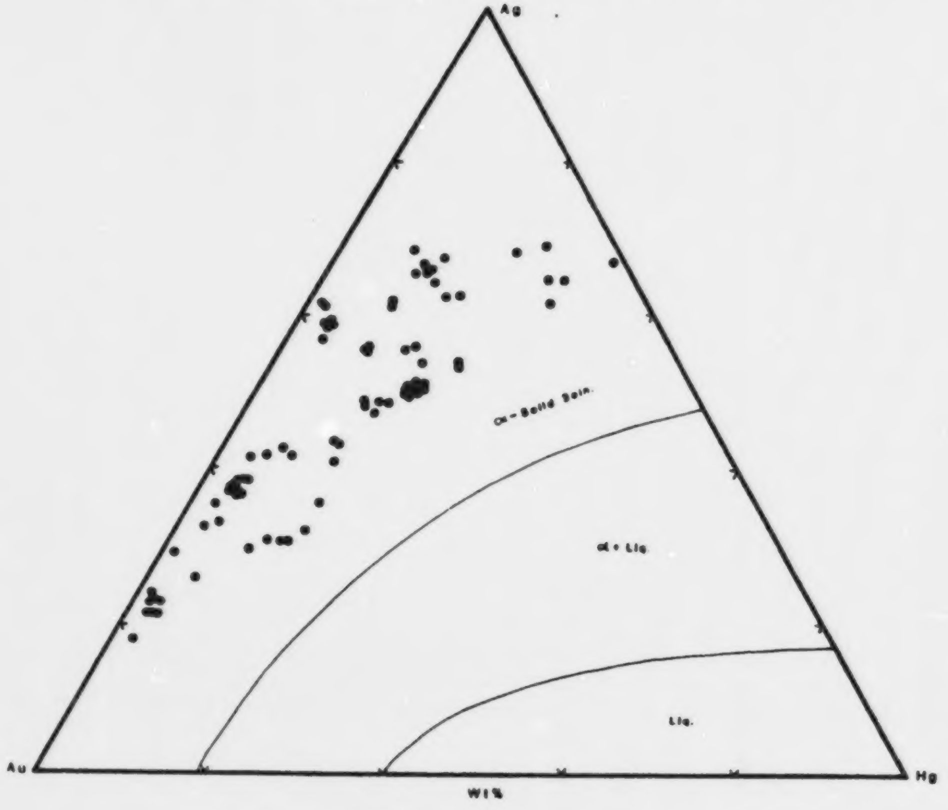

DYSCRASITE (Ag_3Sb)

Dyscrasite is a rare constituent of the ores. It was found in two samples of the Banded Pyrite + Sphalerite ore type. In sample TLS.5-83A, the dyscrasite occurs as fine-grained (≤10um) inclusions in freibergite that is associated with galena which cements large fractures in pyrite porphyroblasts (Plate 11d). Dyscrasite was also observed as globular fine-grained (≤5um) inclusions in galena that also contained intergrowths of lesser gudmundite in sample TLS.5-84. The mineralogical association of dyscrasite with freibergite, galena and gudmundite in Banded Pyrite + Sphalerite ores is consistent with the strong geochemical affinity of Pb, Sb and Ag in Zn-rich ores.

One quantitative wavelength dispersive electron microprobe analysis of the dyscrasite was generated using the JEOL 733 at CANMET. The determined composition of 75.43 Wt % Ag and 23.61 Wt % Sb (total = 99.03 Wt %) yields a unit formula of $Ag_{3.1}Sb_{0.9}$, which corresponds closely to the stoichiometric dyscrasite composition. The composition lies within the narrow dyscrasite subsolidus field (23 to 27 Wt % Sb) between 200° and approximately 500° on the phase diagram for the Ag-Sb system (Petruk et al. 1969). Dyscrasite is included in a group of minerals termed alloy-like compounds (Ramdohr, 1980).

THE ANTIMONIAL SULFOSALTS

FREIBERGITE ($(Cu,Ag)_{10}(Fe,Zn)_2(Sb,As)_4S_{13}$)

Freibergite is the name applied to argentian tetrahedrite with greater than 20 Wt % Ag (Riley, 1974), and tetrahedrite when the mineral contains less than 20 Wt % Ag. Microprobe analyses of the Trout Lake tetrahedrite/freibergite indicated compositions that span this 20 Wt % boundary, but that yield an average Ag content of 21.7 % Ag. For convenience all phases in the tetrahedrite-freibergite solid solution series are referred to as freibergite in this study.

Freibergite is a trace constituent of the ores, and was found only in samples of the Massive Sphalerite, Banded Pyrite + Sphalerite and the Massive Pyrite ore types. Therefore, freibergite is concentrated in the hangingwall to central parts of the stratigraphic sequence. It is most commonly observed in the Banded Pyrite + Sphalerite ores, where it may constitute 0.1 Vol %, as in TLS.2-26, rather than the typical quantities of ≤0.05 % in the Massive Pyrite and Massive Sphalerite ore types. The freibergite occurrred only as inclusions in, or discrete grains associated with galena, and tends to be less abundant where the galena is associated with prominent chalcopyrite. Freibergite along with the other Sb-sulfosalts (except costibite) and dyscrasite are concentrated in the hangingwall Zn-rich ores, but only where galena attains prominence. As stated in the section on dyscrasite, this mineralogical association is consistent with the strong geochemical affinity of Pb, Sb and Ag in the distal, Zn-rich ore, which are the equivalent of the 'Kuroko' or Black' ores of the Kuroko deposits, Japan.

Freibergite is invariably anhedral, and varies from generally fine-grained rounded inclusions in galena, to rare medium-grained (≤500um) interstitial grains associated with galena. The dominant textures exhibited by freibergite are (1) extremely fine-grained (≤25um) rounded inclusions marginally located within interstitial galena in massive sphalerite (Plate 1e), (2) anhedral, fine- to medium-grained inclusions in, or discrete grains associated with interstitial galena in massive sphalerite (Plate 3b), (3) interstitial masses of galena and freibergite that envelope, invade, cement and/or replace fractured pyrite in the Banded Pyrite + Sphalerite ores (Plate 2a, 2e and 2g), (4) freibergite associated with galena, pyrrhotite and foliated scaley masses marcasite replacing pyrite (Plate 2h), and (5) myrmekitic intergrowths in galena (Plate 11e).

Sixty quantitative energy dispersive electron microprobe analyses of the freibergite reveal the consistent abundance of the major elements Cu, Ag, Fe, Sb and S, and the variably minor, trace to undetected concentrations of Zn and As. Seven analyses are presented in Table 18, whereas a complete table of the analyses is presented in Appendix C.

The detection limit for the AsLα line is approximately 0.2 % As, because of its position on the inclined and structured 'front end' of the spectrum, and also because of the severe absorption of this 'soft' wavelength. As a result of the low tennantite component ($Cu_{12}As_4S_{13}$) in the freibergite, the analyses suffer from poor sensitivity in the As-determinations. In addition, the overlap of the CuKß into the ZnKα R.O.I., and its subsequent routine stripping, degraded the peak shape and increased the uncertainty in the Zn-determinations, which were based on the small ZnKα peak. The Ag L-series peaks were also routinely stripped out from the SbLα R.O.I.. Because of the uncertainties generated in the analyses by these limitations in the energy dispersive analysis of freibergite, and because of the probability of non-stoichiometric compositions, the number of atoms per unit formula was calculated on the basis of 13 sulfur atoms, rather than a given number of cations.

The most notable deviations in stoichiometry are the consistently (except one analysis) high number of atoms of Fe + Zn per unit formula ($\bar{x} = 2.23$), and the deficiency in the Cu + Ag ($\bar{x} = 9.88$). It is apparent that the widely used general formula for the tennantite-tetrahedrite solid solution $(Cu,Ag)_{10}(Fe,Zn)_2(Sb,As)_4S_{13}$ does not fully describe the substitution of Ag, Fe and Zn into the ideal end-members tetrahedrite ($Cu_{12}Sb_4S_{13}$) and tennantite ($Cu_{12}As_4S_{13}$). The author suggests that the use of the general formula $(Cu,Ag,Fe,Zn)_{12}(Sb,As)_4S_{13}$ better describes the composition of the Trout Lake freibergite.

The 60 analyses yield an average composition of 22.78 % S, 5.58 % Fe, 1.14 % Zn, 21.58 % Cu, 21.68 % Ag, 0.20 % As and 26.66 % Sb, with a mean total of 99.82 %. This composition translates into the unit formula

$$(Cu_{6.18},Ag_{3.70})(Fe_{1.83},Zn_{0.40})(Sb_{4.00},As_{0.05})S_{13.00}$$

or

$$(Cu,Ag,Fe,Zn)_{12.11}(Sb,As)_{4.05}S_{13.00}$$

TABLE 18

Representative Microprobe Analyses of Freibergite.

Wt %.	1	2	3	4	5	6	7	Uncertainty.
S.	22.53	23.63	21.77	24.24	24.02	23.03	22.19	± 0.1 - 0.2
Fe.	5.59	5.67	6.52	5.88	5.98	5.62	4.83	± 0.2 - 0.3
Zn.	1.54	1.46	1.20	1.45	1.89	----	2.65	± 0.4 - 0.5
Cu.	20.37	23.26	14.73	28.46	27.51	24.12	22.80	± 0.5 - 0.6
Ag.	22.22	18.83	30.31	14.76	13.05	18.97	20.21	± 0.2 - 0.4
As.	-----	-----	-----	2.83	-----	-----	-----	± 0.0 - 0.5
Sb.	26.61	28.10	26.33	23.64	27.97	27.25	26.30	± 0.4 - 0.5
Total.	98.86	101.04	100.85	101.27	100.42	98.99	98.97	
Number of atoms.								**Ideal.**
S.	13.00	13.00	13.00	13.00	13.00	13.00	13.00	13.00
Fe.	1.85	1.79	2.23	1.81	1.86	1.82	1.62	
Zn.	0.44	0.39	0.35	0.38	0.50	----	0.76	2.00
Cu	5.93	6.48	4.44	7.70	7.52	6.87	6.74	
Ag.	3.81	3.08	5.38	2.35	2.10	3.18	3.52	10.00
As.	----	----	----	0.65	----	----	----	
Sb.	4.04	4.07	4.14	3.34	3.99	4.05	4.06	4.00
Comment.	Average type.	High Sb.	High Ag.	High Cu, As.	Low Ag.	Low Zn.	High Zn.	

* Uncertainty quoted at the 95% confidence limits.
* Unit formula calculated on the basis of 13 sulfur atoms.
* A pyrite standard was employed for S and Fe, whereas a chalcopyrite, sphalerite, arsenopyrite, Ag-metal and a stibiotantalite ($SbTaO_4$) standard were employed for Cu, Zn, As, Ag and Sb, respectively.

which constitutes near stoichiometric freibergite close to the tetrahedrite composition.

The analyses exhibit the diadochic substitutions of Sb-As, Cu-Ag and Fe-Zn. The coupled substitution of Sb + Ag = Cu + As is not clearly defined because of the detection limit and sensitivity for As. Miller and Craig (1983) point out that the correlation of Ag with Sb is not linear, but merely 'permissive', such that high Sb may be accompanied by high Ag, whereas high As is always accompanied by high Cu and low Ag. This is apparent from analyses 4 and 5, where analysis 5 contains higher Sb, yet lower Ag than analysis 4. The Ag values for all 60 analyses range from 13.05 to 30.31 % Ag, yet the As values do not exceed 2.83 % As, ie., 0.65 atoms per unit formula. It is noteworthy that the most Ag-poor analyses were collected on a large mass of freibergite with networked blebs of chalcopyrite interpreted as an exsolution product, and euhedral inclusions of arsenopyrite.

GUDMUNDITE ($FeSbS$)

Gudmundite is observed in the occassional sample and invariably constitutes a trace constituent. It was observed in the hangingwall Banded Pyrite + Sphalerite and Massive Sphalerite ores, where galena attains prominence. However, it was also observed (1) associated with pyrrhotite in a rim of sphalerite at the contact with a quartz vein, and (2) associated with graphic-textured clausthalite-galena solid solution in late Fe-poor sphalerite. Gudmundite is less abundant than freibergite, but more abundant than pyrargyrite. Both freibergite and gudmundite are characteristic and essential minerals of the Zn, Pb, Sb and Ag geochemical association, whereas pyrargyrite, boulangerite, freieslebenite and native silver are non-essential.

The gudmundite varies from fine-grained to rarely medium-grained (≤150um). It also varies from euhedral to anhedral depending on the textural association. The dominant textures exhibited by gudmundite are (1) fine-grained, euhedral, bladed to tabular, subhedral to rounded inclusions in galena (Plates 1e, 3a and 11h), (2) lobate and myrmekitic intergrowths with galena (Plate 11g), (3) myrmekitic intergrowths with pyrrhotite and associated with freibergite, as a reaction rim on pyrite (Plate 11f), and (4) anhedral grains associated with pyrrhotite that are disseminated in the matrix sphalerite.

Gudmundite was found to contain neither detectable trace elements nor any significant deviations from stoichiometry. Eight microprobe analyses are presented in Table 19.

TABLE 19

Microprobe Analyses of Gudmundite.

Wt %.	1	2	3	4	5	6	7	8	Uncertainty.
S.	15.28	15.36	15.20	15.42	15.19	15.13	15.66	15.18	± 0.2
Fe.	26.63	26.66	26.96	27.09	26.48	27.25	26.58	26.22	± 0.4
Sb.	57.63	57.89	58.12	57.96	57.94	58.29	57.65	57.84	± 0.7
Total.	99.54	99.91	100.28	100.47	99.60	100.67	99.89	99.24	
Number of atoms.									
S.	1.00	1.00	0.99	1.00	1.00	0.98	1.02	1.00	
Fe.	1.00	1.00	1.01	1.01	1.00	1.02	0.99	0.99	
Sb.	1.00	1.00	1.00	0.99	1.00	1.00	0.99	1.01	

* Uncertainty quoted at the 95% confidence limits.
* Unit formula calculated on the basis of 3 atoms.
* A pyrite and a stibiotantalite standard were employed for Fe and S and Sb, respectively.

PYRARGYRITE (Ag_3SbS_3)

Pyrargyrite otherwise known as 'Ruby Silver' is a rare constituent of the ores. It invariably occurs as anhedral inclusions associated with pyrrhotite and/or gudmundite inclusions within interstitial masses of galena in the Massive Sphalerite, and less commonly the Banded Pyrite + Sphalerite ore type (Plate 11h). The pyrargyrite occurs in sphalerite-rich ores with abundant galena, and is invariably subordinate to freibergite (except in TLS.5-64 i.e., 0.02 Vol % pyrargyrite and 0.01 Vol % freibergite). It is a characteristic, but non-essential mineral of the Zn, Pb, Sb and Ag geochemical association.

Several microprobe analyses of pyrargyrite were attempted, but the fine-grained (≤20um) nature of the pyrargyrite, and calibration and tarnishing problems resulted in only one acceptable analysis. This analysis is given below.

17.25 % S, 59.38 % Ag and 22.46 % Sb (Total = 99.09 %).

which translates into the unit formula

$$Ag_{3.07}, Sb_{1.03}, S_{3.00}$$

No As was detected.

BOULANGERITE ($Pb_5Sb_4S_{11}$)

Boulangerite is an extremely rare trace constituent of the hangingwall Banded Pyrite + Sphalerite ores. It was observed as a single 15um inclusion that was associated with freibergite within an interstitial mass of galena in a massive sphalerite of Sample TLS.2-26. No detectable minor or trace elements were observed. Quantitative microprobe analyses (at 15 and 20 kV) were unattainable because of the grain size, resulting in contamination by adjacent phases, and because of the failure to adequately resolve the PbMα and the SKα overlap. The determined variations in stoichiometry may indicate either solid solution towards falkmanite ($Pb_3Sb_2S_6$), or more probably poor resolution of the overlap phenomena. Sample TLS.2-26, the only sample in which boulangerite was observed, contains 0.1 Vol % freibergite and 3 Vol % galena, and is therefore characterised by the Zn, Pb, Sb and Ag association.

COSTIBITE (CoSbS)

One grain (≤10um) of costibite was identified in sample TLN.2-63, by the use of B.S.E. imagery and qualitative microprobe analysis as a check of the grey level compositional integrity, during routine image analysis on the JEOL 733, CANMET. No quantitative microprobe analyses have been attempted, as the grain has not been located since. In addition to Co, Sb and S, the presence of minor Fe was also detected. Sample TLN.2-63 is classified as a Sheared Chalcopyrite + Sphalerite ore and contains negligible pyrite. It is suggested that during the deformation and breakdown of pyrite, Co in solid solution was liberated. Much of the Co may have entered the pyrrhotite structure, but a given fraction may have combined with available Sb and S. The identification as costibite is tentative, as this composition may correspond to costibite or its polymorphs paracostibite or willyamite.

FREIESLEBENITE ($Ag_2Sb_2Pb_2S_6$)

Freieslebenite is an extremely rare trace constituent of the hangingwall Banded Pyrite + Sphalerite ores. Only one anhedral grain (approximately 20 x 10um) associated with pyrargyrite, freibergite, gudmundite and pyrrhotite as inclusions within interstitial galena in the massive sphalerite of TLS.5-84, was observed (Plate 3a). In addition to galena, freibergite, gudmundite and pyrargyrite Sample TLS.5-84 also contains dyscrasite, all of which are characteristic of the Zn, Pb , Sb and Ag geochemical association.

Two microprobe analyses of this one grain failed to detect any minor or trace elements. The analyses were processed by itterative stripping of the overlapping peak flanks of SKα and PbMα, and in the case of one analysis, the PbMα was itteratively stripped and Pb was calculated by difference from 100 %. The analyses are considered as semi-quantitative, but clearly confirm the identification of freieslebenite. The analyses are presented below.

TABLE 20

Microprobe Analyses of Freieslebenite.

	Wt %.					Number of Atoms.			
	S	Ag	Sb	Pb	Total	S	Ag	Sb	Pb
Freies-1.	18.50	19.96	23.16	38.38	-----	6.148	1.972	2.028	1.975
Freies-1.	18.35	19.94	23.17	37.03	98.49	6.065	1.971	2.029	1.905
Freies-2.	18.64	21.11	21.97	38.40	100.12	6.183	2.008	1.992	1.905
Uncertainty.	± 0.2	± 0.3	± 0.4	± 0.4					

* Uncertainty quoted at the 95% confidence limits.
* Unit formula calculated on the basis of 4 atoms of Ag + Sb.
* A pyrite, Ag-metal, stibiotantalite and an altaite (PbTe) standard was employed for S, Ag, Sb and Pb, respectively.
* The first analysis of Freies-1 was processed by itteratively stripping the PbMα and calculating Pb by difference from 100 %.

PLATE 11.

PLATE 11.

PHOTOGRAPH A

SAMPLE TLS.2-40(#2) : Detail of the area indicated by the lower arrow in plate 2e. The electrum (El) is intimately associated with galena (Gal) and freibergite (Fr) filling fractures and interstitial spaces in the pyrite (Py). Plane polarised light. Bar scale = 40 µm.

PHOTOGRAPH B.

SAMPLE TLS.5-83A : Galena (Gal), freibergite (Fr), sphalerite (Sp) and electrum (El) invading and replacing fractured pyrite (Py). Note the poorly formed dendritic-textured galena to the left of centre. Plane polarised light. Bar scale = 160 µm.

PHOTOGRAPH C.

SAMPLE TLN.1-89 : A detail of the bottom centre area of Plate 10e. Chalcopyrite (Cp) is enveloped and corroded by the electrum (El), which also invades the dilated cleavage traces of some of the chlorite grains. Cc denotes persistent carbon coat. Plane polarised light. Bar scale = 40 µm.

PHOTOGRAPH D.

SAMPLE TLS.5-83A : High magnification, high contrast BSE photograph showing dyscrasite (Ag - bright white) and freibergite (Fr - light grey to dark grey) filling fractures in pyrite (black). Note the inhomogeneity of the freibergite. BSE. Bar scale = 15 µm.

PHOTOGRAPH E.

SAMPLE TLN.1-87 : A mass of myrmekitic freibergite (Fr) within a grain of galena (Gal) from a Massive Sphalerite (Sp) ore. Plane polarised light. Bar scale = 40 µm.

PHOTOGRAPH F.

SAMPLE TLS.5-64 : A thin reaction rim of myrmekitic pyrrhotite (Po) and gudmundite (Gud), and associated freibergite (Fr) and sphalerite (Sp) forming on a corroded pyrite (Py) porphyroblast. Plane polarised light. Bar scale = 40µm.

PHOTOGRAPH G.

SAMPLE TLS.5 -84 : Myrmekitic gudmundite (Gud) in galena (Gal), which is associated with sphalerite (Sp) forming the matrix material to a large pyrite (Py) grain. Plane polarised light. Bar scale = 40 µm.

PHOTOGRAPH H.

SAMPLE TLS.5-64 : Interstitial galena (Gal) containing inclusions of pyrargyrite (Pyr), pyrrhotite (Po), sphalerite (Sp) and gudmundite (Gud), within a matrix of sphalerite. Plane polarised light. Bar scale = 40 µm.

PLATE 11.

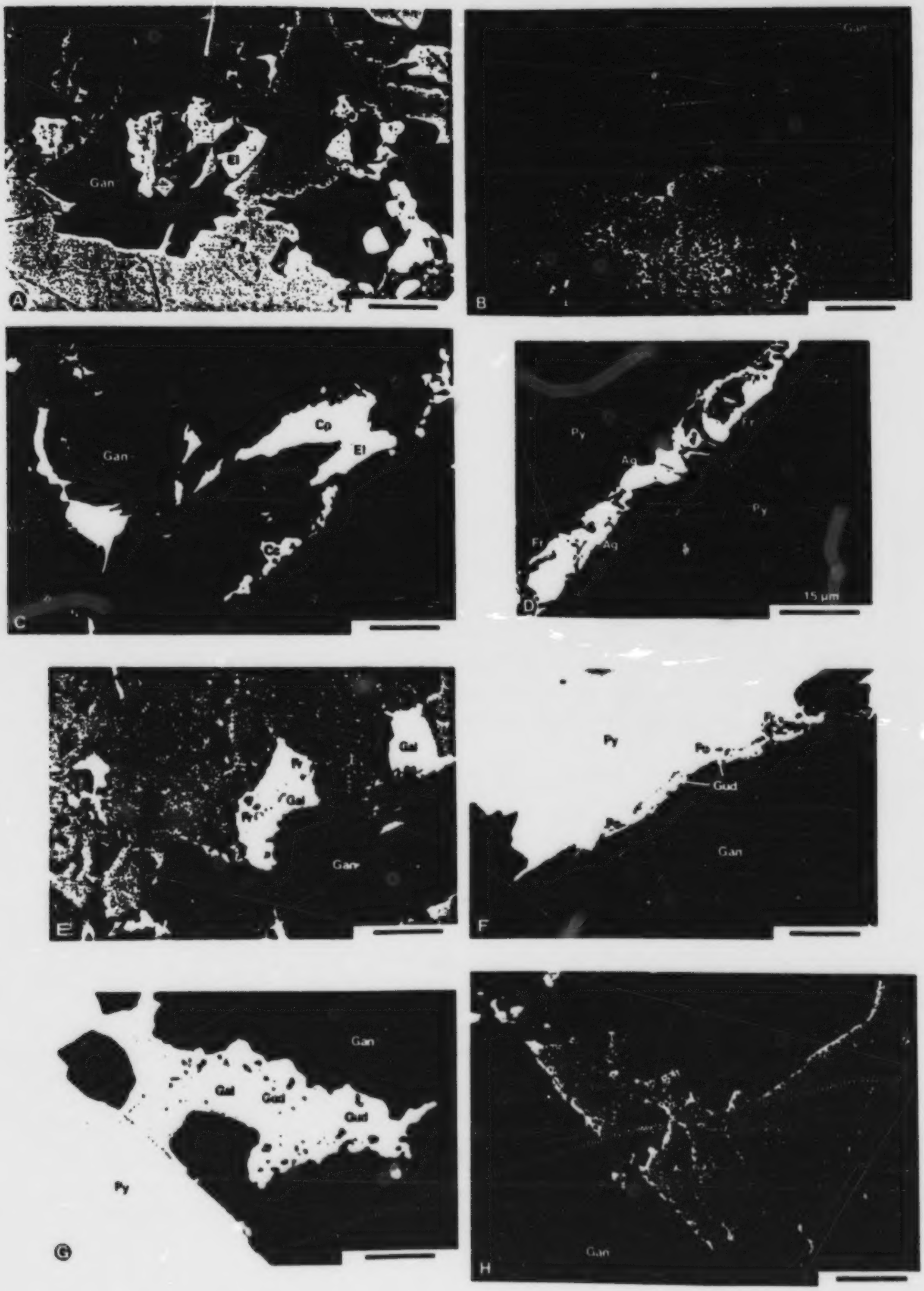
A
Gan
El
B
Gan
C
Gan
Cp
El
Cs
D
Py
Ag
Fr
Py
Fr
Ag
15 µm
E
Gal
Pr
Gal
Pr
Gan
F
Py
Po
Gud
Gan
G
Gan
Gal
Gud
Gud
Py
H
Gan

BOURNONITE (Pb,Cu,Sb,S_1)

Bournonite is an extremely rare constituent of the ores, that was identified during image analysis of several of the mill products. Because it was not detected in any of the ore samples, it cannot be ascribed to any of the ore types. It occurs in the mill products as fine-grained (≤10um) euhedral grains with stubby to prismatic habit. It occurs associated with freibergite as inclusions in sphalerite. Because of its association with sphalerite and freibergite, and because of the known geochemical asociation of Sb and Pb with Zn, it is suggested that bournonite occurs in the hangingwall Massive Sphalerite and the Banded Pyrite + Sphalerite ore types.

Qualitative electron microprobe analysis of the bournonite detected a minor Fe content in addition to the major elements Pb, Cu, Sb and S.

THE TELLURIDES

HESSITE (Ag_2Te)

Hessite is a rare trace constituent of the ores, and was observed in the Sheared Chalcopyrite + Sphalerite and the Chalcopyrite Stringer ore types. Hessite occurs as fine-grained (≤20um) euhedral to anhedral grains in two textural associations. These are (1) euhedral to anhedral grains intimately associated with pilsenite, lesser electrum and abundant chalcopyrite invading and replacing sphalerite and/or pyrrhotite in sample TLS.1-47 (Plate 5d), and (2) as inclusions in galena associated with and enveloped in chalcopyrite, which occassionally forms veinlets in fractured gangue (Plate 6h). Hessite occurs in the Cu-rich footwall ores, and is generally associated with and forms inclusions in galena and/or chalcopyrite.

Three microprobe analyses of hessite reveal trace S, and slight apparent cation-deficiency. The cation-deficiency may constitute a real deviation from stoichiometry, or more probably reflects (as do the low totals) the use of a Ag-metal standard, and the consequent increased potential error in the matrix corrections for Ag.

TABLE 21

Microprobe Analyses of Hessite.

Wt %.	1	2	3	Uncertainty.
S.	0.27	0.25	0.32	± 0.1
Ag.	61.38	61.18	61.19	± 0.4
Te.	37.21	36.98	36.77	± 0.5
Total.	98.86	98.41	98.27	
Number of atoms.				
S.	0.03	0.03	0.04	
Ag.	2.00	2.00	2.00	
Te.	1.03	1.02	1.02	

* Uncertainty quoted at the 95% confidence limits.

* Unit formula calculated on the basis of 2 silver atoms.

* A pyrite, Ag-metal and altaite standard were employed for S, Ag and Te, respectively.

PILSENITE(?) ($(\underline{Bi},\underline{Pb})_{2}(\underline{Te},\underline{Se})_{2\cdot 2}$)

Pilsenite(?) is an extremely rare trace constituent of the ores that was observed in sample TLS.1-47, a Chalcopyrite Stringer ore. Wehrlite has been previously identified at Trout Lake, in what was termed the Pyrite-Chalcopyrite ores (Muzylowski, 1979). Wehrlite (BiTe(?)) is recognised by Fleischer (1983) as an accredited mineral specie, whereas Ramdohr (1980) considers wehrlite as being possibly identical to pilsenite (Bi_3Te_2). However, recent revisions to the Glossary of Mineral Species (Mineralogical Record, Misc., 1983-1985) have discredited wehrlite and recognised pilsenite as Bi_4Te_3.

Numerous grains of pilsenite(?) were observed as fine-grained (≤25um) euhedral to anhedral grains intimately associated with hessite, lesser electrum and abundant chalcopyrite invading and replacing sphalerite and pyrrhotite (Plate 5d). Hessite was observed forming rare intricate intergrowths within a single grain of pilsenite. The identification of 'wehrlite' in the Pyrite-Chalcopyrite ores (Muzylowski, 1979), and the observation of pilsenite(?) in only one sample of the Chalcopyrite Stringer ores, suggests that the pilsenite(?) is restricted to the footwall Cu-rich ores i.e., the Chalcopyrite Stringer and the Disseminated Pyrite + Chalcopyrite ore types.

Two microprobe analyses of the pilsenite(?) reveal several minor and trace elements. The analyses were generated with an excitation voltage of 20 kV, such that the Bi and PbLα peaks could be modelled, and the scaled Bi and PbMα peaks stripped off the SKα R.O.I.. No SKα peak was detected, and both Bi and Pb were analysed by their respective mutually overlapped (partial) Lα peaks.

The two analyses yield an average composition of 0.62 % Fe, 0.87 % Se, 32.19 % Te, 3.26 % Pb and 60.81 % Bi (mean total = 97.73 %), which translates into the unit formula $(Bi_{1.84},Pb_{0.10},Fe_{0.07})(Te_{1.59},Se_{0.07})$. These compositions are non-stoichiometric relative to the known Bi- and Te-bearing minerals (Ramdohr, 1980, Miller, 1981 and Fleischer, 1983). The analyses may therefore represent (1) inferior analyses due to inappropriate standards, poor peak resolution due to overlap correction, as well as sample decomposition (severe scorch marks at the point of analysis), as reflected in the low totals, (2) intermediate compositions in a solid solution such as Tsumoite (Bi,Te) and Pilsenite (Bi_4Te_3), and (3) submicroscopic intergrowths of two or more related phases.

The observed high reflectivity, white colour and weak brownish anisotropy are characteristic of many of the structurally similar 'Te-Bi compounds' (Ramdohr, 1980), but are not sufficiently diagnostic of a given mineral specie. The identification as pilsenite therefore remains tentative.

TABLE 22

Microprobe Analyses of Pilsenite(?).

Wt %.	1	2	Uncertainty.
Fe.	0.15	1.09	± 0.1
Se.	0.71	1.02	± 0.1
Te.	33.06	31.31	± 0.3
Pb.	3.79	2.72	± 0.3
Bi.	60.70	60.92	± 1.4
Total.	98.40	97.05	
Number of atoms.			
Fe.	0.03	0.12	
Se.	0.06	0.08	
Te.	1.66	1.52	
Pb.	0.12	0.08	
Bi.	1.87	1.80	

- * Uncertainty quoted at 95% confidence limits.
- * Unit formula calculated on the basis of 2 cations.
- * A pyrite, pure-Se, pure-Te, galena and a Bi-metal standard were employed for Fe, Se, Te, Pb and Bi, respectively.

RUCKLIDGEITE ($(\mathrm{Bi,Pb})_3\mathrm{Te}_4$)

Rucklidgeite is a rare trace constituent of the ores, that was observed in sample TLS.3-14, a Chalcopyrite Stringer ore. Abundant fine-grained (approximately 15um) rucklidgeite, clausthalite and lesser electrum, associated with chalcopyrite and pyrrhotite were observed in Sample TLS.3-14. These phases infilled and corroded deformed pyrite porphyroblasts along fractures and grain boundaries, formed interstitial films and wedges, as well as occurring as variably idiomorphic and commonly composite inclusions in the pyrite. The rucklidgeite inclusions varied from blocky to rounded, lenticular, lobate and tabular, with aspect ratios varying from 1 to 20 (Plate 5b and 5c). The association with clausthalite and electrum is consistent with the rare occurrences of rucklidgeite "in contact with native gold, galena and pyrite" in the Ashley deposit, Ontario (Harris et al. 1983). Both the rucklidgeite and pilsenite(?) probably correspond to the wehrlite observed by Muzylowski (1979), and are restricted to the footwall chalcopyrite-rich ores i.e., the Chalcopyrite Stringer ores, and probably also the Disseminated Pyrite + Chalcopyrite ores.

Three microprobe analyses of rucklidgeite were obtained and reveal Fe and Se as non-essential minor to trace elements. These analyses were generated with a 20 kV excitation potential, during the same analytical run in which the pilsenite analyses were collected. As with the pilsenite, the Bi and PbLα peaks were modelled, and the scaled Bi and PbMα peaks were stripped off the SKα R.O.I.. No SKα was observed, and both Bi and Pb were analysed by their respective mutually overlapped (partial) Lα peaks. The analyses are presented below.

The 3 analyses yield an average composition of 0.55 % Fe, 1.69 % Se, 41.38 % Te, 15.46 % Pb and 39.73 % Pb (mean total = 98.81 %), which translates into the unit formula of $(\mathrm{Bi}_{2.20}, \mathrm{Pb}_{0.86}, \mathrm{Fe}_{0.12})(\mathrm{Te}_{3.75}, \mathrm{Se}_{0.25})$ or $(\mathrm{Bi,Pb,Fe})_{3.18}(\mathrm{Te,Se})_{4.00}$. The slight cation excess probably reflects the poor resolution of the overlapped Bi and PbLα peaks, and also the inappropriate selection of standards.

TABLE 23

Microprobe Analyses of Rucklidgeite.

Wt %.	1	2	3	Uncertainty.
Fe.	0.74	0.46	0.44	± 0.1
Se.	1.51	1.73	1.84	± 0.1
Te.	43.30	39.93	40.92	± 0.4
Pb.	15.42	15.43	15.52	± 0.6
Bi.	39.36	40.23	39.61	± 1.0
Total.	100.32	97.77	98.33	

Number of atoms.				$\bar{x}$.
Fe.	0.15	0.10	0.09	0.12
Se.	0.21	0.26	0.27	0.25
Te.	3.79	3.74	3.73	3.75
Pb.	0.83	0.89	0.87	0.86
Bi.	2.10	2.30	2.20	2.20

* Uncertainty quoted at the 95% confidence limits.

* Unit formula calculated on the basis of 2 anions (Te + Se).

* A pyrite, pure-Se, pure-Te, galena and a Bi-metal standard were employed for Fe, Se, Te, Pb and Bi, respectively.

VOLYNSKITE ($BiAgTe_2$)

Volynskite is an extremely rare trace constituent of the ores, that was identified during image analysis of the Cu-concentrate (#12). Because it was not identified in any of the ore samples, it cannot be ascribed to any of the ore types. It was observed as a single fine-grained (10 um diameter) anhedral grain locked with hessite (Plate 12a). Because of the association with hessite it is probable that volynskite occurs in the footwall Cu-rich ores.

Three quantitative wavelength dispersive electron microprobe analyses of the volynskite were generated using the JEOL 733. These analyses are presented below and indicate minor element-free volynskite, with slightly Ag-poor, Bi-rich stoichiometry.

TABLE 24

Three Microprobe Analyses of Volynskite.

Wt %.	1	2	3	$\bar{x}$	Std. Dev.
Ag.	17.96	17.55	16.52	17.35	± 0.5
Bi.	40.73	40.36	39.57	40.22	± 0.7
Te.	44.50	44.63	41.52	43.55	± 0.5
Total.	103.19	102.52	97.58	101.10	
At %					
Ag.	23.46	23.08	22.96	23.17	
Bi.	27.49	27.42	28.39	27.77	
Te.	49.05	49.50	48.67	49.07	

* Standard Deviation quoted at the 95% confidence limits.

* Operating Conditions :

Excitation voltage : 20 kV.

Sample Current : 15 nA on the Faraday Cup.

Count Time : 60 secs or until 0.5 % standard deviation on the standard or unknown is reached.

Ag : AgLα analytical line; PET crystal; Matildite ($AgBiSe_2$) standard.

Bi : BiMα analytical line; PET crystal; Bismuthinite (Bi_2S_3) standard.

Te : TeLα analytical line; PET crystal; Altaite (PbTe) standard.

SELENIDES

CLAUSTHALITE-GALENA SOLID SOLUTION (Pb(Se,S))

As stated previously (See GALENA) this section will treat only those 'galenas' that are texturally and/or optically distinguishable from the common, minor element-free, stoichiometric galena. Three distinct varieties of clausthalite-galena are recognised, and will be treated as such below.

1. Abundant fine-grained (≤30um), graphic-textured clausthalite-galena solid solution in Fe-poor sphalerite was observed in sample TLN.1-87, a Massive Sphalerite ore (Plate 9b). The Fe-poor sphalerite and the associated clausthalite-galena, as well as lesser gudmundite are observed interstitial to, invading and corroding the Fe-rich common matrix sphalerite. Semi-quantitative microprobe analyses of this 'clausthalite' reveals a wide range in the Se and S contents, as well as minor Ag (≤3 % Ag). The Ag content is highly erratic and may reflect contamination from an undetected Ag-bearing inclusion. The Se content varies from undetected (<0.05 % Se) to 23 % Se (i.e., approximately 80 % clausthalite component). Considerable inhomogeneity was observed within apparently single grains.

2. 'Galenas' with a high reflectivity and a slight blue-white colour (when viewed with a daylight filter) were observed in the Sheared Chalcopyrite + Sphalerite, the Mixed/Banded Chalcopyrite + Sphalerite and the Chalcopyrite Stringer ores. Qualitative microprobe analyses of some of these galenas revealed highly variable Se-contents, varying from trace to major concentrations. The analyses suggest a trend of increasing Se content (clausthalite component) in the galenas passing towards the footwall Cu-rich ores. No Te or Ag was detected.

3. 'Galenas' with a high reflectivity and blue-white colour were observed associated with rucklidgeite and lesser electrum in sample TLS.3-47 (Plate 5b). Two microprobe analyses of these galenas generated at 20 kV excitation potential (during the same analytical run in which the pilsenite and rucklidgeite were analysed), indicate a significant clausthalite component (Se), and a trace altaite component (Te). The analyses are presented in Table 25.

The average composition and the calculated unit formula are also presented, and exhibit good stoichiometry despite the stripping procedure employed to generate the SKα, as well as the probable contamination of the analysis by adjacent pyrite, as indicated by the Fe-peak. Analysis 1 corresponds to clausthalite-galena that occurred along with chalcopyrite (with myrmekitic pyrrhotite) as a composite inclusion in pyrite, whereas analysis 2 corresponds to clausthalite-galena that occurred along with electrum and pyrrhotite, also as a composite inclusion in pyrite.

These 'clausthalites' differ significantly from those of the previous two varieties in that they contain minor Te, consistent with their association with rucklidgeite.

TABLE 25

Microprobe Analyses of Clausthalite-Galena from TLS.3-47.

Wt %.	1	2	$\bar{x}$.
S.	10.96 ± 0.3	3.80 ± 0.3	7.38
Se.	5.81 ± 0.3	19.22 ± 0.6	12.52
Te.	0.45 ± 0.1	1.55 ± 0.3	1.00
Fe.	1.11 ± 0.2	1.69 ± 0.2	1.40
Ag.	0.00	0.66 ± 0.2	0.33
Pb.	81.74 ± 1.6	70.12 ± 1.7	75.93
Total.	100.07	97.04	98.56
Number of atoms.			
S.	0.82	0.32	0.57
Se.	0.18	0.65	0.42
Te.	0.01	0.03	0.02
Fe.	0.05	0.08	0.07
Ag.	0.00	0.02	0.01
Pb.	0.94	0.90	0.92

* Uncertainty quoted at the 95% confidence limits.

* Unit formula calculated on the basis of 1 anion (S, Se and Te).

* A pyrite, pure-Se, pure-Te, Ag-metal and galena standards were employed for S and Fe, Se, Te, Ag and Pb, respectively.

* The SKα peak was generated by modelling the PbLα peak and stripping the scaled PbMα peak off the SKα R.O.I..

NAUMANNITE (Ag_2Se)

Naumannite is an extremely rare trace constituent of the ores, that was identified during image analysis of a Cu-rougher concentrate (#4). It was not identified in any of the ore samples and is not therefore ascribed to any ore type. It was observed as a single fine-grained (<5um) anhedral grain containing an inclusion of clausthalite (Plate 12b). Several wavelength dispersive microprobe analyses of the naumannite were attempted, but the fine-grained nature of this single grain prohibited contamination free analysis. However, the analyses did confirm the composition as being essentially Ag_2Se.

RARE EARTH MINERALS

MONAZITE AND BASTNAESITE

Monazite and a mineral tentatively called bastnaesite were observed during image analysis of the ores. Both constitute rare, trace minerals, and were observed in most of the ore types including the hangingwall Massive Sphalerite ores and the footwall Chalcopyrite Stringer ores. They appear to be relatively more abundant in the latter ores.

Monazite formed anhedral grains with a median grain size of approximately 10 to 15 um, and was generally associated with chalcopyrite (Plate 12c). The bastnaesite in sample TLN.2-11 was observed replacing a prismatic mineral of porphyritic character, and exhibited a characteristic needlelike form (Plate 12d). Relatively abundant bastnaesite was also observed in TLS.1-52, and exhibited a 'spongy' form. Both these textures suggest a late replacement phase of metamorphic origin. REE's generally occur as trace elements in rock-forming minerals, and rarely form minerals of their own (Graf, 1977). The absence of xenotime, the heavy REE phosphate, and the mere presence and abundance of monazite and bastnaesite suggests fractionation and enrichment of the light REE Ce and La. It is interpreted that seawater-rock interactions and dissolution of primary REE-bearing minerals in the volcanic pile, enriched the ore-bearing fluids in Ce and La. The REE's were precipitated during the discharge of the hydrothermal ore-bearing fluids and are thus enriched in the ore zone.

Qualitative microprobe analysis of the monazite revealed the major elements P, Ce and La, and a variably minor to undetected Ca content, which corresponds to $(Ce, La, Ca) PO_4$. Qualitative microprobe analysis of the mineral tentatively identified as bastnaesite revealed the major elements Ce and La, while O, C and F being 'invisible' to the microprobe technique are assumed to be present. The composition of this mineral possibly corresponds to $(Ce, La)(CO_3)F$, and is therefore tentatively called bastnaesite.

PLATE 12.

PLATE 12.

PHOTOGRAPH A.

SAMPLE TL.MP-12 : A high magnification, high contrast BSE photograph showing a particle consisting of volynskite (Vol) and hessite (Hess), surrounded by the mounting medium (Mm). The sample is a mill product, i.e., the Cu-1st Cleaner concentrate. BSE. Bar scale = 5 µm.

PHOTOGRAPH B.

SAMPLE TL.MP-4 : A high magnification, high contrast BSE photograph showing a particle of naumannite (Nau) containing an inclusion of clausthalite (Cl), surrounded by the mounting medium (Mm). The sample is a mill product, i.e., the Cu-Rougher concentrate. BSE. Bar scale = 2 µm.

PHOTOGRAPH C.

SAMPLE TLN.1-89 : Fine-grained, rounded inclusions of monazite (Mon) hosted in chalcopyrite (Cp), which is interstitial to the gangue (Gan). BSE. Bar scale = 20 µm.

PHOTOGRAPH D.

SAMPLE TLN.2-11 : Basnaesite (Baes) exhibiting needle-like form, and replacing (pseudomorphing) a prismatic mineral of porphyritic character, i.e., a primary volcanic phenocryst. BSE. Bar scale = 150 µm.

PHOTOGRAPH E.

SAMPLE TLN.2-83 : A large area of matrix pyrrhotite (Po - white to dark grey) exhibiting 120° triple junctions, and relatively equiganular grains in a mosaic texture. Partially crossed polars. Bar scale = 160 µm.

PHOTOGRAPH F.

SAMPLE TLN.2-11 : A Chalcopyrite Stringer ore exhibiting chalcopyrite (Cp) and lesser pyrrhotite (Po) invading fractures in folded and ruptured laminae of chloritic-schist (Gan). Plane polarised light. Bar scale = 325 µm.

PHOTOGRAPH G.

SAMPLE TLN.2-9 : The nose of a tight, isoclinally folded and ruptured lamination of chloritic-schist (Gan) enveloped and invaded by a matrix of chalcopyrite (Cp) with streaks of carious blebs and myrmekitic masses of sphalerite (Sp) and pyrrhotite (Po). These streaks sweep around the folded nose of the lamination. Plane polarised light. Bar scale = 325 µm.

PHOTOGRAPH H.

SAMPLE TLN.2-6 : Fine-grained swirls (Sw) form in the vortices of compression around the competent augens of gangue (Gan), which have been milled and rotated by the shearing that has also produced the diablastic-textured sphalerite (Sp) within the chalcopyrite (Cp) matrix. Plane polarised light. Bar scale = 160 µm.

PLATE 12.

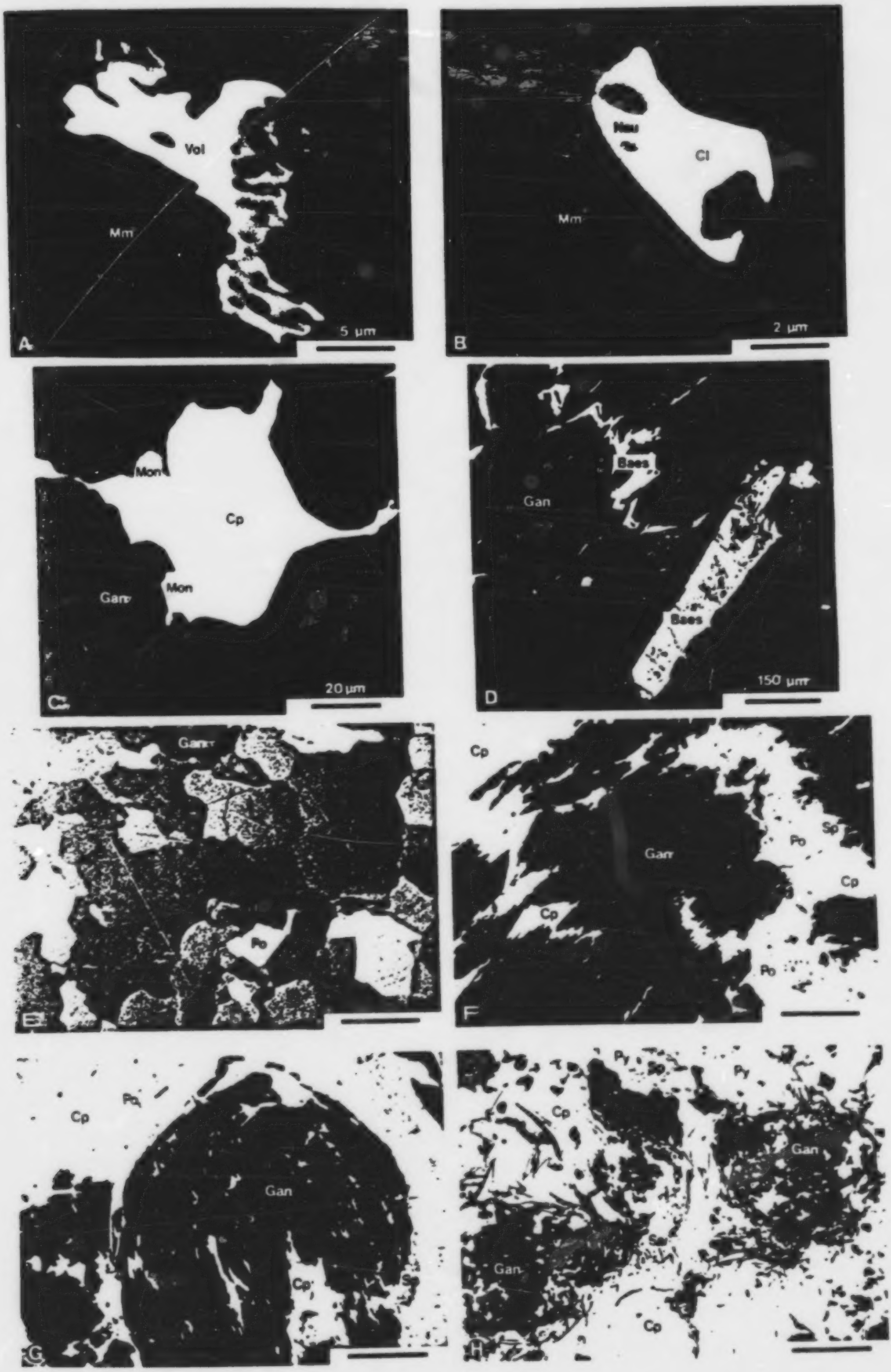
Vol
Mm
A
5 µm
Nau
Cl
Mm
B
2 µm
Mon
Cp
Mon
Gan
C
20 µm
Baes
Gan
Baes
D
150 µm
Gan
Po
E
Cp
Gan
Sp
Po
Cp
Cp
Po
F
Cp
Po
Gan
Cp
G
Py
Sp
Py
Cp
Gan
Sp
Gan
Cp
H

Chapter VIII

MINERAL - METAL BALANCE

In order to elucidate the underlying 'structure' of the chemical composition of the ores, the chemical assays of the 27 representative ore samples were treated statistically by the SAS statistics package. R-Mode Factor Analysis was also performed on the same dataset. In so doing it was hoped to simplify the inter-relationships of the the 17 elements, by (1) evaluating the strength of any linear relationship between pairs of elements, through construction of a Correlation Coefficient Matrix, and by (2) clustering the elements into a small number of mutually uncorrelated (orthogonal) generalised factors through Factor Analysis. These techniques provide invaluable information on the mineral chemistry, permitting interpretation of the host mineralogy of the elements and thus permitting elements to be assigned to previously identified minerals and particularly those trace elements whose host mineral(s) had not been identified i.e., Indium. In addition, the results were equally invaluable in evaluating the mineral associations that characterise the ore, and the control the differentiation of the ore.

All the analyses for Bi yield concentration levels below the detection limit of 0.001 % or 10 ppm Bi. The analyses for Ni indicate concentrations of less than 0.003 % or 30 ppm Ni (except for one analysis of 0.006 % Ni). The variance exhibited by Ni is therefore probably of the same order as the analytical uncertainty, due to the proximity to the detection limit. In consequence, the Bi and Ni are excluded from the statistical treatment. The mean, maximum and minimum elemental concentrations, and coefficient of variation are provided below in Table 26.

The mean values provide limited information on the relative abundances of the elements in the ores. Clearly the mean values represent elevated values with respect to the mine reserves and analyses of concentrate feed i.e., 14.51 % Zn versus 5.6 % Zn for the proven ore reserves. This disparity reflects (1) that the mean analyses are unweighted with respect to the relative abundances of the ore types, and (2) mine dilution and recovery is not included in the mean analyses. In addition, the preferential elevation of the Zn with respect to the Cu compared to that of the proven reserves, suggests that the suite of 27 samples is biased towards the Zn-rich ores.

Assuming that sphalerite and chalcopyrite are the sole Zn- and Cu-bearing minerals, respectively, then the maximum analysis for Zn and Cu indicate ores with up to 75 % sphalerite and 64 % chalcopyrite. In addition, a maximum analysis of 44 % Fe indicates ores with up to 98 % pyrite (± pyrrhotite). The coefficient of variation for Fe and S indicates that these elements exhibit the least range in concentration. This reflects (1) the undifferentiated character of S, being for all intents and purposes the sole anion,

TABLE 26

SOME BASIC PARAMETERS OF THE ELEMENT DISTRIBUTIONS.

Element.	Mean.	Maximum.	Minimum.	Coef. of Var.
Wt %.				
Cu.	4.97	21.89	0.02	126.
Zn.	14.51	44.7	0.19	103.
Mn.	0.084	0.270	0.014	81.
Pb.	0.688	12.1	0.001	358.
Fe.	23.4	44.0	5.6	47.
S.	26.5	45.0	3.9	38.
ppm .				
Au.	3.295	13.75	0.377	108.
Ag.	61.05	445.9	4.631	156.
Cd.	0.031	0.126	0.001	107.
Co.	0.016	0.123	0.001	148.
As.	2795.	54000.	<2.	374.
Se.	65.	302.	<1.	117.
Te.	1.6	5.	<0.2	90.
Hg.	38.	114.	7.	60.
Sb.	85.	377.	2.	99.
In.	34.	63.	<1.	47.
Sn.	36.	54.	<1.	44.

* 'Coef. of Var' denotes coefficient of variation, which is a measurement of variation in a population calculated from [CV = std dev / mean . 100].

irrespective of ore type, and (2) the ubiquitous nature of pyrite and/or pyrrhotite in each ore type, and the generally undifferentiated nature of pyrite. In addition, the lower concentration levels of Fe are sustained by silicate-Fe, Fe in chalcopyrite, sphalerite and pyrrhotite, even where pyrite and/or marcasite are present in minor to trace amounts. Conversely Pb, As and Ag exhibit the largest range in concentrations reflecting the differentiated nature of the ores with respect to these elements, and their respective lognormal distributions. Surprisingly, Au exhibits a coefficient of variation of 108, which is inconsistent with its general tendency for erratic distribution. However, observed abundances of electrum in samples TLN.1-89, TLN.2-8, TLN.2-11 and TLS.2-40, all of which were not included in the suite of ores upon which the chemical analyses were performed, indicate that the coefficient of variation for Au is unrepresentative of the entire ore population. The Au is erratically distributd and probably also lognormally distributed. For example, the derived Au content of TLN.1-89 (from modal analysis of the electrum, See Table 8) is 3,300 ppm Au, at least within the area of the polished section.

FIGURE 19

ELEMENT PAIR SCATTER DIAGRAMS.
(Values for Sb, Pb, and Se log-transformed).

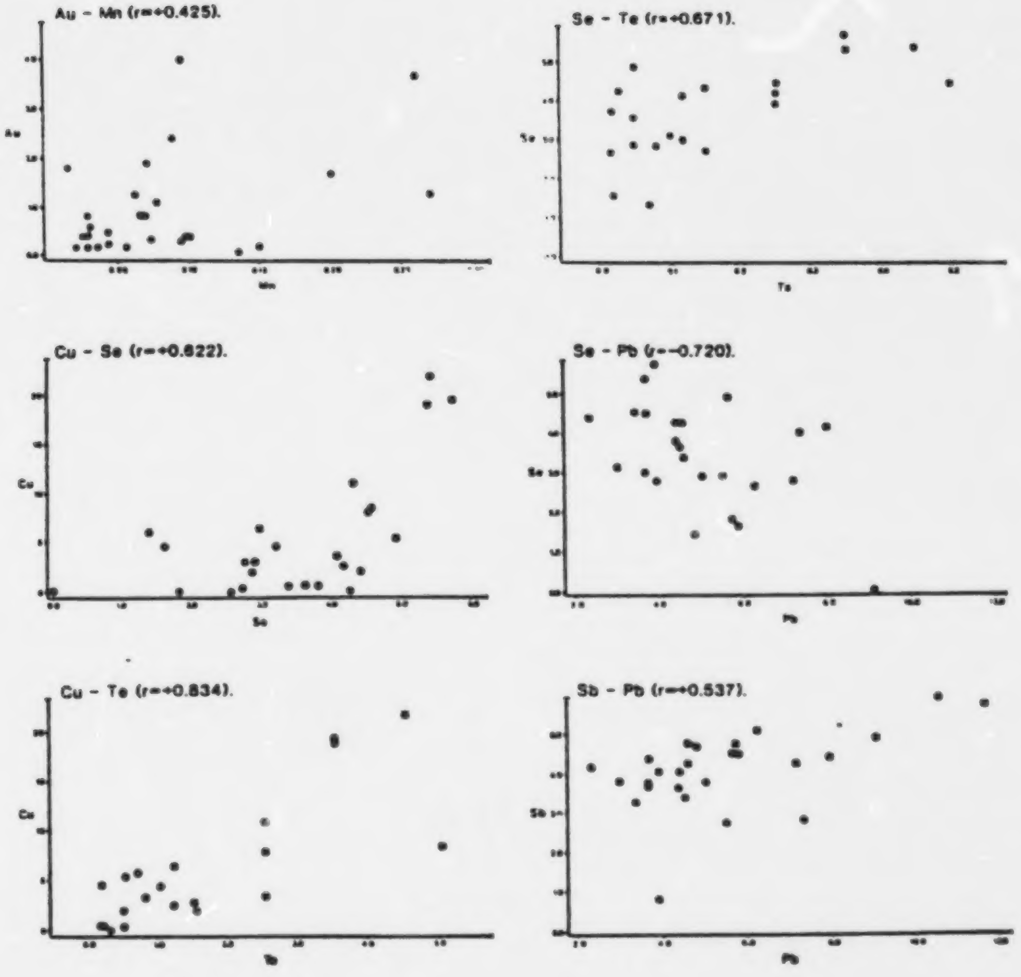

FIGURE 20

ELEMENT PAIR SCATTER DIAGRAMS.
(Values for Sb, Pb, and Ag log-transformed).

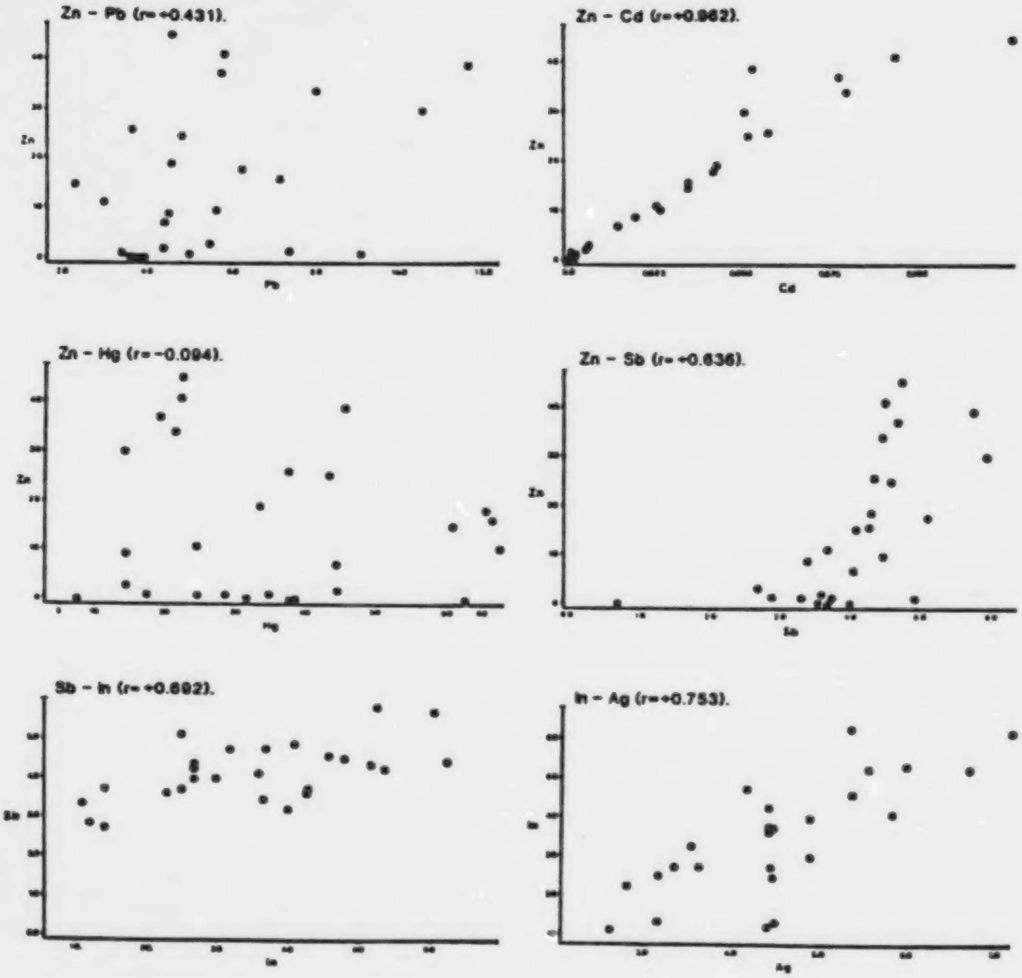

CORRELATION ANALYSIS

Elements with lognormal distributions i.e., Ag, Sb, Pb, Se, As and Co were log-transformed to normal distribution in preparation for multivariate statistical analysis. Table 27 contains the correlation coefficient matrix consisting of possible 'r-values' of + 1.000 to - 1.000. For a sample size of 27 observations (the number of samples analysed) r-values less than ± 0.38 are not significantly different from zero at the 95 % confidence limits. Therefore the author will not attempt interpretation of linearity between two elements, where the r-value is less than ± 0.38. However, even a correlation coefficient of ± 0.38 indicates that only 14.4 % of the total variance in 'X' and 'Y' can be explained by their linear relationship. Of the 120 coefficients in the matrix, 45 yield r-values greater than ± 0.38, and indicate a significant linear relationship for the respective element pairs. In addition, groups of elements that exhibit a high degree of covariance are readily identified. Two such groups of elements that covary are recognised by their positive correlations between elements of the same group, and negative correlations with elements of the second group. These groups define the fundamental geochemical associations of the ores. These are given below.

1. The Zn-Group : Zn, Cd, Pb, Sb, Ag, Hg, As, In and Sn.
2. The Cu-Group : Cu, Se, Te, Co and Fe.

Au and Mn do not exhibit any significant covariance with the above element groups. Sulfur exhibits marked significant covariance with elements of the Zn-group, and no significant covariance with elements of the Cu-Group, except Fe. It is interpreted that this reflects the elevated concentration of Hg, Sn, Sb and In in high sulphide, and hence S-rich samples, where the Zn-rich ores tend to consist of more massive sulphides than the Cu-rich ores. This relationship can be considered as a product of induced covariance resulting from S being the sole significnat anion in the sulphide ores. Therefore, S is not included in Zn-group. The S-Fe pair yields an r-value of + 0.661, and this is readily understood in terms of S being the sole significant anion and Fe being the dominant cation of the sulphides. In addition, the greater weight fraction of S in pyrite (55 % S) versus chalcopyrite (35 % S) and sphalerite (30 % S) also tends to strengthen the positive covariance of Fe with S.

The Au-Mn pair yields an r-value of + 0.425, and represents the only significant correlation of Au. The Mn is probably hosted in the gangue, and most probably in chlorite and/or calcite. It may be postulated on the basis of this weak correlation (Fig 19) that Au-rich ores are coincident with a primary (non-metamorphic) Mn-rich alteration suite, and/or where the latter is related to the fluid state mobilisation of Au during metamorphism. Most surprisingly Au exhibits no correlation with As or Cu. Gold is commonly associated with As-rich pyrite and arsenopyrite in many types of deposits (Boyle, 1979, Gasparrini, 1983). Both the petrographic and chemical analyses failed to identify any such association at Trout Lake. Conversely, the apparent tendency of Au to be concentrated in the Cu-rich ores, as observed petrographically, is not substantiated by the chemical analyses. However, the chemical analyses for Au are considered to be unrepresentative of the ores, for reasons stated earlier.

TABLE 27

CORRELATION COEFFICIENT MATRIX OF THE CHEMICAL ANLAYSES.

	Zn	Cd	Ag	Pb	Sb	As	In	Sn	Hg	Cu	Se	Te	Co	Fe	Mn	Au
Zn	1.000															
Cd	0.962															
Ag	0.269	0.107														
Pb	0.431	0.273	0.439													
Sb	0.636	0.545	0.465	0.537												
As	0.136	0.091	0.094	0.371	0.431											
In	0.457	0.364	0.753	0.217	0.692	0.195										
Sn	0.389	0.355	0.423	-0.078	0.662	-0.005	0.743									
Hg	-0.094	-0.104	-0.010	-0.109	0.321	0.493	0.300	0.482								
Cu	-0.381	-0.344	0.160	-0.531	-0.223	-0.591	0.187	0.374	0.051							
Se	-0.503	-0.355	-0.376	-0.720	-0.456	-0.413	-0.222	0.073	0.229	0.622						
Te	-0.507	-0.470	0.104	-0.504	-0.405	-0.512	-0.005	0.212	-0.009	0.834	0.671					
Co	-0.071	0.036	-0.161	-0.503	-0.043	0.064	0.135	0.252	0.303	0.292	0.435	0.273				
Fe	-0.594	-0.562	-0.092	-0.108	0.017	0.110	0.047	0.355	0.611	0.364	0.405	0.380	0.283			
Mn	0.010	0.087	-0.029	-0.164	-0.177	-0.137	-0.060	-0.088	-0.125	-0.018	0.127	0.093	0.229	-0.348		
Au	-0.127	-0.118	0.034	-0.134	-0.190	0.237	-0.036	-0.110	0.107	0.043	0.002	0.053	0.086	-0.054	0.425	
S	0.126	0.127	0.079	-0.020	0.571	0.269	0.473	0.732	0.641	0.063	-0.001	-0.064	0.079	0.661	-0.248	-0.225

TABLE 28

CORRELATION COEFFICIENT MATRIX OF THE CHEMICAL ANALYSES PORTRAYING ONLY THE SIGN OF THE SIGNIFICANT CORRELATIONS.

	Group 1.								Group 2.						
	Zn	Cd	Ag	Pb	Sb	As	In	Sn	Hg	Cu	Se	Te	Co	Fe	Mn	Au
Zn																
Cd	+															
Ag																
Pb	+		+													
Sb	+	+	+	+												
As					+											
In	+		+		+											
Sn	+		+		+		+									
Hg						+		+								
Cu	–			–		–										
Se	–			–	–	–				+						
Te	–	–		–	–	–				+	+					
Co				–							+					
Fe	–	–							+		+	+				
Mn																
Au															+	
S					+		+	+	+					+		

As stated earlier two groups of elements exhibiting marked covariance are recognised, and characterise the ores in terms of their mutual differentiation. These groups can be considered endmembers of a differentiation series from the footwall Cu-rich ores to the hangingwall Zn-rich ores. In addition, each lens may exhibit a greater tendency towards differentiation with a predominence of one association, eg., Lens 5 of the South Zone is enriched in the Zn-Group with respect to all other lenses. Table 28 contains the correlation coefficient matrix portraying only the sign of the 40 significant correlations. The groups of elements displaying positive covariance are identified by fields of '+' signs, whereas the field of '-' signs identifies the antipathetic relationship or negative covariance between elements of the different groups. The coherence of the covariance exhibited by the two element groups is given in Table 29, with the elements ordered in terms of the strength of their covariance i.e., geochemical affinity within that group. Sb, Zn, Se, Pb and Te exhibit the highest degree of coherence, Sn, Cu, As, In, and Ag exhibit moderate coherence, while Cd, Co, Hg and Fe exhibit low coherence. Fe exhibits negative covariance with Zn and Cd and positive covariance with Se and Te, as well as the Zn-group element Hg. The groups are discussed below.

The Zn-Group (Hangingwall Association).

Elements : Zn, Sb, Pb, Sn, As, In, Ag, Cd, and Hg.

This group contains the highest r-value of any element pair in the matrix, i.e., Zn-Cd (+ 0.962), and is consistent with the universal hypogene geochemical coherence of these two elements (Mielke, 1979). Regression analysis of Cd on Zn yields a calculated Cd content of 0.14 % Cd in sphalerite, assuming that sphalerite is the sole host of Cd. This value agrees favourably with the calculated 0.16 % Cd from the microprobe analyses of sphalerite, and the 0.14 % Cd calculated from the 1983 concentrate assays. The r-value of + 0.962 indicates that 93 % of the variance in Zn and Cd is explained by their linear relationship. This is interpreted as the systematic diadochic substitution of Cd for Zn in sphalerite (Fig 20). Despite the high r-value, and thus linearity for the Zn-Cd pair, Cd exhibits distinctly lower covariance than Zn with the other elements of the Zn-group. However, it does exhibit numerous insignificant (note that this is at the 95 % confidence level) positive corelations with all other elements of the Zn-group, and conversely with elements of the Cu-group. The decreased covariance of Cd is probably attributable to the greater analytical uncertainty in the Cd determinations, due to proximity to the detection limit at these low levels of concentration. This results in a greater scatter in the Cd determinations relative to the Zn determinations, and possibly also results in the decreased strength of the covariance of the Zn-Cd pair from the ideal of + 1.000 to + 0.962, and the decreased coherence in the apparent geochemical coherence of Cd.

The assumption that sphalerite is the sole Hg-bearing phase (See SPHALERITE) is not substantiated by the correlation coefficient of - 0.094 for the Zn-Hg pair. Hg exhibits no significant covariance with elements of the Cu-

TABLE 29

COHERENCE OF THE GEOCHEMICAL ASSOCIATIONS.

The number and sign of the significant correlations exhibited by each element within its respective group, and within the opposing group.

Element.	Within Respective Group.	Within Opposing Group.
Sb.	+ 7.	- 2.
Zn.	+ 5.	- 4.
Se.	+ 4.	- 4.
Te.	+ 3.	- 5.
Pb.	+ 3.	- 4.
Sn.	+ 5.	- 0.
Cu.	+ 2.	- 3.
As	+ 2.	- 3.
In.	+ 4.	- 0.
Ag.	+ 4.	- 0.
Cd.	+ 2.	- 2.
Co.	+ 1.	- 1.
Hg.	+ 2.	+ 1.
Fe.	+ 2.	- 2, and + 1.

group, except with Fe, whereas it exhibits significant positive covariance with the Zn-group elements As and Sn, with which it yields a moderate r-value of - 0.498 and - 0.482, respectively. The scatter diagram of Zn-Hg (Fig 20) reveals a distinct lack of linearity, suggesting that the Hg content of sphalerite is highly variable, and/or that additional Hg-bearing phases are present. Hg is known to occur in the electrum ($\bar{x}$ = 10.64 % Hg), but the contribution of this component to the total variance in Hg is considered insignificant. The Hg content of the ores is a minimum of one order of magnitude greater than can be explained by the presence of electrum, i.e., mean analyses of 3.29 ppm Au compared to 38 ppm Hg, and where the Hg content of electrum is approximately 25 % of the Au content of the electrum. It is the author's contention that the Hg analyses are possibly inaccurate, as indicated by the lack of Zn-Hg positive covariance, which is suggested by the 1983 concentrate assays and the known occurrence of Hg in sphalerites from the Flin Flon belt (Chen, pers. comm., 1986). The process by which the Hg-bearing mineral(s) relates to arsenopyrite and cassiterite, the only significant hosts of As and Sn, respectively, is not readily explained. It is however noteworthy that the Hg content of sphalerite calculated from the 1983 concentrate assays is 0.014 Wt % Hg (See SPHALERITE). The average Hg and Zn content of the 27 ore samples is 38 ppm Hg and 14.51 Wt % Zn, which assuming sphalerite to be the only Hg- and Zn-bearing phase, yields a calculated Hg content of sphalerite of 0.016 Wt % Hg. This good agreement tends to suggest that indeed the Hg determinations are accurate, but that the Hg content of sphalerite from different ore samples and/or ore types is highly variable, but yields a consistent average for the ore. The metal-balance to be performed using the Matbal program on the mill products (Part 2 of Project) will help to clarify the question of the accuracy of these Hg determinations.

Arsenic exhibits a low positive correlation with Sb (+ 0.431) and with Hg (+ 0.493), and a low negative correlation with Cu (- 0.591), Se (- 0.413) and Te (- 0.512). The correlation of As with Sb reflects the greater abundance of arsenopyrite, which is interpreted to be the only significant host of As, in Sb-rich ores, where the latter tend to be Massive Sphalerite, and more typically Banded Pyrite Sphalerite ores with abundant galena, freibergite and pyrargyrite. The trace concentrations of As in freibergite, which behaves antipathetically to the Sb, is relatively insignificant, and is masked by the greater contribution to the total variance in As by the dominant arsenopyrite component. Arsenopyrite is also observed in the footwall Cu-rich ores, but invariably as a trace constituent, resulting in the Cu-As r-value of - 0.581. The low chalcopyrite content of Sb- and Ag-rich ores (galena associated with chalcopyrite tends to contain negligible freibergite) is consistent with the negative correlation of As with Cu, Se and Te, where arsenopyrite tends to be concentrated in these ores.

Antimony displays the highest degree of coherent covariance of all the elements, exhibiting significant positive covariance with all elements of the Zn-group, except Hg (Sb-Hg r-value = + 0.321), and conversely with elements of the Cu-group. Seven Sb-sulfosalts and dyscrasite were observed in the ores, where freibergite, gudmundite and pyrargyrite are by far the most abundant. Lead exhibits the next highest coherence, while Ag exhibits moderate coherence. Galena is by far the most significant Pb-bearing mineral, while Ag was identified as a major or essential substituent cation in 9 minerals (in 5 of which Sb is also an essential substituent), and as a minor or trace element in an additional 2 minerals. The positive covariance of Sb, Ag and Pb is characterised by moderate r-values, and reflects the wealth of host phases of Sb, Ag and Pb (Fig 20). In general Sb, Ag and Pb positively covary, and are coupled with the Zn-Cd pair, being enriched in sphalerite-rich ores. The lower coherence of Ag reflects the occurrence of Ag-minerals such as hessite, volynskite and naumannite, which are interpreted to predominate in the footwall Cu-rich ores. This association of Ag with elements of the Cu-group reduces the strength of the linear relationship of Ag with Sb, Pb and Zn. However, the contribution of Ag in freibergite, pyrargyrite, and other lesser sulfosalts, as well as galena and most probably sphalerite to the total variance in Ag, is dominant.

Indium and tin are also included in the Zn-group, and exhibit moderate coherent covariance. Neither element exhibits significant negative covariance with elements of the Cu-group. Cassiterite was the only Sn-bearing mineral identified, whereas no In-bearing mineral was identified. Both elements exhibit significant positive covariance with Zn, Ag, Sb and one another (Fig 20). Petruk (1985) reports that sphalerite in complex sulphide ores contains trace In, and that the In reports to the Zn concentrate. Petruk also reports that cassiterite in these ores generally occurs as fine-grained inclusions in sphalerite, which is in general agreement with the observations of this study. Thus, the mineral association of cassiterite with sphalerite explains the Zn-Sn r-value of + 0.389, whereas the observed occurrence of cassiterite as inclusions in chalcopyrite reduces the strength of this linear relationship and results in the marginally insignificant r-value of + 0.374 for the Cu-Sn pair. Indium is probably largely hosted in sphalerite, though the moderate Zn-In r-value of + 0.457 suggests either that the In content of sphalerite is highly variable or that additional In-bearing minerals exist. The moderate to high covariance of In with Ag and Sb (Fig 20) tends to confirm the later, and that In occurs in one or more of the Ag-bearing Sb-sulfosalts, or that the In content of sphalerite is elevated in ores with high sulfosalt content.

The Cu-Group (Footwall Association).

Elements : Cu, Se, Te, Co and Fe.

This group of 5 elements is characterised by the coherence of Cu, Se and Te, the less coherent Co, and the loosely included Fe. Cu, Se and Te all exhibit moderate to high (> 0.600) positive correlations with one another, Fe exhibits significant positive covariance with Se and Te, whereas Co exhibits only one significant positive correlation with other elements of the Cu-Group i.e, Co-Se pair. Co is included in the Cu-Group because of the one significant and numerous non-significant negative correlations with elements of the Zn-Group, and the converse for elements of the Cu-Group.

Co exhibits significant negative correlations with Pb, but insignificant correlations with Zn and Cd. In addition, the Co-Fe pair yields an r-value of + 0.283, suggesting that pyrite the dominant host of Fe is not the dominant host of the Co. Hawley and Nichol (1961) determined that partitioning of Co into pyrite, pyrrhotite and chalcopyrite in the Flin Flon ores to be 0.44 :

1.0 : 0.086. The general tendency for pyrrhotite to be concentrated in the Cu-rich footwall ores, and the predominence of pyrite as the Fe-sulphide in the galena- and sulfosalt-rich ores, suggests that pyrrhotite may be the dominant host of the Co. The contribution of the pyrrhotite to the total variance in Fe is masked by the dominant contribution of Fe in pyrite, and results in a loss of linearity in the Co-Fe covariance. In contrast however, minor pyrrhotite is comonly associated with galena, freibergite, gudmundite, etc., and Co has been identified along with Sb in costibite. The lack of significant positive covariance between Co and Fe, and the negative covariance of Co with Pb is probably a multi-phase relationship involving pyrrhotite, pyrite (± marcasite), chalcopyrite, costibite and their association with galena and the Sb-sulfosalts.

Fe is loosely included in the Cu-group because of the two significant positive correlations with Se (Fe-Se r-value = + 0.405) and Te (Fe-Te r-value = + 0.380), and the two significant negative correlations with the Zn-group elements Zn and Cd. Pyrite the dominant host of Fe is observed in all the ore types though it behaves essentially antipathetically to sphalerite by (1) banding and segregation of pyrite and sphalerite in the Banded Pyrite Sphalerite ores, and by (2) the tendency towards decreased pyrite content in the Massive Sphalerite ore type, and the converse in the Massive Pyrite ores. This contributes to the negative covariance of the Fe-Zn and Fe-Cd element pairs, while the tendency towards chalcopyrite-, pyrrhotite- and pyrite-rich footwall Cu-rich ores contributes to the positive covariance of Fe with the Cu-group elements. In addition, in Cu-rich samples that contain low abundances of pyrrhotite and pyrite, the Fe content of chalcopyrite sustains the covariance of Fe with the Cu-group elements. The positive covariance of the Fe-Hg pair (r-value = + 0.611) is not readily explicible, and again defies comment until the accuracy of the Hg determinations is clarified. However, this Fe-Hg covariance suggests that Hg either as a trace element in sphalerite and/or other mineral(s) covaries with pyrite the dominant host of Fe.

Cu, Se and Te all exhibit moderate to high correlation coefficients (ranging from + 0.622 to + 0.834) with one another, whereas Se and Te exhibit moderate to low positive covariance with Fe. The coherent positive covariance of Se, Te and Cu is surprising in view of the number of Te- and Se-bearing phases identified i.e., hessite (Te), clausthalite-galena (Se), rucklidgeite (Te, Se) pilsenite (Te, Se), volynskite (Te) and naumannite (Se). The Se-Pb pair yields an r-value of - 0.720, suggesting that the clausthalite-galena solid solution contributes an insignificant component to the total variance in Pb and Se (Fig 19). Hawley and Nichol (1959) determined variable but comparable ranges (200 to 400 ppm Se) of Se in pyrite, pyrrhotite and chalcopyrite from the Flin Flon ores. This suggests that the positive covariance of Se and Cu is primarily related to the Se content of chalcopyrite, and the paragenetic association of chalcopyrite with Se-bearing pyrrhotite, pyrite, hessite, clausthalite, rucklidgeite, pilsenite and naumannite in Cu-rich ores. The Cu-Te pair yields the highest r-value of the Cu-Group .i.e, + 0.834, and explains 70 % of the variance in Cu and Te (Fig 19). The partial covariance of Ag-Te is not exclusive of the Cu-Te covariance, as hessite is concentrated in the Cu-rich ores. In addition, rucklidgeite and pilsenite are concentrated in the Cu-rich ores, such that the covariance of Cu and Te may be explained by the paragenetic association of chalcopyrite with Te-bearing phases, but principally by Te in solid solution in chalcopyrite.

Petruk (1985a) notes that chalcopyrite in complex sulphide ores may contain a 'few' ppm Te, and this might be sufficient to accomodate much of the Te in the ores, which averages only 1.6 ppm Te. The low positive covariance of Fe with all the Cu-group elements reflects the masking effect of the dominant Fe in pyrite on the contribution of the chalcopyrite Fe to the total variance in Fe.

FACTOR ANALYSIS

As stated earlier, R-Mode Factor Analysis was employed to elucidate the structure of the chemical composition of the ores by attempting to define and interpret intercorrelations amongst the elements in the ore samples. R-Mode Factor Analysis analyses the structure within the standardized correlation coefficient matrix of a multivariate dataset (Davis, 1973). The technique is applied by clustering a large number of elements into a small number of uncorrelated, generalised factors, such that the elements within each factor are highly correlated, as indicated by high negative or positive factor loadings. The number of factors is ideally small with high factor loadings for each element, such that each element is associated with a minimum number of factors, thus simplifying the relationships in a complex dataset. In this manner the original elements can be replaced by the factors with little loss of information. Each factor describes an 'environmental factor' or geological process that contributes to the variation in the data. In addition, each sample receives a factor score for each extracted factor, and this score expresses the degree to which each sample possesses the property of the individual factors.

The principal factor matrix given in Table 30 contains the factor loadings for all 16 elements (S was excluded) in the dataset, for each of the 7 factors extracted. The communality is the fraction of the variation in each element that is described by the 7 factors. It should be noted that the square of the factor loading equals the fraction of the variation of that element described by the factor. It is also noteworthy that orthogonal varimax factor axis rotation was employed on the grounds that the factors are ideally uncorrelated and may reflect the effects of real phenomena which are postulated as being uncorrelated (Harbaugh and Merriam, 1968). For the purpose of interpretation an arbitary cut-off is adopted, below which value the factor loadings are considered insignificant or unrepresentative. Factor loadings below ± 0.400 were therefore disregarded, while the sign (denoted by P or N) of the accepted significant factor loadings are presented in Table 31.

Seven factors were extracted because this was the smallest number of factors to satisfactorily describe over 90 % of the variation in the dataset. Extraction of 6 factors was attempted and described less than 90 % of the variation in the dataset. However, with the extraction of 6 factors the essential changes relative to extracting 7 factors were that Factors 5 and 6 were combined resulting in significant loss of the described variation in the dataset, and specifically in Au and Mn. The element pair scatter diagram for the Au-Mn pair (Fig 19) indicates that the r-value of + 0.425 is a product of the extreme values distorting the correlation, and does not correctly describe that negligible correlation apparently exists. Thus, the extraction of 6

TABLE 30

PRINCIPAL FACTOR MATRIX.

	FACTOR.							
ELEM.	1	2	3	4	5	6	7	COMMUNALITY
Au	-0.017	-0.083	0.026	-0.009	-0.952	0.233	0.020	0.968
Ag	-0.005	0.004	-0.085	-0.956	-0.057	-0.007	-0.115	0.939
Cu	0.900	-0.189	0.092	-0.225	-0.041	-0.073	0.103	0.922
Zn	-0.270	0.910	-0.103	-0.259	0.058	0.003	-0.035	0.983
Cd	-0.197	0.950	-0.088	-0.103	0.058	0.059	0.060	0.971
Co	0.198	0.038	0.192	0.021	-0.012	0.131	0.931	0.963
Mn	0.061	0.048	-0.096	0.038	-0.239	0.948	0.129	0.990
Pb	-0.648	0.092	-0.152	-0.432	0.156	-0.025	-0.408	0.829
Fe	0.218	-0.512	0.758	-0.006	0.157	0.019	0.104	0.919
As	-0.785	-0.057	0.380	-0.138	-0.272	-0.156	0.218	0.928
Se	0.709	-0.200	0.243	0.364	0.008	0.064	0.289	0.822
Te	0.825	-0.377	0.014	-0.147	-0.029	0.046	0.132	0.864
Hg	-0.089	-0.040	0.901	-0.046	-0.142	-0.109	0.175	0.887
Sb	-0.363	0.477	0.416	-0.562	0.213	0.016	-0.073	0.898
In	0.044	0.339	0.274	-0.832	-0.008	-0.055	0.126	0.903
Sn	0.340	0.442	0.598	-0.513	0.096	-0.032	0.061	0.947
VAR.	3.49	2.77	2.30	2.68	1.17	1.03	1.29	
% VAR.	21.8	17.3	14.4	16.7	7.3	6.4	8.1	
CUM % VAR.	21.8	39.1	53.5	70.2	77.5	83.9	92.0	

TABLE 31

PRINCIPAL FACTOR MATRIX
PORTRAYING ONLY THE SIGN OF THE SIGNIFICANT FACTOR LOADINGS.

	FACTOR.						
ELEMENT	1	2	3	4	5	6	7
Au					N		
Ag				N			
Cu	P						
Zn		P					
Cd		P					
Co							P
Mn						P	
Pb	N			N			N
Fe		N	P				
As	N						
Se	P						
Te	P						
Hg			P				
Sb		P	P	N			
In				N			
Sn		P	P	N			

factors was rejected on the grounds that it excessively compresses the variation in the dataset into too small a number of factors or geological processes. By extracting 8 or 9 factors a greater amount of the variation in the dataset was described, but with the creation of meaningless additional factors with insignificant low factor loadings and no apparent geological significance.

The values for communality indicate that 99 % of the variation in Mn and 98 % of the variation in Zn were accomodated for by the 7 factors. Conversely, the 7 factors described only 82 % of the variation in Se and 83 % of the variation in Pb. The combined variation in the 16 elements described by the 7 factors is 92.0 %. One of the more interesting results of the factor analysis is that Factors 5 and 6 contain only one very high significant factor loading for Au and Mn, respectively. This suggests that greater than 90 % of the variation displayed by Au and Mn is controlled by 2 processes that are each independent of the variation in any of the other 15 elements. Factor 6 describes 90 % of the variance in Mn and represents the variation in Mn derived largely from the distribution of the Mn-bearing gangue minerals. Factor 5 describes 91 % of the variance in Au, and indicates that the distribution of Au is independent of all other 15 elements. The mercurian electrum is the sole Au-bearing mineral identified and contains approximately 10 % of the Ag, and 2 % of the Hg in the ore. These two elements behave antipathetically with Au within the compositional range of the electrum, and this togethar with the minor contribution of the Ag and Hg in electrum to the total variance in the respective element, results in a complete lack of significant covariance in Ag and Hg with Au. Factor 5 also confirms the results of the correlation analysis, whereby neither Cu nor As exhibit positive covariance with Au.

Factor 1 describes 21.8 % of the variance in the dataset, and constitutes the most powerful process controlling the variance in the data. Cu, Se and Te exhibit high positive factor loadings, As exhibits a high negative and Pb exhibits a medium negative factor loading. This indicates that Cu, Se and Te behave essentially sympathetically and are antipathetic with respect to approximately 62 % and 42 % of the variance in As and Pb, respectively. This factor is interpreted as describing the distribution of chalcopyrite which is the only significant Cu-carrier and probably the principal host of Se and Te, as well as the mineral association of tellurides and selenides with the footwall chalcopyrite-rich, and hence Cu-rich ores. Simultaneously, As and consequently arsenopyrite, and Pb and principally galena are depleted in the Cu-rich ores. It is interesting that Sn exhibits a marginally insignificant positive factor loading of + 0.340, suggesting that a small portion of the variance in Sn is sympathetic with that of Cu. This may reflect a mineral association of minor cassiterite with chalcopyrite, or stannite (not identified in the ores) with chalcopyrite, or trace Sn in solid solution in chalcopyrite.

Factor 2 describes 17.3 % of the variance in the dataset and contains high positive factor loadings for Zn and Cd and moderate to low positive factor lodings for Sb and Sn, and thus the sympathetic relationship of Zn and Cd with a smaller component of the variance in Sb and Sn. The low negative factor loading on Fe indicates that Fe exhibits an antipathetic relationship with the latter 4 elements. As this factor describes 83 % and 90 % of the variance in

Zn and Cd, respectively, it clearly represents the process controlling the distribution of sphalerite. This process is coupled with a component in the variance of Sb and Sn, which is interpreted to represent the elevated concentration of Sb-sulfosalts and cassiterite in the Zn-rich ores. Conversely, the negative factor loading on Fe confirms the antipathetic relationship of the dominant Fe host pyrite, and also pyyrhotite and chalcopyrite with respect to sphalerite and the associated Ag-bearing sulfosalts.

Factor 3 describes 14.4 % of the variance in the dataset, and contains a high positive factor loading on Hg, a moderate to low positive factor loading on Sn, As and Sb, and a medium to high positive factor loading on Fe. This factor describes 81 % of the variance in Hg. However, as the accuracy of the Hg determinations is questionable on the basis of the complete lack of Zn-Hg covariance, this factor may not represent a real phenomena operating on the ores. If it is assumed that the Hg analyses are accurate, and that the concentration of Hg in sphalerite from different ore samples and/or ore types is highly variable, then this factor describes the process by which the Hg content varies and is coupled with a component of the variance in Fe, Sn, As and Sb. Thus, as the Hg content increases it is interpreted that the abundance of pyrite, arsenopyrite, cassiterite and the Sb-sulfosalts (possibly the more common and non Ag-bearing gudmundite) also increases in the ore. The Banded Pyrite + Sphalerite ore type exhibits the highest factor scores and thus expression of this factor. This reflects the observed increased abundances of arsenopyrite, Sb-sulfosalts and pyrite in this ore type as it grades along a line of differentiation away from the Massive Sphalerite ores and towards the Massive Pyrite ores.

Factor 4 describes 16.7 % of the variance in the dataset and 91 % of the variance in Ag. Ag and In exhibit high negative factor loadings, while Sb, Pb and Sn exhibit low negative factor loadings, and thus the sympathetic relationship of Ag and In with a component of the variance in Sb, Pb and In. As this factor includes 91 % of the variation in Ag, it clearly constitutes a multiphase mineral association encompassing at least 11 known Ag-bearing minerals. The mass balancing of Ag in many of the ore samples indicates that sphalerite and possibly chalcopyrite may contain trace but significant concentrations of Ag. Petruk (1985) notes that sphalerite from complex sulphide ores contains approximatley 20 to 50 ppm Ag in solid solution, while the Kidd Creek sphalerites range from not detected (> 12 ppm) to 308 ppm averaging 45 ppm Ag (Cabri et al. 1985). Similarly, the latter authors found that Kidd Creek chalcopyrites contain trace Ag that ranged from not detected (< 10 ppm) to 1,589 ppm Ag with no average value quoted, whereas In is carried in chalcopyrite and to a lesser extent in sphalerite. Factor 4 is interpreted to describe the distribution of Ag and In and partly that of Sb, Pb and Sn, where Ag and In are partly hosted in sphalerite and possibly chalcopyrite, but whose concentration is independent of that of Zn and Cu, and hence the abundance of sphalerite and chalcopyrite. In addition, high Ag values are coincident with high Sb, Pb and Sn in the form of elevated abundances of Sb-sulfosalts, many of which are Ag-bearing, galena and cassiterite. The lack of strong Zn-Ag covariance (r-value = + 0.269) reflects the independence of this Ag+In+Sb+Pb+Sn association with Zn, though it tends to coincide, in a permissive rather than linear manner with Zn-rich ores. The In-Ag covariance reflected in the r-value of + 0.753 and confirmed by Factor 4 may partially reflect the known coupled substitution of $Ag^{+} + In^{3+} = 2 Zn^{2+}$ in synthetic sphalerites (McIntyre et al. 1984), and possibly similar substitution for Cu^{2+} in chalcopyrite. There is however no evidence that the chalcopyrite at Trout Lake contains significant Ag, other than the diffulties encountered in mass balance calculations of Ag while disregarding chalcopyrite as a Cu-carrier.

Factor 7 describes 8.1 % of the variance in the dataset and contains significant antipathetic factor loadings for Co (+ 0.931) and Pb (- 0.408). This factor indicates that 87 % of the variance in Co is independent of all other elements, except for a minor (17 %) component in the variance in Pb. Costibite is the only Co-bearing mineral identified, though pyrrhotite and possibly also chalcopyrite and pyrite are interpreted as the principal Co-carriers. The lack of Fe-Co covariance is in agreement with the correlation analysis and confirms that pyrite the dominant host of Fe is not a significant Co-carrier, while the complete lack of Co-As covariance indicates that arsenopyrite is not a Co-carrier. It is interpreted that Co is principally hosted in pyrrhotite and that the covariance of Co with the Fe in pyrrhotite is completely masked by the dominant contribution of the Fe in pyrite to the total variance in Fe. The partial antipathy of Pb with Co remains unexplained, though galena and pyrrhotite tend to be concentrated in the hangingwall and footwall, respectively.

Factors 1, 2, 3, 4 and 7 are multi-element factors describing distinct element associations whose behaviour are controlled by five ideally independent geological processes. For example, chalcopyrite and sphalerite tend to be concentrated in different ores, though the relationship is distinctly non-linear with numerous combinations of the two extremes. The factors can be regarded as independent processes that are all superimposed on one another in the ores, but that display variable expression independent of the expression of the superimposed factors. Thus a high Zn sample will contain high Cd, but potentially high or low Cu, As, Ag or Hg values, whereas a high Cu sample will exhibit high Se and Te values, low As and Pb, but potentially variable Zn, Cd Ag, Au, etc. These five factors are summarised in to the following associations.

1. Factor 1 : Cu + Te + Se - As - Pb.
2. Factor 2 : Zn + Cd + Sb + Sn - Fe.
3. Factor 3 : Hg + Fe + Sn + Sb.
4. Factor 4 : Ag + In + Sb + Sn + Pb.
5. Factor 7 : Co - Pb.

These five factors describe the independent processes whose combined expression results in the generalised two-fold division of the ores into the Zn-group and the Cu-group elements. Thus, the principal of the ores representing a simple differentiation series from Zn-rich to Cu-rich is a simplified or generalised trend of the fundamental processes at work. In addition, if the ores were differentiated primarily on the basis of Cu and Zn, then these two elements would contribute high antipathetic factor loadings on a single factor. Clearly, these elements are not mutually exclusive and do not exhibit a strong linear relationship describing such a negative covariance. However, this generalisation is largely valid, because the factors are apparently not truely independent, in that Factors 2, 3 and 4 typically exhibit compatible expression, whereas Factors 1, 5 and 7 exhibit compatible expression. Oblique factor axis rotation is preferred where the factors are partially correlated, as indicated by these non-orthogonal dependent relationship of the factors (Harbaugh and Merriam, 1968). However, the R-Mode Factor Analysis program employed in this study does not have an oblique factor axis rotation option.

SUMMARY

Copper is carried in chalcopyrite, cubanite, bournonite and freibergite, where the latter three phases represent insignificant contributions of Cu to the total Cu tonnage. Te was determined to occur in hessite, rucklidgeite, pilsenite(?), volynskite and in the clausthalite-galena solid solution that was associated with rucklidgeite. The Cu-Te element pair yields the highest r-value of the Cu-Group elements i.e., + 0.834, and is interpreted as the result of the paragenetic association of the Te-bearing minerals with chalcopyrite, probably with a significant contribution from trace Te in solid solution in chalcopyrite (undetected; <0.01 Wt % Te). Selenium was identified in the clausthalite-galena solid solution, rucklidgeite, pilsenite(?) and naumannite. The Se-Pb pair yields an r-value of - 0.720, indicating that the clausthalite-galena solid solution contributes an insignificant component to the total variance in Se and Pb. The positive covariance of Cu and Se (r-value = + 0.622) is interpreted as resulting from the Se content of chalcopyrite, and the paragenetic association of chalcopyrite with Se-bearing pyrrhotite and pyrite (Hawley and Nichol, 1959), rucklidgeite, pilsenite(?) and naumannite in Cu-rich ores.

Zn is carried in sphalerite and freibergite, where the latter is an insignificant contributor to the total Zn tonnage. Cd and possibly Hg are also hosted in the sphalerite. The extremely strong positive covariance of Cd and Zn demonstrates that sphalerite is the host of the Cd. The complete lack of Zn-Hg covariance suggests that (1) Hg is only partly hosted in sphalerite, (2) does largely occur in sphalerite, but exhibits highly variable content, or (3) the Hg determinations are inaccurate. The latter option is without factual foundation at present and is disregarded. In light of the known occurrence of Hg dominantly in sphalerite from Flin Flon ores (Chen, pers. comm., 1986), it is probable that the Hg is largely hosted in sphalerite with extremely variable concentrations. The sole mineral positively identified as being Hg-bearing is electrum, which is interpreted to contain approximately 2 to 3 % of the Hg in the ore. The variation in Hg content is coupled with bulk variations in Fe, Sn and Sb, and achieves maximum expression in the Banded Pyrite + Sphalerite ores, where pyrite, Sb-sulfosalts and probably cassiterite are most abundant.

Au is interpreted to be largely carried in mercurian electrum which is the only Au-bearing mineral identified. The correlation and factor analyses failed to identify any geochemical association of Au with any element, other than Mn, which probably reflects a distorted (non-normally distributed variables) correlation coefficient or an unidentified paragenetic association with a Mn-bearing gangue phase. No association of Au with As was apparent, nor was any association of arsenopyrite with electrum observed petrographically. The lack of covariance between Au and Hg and Ag reflects the minor contribution of the Ag and Hg in electrum to the total variance in these elements, which occur in concentration levels that are at least one order of magnitude greater than can be explained by their occurrence in electrum. The abundance and relative ease with which electrum was observed (417 grains and two anastomosing masses) suggests that electrum may indeed be the sole Au-bearing mineral, though the existence of trace Au in solid solution in pyrite cannot be discounted or confirmed without the use of an ion microprobe or micropixie.

Arsenic occurs principally in arsenopyrite, but also in solid solution in freibergite, where it's level of concentration ($\bar{x}$ = 0.20 Wt % As), and the trace abundance of freibergite in the ores, implies that arsenopyrite can be assumed to be the sole host of As.

Costibite is the only Co-bearing mineral identified, but is interpreted to be a minor Co-carrier because only one grain was observed, and because of the complete lack of Co-Sb positive covariance. The principal host of Co was not identified, but was interpreted to be pyrrhotite and possibly chalcopyrite to a lesser extent.

Cassiterite is the only Sn-bearing mineral identified, though it may be cautiously inferred that stannite may occur associated with chalcopyrite and remains to be observed. The metallurgically troublesome element Sn, which averages 36 ppm in the ores, is interpreted to be largely hosted in cassiterite associated with sphalerite, and a lesser component either as cassiterite or stannite associated with chalcopyrite, or in solid solution in chalcopyrite.

The metallurgically troublesome element Bi occurred consistently at concentration levels below the detection limit of the chemical analyses (0.001 Wt % or 10 ppm Bi). Bi was detected in the tellurides rucklidgeite, pilsenite(?) and volynskite. Galena is a potential host phase of trace Bi, but the severe Bi and PbMα overlap prohibits detection of less than 1 or 2 % Bi.

Indium which occurs at trace concentrations in the ores ($\bar{x}$ = 34 ppm In) is interpreted to occur in sphalerite, possibly chalcopyrite and/or Sb-sulfosalts. Indium exhibits moderate positive covariance with Zn, but high positive covariance with Ag, Sn, Sb and Pb. The strong covariance with Ag may reflect their geochemical association rather than necessarily being co-hosted in the same mineral. However, it is interpreted that a major component of both In and Ag are carried in sphalerite, especially where associated with Sb-sulfosalts in the Banded Pyrite Sphalerite ores.

Antimony is carried in freibergite, gudmundite, pyrargyrite, boulangerite, freislebenite, dyscrasite, bournonite and costibite, where the first three most abundant Sb-sulfosalts may be assumed to contribute the only significant components to the total variance in Sb. Four of the above minerals are Ag-bearing, particularly the more abundant freibergite and pyrargyrite, and this togethar with the association of these minerals with sphalerite and galena, both of which are interpreted as major Ag-carriers, results in a moderately strong Ag-Sb positive covariance.

Silver is carried in freibergite, pyrargyrite, hessite, electrum, dyscrasite, freieslebenite, naumannite, volynskite, acanthite, galena, probably sphalerite and possibly in chalcopyrite. Minor but erratic Ag was also detected in the clausthalite-galena solid solution. Despite the number of Ag-bearing minerals Factor 4 describes 91 % of the variance in Ag, suggesting that the distribution of Ag is extremely systematic, covarying with significant components of the variance in In, Sb, Sn and Pb. Both Zn and Cu exhibit insignificant positive covariance with Ag, suggesting that both sphalerite and chalcopyrite are not the principal Ag-carriers, or that the Ag content of either of these minerals is highly variable and independent of the Zn and Cu abundances in the same sample. The strong In-Ag covariance suggests that sphalerite is a principal host of Ag, though chalcopyrite being a simple derivative structure of sphalerite may also demonstrate the coupled substitution of $Ag^{+} + In^{3+} = 2\ Me^{2+}$, where Me denotes Zn or Cu. Microprobe analysis of the Ag in galena indicated a minimum average content of 250 ppm Ag, and this suggests that galena hosts approximately 3 to 5 % of the Ag in the ore. Microprobe analyses of the mercurian electrum yields an average Au/Ag ratio of 0.9 and indicates that this mineral accounts for approximately 11 % of the Ag in the ore, assuming the electrum is the sole significant Au-carrier. If one assumes that sphalerite and chalcopyrite contain an average of 50 ppm Ag in solid solution, then the sphalerite hosts 20 % of the Ag and chalcopyrite 15 % of the Ag in the ore, based on the average Ag, Zn and Cu assays of this study. It is noteworthy that modal analysis of the Sb-sulfosalts, and the subsequently derived chemical compositions of TLS.5-64, when compared to the bulk chemical compositions indicated that the Sb-sulfosalts account for approximately 50 % of the Ag in this sphalerite- and galena-rich, chalcopyrite-poor sample. The principal Ag-carriers are interpreted to be freibergite, sphalerite, pyrargyrite, galena, chalcopyrite and electrum. It is also interpreted that the Ag content of sphalerite, galena and chalcopyrite varies in different ore types and/or samples, and is partly dependent on the abundance of other minerals capable of carrying significant Ag. For example, the highest determined Ag content of galena (1,200 ppm Ag) was observed in a Massive Pyrite ore with abundant galena, freibergite and trace dyscrasite.

Chapter IX

PREDICTION OF MINERAL LIBERATION

The grain size distributions for pyrite, chalcopyrite, sphalerite, freibergite and galena were determined for each of the 27 representative samples (plus the Chalcopyrite Stringer ore TLN.1-89) in order to predict liberations that would be obtained at certain grinds. Histograms and cumulative grain size distributions were plotted for the minerals of interest. The grain size distributions were condensed into mean distributions for each ore type, and histograms and cumulative grain size curves were plotted (Fig 7 to Fig 15). The 80 % 'passing' or 'less than' fraction is given for each detected mineral in each ore type. It is interpreted by Petruk's liberation model that the minimum grind to liberate the mineral, is a grind that gives the same size distribution of the mineral in the unbroken ore. The same model gives the optimum grind as the point on the cumulative grain size curve where the curve flattens, and beyond which point further grinding would not yield a significant (>10 %) increase in liberation (Petruk, 1976). The minimum and optimum grinds for the minerals of interest in each ore type and for an average Trout Lake ore are presented in Table 32. The average Trout Lake ore is a weighted average in terms of the Wt % of the mineral in each ore type (excluding the Vein Quartz Chalcopyrite ores), and not in terms of the relative abundance of each ore type, which is unknown. Thus, the predicted average grinds for liberating sphalerite are not significantly affected by the minor fine-grained sphalerite in the Chalcopyrite Stringer ores, but is dominated by the the major coarse-grained sphalerite in the Massive Sphalerite ores. The grain size distributions of pyrite, sphalerite, chalcopyrite, galena and freibergite for the average Trout Lake ore are presented in Figure 21.

Petruk's liberation model assumes that 50 % of the mineral would be liberated at the minimum grind, and provides a method for calculating the approximate liberation that would be produced at finer grinds. The method involves (1) determining the 95 % passing size of the grind, (2) drawing a vertical line on the cumulative size distribution curve for the mineral of interest, and (3) noting the point where the vertical line intersects the cumulative size distribution curve. To determine the predicted liberation one uses the values on the cumulative size distribution axis. The predicted liberation is [100 - (value at the point of intersection) + (value at point of interest) / 2]. The predicted liberation that would be obtained when an assumed average Trout Lake ore is ground to 95 % minus 147 um, the nominal grind used for processing Trout Lake ore, is 55 % for pyrite, 62 % for chalcopyrite, 66 % for sphalerite, 52 % for galena, 52 % for freibergite and 31 % for electrum. The above predicted liberations are minimum liberations because they assume that all these minerals are cemented in a matrix that is composed of minerals that have the same breakage characteristics as the ore minerals. In practise soft minerals like sphalerite, chalcopyrite and galena will break into finer grains than the hard minerals like pyrite, hence inclusions within these soft minerals will achieve higher liberations than predicted. Furthermore, pyrite tends to break along grain boundaries, and consequently releases the small interstitial minerals. Therefore, liberation of the interstitial minerals depends upon the liberation of the host mineral, i.e., pyrite, rather than upon the size of the interstitial mineral. On the other hand, minerals that are completely enclosed in pyrite will probably not be liberated unless the ore is ground to an extremely fine size.

Following the above guidelines, it is likely that the sphalerite liberation will be slightly higher than predicted due to interstitial sphalerite in pyrite. Similarly, the chalcopyrite liberation will be higher than predicted due to (1) interstitial chalcopyrite in pyrite, (2) veinlets in pyrite, and (3) intergrowths with sphalerite. It is noteworthy that Petruk (1986) found that only a small percentage of "chalcopyrite-disease" was still present as rods and blebs in sphalerite from New Brunswick, after the ore had been ground.

It is likely that the galena liberation will be much higher than predicted because it mostly occurs as (1) interstital material or inclusions in sphalerite, and (2) in fractures and interstices in pyrite. Sphalerite is a soft mineral that breaks into smaller grains than the screen analysing the ore would indicate, and hence would liberate more galena than predicted. The interstital galena in pyrite would also be liberated from pyrite when pyrite is liberated, regardless of the size of the galena grains. The rare minerals freibergite, electrum, hessite, etc., occur largely as minute grains associated with galena, chalcopyrite and sphalerite, commonly in fractures and interstices in pyrite. Their liberation therefore depends upon the breakage of the ore to a size that will liberate the host mineral, eg., pyrite, as well as the breakage that would release the minute grains. Therefore, the liberation of these minerals will likely be much higher than predicted by the liberation model.

It is possible to make a very generalised prediction on metal recoveries, taking into consideration that concentrate grades can substantially alter this prediction, and as stated above, actual liberations are subject to variation. In general it can be expected that 95 % of free minerals plus 33 % of unliberated minerals would be recovered in relatively high grade concentrates i.e., 26 to 28 Wt % Cu, and 50 to 54 % Wt % Zn in the respective concentrates. Following these guidelines the predicted recovery for sphalerite from Trout Lake ore is 78 % and chalcopyrite 75 %. Actual observed recovery of Zn in the Zn concentrate is 77 %, whereas 92 % of the Cu is actually recovered in the Cu concentrate. However, an additional 14 % of the Zn is lost/recovered to the Cu-concentrate.

Electrum was observed in 37 of the 112 samples, while thirty two samples contained the total of 417 grains of electrum of type 1 and 3 (See ELECTRUM), whereas sample TLN.1-89 and TLN.2-11 contained anastomosing masses of electrum of type 2. The grain size distribution of electrum of type 1 and 3 was measured using an optical microscope with calibrated graticules, whereas that of type 2 was determined with the image analyser. Because electrum of type 1 and 3 tends to assume a rectangular shape in the plane of the section, it is not amenable to measurement by a single dimension. Each grain was measured

FIGURE 21

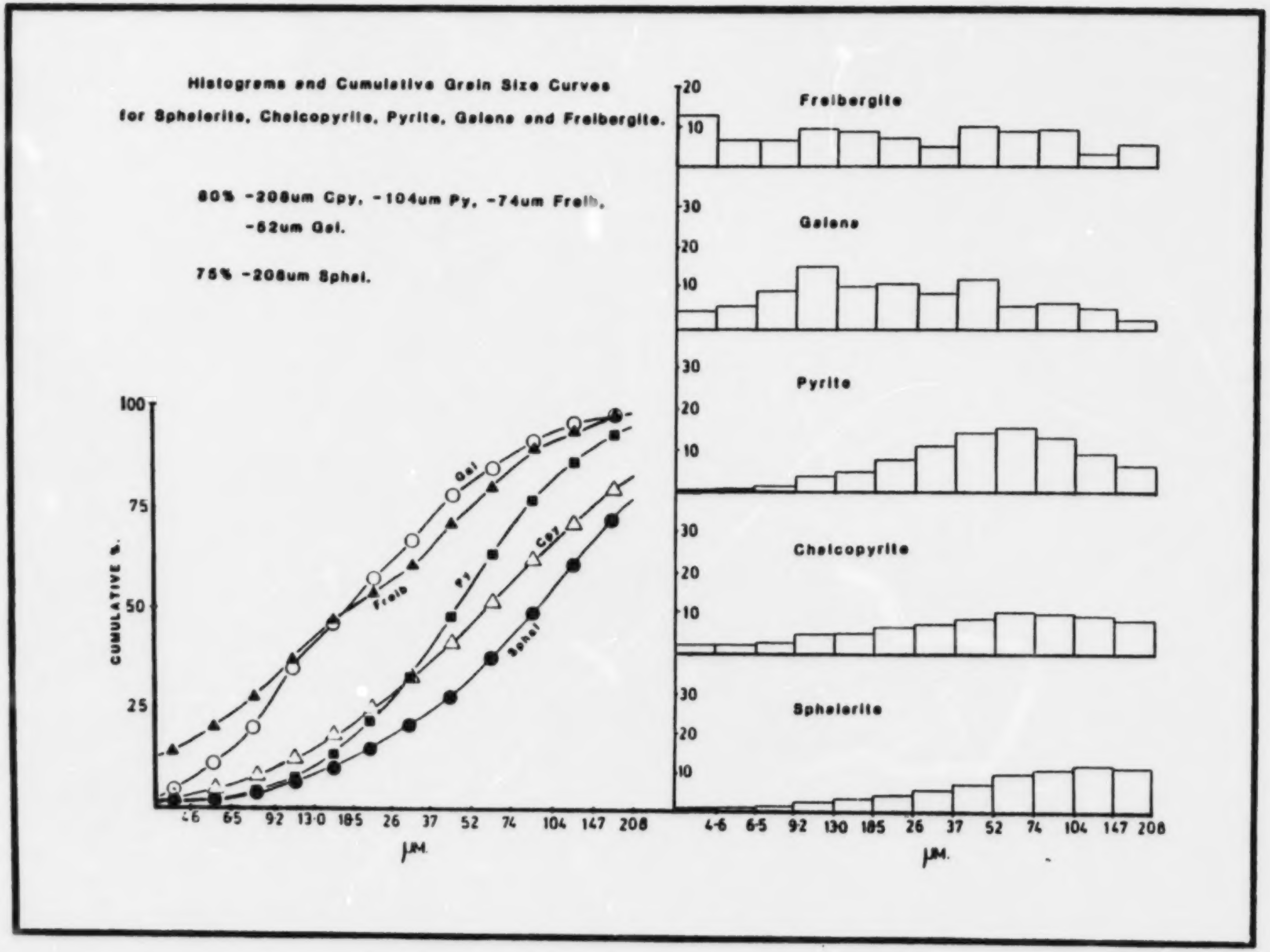

Histograms and Cumulative Grain Size Curves for Sphalerite, Chalcopyrite, Pyrite, Galena and Freibergite.

80% -208um Cpy, -104um Py, -74um Freib, -52um Gal.

75% -208um Sphal.

TABLE 32

THE MINIMUM AND OPTIMUM GRINDS FOR THE MINERALS OF INTEREST.

Ore Types.	Pyrite		Sphalerite		Chalcopyrite		Galena		Freibergite		Electrum	
	M.G.	O.G.	M.G.	O.G.	M.G.	O.G.	M.G.	O.G.	M.G.	O.G.	M.G	O.G.
M. Sp.	147	52	>208	147	74	6.5	74	13	13	4.6	-	-
B. Py+Sp.	104	37	208	74	26	4.6	52	13	74	52	-	-
M. Py.	147	37	52	13	18	4.6	18	4.6	26	4.6	-	-
M/B. Cp+Sp.	37	13	147	74	147	52	-	-	-	-	-	-
M. Cp+Po.	104	37	52	13	>208	74	-	-	-	-	-	-
Cp. Stgs.	208	52	52	9.2	>208	104	-	-	-	-	-	-
D. Py+Cp.	104	37	104	26	104	37	-	-	-	-	-	-
S. Cp+Sp.	104	52	74	37	147	18	-	-	-	-	-	-
V. Qtz+Cp.	208	52	104	37	>208	208	-	-	-	-	-	-
Mean.	95	26	>208	52	175	52	48	9.2	60	4.6	23	4.6

M.G. denotes the Minimum Grind, quoted at 80 % passing.

O.G. denotes the Optimum Grind, quoted at 80 % passing.

along its maximum dimension (dm), and then an average dimension (di) perpendicular to dm was estimated. The 'equivalent square diameter' was calculated from the product of dm and di.

The grain size distribution for electrum in type 1 and 3 is presented in Fig 22, and is defined by 80 % - 18 um. The grain size of electrum of type 2 was determined by chord analysis of TLN.2-11 and TLN.1-89. The latter sample contained 0.2 Area % electrum and corresponds to approximately 900,000 um^2 of electrum. This contrasts with approximately 9,000 um^2 in TLN.2-11, and approximately 11,000 um^2 for all 417 grains of type 1 and 3. A weighted average grain size distribution for type 2 was calculated and is defined by 80 % - 37 um (Fig 22). A 'sample' (statistical) of 417 grains in 32 samples is considered representative of type 1 and 3, whereas 2 anastomosing masses, especially the overwhelming influence of the electrum in TLN.1-89, cannot be considered as a large enough 'sample' to be representative of type 2. The relative abundance of type 1 and 3 relative to type 2 is therefore unknown, and an unweighted average grain size distribution of type 1, 2 and 3 was generated (Fig 22). The resulting distribution for electrum is defined by 80 % - 26 um. The calculated predicted liberation using Petruk's model is 25 % for type 1 and 3 electrum, and 37 % for type 2 electrum, and corresponds to predicted recoveries of 50 % and 58 %, respectively. It is noted that the actual recovery of Au in the Cu concentrate is 59.6 %.

Sample TLS.5-64, a representative Massive Sphalerite ore, contained abundant freibergite, pyrargyrite and gudmundite. Because of their abundances in this sample image analysis of these 3 phases and galena (in addition to the routine mineral list) was possible, and was performed to determine the mineral quantities and the grain size distributions of these minerals, three of which are Ag-bearing. The results of the chord analyses are plotted in Fig 23, and demonstrate the consistently fine-grained nature of the Sb-sulfosalts i.e., 80 % - 13 um for freibergite, pyrargyrite and gudmundite. Except for freibergite, which exhibits a fine- to medium-grained nature in some of the Banded Pyrite + Sphalerite ores, the distributions are considered representative of the bulk of the pyrargyrite and gudmundite in the ores. The derived chemical compositions of TLS.5-64 is of particular interest in evaluating the Ag-bearing minerals. The derived compositions compare favourably with the chemical analyses (See Table 7). The derived Sb content of 0.03 Wt % (300 ppm) Sb is in excellent agreement with the chemical analysis of 310 ppm Sb, whereas the derived Ag content of 0.02 Wt % (200 ppm) Ag is approximately half of the chemical analysis of 0.04 Wt % (446 ppm) Ag. This suggests that despite accommodation of all the Sb-sulfosalts, only 45 % of the Ag could be accounted for, and that galena and probably sphalerite are Ag-bearing. If galena is the host of the excess Ag, then it contains approximately 0.15 Wt % (1,500 ppm) Ag, a detectable concentration that was not observed, and which far exceeds the tentative average 250 ppm Ag content in galena. The derived Ag content however, is subject to large uncertainty due to the poor sensitivity of the determination of the Area % of freibergite and pyrargyrite at these levels of abundance, as well as the uncertainty due to sample inhomogeneity. However, it is suggested here that the uncertainty in the derived compositions and principally the existence of Ag in solid solution in sphalerite and galena, both contribute to the discrepancy between the derived and the chemical analyses.

FIGURE 22

Histograms and Cumulative Grain Size Curves For The Trout Lake Electrum.

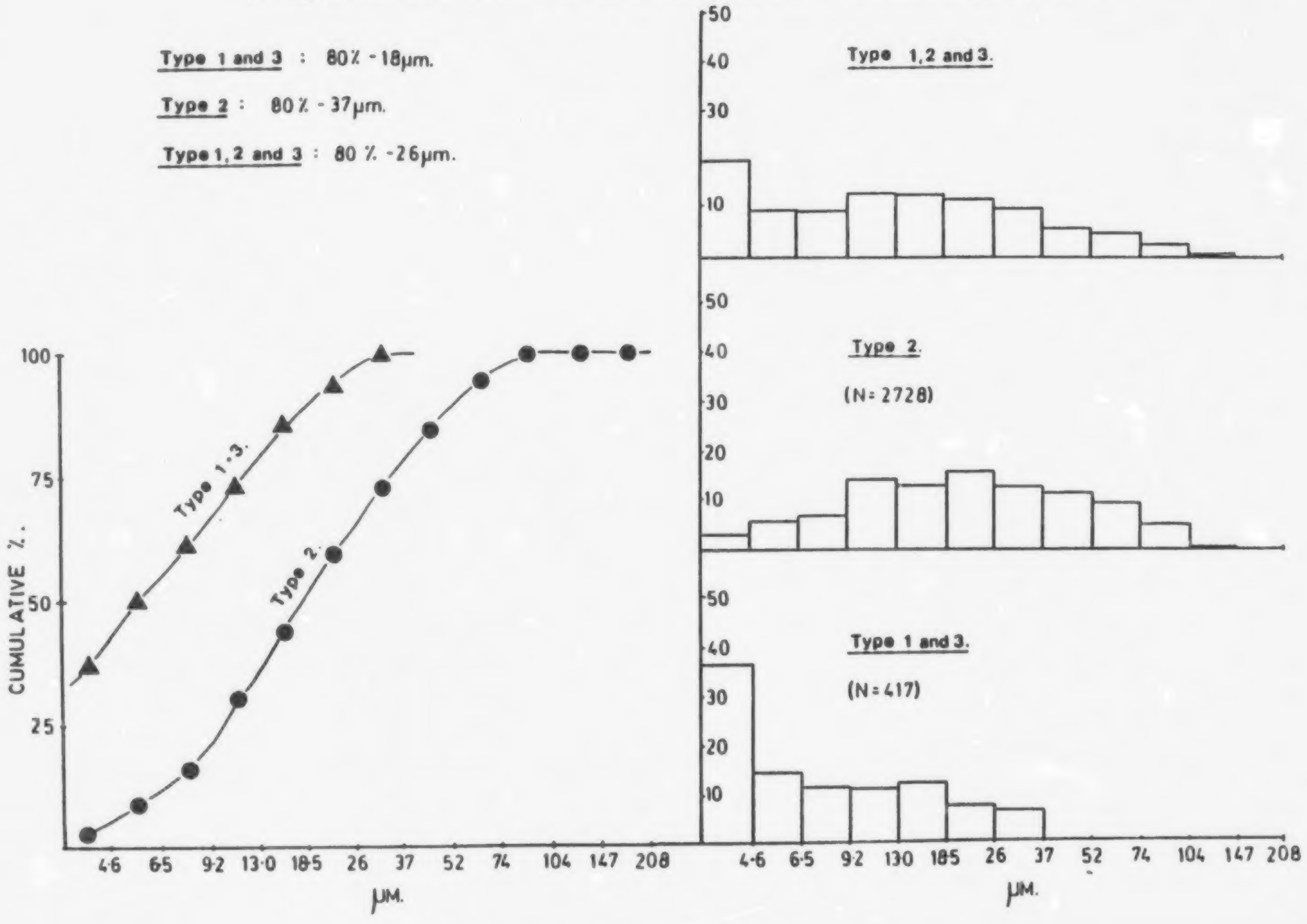

FIGURE 23

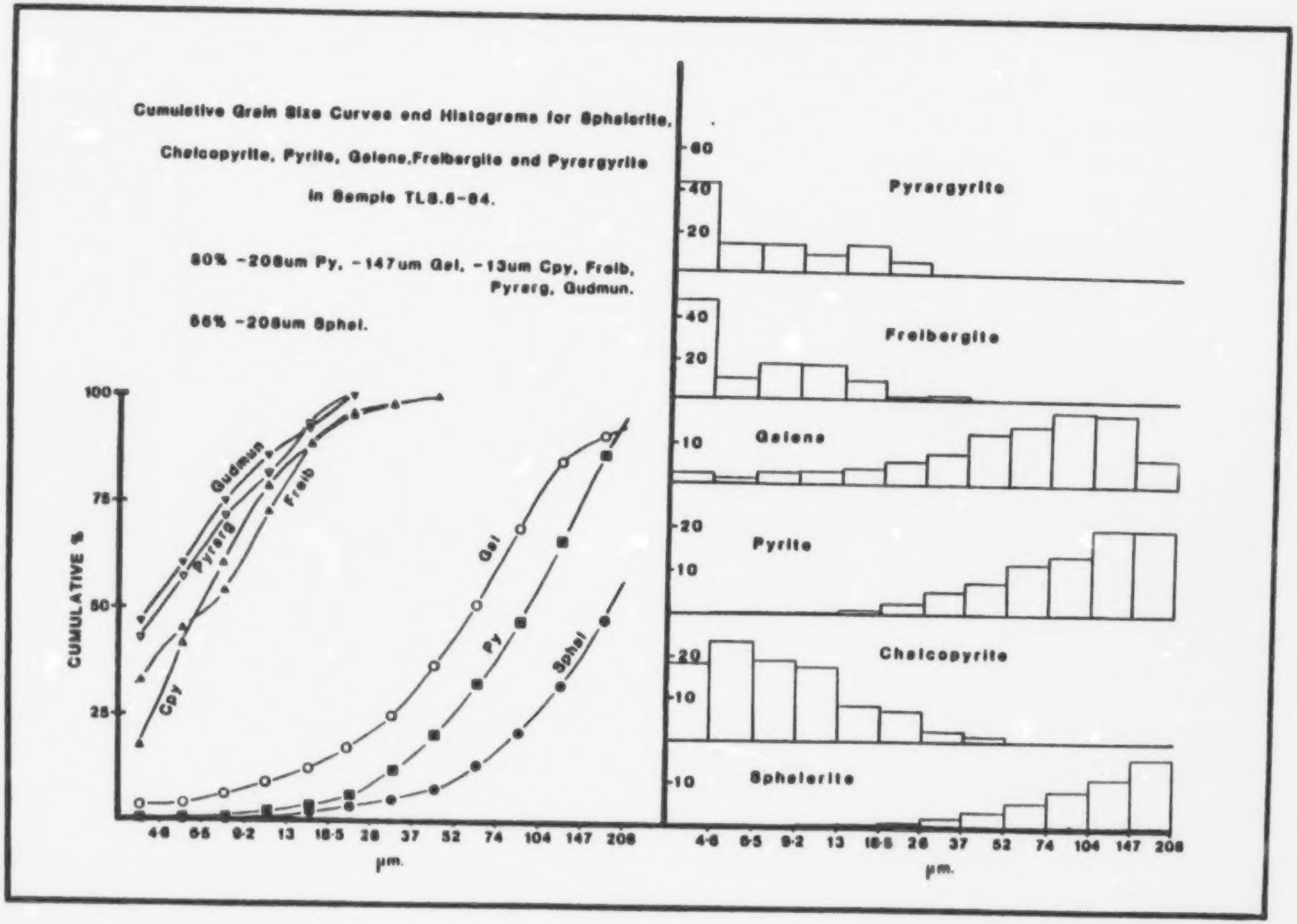

Cumulative Grain Size Curves and Histograms for Sphalerite, Chalcopyrite, Pyrite, Galena, Freibergite and Pyrargyrite in Sample TLS.5-84.

80% -208um Py, -147um Gal, -13um Cpy, Freib, Pyrarg, Gudmun.

55% -208um Sphal.

As stated earlier the predicted liberations for freibergite, galena, sphalerite and chalcopyrite, all of which are interpreted to be Ag-carriers in that approximate order of confidence and/or significance, are 52, 52, 66 and 62 %, respectively. The predicted liberation for freibergite and pyrargyrite in sample TLS.5-64 is 23 % and 19 %, respectively, while the petrographic observations on the grain sizes of pyrargyrite, hessite, dyscrasite and the other lesser Ag-bearing minerals suggests that comparable predicted liberations would have been obtained had the grain size distributions been determined. All of these Ag-bearing minerals are 'soft' relative to pyrite and quartz and will tend to concentrate preferrentially in the finer sieve fractions of the grind, and thus probably achieve somewhat higher actual liberations. Thus, the flotation behaviour of these minerals (excluding the greater portion of sphalerite and chalcopyrite which are liberated) will be largely determined by the flotation characteristics of the host mineral.

Chapter X

THE ORE TEXTURES AND METAMORPHISM AT TROUT LAKE

The Trout Lake ore deposit comprises a series of steeply dipping stacked lenses (6 proven), that are interpreted to represent a metamorphosed volcanogenic massive sulfide deposit as defined by Franklin et al. (1980). The ores were deposited by metal-bearing hydrothermal fluids mixing with seawater, either just below or above an exhalative vent on the Aphebian seafloor. The ore lenses are interpreted to have formed as mounds of sulfide mud produced by a 'snowfall' of fine-grained sulfide precipitates above the vent, with associated deposition of a cross-cutting vein system beneath the vent, representing the 'plumbing system', and generally referred to as the stockwork or stringer mineralisation. The lenses (both exhalative and stockwork ores) generally exhibit a pronounced metal zonation of decreasing Cu / (Cu + Zn) stratigraphically upwards and towards the margins of the lenses. Lenses that exhibit both the Cu / (Cu + Zn) zonation and an underlying stockwork mineralisation are termed proximal, having formed in the immediate area of the vent and not having undergone downslope transportation or reworking. The lenses at Trout Lake conform to the configuration of proximal type deposits.

Contemporaneous with the deposition of the sulfide lenses was the deposition of fine-grained subaqueous pyroclastics of quartz - phyric character. These pyroclastics were produced by volcanic extrusions from distant and/or adjacent magmatic bodies, where the latter may have been directly related to the ore deposition, providing the 'heat engine' to drive the ore-forming hydrothermal cells. Thus, during each of the hydrothermal cycles, each of which produced one or more ore lenses, a variable amount of pyroclastics were also deposited. The pyroclastic deposits formed the seafloor on which the exhalative vent formed, and the 'capping-rock' that encloses each of the lenses. It also contributed to the interbedded and disseminated wallrock within the lenses.

The supracrustal rocks of the Flin Flon belt, which include the Amisk Group, the host of all the volcanogenic massive sulfide deposits, were deformed and metamorphosed prior to 1,750 Ma during the Hudsonian Orogeny (Syme et al. 1982). The metamorphic grade of the Flin Flon area rocks corresponds to lower and middle greenschist facies. The absence of almandine (garnet) and the presence of biotite (and/or phlogopite) in pelitic rocks from the Trout Lake locality indicates that the rocks of this locality were metamorphosed at least to the biotite isograd, corresponding to the middle greenschist facies. The metamorphic peak occurred during the second of three deformation events (Price, 1977, and Syme et al. 1982).

The textures displayed by the ores reflect, to varying degrees, the processes of initial deposition, metamorphism and deformation. However, because of the generally large stability fields of the common sulfides, a clear succession of mineralogical changes produced by progressive metamorphism, as observed in silicate rocks, is not observed. In addition, the relatively rapid equilibration times of sulfide minerals facilitates (1) the obliteration of all textures inherited from prior processes and events (i.e., primary ore depositional textures), and (2) the reversion of sulfide minerals (formed at the elevated temperatures of the metamorphic peak) to low temperature minerals, during the period of falling temperature (i.e, retrograde). Thus, the sulfide mineral assemblage we observe today is typically a retrograde assemblage, and not that formed at the temperature maximum (Vokes, 1969), while the textures reflect principally the latest event. However, certain minerals and mineral textures produced at each stage in the history of the deposit survive, and permit at least partial deciphering of this history.

RELICT TEXTURES

Two ore textures observed in the Trout Lake ores are interpreted to be relict textures i.e., preserved primary ore depositional textures, that have survived the metamorphic recrystallisation and deformation largely unmodified. These textures are (1) spheroidal pyrite, and (2) mineral banding. Spheroidal pyrite was observed in only two samples and consisted of radiating cracks, pits and/or inclusions of chalcopyrite, sphalerite and/or pyrrhotite in the pyrite (Plate 4b and 5g). This texture formed during or deposition and subsequent diagenesis, with recrystallisation of the pyrite and the segregation of the chalcopyrite, sphalerite and pyrrhotite into the radiating cracks.

Mineral banding constitutes the most commonly preserved texture in metamorphosed sulfide deposits, and at Trout Lake it is prominent, particularly in the Banded Pyrite + Sphalerite ore type. Such banding is the expression of the alternating types and concentrations of various minerals (Vokes, 1969), eg., sphalerite-rich alternating with pyrite-rich laminae, with variably superimposed banding of arsenopyrite-, galena- and/or gangue-rich laminae (Plate 2f, 2g and 6a). Banding of this type, produced principally by changes in the ore fluid composition and subsequent sedimentation, is observed in the 'Black Ores' of the unmetamorphosed Kuroko deposits (Lambert and Sato, 1974, Craig and Vaughan, 1981, and Shimazaki,1974). The latter author also reports banding due to size grading, particularly of pyrite grains. Banding of this type is unlikely to be preserved even during low grade metamorphism, due to the recrystallisation which will tend to modify the grain size, but not the distribution of the mineral components. The banding is generally parallel to the sedimentary stratification in the enclosing wallrocks, which is also parallel to the metamorphic foliation, as is commonly observed in many metamorphosed deposits (Vokes, 1969). Discontinuous banding in the Chalcopyrite Stringer ores, consisting of alternating chalcopyrite- and gangue-rich laminae (Plate 4e) is interpreted as the product of metamorphic segregation under conditions of directed stress in this highly chloritised 'plastic' zone, and is thus not a primary feature of these ores.

CHANGES IN THE MINERALOGY DUE TO METAMORPHISM

Despite the tendency of sulfides to re-equilibrate rapidly, much textural and compositional evidence is observed that indicates the prior existence of high temperature minerals, and/or successive stages in a discernible mineral paragenesis.

A. INVERSION TWINNING.

Spindle-shaped or lance-like and doubly concave twin lamellae are rarely visible in chalcopyrite from Trout Lake ores. These twins are particularly visible in samples containing coarse-grained chalcopyrite. This texture is due to structural transformation from a high temperature form, which possessed a higher symmetry structure than the present low temperature form, while retaining the same composition.

B. EXSOLUTION.

Chalcopyrite exhibits textures diagnostic of exsolution due to the decomposition of a pre-existing high temperature mineral of homogeneous composition. Rare sphalerite stars form clusters and linear features within coarse-grained chalcopyrite, particularly in the Vein Quartz + Chalcopyrite ores. The stars are typically 20 um in diameter, though rare exquisitely formed stars up to 90 um in diameter are observed (Plates 5a and 7a). The similarity in structures between chalcopyrite and sphalerite (chalcopyrite is a derivative structure of sphalerite) provides for crystallographic continuity and this coherent exsolution (Craig and Vaughan, 1981). The high temperature intermediate solid solution (iss) of the Cu-Fe-S system is structurally similar to sphalerite and permits extensive solid solubility of one phase in the other (Vaughan and Craig, 1978). Barton and Skinner (1979) report that 4 Mole % ZnS is soluble in the iss at 500°C and that chalcopyrite and sphalerite are incompatible down to just below 500°C. Thus, on cooling it is interpreted that the iss breaks down eutectoidally to produce sphalerite exsolution bodies (stars) in chalcopyrite, and implies that temperatures in the proximity of 500°C were achieved in the Trout Lake locality during metamorphism. Similarly iss being soluble in sphalerite at higher temperatures, results in exsolution of chalcopyrite from sphalerite on cooling. This exsolution can produce the texture known as 'chalcopyrite-disease' (Plate 1c and 1d), also attributed to epitaxial growth of chalcopyrite on sphalerite, and replacement of sphalerite by reaction with Cu-rich fluids (Craig and Vaughan, 1981). However, Hutchinson and Scott (1981) demonstrated that significant amounts of chalcopyrite will not dissolve in sphalerite at the temperatures indicated for many deposits exhibiting 'chalcopyrite-disease'. The 'chalcopyrite-disease' observed at Trout Lake is interpreted to be essentially replacement in origin.

Coarse-grained chalcopyrite at Trout Lake commonly displays exsolution lamellae of cubanite up to 5 mm in length and 50 um in width, and which exhibit composite or finely-lamellar habit (Plate 5a). The cubanite forms by breakdown of the high temperature iss with a slight excess of Fe and S relative to stoichiometric chalcopyrite. Naturally occurring cubanite transforms to iss at 205 ± 5°C (Craig and Scott, 1976) and this represents the upper stability of cubanite and a minimum temperature estimate for the ores. Ramdohr (1980) reports that the cubanite lamellae commonly overprint the sphalerite stars, indicating that the sphalerite stars had already formed when the chalcopyrite and cubanite still formed a homogeneous intermdiate solid solution (iss). Though, this was not observed at Trout Lake, it indicates that the exsolution of sphalerite from iss is not eutectoidal as suggested by Vaughan and Craig (1978), as chalcopyrite is not formed, with the iss persisting as the host phase to lower temperatures.

Fine-grained blebs and rods of pyrrhotite occassionally occur in sphalerite from deformed samples, that also exhibit sphalerite replacement of pyrite (Plate 7g). This 'chalcopyrite-disease'-like texture may have formed by exsolution of excess FeS from the sphalerite due to recrystallisation associated with the deformation, and subsequent reduction in the ability of the lower temperature sphalerite to dissolve FeS. Ramdohr (1980) reports such a texture from metamorphosed ores in Sweeden.

C. COMPOSITION.

The ore mineral assemblages and the compositions of the constituent minerals may be useful in estimating temperature and pressure during the metamorphism of the ores by reference to relevant phase equilibrium diagrams. The equilibrated mineral pair pyrite + arsenopyrite, which is observed in the Trout Lake ores (eg., polygonal equigranular mosaics in massive pyrite bands), constitutes a fixed point geothermometer. This mineral pair must have formed below 520°C (Sharp et al. 1985), and not 490°C (Koo, 1973). In addition, the As content of buffered arsenopyrite increases with increasing temperature. Because of the refractory nature of arsenopyrite it tends to retain its high temperature composition during cooling (Craig and Vaughan, 1981). The effect of pressure on such a composition is not large (Sharp et al. 1985), and can be ignored for the purpose of an estimation based on only eight arsenopyrite analyses. The average As content of these analyses is 32 At % and yields a temperature estimate of 425 ± 30°C. This value for the temperature of crystallisation of arsenopyrite is in good agreement with the P + T conditions of middle greenschist facies metamorphism. Failure to account for the effects of (1) pressure, (2) trace element content (i.e., Co, Ni and Sb, which were not determined, but are considered low as they were not observed by EDS), as well as the relatively few analyses, prohibits a truely quantitative statement.

Sphalerite constitutes another refractory sulfide which displays compositional dependence on the conditions of formation. Sphalerite may contain up to 30.1 Wt % Fe (Craig et al. 1984), and when equilibrated with pyrite and hexagonal pyrrhotite it is temperature independent between 300 and 600°C, but is pressure dependent, and therefore, of use as a geobarometer. Thus, in the Fe-Zn-S system where the activity of FeS is buffered by pyrite + hexagonal pyrrhotite, sphalerite will become enriched in FeS with decreasing pressure (Craig and Scott, 1976). However, sphalerite also commonly undergoes partial re-equilibration resulting in decreased FeS contents, and thus higher calculated pressures during formation. Hexagonal pyrrhotite was not observed in this study, though undoubtedly much of the monoclinic pyrhotite formed by decomposition of the hexagonal pyrrhotite below 254°C. The Trout Lake sphalerites are generally observed in equilibrium with monoclinic pyrrhotite and corroding and replacing pyrite (Plate 8d and 8e), and is therefore unsuitable for geobarometric use. The average Fe content of 56 sphalerite analyses is 6.82 Wt % Fe, whereas 3 analyses of an optically and texturally distinct later population of sphalerite (i.e., invaded and partially replaced the common sphalerite in sample TLN.1-87) had an average Fe content of 1.96 Wt % Fe. This late Fe-poor sphalerite is interpreted as a retrograde reaction during the period of falling temperature following the metamorphic peak. The sphalerite from Trout Lake exhibits a low but somewhat variable Fe content due to (1) re-equilibration from the high temperature composition, or (2) initial equilibration with pyrite under conditions of high sulfur activity during the period of pyrite metablastesis. In addition, the abundance of 'chalcopyrite-disease' may have had an adverse influence on the sphalerite, because Cu is known to affect the equilibration of the sphalerite composition (Hutchinson and Scott, 1981).

D. REPLACEMENT.

Replacement of one mineral by another implies that the mineral being replaced predates the one replacing it. It therefore provides information useful in determining the mineral paragenesis. Replacement is produced by one of the following processes (1) dissolution and subsequent re-precipitation, (2) oxidation, and (3) solid state diffusion (Craig and Vaughan, 1981).

Several replacement textures of pyrite are common in the Trout Lake ores. Fractured and granulated pyrite with deformation cleavage commonly exhibits relacement (rather than merely injection or infilling and cementing by matrix sulfides) by chalcopyrite, sphalerite pyrrhotite and galena (Plate 2a, 2b and 8g). In fact, the cataclastic deformation of pyrite porphyroblasts to produce what are termed porphyroclasts facilitates the replacement of the pyrite. Pyrite idioblasts (euhedral metablasts) enveloped in a chalcopyrite matrix commonly displays corrosion and replacement resulting in rounded islands of pyrite in the chalcopyrite (Plate 3f and 4a). Similarly, pyrite idioblasts in a sphalerite matrix exhibit corrosion and embayment and in an advanced stage, the development of 'atoll' texture (Plate 1b). The latter forms by preferential replacement of the core of zoned pyrite grains, which is chemically distinct, possibly containing a distinct difference in trace element contents eg., Ni, or a subtle variation from stoichiometry. The core may represent a pre-metamorphic or possibly early stage of metamorphic recrystallisation prior to the main pyrite metablastesis (pyrite porphyroblastic growth).

Pyrrhotite is commonly observed replacing pyrite along fractures and grain boundaries (Plate 8d and 8e), particularly as rounded islands in a matrix of pyrrhotite and chalcopyrite (Plate 4a). In fact pyrrhotite-rich ores are generally pyrite-poor and/or exhibit deformed pyrite partially replaced by pyrrhotite, suggesting that much of the pyrrhotite formed by the breakdown of pyrite and the release of S in a partly open system i.e.,

$$FeS_2 = FeS + S$$

Marcasite relaces pyrite along fractures and grain boundaries in a variety of textures. These are (1) fringes of bladed grains and flecks on the pyrite, (2) comb-textured marcasite on pyrite grain boundaries and fractures, (3) 'sooty-textured' pyrite (Plate 4c), and (4) fine- to medium-grained interlocking aggregates in polygonal masses of recrystallised pyrite (Plate 4g). These textures are most common in highly deformed samples and are typically concentrated along shear zones or schlieren. Rare foliated scaley masses of marcasite associated with galena, freibergite and pyrrhotite are observed enveloping and corroding cataclastic pyrite along distinct schlieren in some Banded Pyrite + Sphalerite ores (Plate 2h). All these textures involving the replacement of pyrite by marcasite are interpreted as retrograde adjustments associated with deformational events that postdate the pyrite metablastesis, possibly contemporaneous with the D3 event. A rare fine-grained, concentrically-ringed mixture of marcasite and pyrite replacing pyrrhotite, called 'birds eye' texture, was observed. This texture occurs in contact with pyrite grains enveloped in the pyrrhotite, and appeared to be nucleated by this pyrite (Plate 4h).

Pyrite may exhibit dendritic replacement by galena, sphalerite, chalcopyrite and rarely pyrrhotite (Plate 2d, 5h, 8b and 8c), particularly in the Massive Pyrite and the Banded Pyrite + Sphalerite ores. This texture is interpreted as resulting from preferential invasion and replacement of pyrite along crystallographically controlled directions, either deformation cleavages or planes of lattice defects i.e., dislocations in the pyrite.

As discussed earlier, the abundant 'chalcopyrite-disease' in Trout Lake sphalerites is interpreted to be principally a replacement texture, with a possible minor component from exsolution. Cu-bearing fluids replace the FeS component and possibly also the ZnS component of sphalerite, and is generally developed along grain margins, fractures and twin planes in the sphalerite (Eldridge et al. 1983). This process will tend to deplete the sphalerite in FeS, possibly contributing to the low Fe contents and rendering such sphalerites unuseable for geobarometric measurements. The 'chalcopyrite-disease' is commonly observed lying on the bent lamellar twin planes of the sphalerite, where the latter are produced by twin gliding in response to stress. This suggests that the 'chalcopyrite-disease' was imposed on a pre-existing and deformed sphalerite. The 'chalcopyrite-disease' is most common and intensely developed in samples displaying intense deformation and abundant matrix chalcopyrite. A discernible trend with increasing deformation is observed from (1) sphalerite with weak 'chalcopyrite-disease', to (2) sphalerite with 'chalcopyrite-disease' and interstitial blebs, films and wedges of chalcopyrite to, (3) sphalerite with intense 'chalcopyrite-disease' and abundant interstitial films, wedges and xenoblastic masses of chalcopyrite enveloping the sphalerite (Plate 1c and 1d), to (4) where this sphalerite (in 3) develop carious interpenetrative contacts with the enveloping chalcopyrite (Plate 6b and 6g), to (5) where chalcopyrite and sphalerite form fine-grained myrmekitic intergrowths (Plate 6a). The development of 'chalcopyrite-disease thus appears to be facilitated by the deformation of the host sphalerite.

CHANGES IN THE FABRIC DUE TO METAMORPHIC RECRYSTALLISATION

Metamorphic recrystallisation or metablastic growth plays a major role in the ore textures of metamorphic deposits. Recrystallisation results from the effect of applied thermal energy inducing the growth of strain-free grains and the minimisation of the interfacial tension i.e., the area of the grain interfaces. During the process of recrystallisation stored energy of strained grains is released, work-hardened minerals are replaced by softer annealed grains, re-orientation occurs, grain size increases, and essentially equidimensional grains in a polygonal mosaic or 'foam' texture are developed. Stanton (1972) strictly defines recrystallisation as the process of grain boundary migration. Recrystallisation involves (1) 'nucleation' of strain-free domains by thermal activation at preferred points in the grains, (2) 'primary recrystallisation' where new strain-free grains propagate from the nuclei to the point where they mutually impinge, (3) 'normal growth' of the now strain-free grains in order to minimise the total energy of the boundaries i.e., total interfacial surfaces, to produce slightly curved surfaces meeting at the characteristic dihedral angles (120° in monomineralic aggregates (Plate 12e), (4) 'secondary recrystallisation' where certain grains are coarsened in grain size at the expense of other smaller matrix grains to produce porphyroblasts, and (5) 'differential recrystallisation' with temperature dependent recrystallisation preferentially producing recrystallisation and annealing in one phase and not another.

In general the grain size increases with grade of metamorphism as a direct result of recrystallisation. In consequence, the majority of textures inherited from the period of ore deposition are obliterated. Non-metamorphosed volcanogenic massive sulfide deposits contain fine-grained sedimentary material with abundant pyrite framboids and colliform textured pyrite, whereas the metamorphosed Trout Lake deposit contains pyrite grains up to several cm in diameter, and a calculated median grain size of between 52 and 74 um. Sato (1974) reports that sphalerite and chalcopyrite usually occur as grains under 10 and 50 um, respectively, in the non-metamorphosed Shakanai mine, Japan. This contrasts with the observed grain size distributions of these two minerals at Trout Lake; median grain size of between 104 and 147 um, and 52 and 74 um, respectively. Therefore, it is interpreted that there is a general increase in grain size of the constituent sulfides due to mineral growth. However, the effects of deformation (discussed in the next section) tend to reduce the grain sizes that were produced by pure metamorphic recrystallisation. Thus, the median grain sizes mentioned above are probably lower than those initially produced during the metamorphic peak, prior to the deformation of D3.

The most distinctive texture attributed to metamorphic recrystallisation is the development of annealed polygonal mosaics of equidimensional grains displaying 120° triple junction angles. Bands and masses of pyrite at Trout Lake commonly display this recrystallised granuloblastic texture (Plate 7b). Recrystallised masses of pyrite + arsenopyrite also exhibit this texture, with the development of characteristic (not 120°) dihedral angles for this polymineralic assemblage. Similarly, massive magnetite commonly displays 120° dihedral angles (Plate 9g). Minor minerals typically occur within the interstices between the major mineral (i.e., galena, sphalerite or chalcopyrite in pyrite masses), and rarely as entrapped inclusions (eg., rounded sphalerite inclusions in pyrite, See Plate 2c and 8h)). This granuloblastic texture is developed in an essentially solid medium where the 'force of crystallisation' of the constituent minerals to form euhedral shapes are the same or similar, such that when the growing minerals mutually impinge, one mineral does not develop euhedrism at the expense of another. Stanton (1972) proposed a 'Crystalloblastic Series' for common rock-forming minerals and sulfide minerals, which is based on the 'force of crystallisation' or tendency to form euhedral or idiomorphic grains. The series in order of decreasing tendency to euhedrism is; garnet, magnetite - arsenopyrite, pyrite, dolomite, tremolite, muscovite, chlorite, pyrrhotite, sphalerite, chalcopyrite and galena. Stanton also points out that other minerals of the same structural groups as those in the series, will likely display equivalent euhedrism and thus positions in the series i.e., pyrite - marcasite.

When grains of pyrite are disseminated in a matrix of sphalerite, chalcopyrite and/or galena, they tend to develop as large euhedral grains with well formed crystal faces (and are termed porphyroblasts) in a matrix of anhedral minerals which rarely develop crystal faces, but tend to form mosaic textures. Thus, disseminated pyrite, arsenopyrite and magnetite develop porphyroblastic texture within matrices of sphalerite, chalcopyrite, pyrrhotite and/or galena (Plate 7c). This is particularly pronounced in the Banded Pyrite + Sphalerite ores, where pyrite and lesser arsenopyrite form euhedral cubes and prisms with rhombic sections, respectively, in the sphalerite matrix. Within the matrix, chalcopyrite tends to occupy the interstices between sphalerite grains rather than forming an equidimensional mosaic. Similarly, galena forms as interstitial masses between sphalerite grains, commonly forming on the sphalerite - pyrite, or sphalerite - gangue contacts, in preference to the sphalerite - sphalerite contacts (Plate 7h). It is noteworthy that when sphalerite forms the interstitial material to pyrite the pyrite tends to be idiomorphic, whereas as also noted by Vokes (1969), pyrite with interstitial galena has decreased idiomorphism appearing more rounded (Plate 2g and 8a). Paragenetic sequences are commonly constructed on the basis of these textures, where these textures are erroneously interpreted as replacement or cross-cutting textures, rather than merely reflecting the position of the constituent minerals in the 'Crystalloblastic Series'. In this study these textures are interpreted in light of the mineral(s) position within the 'Crystalloblastic Series', and generally imply contemporaneous rather than sequential crystallisation.

The grain size of pyrite exhibits a strong dependence on the surrounding matrix in which it grows. Pyrite forming in a chlorite gangue tends to be considerably coarser-grained than pyrite in a sphalerite matrix or in a band of massive pyrite. This phenomena may be attributed to (1) more widely spaced crystallisation nuclei from which the pyrite grows, and (2) the lower 'force of crystallisation' of the minerals forming the matrix. Thus, there is an observed trend of decreasing pyrite grain size from pyrite in (1) a gangue matrix, (2) a sphalerite or chalcopyrite matrix, where the pyrite is generally porphyroblastic, and in (3) a band or mass of monomineralic pyrite. Occassionally, the pyrite porphyroblasts overgrow and enclose residual 'foreign' minor minerals, which typically develop rounded or spherical forms to minimise interfacial energies with the host pyrite. When this texture is well developed it is called poikiloblastic pyrite, and sphalerite is the most common inclusion in pyrite (Plate 2c and 8h). Similarly, magnetite may exhibit this texture, overgrowing and entrapping pyrite, sphalerite and chalcopyrite (Plate 9b and 9c).

CHANGES IN THE FABRIC DUE TO DEFORMATION

The term deformation is normally used to encompass folding, faulting and other mechanically induced features produced by tectonic forces. Deformation is most pronounced when the stress is applied either at rapid rates or at relatively low temperatures such that the body of rock experiences high strain rates or lacks plasticity, respectively. Deformation tends to reduce the grain size of the constituent ~~mi~~nerals, and thus competes with the effect of increased grain size produced by recrystallisation. At Trout Lake the textural evidence suggests that deformation accompanied (preferred orientation, schistosity, segregation and other foliated textures) and also outlasted (numerous cataclastic textures, and the diablastic intergrowths of the matrix sulfides) the main recrystallisation event. This is in general agreement with the known coincidence of the metamorphic peak with the D2 deformational event, which preceeded a third deformational event (D3) at lower temperatures (Price, 1977). Therefore, many of the textures developed during the metamorphic peak have been modified by the final deformation event.

The most subtle effects of deformation involve the development of lattice defects, which are occassionally the sole evidence of deformation in moderately deformed ore minerals. Pyrite commonly displays pronounced anisotropy in deformed samples, suggesting that the anisotropy is due to lattice defects eg., dislocations. Ramdohr (1980) points out that gliding and twin gliding are not observed in pyrite. Pyrite deforms in a brittle manner, with dislocations and particularly the development of deformation cleavage, whereas lattice bending is improbable. The dendritic replacement of pyrite by galena, sphalerite, chalcopyrite and/or pyrrhotite, which is common in samples exhibiting distinct deformational textures, exhibits distinct crystallographic control by the host pyrite (Plate 2d, 5h, 8b and 8). Commonly the pyrite does not display deformational cleavage, and thus the dendritic pattern is interpreted as being due to minute lattice dislocations.

Sphalerite commonly displays deformational twinning consisting of straight to curved repeated lamellar twinning of relatively uniform thickness (Plate 1c). The intensity of the twinning appears to vary with the orientation of the grains and the character of the surrounding minerals, eg., galena which may accomodate and absorb the stress by readily deforming, resulting in less defomed sphalerite.

The brittle idioblastic minerals pyrite, arsenopyrite and magnetite, if subjected to stress above that which merely produces lattice defects, will deform cataclastically with the development of cleavage, granulation, fractures and/or brecciation. Commonly these minerals exhibit granulated margins, where the grain edges are shattered and the dislodged fragments 'float' in the surrounding matrix. Deformation cleavage parallel to (100) in pyrite is common, and becomes highlighted when matrix sulfides, particularly chalcopyrite, cement or replace the pyrite along the cleavage planes (Plate 2b). Similarly, irregular fractures are produced by deformation and also become infilled by matrix minerals or by the products of the attrition (Plate 2a, 6f and 8g). 'Blow Apart' texture is occassionally well developed, with the drawing apart of the fragments of cataclastic pyrite and the injection or infilling of matrix sulfides, which cement the fragments without replacing them (Plate 6f). The matrix minerals have behaved plastically, 'flowing' between the fragments of the brecciated brittle sulfide mineral. This texture has been interpreted to mean that the matrix sulfides are younger, though clearly they existed in the ore prior to the deformation and merely flowed over minute distances. Even when accompanied by corrosion or minor replacement of the pyrite porphyroclast Vokes (1969) refers to these textures as pseudo-epigenetic. The effects of deformation on the matrix sulfides, which have relatively rapid equilibration times, are partly obliterated by the subsequent recrystallisation and tendency to develop a granuloblastic fabric during the period of falling (Plate 12e), yet still elevated temperature conditions that endured after the cessation of deformation.

Elongation and the development of a foliation within the sulfide mass is observed at Trout Lake. Such directed textures are produced by deformation accompanying recrystallisation. Numerous ore samples contained coarse-grained elongate pyrite and/or oval rather than equidimensional matrix sphalerite grains exhibiting a preferred orientation parallel to that in the adjacent schist bands i.e., schistosity (Plate 1a and 6b). Similarly, recrystallised masses of pyrite occassionally exhibit polygonal, yet elongate grains displaying a preferred orientation, rather than ideally equidimensional grains in a foam texture. This texture is due to growth under conditions of directed stress, and thus a deformational or dynamic component during crystallisation. Galena commonly forms on the sphalerite - sphalerite and sphalerite - gangue contacts that are parallel to this foliation, and thus accentuate it (Plate 7h). The silicates also define a foliation by (1) the distribution and banding of the wallrock laminae and the orientation of the constituent gangue minerals, and by (2) the preferred orientation of individual gangue grains, particularly chlorite and biotite, that are disseminated vitin the sulfide matrix (Plate 1a and 7h). The banding observed in the Chalcopyrite Stringer ores (Plate 4e), consisting of alternating chalcopyrite-rich and gangue-rich (eg., chlorite) laminae is in apparent conflict with the mode of origin of these 'stockwork' ores. However, the stratabound attitude of these ores is interpreted to have resulted from intense shearing in this highly chloritised plastic zone. During this shearing the chalcopyrite segregated into distinct layers, thus developing a pseudo-primary banding that in fact constitutes a metamorphic foliation. All these textures are produced by crystallisation under the directional stress that is characteristic of regional metamorphism and results in oriented textures rather than purely cataclastic textures.

In ores that have undergone intense deformation the cataclasis affects both the sulfides and gangue minerals to produce thoroughly tectonised ores. This penetrative deformation which is dominated by internal rotational movements is termed 'Durchbewegung' (literally "move through") (Vokes, 1969, and Craig and Vaughan, 1981). In such ores the original primary banding is generally totally disaggregated with a general sequence recognised for the deformation of gangue laminae. These schist laminae become (1) fractured and dislocated (Plate 12f), then (2) completely disoriented as rafts floating in a sulfide matrix, then (3) folded and recrystallised detached cores of schist in the sulfide matrix (Plate 12g), and finally (4) become rotated, rounded and milled to produce 'balls or augens of gangue (Plate 6b and 6c). All these stages are found at Trout Lake. Gangue that was originally disseminated through the sulfide matrix develops a pronounced schistosity, commonly flowing around pyrite porphyroblasts or other competent augen-shaped features in a lepidoblastic texture. The matrix sulfides invade and infill fractures in the augens of gangue, as well as fractures and dilated cleavages in the individual grains of chlorite and biotite. Similarly, pyrite is commonly milled to form pyrite balls or 'pebbles' in a fine-grained tectonised sulfide matrix (Plate 6g). Under conditions of intense deformation the pyrite breaks down, partially or completely to form pyrrhotite.

In several highly deformed samples swirls of extremely thin (≤ 3 um) plates of an unidentified micaceous mineral, possibly chlorite, having almost a filamentous form in the 2 dimensions of the plane of the section are observed around competent augens of gangue and porphyroblasts of pyrite (Plate 12h). These swirls formed in the vortices of compression around these augens during, and attest to, the rotational movements that deformed the host sulfides. The swirls are thus unfractured, unlike many of those gangue minerals eg., biotite that are interpreted to have formed earlier at the metamorphic peak.

Deformational textures are observed in most of the ore samples examined, but tend to be concentrated or are more pronounced along linear features interpreted to be shear zones. However, in several samples the deformation is indeed penetrative, and affects the entire body of the sample.

Whereas pyrite, arsenopyrite magnetite and many of the gangue minerals deform brittley, sphalerite, chalcopyrite, pyrrhotite and galena deform plastically as suggested by the manner in which they infill fractures etc, in the former more competent minerals. These 'softer' matrix minerals develop a fine-grained myrmekitic texture (Plate 6a) due to diablastic growth i.e., collection crystallisation during and after shearing (Ramdohr, 1980). The development of this diablastic texture is characterised by a trend with increasing deformation from straight or curved to carious to myrmekitic interpentrative contacts between these 'softer' minerals. This texture is variable developed and accompanies many of the other deformational textures in virtually all of the 9 ore types, and in ores from each of the 6 proven ore lenses. In highly deformed Chalcopyrite Stringer ores pyrrhotite and rarely minor sphalerite form carious blebs in and myrmekitic intergrowths with chalcopyrite, whereas in highly deformed Banded Pyrite + Sphalerite ores that contain abundant galena, the latter forms blebs in and lesser myrmekitic intergrowths with sphalerite.

The most intense development of Durchbewegung texture is observed in Sample TLN.2-12, a Sheared Chalcopyrite + Sphalerite ore (Plate 6a, 6c and 6d). No pyrite was observed, and is interpreted to have been completely granulated and replaced by pyrrhotite. The gangue consists of milled, rounded and fractured augens around which the matrix of chalcopyrite, sphalerite and pyrrhotite flow in a mylonitic texture (Plate 6c). This matrix consists of fine-grained diablastic-textured chalcopyrite, sphalerite and pyrrhotite, which are admixed to form mutual intergrowths of one another to varying degrees depending on their proportions in a given layer (Plate 1f and 6e). The layering produced by shearing and plastic flow sweeps across the plane of the section, resembling flow lines. At the termination of the augens coarse-grained matrix sulfides forming in the 'pressure shadows' contrast with the bulk of the fine-grained matrix (Plate 6d).

The Sheared Chalcopyrite - Sphalerite ore type was defined where the bulk of the constituent chalcopyrite and sphalerite exhibit diablastic texture. The definition of such an ore type, based on a specific textural criteria, is warranted in that it is the fine-grained intricate intergrowth of the two principal valuable minerals, chalcopyrite and sphalerite. All but one of the samples assigned to this ore type were collected from the No. 2 Lens of the North Zone. This lens is somewhat unique in that (1) it is clearly the largest and richest lens, (2) it lacks a well defined metal zonation i.e., it is disrupted, and (3) it is characterised by the intrusion of a 5 to 25 m thick quartz - diorite sill that is discontinuously interlaced with the lens down dip, at least to the 425 m level (Plate 6e). It is interpreted that the quartz - diorite was intruded along this highly chloritised, sulfide-rich horizon as a syn- or post-tectonic sill. The sill and the associated deformation are clearly not pre-metamorphic, as the recrystallisation of the metamorphic peak would have obliterated the diablastic texture (and its association with the intrusion), producing instead a typical mosaic textured sulfide matrix. Similarly, the preserved cataclastic textured pyrite and the diablastic textured matrix sulfides, observed in all the ore lenses, indicate that deformation outlasted (or recurred after) the metamorphic peak, and the associated major sulfide recrystallisation or metablastic event. However, the temperature was still somewhat elevated at the time of deformation allowing moderate recrystallisation i.e., collection crystallisation of the 'smeared' sulfides.

SULFIDE MOBILISATION

As discussed earlier, the plastic flow of matrix sulfides infilling fractures in pyrite porphyroclasts and gangue, etc., has been observed repeatedly at Trout Lake. This texture may be referred to as mobilisation, as might the plastic flow that thickens up sulfides in the nose of folds. However, sulfide movement of this type, though observed at Trout Lake, does not occur over distances greater than probably several centimeters. The preservation of the primary ore depositional Cu / (Cu + Zn) zonation suggests that in general large scale redistribution of elements and thus minerals has not occurred at Trout Lake. The disruption of the Cu (Cu + Zn) zonation in Lens No. 2 of the North Zone was probably produced by shearing, plastic flow, overfolding and minor faulting, and constitutes redistribution of the metals over relatively short distances, and essentially in the solid state.

However, the Vein Quartz + Chalcopyrite ore type does constitute a mobilisation and redistribution of elements over large distances i.e., several tens of meters. These veins consist principally of quartz, carbonate and chalcopyrite with lesser pyrrhotite, sphalerite, pyrite and galena. The veins are interpreted to be a hydrothermally remobilised fraction of metamorphic origin. Quartz is readily 'sweated out' during the metamorphism, and together with sulfides which were selectively dissolved, and migrated over large distances in the pore fluids. Recrystallisation occurred as coarse-grained veins that cross-cut the foliation in both the ore lenses and the surrounding wallrock. The sulfide fraction of the veins is relatively enriched Cu, and possibly Au, while other commonly fugitive metals such as Pb, As and Sb do not appear to have been selectively concentrated in these veins.

The type 2 electrum observed in the Chalcopyrite Stringer ores TLN.2-11 and TLN.1-89 is also interpreted to have been formed by fluid state mobilisation i.e., transported in solution to the point of crystallisation. Type 2 electrum consists of anastomosing masses and lesser disseminations that are distributed along the chalcopyrite - chlorite schist contact, and which envelope and corrode the chalcopyrite. This contact is interpreted to have behaved as the channelway along which the Au, Ag and Hg migrated in solution. Crystallisation occurred in areas of low stress and strain rates, such as the contact (possibly dilational) at the crest of a minor overturned and tightly closed fold in TLN.1-89 (Plate 5e and 10e). Because of the abundance of electrum in this mass, it is improbable that it was concentrated by solid state diffusion from the surrounding sulfides, particularly pyrite, or by plastic flow. Therefore, the present distribution of Au in Trout Lake, probably reflects both its original distribution as well as a modified distribution due to limited solid state diffusion, hydrothermal mobilisation, migration and recrystallisation.

Chapter XI

DISCUSSION AND CONCLUSIONS

The sulphides pyrite, chalcopyrite, sphalerite, pyrrhotite, marcasite, galena, arsenopyrite, cubanite and acanthite; the oxides magnetite and cassiterite; the Sb-sulfosalts freibergite, gudmundite, pyrargyrite, freieslebenite, boulangerite, bournonite and costibite; the intermetallic and alloy-like compounds mercurian electrum and dyscrasite; the tellurides hessite, rucklidgeite, pilsenite and volynskite; and the selenides clausthalite and naumannite have all been identified in the ores, in that general order of abundance. The ores are dominated by the textural and spatial distribution of the first three most abundant sulphides, pyrite, chalcopyrite and sphalerite. The differentiation of the ores in terms of Cu and Zn, results in a differentiation series characterised by near end-member mono-mineralic sulphide components of chalcopyrite in the footwall Chalcopyrite Stringer ores, and sphalerite in the hangingwall Massive Sphalerite ores. The pyrite tends to be concentrated in the footwall Cu-rich ores, or in the hangingwall Zn-rich ores as distinct segregated pyritic bands.

The differentiation of Cu and Zn yields a distribution of the Cu / Cu + Zn ratios that is characteristic of many volcanogenic massive sulphides (Franklin et al. 1980). This metal zonation is widely accepted as the result of the physiochemical trend encountered by the ore-forming fluids as they emanate upwards and outwards from the point of sea-floor discharge (Franklin et al. 1980). These authors also note that proximal deposits which overlie the emanative centre, have well defined stringer zones and prominent vertical compositional gradations of decreasing Cu / Cu + Zn ratios, as is the case in Trout Lake. The metal distributions are thus primary and do not reflect remobilisation during the lower greenschist facies metamorphism. Limited sulphide mobilisation is observed in the form of fluid state remobilisation and subsequent deposition as quartz- and chalcopyrite-rich hydrothermal veins of metamorphic origin. Fluid state remobilisation is also proposed as the principal mechanism by which electrum attained its present distribution, possibly in all observed occurrences, but certainly in the fold nose of a pinch structure in the highly sheared Chalcopyrite Stringers of TLN.1-89.

Deformational textures are numerous and widespread in the Trout Lake ores. The most conspicuous evidence of deformation on the megascopic scale is the conformable or stratabound attitude assumed by the stockwork ore zones, due to shearing in this highly chloritised 'plastic' zone. Open to tightly closed and isoclinal folding are common on the meso- and microscopic scale. The foliated ores commonly consist of lepidoblastic to augen-textured gangue and the enveloping, foliated and occassionally gneissic-textured sulphides. The commonest deformational texture observed in the ores is the cataclastic deformation of pyrite porphyroblasts. Depending on the intensity of the deformation and the nature of the host or surrounding sulphides, the pyrite texture varies from disaggregated annealed polygonal masses, granulated, rounded, fractured, deformation cleavage developed, 'blow-apart' textured, schistose pyrite with rare crenulation cleavage developed, and mobilisation of pyrite into the cleavages of gangue minerals and veinlets. Such deformation facilitates the cementation and/or replacement of pyrite by sphalerite, chalcopyrite, pyrrhotite, marcasite and galena. Under conditions of intense deformation, the pyrite completely breaks down to form pyrrhotite.

The most significant deformational texture observed in the ores is the development towards a myrmekitic texture due to diablastic growth i.e., collection crystallisation during and after shearing (Ramdohr, 1980, pp. 118.). This diablastic texture is characterised by a trend with increasing deformation from straight or curved to carious to myrmekitic interpenetrative contacts between chalcopyrite, sphalerite, pyrrhotite and/or galena. Most of the ore types exhibit a trend towards this texture, at least locally along shear zones or 'schlieren'. In ores where the bulk of the chalcopyrite and sphalerite exhibit this texture they were assigned to the Sheared Chalcopyrite + Sphalerite ore type.

The diablastic texture is also characterised by reduced grain size distributions relative to the unsheared equivalent, and also reduced optimum grinds i.e., sphalerite 37 um, chalcopyrite 18.5 um. However, of greater significance is the interpenetrative contacts of the two main minerals of interest chalcopyrite and sphalerite. Petruk's mineral liberation model is partly based on the empirical observation that approximately one third of the unliberated grains will be recovered in the appropriate concentrate. For most ore types the dominant contaminant phase in these composite particles are likely to include pyrite, gangue and pyrrhotite, whereas in the Sheared Chalcopyrite Sphalerite ores the predominant contaminant phase is likely to be sphalerite where chalcopyrite is floated first, and then chalcopyrite where sphalerite is subsequently floated. In consequence, high Zn values may report to the Cu-concentrate, and reduce the availability and resulting recovery of sphalerite in the Zn-concentrate. In addition, chalcopyite-bearing sphalerite composite particles will be floated and thereby raise the Cu recovery in the Zn-concentrate.

All but one of the samples recognised as comprising this ore type were collected from the No. 2 Lens of the North Zone. Nine of the 21 samples from this lens were assigned to this ore type. Lens 2 of the North Zone is characterised by the disruption of the generalised metal zonation, and also by the intrusion of a 5 to 25m thick quartz-diorite sill that is discontinuously interlaced with the lens down dip, at least to the 425m level. A recent high grade intersection of the lens at the 425m level confirmed the continuation of the direct relationship between the quartz-diorite and the predominance of the Sheared Chalcopyrite Sphalerite ore type. This suggests that the quartz-diorite was intruded along this highly chloritised and sulphide-rich horizon as a syn- or post-tectonic sill. The sill is clearly not pre-metamorphic as it is interpreted to cause the deformation and distinctive rounding of the pyrite porphyroblasts, and thus postdates the metamorphic recrystallisation of pyrite. In addition, the metamorphic recrystallisation of the sulphides would have obliterated the diablastic texture, and its direct association with the intrusion. The quartz-diorite exhibits a schistosity, suggesting that it's intrusion was contemporaneous with the metamorphic maxima of D_2, or merely predates D_3.

Lens 2 of the North Zone is the richest of the 6 proven ore lenses, containing 2,213,000 tons (combined production and reserves) averaging 0.069 oz/ton Au, 0.51 oz/ton Ag, 2.69 % Cu and 7.4 % Zn (Ko, 1986). This constitutes 35 % of the total proven ore tonnage, but also constitutes 48 % of the Au, 39 % of the Ag, 41 % of the Cu and 47 % of the Zn (See Table 2). The lens is still open at depth. If and when (Part 2 of the project) it is determined that the cause of the high Zn reporting to the Cu-concentrate is due to chalcopyrite-sphalerite composite particles, a serious re-evaluation of the processing of diablastic-textured ore, and in particular ore from Lens 2 of the North Zone, should be undertaken. A possible scenario might involve reducing the 'pull' of the Cu-Rougher and regrinding the Cu-Scavenger concentrate to liberate the sphalerite from the recovered chalcopyrite-sphalerite composite particles. Regrinding the Cu-Scavenger concentrate is advantageous in that (1) a smaller fraction (approximately 5 %) of the feed is reground, (2) already liberated sphalerite is not ground to the size range of slimes, and (3) the smallest fraction of the flow with the highest probable concentration (approximately 11 % of the Zn in the feed) of chalcopyrite-sphalerite composite particles is reground.

Another apparently lens-specific texture, though not exclusively so, is the prevalence of fine-grained dendritic sphalerite, galena and freibergite in pyrite porphyroclasts from Massive Pyrite and Banded Pyrite Sphalerite ores of Lens 5 of the South Zone. When ores from stope 2451 of Lens 5 (210 and 215m level) were milled, high Zn-losses to the tailings were experienced. Fine-grained inclusions of sphalerite in pyrite are not liberated until the pyrite is broken to the same size as the sphalerite inclusions (Petruk, in prep.). The same is probably true for freibergite and galena inclusions in pyrite, with resultant poor recovery of Zn, Pb and Ag. Because of the poor sampling coverage of Lens 5, a general statement concerning probable losses of this type for the entire lens is conjectural. However, the low Cu content (0.29 % Cu, See Table 2) of this lens and it's enrichment in Zn-Group elements (Zn, Ag and Pb specifically) suggests that this texture may persist throughout the lens.

Copper is carried in chalcopyrite, cubanite, freibergite and bournonite, where the latter three phases represent insignificant contributions of Cu to the total Cu tonnage. The optimum grind for chalcopyrite is 52 um and is finer than the particle size of the grinding curve defined by 80% -74 um. However, chalcopyrite will preferentially concentrate in the finer sieve fractions due to its grindability (Petruk et al. 1985), and thereby tend to approach the optimum grind. The total recovery of Cu is 95 %, with 93 % in the Cu-concentrate, and represents an excellent recovery with little apparent scope for improvement. Te was determined to occur in hessite, rucklidgeite, pilsenite(?), volynskite and in the clausthalite-galena solid solution that was associated with rucklidgeite. The Cu-Te element pair yields the highest r-value of the Cu-Group elements i.e., + 0.834, and is interpreted as the result of the paragenetic association of the Te-bearing minerals with chalcopyrite, but principally due to the contribution from trace Te in solid solution in chalcopyrite (undetected; <0.01 Wt % Te). Rucklidgeite and the associated Te-bearing clausthalite-galena occurred as fine-grained inclusions along with chalcopyrite and pyrrhotite in pyrite, and may be expected to report to the tailings and/or the Cu-concentrate. Both hessite and pilsenite(?) occur as fine-grained inclusions in chalcopyrite and are expected to report to the Cu-concentrate. Selenium was identified in the clausthalite-galena solid solution, rucklidgeite, pilsenite(?) and naumannite. The Se-Pb pair yields an r-value of - 0.720, indicating that the clausthalite-galena solid solution contributes an insignificant component to the total variance in Se and Pb. The positive covariance of Cu and Se (i.e., + 0.622) is interpreted as resulting from the Se content of chalcopyrite, and the paragenetic association of chalcopyrite with Se-bearing pyrrhotite and pyrite (Hawley and Nichol, 1959), rucklidgeite, pilsenite(?) and naumannite in Cu-rich ores. It is therefore expected that the bulk of the Se will report to the Cu-concentrate, and thereby degrade the quality of the copper (Petruk, 1985).

Zn is carried in sphalerite and freibergite, where the latter is an insignificant contributor to the total Zn tonnage. Cd and possibly Hg are hosted in sphalerite. The strong linear relationship of Zn and Cd demonstrates that sphalerite is the host of Cd. The lack of Zn-Hg covariance suggests that (1) Hg is only partly hosted in sphalerite, (2) Hg does wholely occur in sphalerite, but exhibits variable contents, or (3) the Hg determinations are inaccurate. Hg is known to occur dominantly in sphalerites from Flin Flon ores (Chen, pers. comm., 1986), though it is interpreted that the Sb-sulfosalts freibergite, pyrargyrite and gudmundite are the most significant Hg-carriers. The elements Zn and Cd will report principally to the Zn-concentrate, but also to the Cu-concentrate, because of the 10 to 15 % of the sphalerite in the feed that reports to the Cu-concentrate. The path of Hg during flotation will be partly defined by the behaviour of sphalerite as above, but also by that of the Hg-bearing Sb-sulfosalts. The optimum grind for sphalerite of 52 um is probably elevated by the sampling bias towards, and over-representation of coarse-grained sphalerite in Zn-rich ores, but is compensated for by the tendency for sphalerite to concentrate in the finer sieve fractions. The grinding curve defined by 80 % - 74 um, and thus approaches the optimum grind for sphalerite. However, this optimum grind assumes that 28.5 % of the sphalerite (Fig 21) is finer than the particle size of the grind, and will therefore be partly unliberated (approximately 15 %). The total recovery of Zn is 91.02 % with 77.25 % in the Zn-concentrate, 13.78 % in the Cu-concentrate and 8.97 % in the tailings (See Table 2). The possible causes of the high Zn reporting to the Cu-concentrate are (1) locked or composite particles consisting of chalcopyrite-sphalerite (discussed above), (2) 'drag-over' of sphalerite slimes (<5 um), and (3) activation of sphalerite by dissolution of reactive minerals with the reagents e.g., marcasite. A linear traverse grain counting procedure was performed on the polished section of the float feed, and determined that the ore contains 0.17 Wt % marcasite. Marcasite is relatively unstable and may dissolve in the pulp to produce ferrous ions in solution. These ions togethar with dixanthogen (oxygenated xanthate) at a Ph range of 9.5 to 11, can produce activation of sphalerite (Leroux et al. 1986). However, the minimum storage capacity at the mine and the fast turnover of the 'dry' ore (1 to 3 days) minimises the probability of marcasite oxidising and subsequently reacting in the pulp. The possible drag-over of sphalerite slimes cannot be evaluated at this point, though the present practise of regrinding 60 % (split stream) of the Cu-Rougher underflow/tailings may contribute to increased slime production. Initial work from Part 2 of the project suggests that abundant coarse- to medium-grained free sphalerite, as well as minor sphalerite-chalcopyrite composite particles are floated into the Cu-Scavenger concentrate. This indicates that problems with liberation of sphalerite are of secondary importance compared to the loss of selective flotation between sphalerite and chalcopyrite.

Au is interpreted to be dominantly carried in mercurian electrum which is the only Au-bearing mineral identified. The correlation coefficient matrix failed to identify any geochemical association of Au with any element, other than Mn, which probably reflects a distorted correlation coefficient (non-normally distributed variables) or an unidentified paragenetic association with a Mn-bearing gangue phase. No association of Au with As was apparent, nor was any association of arsenopyrite with electrum observed petrographically. The lack of covariance between Au and Hg and Ag reflects the minor contribution of the Ag and Hg in electrum to the total variance in these elements, which occur in concentration levels that are at least one order of magnitude greater than can be explained by their occurrence in electrum. It is noteworthy that the Au/Ag ratio of the deposit is 0.11. The mercurian electrum yields an average Au/Ag ratio of 0.95, indicating that if the electrum is the sole host of the Au, then it accounts for a maximum of approximately 10 % of the Ag in the deposit. Assuming that electrum is the sole host of the Au, then the loss of 33 % Au to the tailings can explain only 10 % of the total of 30 % Ag losses to the tailings. The abundance and relative ease with which electrum was observed (417 grains and two anastomosing masses) suggests that electrum may indeed be the sole Au-bearing mineral, though the existence of trace Au in solid solution in pyrite cannot be discounted or confirmed without the use of an ion microprobe or micropixie, or cyanidation tests on a pyrite concentrate of the tailings. The finer-grain size of type 1 and 3 (80 % - 18 um) and the correlation between Au and pyrite reporting to the Cu-concentrate or reciprocally to the tailings (McEachern, pers. comm., 1986) suggests that the loss of Au to the tailings is primarily attributable to the electrum of type 1, entrapped in pyrite, and/or Au in solid solution in pyrite. Electrum of type 2 is coarser-grained (80 % - 37 um) and occurs as anastomosing masses in chalcopyrite. Gasparrini (1984) reports that electrum whose grain size is sufficient to ensure liberation, was almost totally recovered in laboratory experiments using standard flotation techniques. The latter author also notes that the electrum generally reports to the Cu-concentrate because of the similar flotation characteristics and spatial association with chalcopyrite. This supports the author's contention that electrum of type 2 is readily recovered, while that of type 1 is not.

Arsenic occurs principally in arsenopyrite, but also in solid solution in freibergite, where it's level of concentration ($\bar{x}$ = 0.20 Wt % As), and the trace abundance of freibergite in the ores, implies that arsenopyrite can be assumed to be the sole host of As. Thus, the environmentally toxic element As is expected to report largely to the tailings, which is then returned to the mine as backfill. Minor As is expected to report to the Zn-concentrate in the form of sphalerite-arsenopyrite composite grains, derived from the common disseminated, fine-grained, euhedral grains of arsenopyrite in the sphalerite of the Massive Sphalerite and the Banded Pyrite + Sphalerite ore types.

Costibite is the only Co-bearing mineral identified, but is interpreted to be a minor Co-carrier, because only one grain was observed and because of the lack of Co-Sb covariance. The principal host of Co was not identified, but was interpreted to be pyrrhotite, and thereby suggests that Co should report largely to the tailings.

Cassiterite is the only Sn-bearing mineral identified, though it may be inferred that stannite may occur in the ores associated with chalcopyrite, or that Sn occurs in solid solution in chalcopyrite. The metallurgically troublesome element Sn occurs at trace concentrations ($\bar{x}$ = 36 ppm Sn) in the ores. It is interpreted to be largely hosted in cassiterite associated with sphalerite, and a lesser component as cassiterite or stannite associated with chalcopyrite, or in solid solution in chalcopyrite.

The metallurgically troublesome element Bi occurred consistently at concentration levels below the detection limit of the chemical analyses (0.001 Wt % or 10 ppm Bi). Bi was detected by microprobe in the tellurides rucklidgeite and pilsenite(?), which formed inclusions in pyrite and chalcopyrite, respectively, and was also detected in volynskite. As a result, Bi would be expected to report at low levels of concentration to the Cu-concentrate and the tailings. Galena is a potential host phase of trace Bi, but the severe Bi and PbMα overlap prohibits detection of less than 1 or 2 Wt % Bi.

Indium which occurs at trace concentrations in the ores ($\bar{x}$ = 34 ppm In) is interpreted to occur in sphalerite, possibly chalcopyrite and/or the Sb-sulfosalts. Indium exhibits high positive covariance with Ag, Sn, Sb and Pb, and moderate covariance with Zn. The strong In-Ag covariance is interpreted to reflect the coupled substitution for Zn in sphalerite, in which it is interpreted that the bulk of the In is hosted. This suggests that In will report principally to the Zn-concentrate, and to a lesser extent to the Cu-concentrate and the tailings.

Antimony is carried in freibergite, gudmundite, pyrargyrite, boulangerite, freislebenite, dyscrasite, bournonite and costibite, where the first three more abundant Sb-sulfosalts may be assumed to contribute the only significant components to the total variance in Sb. Pyrargyrite occurs only as fine-grained inclusions in galena, whereas freibergite and gudmundite generally occur as inclusions in galena, but also as discrete grains intimately associated with galena. Gudmundite and pyrargyrite are generally most abundant in Massive Sphalerite ores. The fine-grained Sb-sulfosalt inclusions are expected to be largely unliberated and their behaviour will be defined by the host galena. In the Banded Pyrite + Sphalerite ores, the fine-grained dendritic freibergite and galena in pyrite, as well as the interstitial and fracture-filling freibergite and galena in pyrite, are expected to be partly unliberated and report to the tailings as composite grains of pyrite with galena, freibergite and/or sphalerite. Gasparrini (1984) reports that Ag-rich tetrahedrite is readily recovered by normal flotation techniques, and indicates that liberated freibergite should report to the Cu-concentrate. However, Gasparrini (1984) also reports that lime has a deleterious effect on the recovery of pyrargyrite, which if free, is therefore expected to report to the tailings, while the flotation characteristics of gudmundite are unknown. As a result, Sb is expected to report to the Cu-concentrate, the Zn-concentrate and the tailings. Assays of 'unbalanced' 1983 feed and concentrates indicates that 60 % of the Sb reports to the tails with 33 % reporting to the Cu-concentrate. This high Sb content of the tailings suggests that the high Ag losses to the tailings (30 %) are at least partly related to the failure to effectively recover the Sb-sulfosalts (four of which are Ag-bearing) and/or that undetected trace Sb occurs in solid solution in arsenopyrite. However, because the As and Sb contents of the feed are 0.16 % and 0.017 %, respectively, and because the Sb content of arsenopyrite is less than 0.02 Wt % Sb (detection limit), Sb in solid solution in arsenopyrite can only account for a maximum of less than 0.5 % of the Sb in the ore. Due to their common occurrence in many of the sulfosalts, the metallurgically troublesome element Sb is partly inseparable from the valuable element Ag during ore dressing. The behaviour of Sb therefore provides an insight into the causes of the poor recovery of Ag.

Silver is carried in freibergite, pyrargyrite, hessite, electrum, dyscrasite, freieslebenite, naumannite, volynskite, acanthite, galena, probably in sphalerite, and possibly in chalcopyrite. Minor but erratic Ag was also detected in the clausthalite-galena solid solution. Freibergite and lesser pyrargyrite and hessite constitute the most abundant Ag-bearing phases, while galena and sphalerite are interpreted to contribute a subordinate, but significant portion of the Ag content of the ores. The calculated optimum grind for freibergite is 4.6 um (See Table 32) with a weighted average grain size curve defined by 80 % - 60 um. Image analysis of pyrargyrite from TLS.5-64 indicates a grain size curve defined by 80 % - 13 um, while that of hessite in the Cu-rich ores was not determined, but is probably of equivalent grain size to pyrargyrite. The fine-grained nature of these Ag-bearing phases dictates that they will be largely unliberated, and that their behaviour will be determined by the flotation characteristics of the host phases. Hessite occurs associated with and hosted in chalcopyrite, and is therefore likely to be readily recovered in the Cu-concentrate. Pyrargyrite occurs as fine-grained inclusions in interstitial galena in Massive Sphalerite and Banded Pyrite + Sphalerite ores. Freibergite in the Massive Sphalerite ores occurs as fine-grained rounded inclusions in galena. Thus, freibergite and pyrargyrite will be largely unliberated, and their behaviour will be determined by the flotation characteristics of the host galena. The freibregite and galena in Massive Pyrite and Banded Pyrite + Sphalerite ores assumes two textural styles, which may retard recovery. These are (1) fine-grained dendritic freibergite and galena (and sphalerite) in pyrite porphyroclasts and (2) freibergite and galena (and sphalerite) interstitial to and invading, cementing and/or replacing fractured pyrite. The grain size curves of freibergite and galena from TLS.5-83A, a Banded Pyrite Sphalerite ore exhibiting strong development of both the above textures, are defined by 80 % - 74 um and 80 % - 37 um, respectively, or 50 % - 13 um for both freibergite and galena. Because of the tendency for pyrite to be concentrated in the coarser-grained sieve fractions, much of the galena and freibergite will be unliberated and report to the tailings. In fact, it is known from assays of 'unbalanced' 1983 feed and concentrates, that approximately 50 % of the Pb (galena) is lost to the tailings. The loss of 50 % of the galena implies the loss of (1) a significant proportion (5 to 10 %) of the Ag in the ore that is hosted in solid solution in galena, (2) Ag present as inclusions of freibergite in the galena, and (3) freibergite associated with, but not as inclusions in galena, and which occurs in the above textures in pyrite. The loss of 9 % of the Zn and 5 % of the Cu, suggests additional losses of Ag in solid solution in sphalerite and possibly chalcopyrite. If and when (Part 2 of the project) it is determined that the cause of the high losses of Pb and Ag to the tailings is due to entrapped inclusions in pyrite, regrinding of a 'coarser-grained pyrite concentrate' might warrant consideration. The coarser-grained pyrite probably contains the bulk of the lost galena and freibergite, as well as sphalerite, chalcopyrite and electrum of type 1. Regrinding the entire tailings or entire pyrite concentrate would be energy consuming and wasteful in that being non-specific it would fail to target the probable host phase; coarse-grained pyrite containing inclusions of the above minerals.

BIBLIOGRAPHY

Ahlrichs, J. W. (1984). Application of quantitative mineralogy for solving metallurgical problems. In Park, W. C., Hausen, D. M. and Hagni, R. D. Ed., AIME/TMS, New York, N. Y., ICAM 84, pp. 279-290.

Barton, P. B. Jr. and Skinner, B. J. (1979). Sulfide Mineral Stabilities. In Geochemistry of Hydrothermal Ore Deposits, ed. H. L. Barnes, 2nd Ed., pp. 236-333. Holt, Rinehart and Winston, New York.

Basu, K., Bortnykov, N., Mookherjee, A., Mozgova, N. and Tsepin, A. I. (1981) Rare minerals from Rajpura-Dariba, Rajasthan, India II: Intermetallic compound $Ag_{74.2}Au_{16.4}Hg_{9.4}$. N. Jb. Miner. Abh., Vol. 141, pp. 217 - 223.

Bates, R. L. and Jackson, J. A. (1980). Glossary of Geology. 2nd Edition, American Geological Institute, Falls Church, Virginia.

Boyle, R. W. (1979). The geochemistry of gold and its deposits. Geol. Surv. of Canada Bull., No. 210.

Cabri, L. J., Cambell, J. L., Laflamme, J. H. G., Leigh, R. G., Maxwell, J. A. and Scott, J. D. (1985). Proton-microprobe analysis of trace elements in sulphides from some massive-sulphide deposits. Can. Mineral., Vol. 23, pp. 133-148.

Chen, T.T. and Petruk, W. (1980). Mineralogy and characteristics that affect recoveries of metals and trace elements from the ore at Heath Steele Mines, New Brunswick. CIM Bull., Vol. 73, No. 823, pp. 167-179.

Craig, J. R., Ljokjell, P. and Vokes, F. M. (1984). Sphalerite compositional variations in sulfide ores of the Norwegian caledonides. Econ. Geol., Vol. 79, pp. 1727-1735.

Craig, J. R. and Scott, S. D. (1976). Sulphide phase equilibria. In Ribbe, P. H. Ed., Sulphide Mineralogy, Chap. 5, Reviews in Mineralogy, Vol. 1, Mineral. Soc. of America.

Craig, J. R. and Vaughan, D. J. (1981). Ore microscopy and ore petrology. Wiley Interscience, John Wiley. New York.

Davis, J. C. (1973). Statistics and data analysis in geology. John Wiley and Sons, New York.

Duval, D. (1985). Trout Lake a moneymaker. The Northern Miner, Oct. 21, 1985, pp. 1-2.

Eldridge, C. S. and Barton, P. B. Jr. (1983). Mineral textures and their bearing on formation of the Kuroko orebodies. Econ. Geol., Monograph 5, pp. 241-281.

Fleischer, M. (1983). Glossary of mineral species, Mineralogical Record, Tucson, Arizona.

Franklin, J. M., Lydon, J. W. and Sangster, D. F. (1981). Massive sulphide deposits. In Skinner, B. J., Ed., 75th Anniversary Volume, Econ. Geol.

Gasparrini, C. (1983). The mineralogy of gold and its significance in metal extraction. CIM Bull., Vol. 76, No. 851, pp. 144-153.

Gasparrini, C. (1984). The mineralogy of silver and its significance in metal extraction. CIM Bull., Vol. 77, No. 866, pp. 99-110.

Graf, J. L., Jr. (1977). Rare Earth Elements as hydrothermal tracers during the formation of massive sulfide deposits in volcanic rocks. Econ. Geol., Vol. 72, pp. 527-548.

Groat, L. A., Carter, R. T., Hawthorne, F. C. and Ercit, T. S. (1985). Tantalian niobian titanite from Irgon claim, southeastren Manitoba. Can. Mineral., Vol. 23, pp. 569-571.

Harbaugh, J. W. and Merriam, D. F. (1968). Computer applications in stratigraphic analysis, Wiley, New York.

Harris, D. C., Sinclair, W. D. and Thorpe, R. I. (1983). Telluride minerals from the Ashley deposit, Bannockburn township, Ontario. Can. Mineral., Vol. 21, pp. 137-143.

Hawley, J. E. and Nichol, I. (1959). Selenium in some Canadian sulphides. Econ. Geol., Vol. 54, pp. 608-628.

Hawley, J. E. and Nichol, I. (1961). Trace elements in pyrite, pyrrhotite and chalcopyrite of different ores. Econ. Geol., Vol. 56, pp. 467-487.

Hutchinson, M. N. and Scott, S. D. (1981). Sphalerite geobarometry in the Cu-Fe-Zn-S system. Econ. Geol., Vol. 76, pp. 143-153.

Jonasson, I. R. and Sangster, D. F. (1975). Variations in the mercury content of sphalerite from some Canadian sulphide deposits. In Elliot, I. L. and Fletcher, W. K. Ed., Geochemical Exploration 1974, pp. 313-332, Elsevier, Amsterdam.

King, R. P. (1979). A model for quantitative estimation of mineral liberation by grinding. Int. Jour. Mineral Processing, Vol. 6, pp. 207-220.

Ko, C. B.(1986). Geology of the Trout Lake Copper-Zinc sulphide deposit. Hudson Bay Mining and Smelting Co. Ltd., Flin Flon, Manitoba. Internal Report.

Koo, J. (1973). Origin and metamorphism of the Flin Flon Cu-Zn sulphide deposit, northern Saskatchewan and Manitoba, Canada. Unpub. Ph.D Thesis, University of Saskatoon, Saskatchewan.

Koo, J. and Mossman, D. J. (1975). Origin and metamorphism of the Flin Flon stratbound Cu-Zn sulphide deposit, Saskatchewan and Manitoba. Econ. Geol., Vol. 70, pp. 48-62.

Lambert, I. B. and Sato, T. (1974). The Kuroko and associated ore deposits of Japan: A review of their features and metallogenesis. Econ. Geol., Vol. 69, pp. 1215-1236.

Leroux, M., Rao, S. R. and Finch, J. A. (1986). Selective flotation of sphalerite from Pb-Zn ore without copper activation. Paper 20.5, Proceedings of the 25th Annual Conference of Metallurgists, Toronto, CIM.

Mainwaring, P. R. and Petruk, W. (1984). SEM-based automatic image analysis and its use in mineral beneficiation - A review. Report MRP/MSL 84-43, CANMET, Dept. Energy, Mines & Resources, Canada.

McIntyre, N. S., Cabri, L. J., Chauvin, W. J. and Laflamme, J. H. G. (1984). Secondary ion mass spectrometric study of dissolved silver and indium in sulphide minerals. Scanning Electron Microsc., III, pp. 1139-1146.

Mielke, J. E. (1979). Composition of the Earth's crust and distribution of the elements. In Siegel, F. R. Ed., Review of research on modern problems in geochemistry. Vol. 16, Int. Assoc. of Geochemistry and Cosmochemistry, UNESCO.

Miller, R. (1981). Kawazulite Bi_2Te_2Se, related bismuth minerals and selenian covellite from the Northwest Territories. Can. Mineral., Vol. 19, Part 2, pp. 341-348.

Miller, J. W. and Craig, J. R. (1983). Tetrahedrite-tennantite series compositional variations in the Cofer deposit, Mineral district, Virginia. Amer. Mineral., Vol. 68, pp. 227-234.

Muzylowski, M. (1979). Copper-Zinc discovery, Flin Flon, Mantoba. CIM Bull., April 1979, pp. 65-67.

Nazmova, G. N. and Spiridonov (1978). Mercury-rich gold. Doclady Acad. Nauk., USSR, Vol. 246, pp. 702-705.

Nysten, P. (1986) Gold in the volcanogenic mercury-rich sulphide deposit Langsele, Skellefte ore district, northern Sweeden. Mineral. Deposita, Vol. 21, pp. 116-120.

Petruk, W. (1976). The application of quantitative mineralogical analysis of ores to ore dressing. CIM Bull., Vol. 69, No. 767, pp. 146-153.

Petruk, W. (1984). Applied mineralogy in ore dressing of volcanogenic massive sulphide ores. In Park, W. C., Hausen, D. M. and Hagni, R. D. Ed., AIME/TMS, New York, N. Y., ICAM 84, pp. 279-290.

Petruk, W. (1985). Recent developments in process mineralogy of complex sulphide ores. Report MRP/MSL 85-148, CANMET, Dept. Energy, Mines & Resources, Canada.

Petruk, W. (In Preparation). Methods of predicting and measuring mineral liberations in ores and mill products, and effect of minerals, textures and grinding methods on liberation.

Petruk, W., Cabri, L. J., Harris, D. C., Stewart, J. M. and Clark, L. A. (1969). Allargentum, redefined. Can. Mineral., Vol. 10, pp. 163-172.

Petruk, W., Pinard, R. G. and Finch, J. (1985). Relationship between observed mineral liberations in screened fractions and in composite samples. SME-AIME Annual Meeting New York, N. Y., 1985.

Price, D. P. (1977). Geology and economic potential of the Flin Flon-Snow Lake Area. Centre for Precambrian Studies, University of Manitoba, Annual Report 1977.

Ramdohr, P. (1980). The ore minerals and their intergrowths. 2 Volumes, 2nd Edition, Int. Series in Earth Sciences, Vol. 35, Pergamon Press, Oxford.

Riley, J. F. (1974). The tetrahedrite-freibergite series, with reference to the Mount Isa Pb-Zn-Ag orebody. Mineral. Deposita, Vol. 9, pp. 117-124.

Sangster, D. F. (1972). PreCambrian volcanogenic massive sulphide deposits in Canada, a review : Geol. Surv. of Canada, Paper 72.

Sato, J. (1974). Ores and ore minerals from the Shakanai mine, Akita Prefecture, Japan. Mining Geology Special Issue, No. 6, pp. 323-335.

Scott, J. D. (1977). Interim report on a mineralogical examination of ore specimens from the Centennial mine, Flin Flon, Manitoba. Internal HBMS report.

Sharp, Z. D., Essene, E. J. and Kelly, W. C. (1985). A re-examination of the arsenopyrite geothermometer: pressure considerations and applications to natural assemblages. Can. Mineral., Vol. 23, pp. 517-534.

Shimazaki, Y. (1974). Ore minerals of the Kuroko-type deposits. Mining Geology Special Issue, No. 6, pp. 311-322.

Stanton, R. L. (1972). Ore Petrology. International Series in the Earth and Planetry Sciences. McGraw-Hill, New York.

Syme, E. C., Bailes, A. H., Price, D. P. and Ziehlke, D. V. (1982). Flin Flon volcanic belt : Geology and ore deposits at Flin Flon and Snow Lake, Manitoba. GAC/MAC Annual Meeting Winnipeg, Manitoba, Field Trip 6.

Vaughan, D. J. and Craig, J. R. (1978). Mineral Chemistry of Metal Sulfides. Cambridge University Press.

Vokes, F. M. (1969). A review of the metamorphism of sulphide deposits. Earth Sci. Rev., Vol. 5, pp. 99-13. poisetup Wills, B. A. (1985). Mineral process technology. 3rd Edition. Int. Series on Materials Sciences and Technology, Vol. 29, Pergamon Press, Oxford.

Appendix A

MICROPROBE ANALYSES OF SPHALERITE.

Wt %.	S.	Zn.	Fe.	Cu.	Cd.	Total.
1.	33.32	62.17	5.76	----	----	101.26
2.	33.32	59.42	7.25	----	----	99.99
3.	33.54	59.53	7.43	----	0.26	100.76
4.	33.05	60.25	7.45	----	----	100.75
5.	33.12	60.27	6.54	----	0.34	100.27
6.	32.97	59.57	5.87	0.52	0.20	99.13
7.	33.06	59.29	7.39	----	0.08	99.83
8.	33.07	58.94	7.18	----	0.22	99.41
9.	33.14	59.40	6.35	----	0.27	99.16
10.	32.99	59.02	5.85	0.81	0.04	98.70
11.	33.01	58.66	6.91	----	0.48	99.07
12.	33.28	59.61	6.30	----	0.41	99.60
13.	33.15	57.72	7.22	----	0.23	100.33
14.	33.03	57.17	8.10	----	0.47	98.77
15.	33.01	58.69	6.26	----	0.18	99.40
16.	33.07	58.74	6.47	----	0.32	98.59
17.	33.20	61.46	5.37	----	----	100.03
18.	32.81	61.04	5.80	----	0.28	99.93
19.	34.05	59.74	7.27	----	0.39	101.45
20.	33.85	59.57	6.82	----	0.31	100.54
21.	33.12	60.23	5.72	0.63	0.32	100.01
22.	33.18	59.09	6.38	----	0.11	98.75
23.	32.81	63.21	3.75	----	----	99.77
24.	32.76	62.74	4.08	----	0.23	99.81
25.	32.59	62.10	4.83	----	----	99.52
26.	32.24	61.59	4.85	----	0.12	98.81
27.	32.65	59.55	7.06	----	0.07	99.32
28.	32.93	57.85	7.01	----	0.26	98.05
29.	33.39	57.95	7.43	----	----	98.77
30.	33.20	58.24	7.47	----	----	98.91
31.	33.38	57.88	7.46	----	----	98.71
32.	34.52	59.27	8.11	----	----	101.90
33.	33.64	56.73	8.23	----	0.26	98.86
34.	34.08	58.34	8.24	----	0.14	100.80
35.	33.00	63.58	2.30	----	0.41	99.28
36.	33.10	60.26	5.39	0.85	----	99.60
37.	32.80	63.19	1.85	----	0.50	98.34
38.	31.98	60.09	6.40	----	----	98.47
39.	33.35	65.61	1.72	----	0.39	101.08
40.	33.60	58.77	7.75	----	----	100.12

Wt %.	S.	Zn.	Fe.	Cu.	Cd.	Total.
41.	33.45	58.06	7.71	----	----	99.22
42.	33.36	60.94	6.78	----	----	101.08
43.	32.86	58.87	7.30	----	----	99.03
44.	33.28	58.99	7.90	----	----	100.17
45.	33.65	59.23	7.50	----	0.27	100.65
46.	33.74	60.43	7.19	----	0.15	101.51
47.	33.55	58.68	8.28	----	----	100.51
48.	33.62	59.15	7.05	----	----	99.81
49.	32.86	59.62	6.31	0.82	----	99.61
50.	33.86	58.70	7.58	----	----	100.14
51.	34.01	59.18	6.80	----	0.40	100.38
52.	33.59	59.64	6.75	----	0.13	100.11
53.	33.31	59.46	7.25	----	0.28	100.30
54.	33.27	60.21	6.42	----	----	99.91
55.	33.43	61.53	6.32	----	----	101.28
56.	33.20	58.46	7.87	----	----	99.53
57.	33.44	58.67	7.76	----	----	99.87
58.	33.36	59.97	7.86	----	0.35	101.54
59.	33.26	59.24	7.22	----	0.36	100.07
$\bar{X}$.	33.25	59.76	6.57	0.06	0.16	99.84
Min.	32.24	56.73	1.72	----	----	98.05
Max.	34.52	65.61	8.24	0.85	0.50	101.90

N = 59.

Appendix B

MICROPROBE ANALYSES OF ELECTRUM.

Wt %.	Ag.	Au.	Hg.	Fe.	Total.	Sample.
1.	62.37	21.24	16.42	0.24	100.24	TLN.1-89.
2.	63.80	22.85	12.78	0.30	99.70	TLN.1-89.
3.	23.69	74.48	1.61	0.60	100.35	TLN.1-89.
4.	49.42	38.40	13.06	0.01	100.86	TLN.1-89.
5.	54.56	29.95	16.47	0.01	100.97	TLN.1-89.
6.	68.20	20.79	12.28	0.03	101.27	TLN.1-89.
7.	67.35	23.38	10.99	0.17	101.86	TLN.1-89.
8.	22.15	74.27	1.86	0.54	98.80	TLN.1-89.
9.	51.20	32.96	17.59	0.02	101.74	TLN.1-89.
10.	68.70	8.04	22.71	0.01	99.43	TLN.1-89.
11.	48.51	38.75	13.20	0.01	100.46	TLN.1-89.
12.	43.08	44.06	12.81	0.09	100.01	TLN.1-89.
13.	22.68	74.99	3.02	0.30	100.97	TLN.1-89.
14.	22.19	73.06	2.50	0.45	98.17	TLN.1-89.
15.	48.39	38.62	14.82	0.09	101.88	TLN.1-89.
16.	34.56	60.80	2.89	0.88	99.11	TLN.1-89.
17.	65.22	23.30	11.24	0.05	99.78	TLN.1-89.
18.	64.42	10.46	24.49	0.06	99.41	TLN.1-89.
19.	68.37	12.36	19.63	0.04	100.37	TLN.1-89.
20.	20.92	75.71	2.39	0.52	99.52	TLN.1-89.
21.	20.79	74.86	3.42	0.52	99.57	TLN.1-89.
22.	63.25	23.09	14.81	0.07	101.20	TLN.1-89.
23.	20.82	75.32	3.02	0.30	99.43	TLN.1-89.
24.	50.09	33.19	17.00	0.04	100.30	TLN.1-89.
25.	40.17	45.03	12.89	0.09	98.16	TLN.1-89.
26.	67.36	23.30	10.49	0.19	101.32	TLN.1-89.
27.	67.28	22.90	11.65	0.17	101.97	TLN.1-89.
28.	65.90	24.92	10.06	0.48	100.92	TLN.1-89.
29.	60.26	11.61	26.29	1.53	99.66	TLS.1-52.
30.	66.28	1.62	30.87	1.59	100.34	TLS.1-52.
31.	63.74	8.34	26.52	1.57	100.15	TLS.1-52.
32.	47.59	35.24	15.02	2.74	100.57	TLS.1-52.
33.	48.09	36.22	13.98	2.60	100.86	TLS.1-52.
34.	25.08	67.71	5.43	0.32	98.50	TL.MP-12.
35.	17.34	79.86	2.68	0.55	100.40	TL.MP-12.
36.	29.00	60.65	9.42	0.67	99.72	TLN.2-11.
37.	32.19	64.50	3.13	0.59	100.39	TLN.2-11.
38.	30.22	57.02	10.96	0.61	98.79	TLN.2-11.
39.	43.03	43.96	11.80	0.30	99.06	TLN.2-11.
40.	29.98	56.47	12.40	0.38	99.20	TLN.2-11.

Wt %.	Ag.	Au.	Hg.	Fe.	Total.	Sample.
41.	40.64	53.40	3.52	0.74	98.27	TLN.2-11.
42.	30.28	55.34	13.12	0.31	99.02	TLN.2-11.
43.	32.03	61.02	4.39	0.82	98.23	TLN.2-11.
44.	36.02	58.33	4.79	0.80	99.92	TLN.2-11.
45.	27.85	67.18	1.29	2.20	98.49	TLN.2-11.
46.	34.30	50.25	14.54	0.74	99.80	TLN.2-11.
47.	42.62	50.33	6.84	0.60	100.37	TLN.2-11.
48.	31.53	52.36	14.06	0.92	98.84	TLN.2-11.
49.	36.91	59.31	3.65	0.72	100.57	TLN.2-81.
50.	36.89	57.68	3.65	0.74	98.93	TLN.2-81.
51.	36.96	57.90	3.46	0.40	98.68	TLN.2-81.
52.	54.75	29.08	14.52	1.14	99.46	TLN.2-81.
53.	55.24	30.48	13.76	0.84	100.30	TLN.2-81.
54.	36.99	57.44	3.98	0.66	99.04	TLN.2-81.
55.	37.38	56.51	3.76	0.51	98.16	TLN.2-81.
56.	40.68	51.15	5.14	1.27	98.24	TLN.2-81.
57.	35.63	57.27	5.05	1.69	99.61	TLN.2-81.
58.	37.47	54.52	4.94	3.49	100.37	TLS.5-83A.
59.	53.79	34.13	9.19	1.98	99.07	TLS.5-83A.
60.	54.00	34.34	9.14	1.39	98.84	TLS.5-83A.
61.	54.15	34.62	9.09	1.22	99.05	TLS.5-83A.
62.	54.62	33.73	9.17	1.50	98.99	TLN.2-40.
63.	49.83	31.52	17.89	0.21	99.43	TLN.2-40.
64.	50.11	31.56	17.06	0.19	98.89	TLN.2-40.
65.	49.41	32.19	16.58	0.29	98.44	TLN.2-40.
66.	49.92	32.45	17.10	0.67	100.12	TLN.2-40.
67.	49.93	30.34	17.71	0.51	98.47	TLN.2-40.
68.	53.32	25.46	20.58	0.49	99.82	TLN.2-40.
69.	53.41	25.10	20.16	0.91	99.56	TLN.2-40.
70.	49.89	33.31	17.09	0.43	100.69	TLN.2-40.
71.	50.82	30.17	18.13	0.39	99.48	TLN.2-40.
72.	50.93	31.07	16.08	0.76	99.59	TLN.2-40.
73.	49.87	30.55	18.58	0.39	99.36	TLN.2-8.
74.	60.84	29.40	9.52	1.51	101.24	TLN.2-8.
75.	68.18	23.36	8.10	1.45	101.07	TLN.2-8.
76.	59.40	35.77	2.00	1.63	98.76	TLN.2-8.
77.	60.34	35.79	1.78	1.68	99.74	TLN.2-8.
78.	40.80	49.08	8.23	0.64	98.72	TLN.2-8.
79.	38.07	56.65	3.99	0.53	99.21	TLN.2-8.
80.	55.47	38.83	3.84	0.51	98.63	TLN.2-8.
81.	58.47	36.61	3.62	0.67	99.35	TLN.2-8.
82.	58.24	36.63	3.79	0.56	99.21	TLN.2-8.
83.	57.62	37.28	2.99	1.26	99.13	TLN.2-8.
84.	57.19	37.24	3.62	0.64	98.67	TLN.2-8.
85.	61.25	28.72	9.11	1.59	100.65	TLN.2-8.
$\bar{x}$.	46.97	41.37	10.64	0.73	99.72	(N = 85)
Max.	68.70	79.86	30.87	3.49	101.97	
Min.	17.34	1.62	1.29	0.00	98.16	

Appendix C

MICROPROBE ANALYSES OF FREIBERGITE.

	S	Fe	Cu	Zn	As	Ag	Sb	Total	S	Fe	Cu	Zn	As	Ag	Sb
	Wt %								Number of atoms.						
	23.07	5.73	23.82	2.00	0.00	19.17	26.98	100.77	13.00	1.86	6.77	0.55	0.00	3.21	4.00
	23.82	5.21	27.02	1.46	0.85	15.54	26.51	100.41	13.00	1.63	7.44	0.39	0.20	2.52	3.81
	24.24	5.88	28.46	1.45	2.83	14.76	23.64	101.27	13.00	1.81	7.70	0.38	0.65	2.35	3.34
	23.27	5.42	23.96	1.66	1.03	19.44	23.80	98.58	13.00	1.74	6.75	0.45	0.25	3.23	3.50
	22.55	5.45	17.60	2.02	0.00	26.34	26.18	100.14	13.00	1.81	5.12	0.57	0.00	4.52	3.98
	22.07	5.35	16.86	1.75	0.00	27.56	26.69	100.28	13.00	1.81	5.01	0.51	0.00	4.83	4.14
	22.44	5.51	17.45	1.79	0.00	27.78	25.42	100.40	13.00	1.83	5.10	0.51	0.00	4.78	3.88
	21.79	5.27	17.18	1.54	0.00	28.50	26.17	100.44	13.00	1.81	5.17	0.45	0.00	5.06	4.11
	23.42	5.67	23.66	1.29	0.43	19.06	27.36	100.89	13.00	1.81	6.63	0.35	0.10	3.14	4.00
	23.59	5.81	23.35	1.27	0.80	19.59	26.83	101.25	13.00	1.84	6.49	0.35	0.19	3.21	3.89
	23.63	5.67	23.36	1.46	0.00	18.83	28.10	101.04	13.00	1.74	6.48	0.39	0.00	3.08	4.07
	22.56	5.53	18.87	1.38	0.00	24.73	27.06	100.15	13.00	1.83	5.69	0.39	0.00	4.24	4.11
	23.07	5.90	26.10	0.91	0.91	16.90	26.52	100.31	13.00	1.91	7.62	0.25	0.22	2.83	3.94
	22.92	5.31	24.18	1.47	0.75	18.36	26.87	99.86	13.00	1.73	6.92	0.41	0.18	3.10	4.01
	22.19	4.83	22.80	2.65	0.00	20.21	26.30	98.97	13.00	1.62	6.74	0.76	0.00	3.52	4.06
	23.03	5.62	24.12	0.00	0.00	18.97	27.25	98.99	13.00	1.82	6.87	0.00	0.00	3.18	4.05
	21.77	5.01	18.36	1.37	0.00	25.47	26.47	98.45	13.00	1.72	5.53	0.40	0.00	4.52	4.16
	21.78	5.47	18.03	0.78	0.00	26.15	27.19	99.39	13.00	1.88	5.43	0.23	0.00	4.68	4.27
	22.85	4.87	23.27	1.37	0.00	19.69	26.92	98.97	13.00	1.59	6.68	0.38	0.00	3.33	4.03
	22.70	4.90	23.19	1.76	0.42	18.37	26.99	98.34	13.00	1.61	6.70	0.50	0.11	3.13	4.07
	22.62	4.98	23.73	1.90	0.00	18.85	26.24	98.33	13.00	1.64	6.88	0.54	0.00	3.22	3.97
	23.31	5.37	23.06	1.19	0.00	18.73	27.52	99.18	13.00	1.72	6.49	0.32	0.00	3.10	4.04
	23.48	5.60	23.54	0.65	0.00	19.06	27.28	99.62	13.00	1.78	6.57	0.18	0.00	3.14	3.97
	23.30	5.46	23.13	1.04	0.00	19.49	27.02	99.45	13.00	1.75	6.51	0.29	0.00	3.23	3.97
	23.26	5.68	22.76	0.91	0.31	19.69	27.47	100.08	13.00	1.82	6.42	0.25	0.08	3.27	4.04
	23.29	5.75	22.14	0.31	0.92	20.03	27.72	100.15	13.00	1.84	6.24	0.09	0.22	3.32	3.32
	23.26	5.72	22.56	2.49	0.68	19.97	26.97	101.64	13.00	1.84	6.37	0.68	0.16	3.32	3.97
	22.14	5.69	19.50	1.62	0.00	24.65	26.45	100.05	13.00	1.92	5.78	0.47	0.00	4.30	4.09
	22.41	6.12	21.54	1.16	0.00	20.70	26.55	98.50	13.00	2.04	6.31	0.33	0.00	3.57	4.06
	22.13	5.87	20.28	0.64	0.00	23.84	26.29	99.06	13.00	1.98	6.01	0.19	0.00	4.16	4.07
	22.53	5.59	20.37	1.54	0.00	22.22	26.61	98.86	13.00	1.85	5.93	0.44	0.00	3.81	4.04
	21.97	5.52	18.02	2.26	0.00	25.19	26.15	99.10	13.00	1.88	5.38	0.66	0.00	4.43	4.08
	21.77	6.52	14.73	1.20	0.00	30.31	26.33	100.85	13.00	2.23	4.44	0.35	0.00	5.38	4.14
	23.57	5.42	21.83	1.52	0.00	20.52	27.08	99.94	13.00	1.72	6.08	0.41	0.00	3.36	3.93
	22.76	5.52	19.43	1.26	0.00	24.39	27.01	100.38	13.00	1.81	5.60	0.35	0.00	4.14	4.06
	21.79	5.95	16.53	0.84	0.00	28.13	25.96	99.20	13.00	2.04	4.98	0.25	0.00	4.99	4.08
	22.70	5.43	19.88	1.28	0.00	24.27	27.22	100.78	13.00	1.79	5.74	0.36	0.00	4.13	4.10
	23.04	6.57	19.64	2.01	0.00	23.15	27.20	101.61	13.00	2.13	5.59	0.56	0.00	3.88	4.04
	22.16	6.04	18.98	1.00	0.00	24.97	26.65	99.81	13.00	2.04	5.62	0.29	0.00	4.36	4.12
	22.56	5.57	18.40	1.95	0.00	24.96	26.84	100.27	13.00	1.84	5.35	0.55	0.00	4.27	4.07
	22.48	5.33	19.41	1.46	0.00	23.72	26.93	99.32	13.00	1.77	5.67	0.42	0.00	4.08	4.10
	22.82	5.42	19.52	2.24	0.00	23.69	26.69	100.38	13.00	1.77	5.61	0.63	0.00	4.01	4.00
	22.29	5.33	20.30	1.66	0.00	23.67	27.00	100.25	13.00	1.78	5.97	0.48	0.00	4.10	4.15
	22.30	5.67	19.26	1.53	0.00	24.25	26.65	99.67	13.00	1.90	5.66	0.44	0.00	4.20	4.09
	22.82	5.52	20.93	1.56	0.00	21.74	27.33	99.89	13.00	1.81	6.02	0.44	0.00	3.68	4.10
	23.23	5.57	20.92	0.71	0.00	22.87	27.86	101.17	13.00	1.79	5.91	0.20	0.00	3.81	4.11
	23.31	5.66	20.75	1.80	0.00	22.92	27.38	101.82	13.00	1.81	5.84	0.49	0.00	3.80	4.02
	21.88	5.34	17.59	1.32	0.00	27.79	24.17	98.09	13.00	1.82	5.27	0.39	0.00	4.91	3.78
	22.65	6.14	20.41	0.39	0.00	22.69	27.44	99.73	13.00	2.02	5.91	0.11	0.00	3.87	4.15
	22.84	5.58	19.53	1.73	0.00	24.04	27.36	101.07	13.00	1.82	5.61	0.48	0.00	4.07	4.10
	21.81	5.59	16.84	1.31	0.00	28.61	25.75	99.91	13.00	1.91	5.07	0.38	0.00	5.07	4.04
	23.00	5.50	20.72	1.32	0.00	22.01	27.48	100.03	13.00	1.79	5.91	0.37	0.00	3.70	4.09
	22.77	5.63	24.44	1.21	0.00	18.41	26.07	98.52	13.00	1.84	7.04	0.34	0.00	3.12	3.92
	23.08	5.49	23.99	1.09	0.48	18.30	25.95	98.38	13.00	1.78	6.82	0.30	0.12	3.06	3.85
	22.90	5.67	24.45	1.76	0.00	17.77	26.97	99.51	13.00	1.85	7.00	0.49	0.00	3.00	4.03
	22.87	5.44	24.29	1.58	0.58	18.97	25.62	99.35	13.00	1.77	6.97	0.44	0.14	3.21	3.84
	22.69	5.28	23.98	1.05	0.25	18.93	25.84	98.02	13.00	1.74	6.93	0.30	0.06	3.23	3.90
	23.14	6.10	26.46	1.05	0.00	15.51	26.79	99.04	13.00	1.97	7.50	0.29	0.00	2.59	3.96
	23.05	5.94	27.94	1.65	0.53	13.37	26.37	98.85	13.00	1.93	7.95	0.46	0.13	2.24	3.92
	24.02	5.98	27.51	1.89	0.00	13.05	27.97	100.42	13.00	1.86	7.52	0.50	0.00	2.10	3.99
Max	24.24	6.57	28.46	2.65	2.83	30.31	28.10	101.82	13.00	2.23	7.95	0.68	0.65	5.38	4.27
Min	21.77	4.83	14.73	0.00	0.00	13.05	23.64	98.02	13.00	1.59	4.44	0.00	0.00	2.10	3.32
Mean	22.78	5.58	21.98	1.41	0.20	21.68	26.66	99.82	13.00	1.83	6.18	0.40	0.05	3.70	4.00

(N = 60)

Appendix D

SAMPLE LOCATIONS AND DERIVED ORE TYPES.

SAMPLE ID.	ZONE.	LENS.	LOCATION.	ORE TYPE.
TLN.1-1.	North.	1.	South End, 110m Level.	Banded Py + Sphal.
TLN.1-2.	North.	1.	South End, 110m Level.	Cpy Stringers.
TLN.1-3.	North.	1.	South End, 110m Level.	Vein Qtz + Cpy.
TLN.1-4.	North.	1.	North End, 110m Level.	(Not Sectioned).
TLN.1-5.	North.	1.	North End, 110m Level.	Cpy Stringers.
TLN.2-6.	North.	2.	North End, 180m Level.	Sheared Cpy + Sphal.
TLN.2-7.	North.	2.	North End, 180m Level.	Cpy Stringers.
TLN.2-8.	North.	2.	South End, 245m Level.	Mixed/Banded Cpy + Sphal.
TLN.2-9.	North.	2.	South End, 245m Level.	Sheared Cpy + Sphal.
TLN.2-10.	North.	2.	North End, 245m Level.	Msv. Cpy + Po.
TLN.2-11.	North.	2.	North End, 245m Level.	Cpy Stringers.
TLN.2-12.	North.	2.	North End, 245m Level.	Sheared Cpy + Sphal.
TLN.2-13.	North.	2.	North End, 245m Level.	Sheared Cpy + Sphal.
TLS.3-14.	South.	3.	South End, 210m Level.	Cpy Stringers.
TLS.3-15.	South.	3.	South End, 210m Level.	Banded Py + Sphal.
TLS.3-16.	South.	3.	North End, 210m Level.	Msv. Cpy + Po.
TLS.3-17.	South.	3.	North End, 210m Level.	Sheared Cpy + Sphal.
TLS.3-18.	South.	3	North End, 210m Level.	Banded Py + Sphal.
TLS.3-19.	South.	3.	North End, 210m Level.	Banded Py + Sphal.
TLS.3-20.	South.	3.	Centre/North, 210m Level.	Banded Py + Sphal.
TLS.3-21.	South.	3.	Centre/North, 245m Level.	Cpy Stringers.
TLS.3-22.	South.	3.	Centre/North, 245m Level.	Cpy Stringers.
TLS.2-23.	South.	2.	North End, 130m Level.	Diss. Py + Cpy.
TLS.2-24.	South.	2.	North End, 130m Level.	Banded Py + Sphal.
TLS.2-25.	South.	2.	South End, 130m Level.	Msv. Py.
TLS.2-26.	South.	2.	South End, 130m Level.	Banded Py + Sphal.
TLN.1-27.	North.	1.	South End, 155m Level.	Banded Py + Sphal.
TLN.1-28.	North.	1.	North End, 80m Level.	Banded Py + Sphal.
TLN.1-29.	North.	1.	North End, 80m Level.	Msv. Py.
TLN.1-30.	North.	1.	North End, 80m Level.	Msv. Py.
TLN.1-31.	North.	1.	Centre, 80m Level.	Banded Py + Sphal.
TLN.1-32.	North.	1.	South End, 80m Level.	Msv. Py.
TLN.1-33.	North.	1.	Centre, 80m Level.	Diss. Py + Cpy.
TLS.3-34.	South.	3.	North End, 80m Level.	Diss. Py + Cpy.
TLS.3-35.	South.	3.	North End, 80m Level.	Msv. Py.
TLS.3-36.	South.	3.	North End, 80m Level.	Diss. Py + Cpy.
TLS.3-37.	South.	3.	North End, 80m Level.	Diss. Py + Cpy.
TLS.2-38.	South.	2.	South End, 80m Level.	Msv. Py.
TLS.3-39.	South.	3.	South End, 180m Level.	Cpy Stringers.
TLS.2-40.	South.	2.	Centre, 180m Level.	Msv. Py.
TLS.3-41.	South.	3.	North End, 180m Level.	Banded Py + Sphal.
TLS.3-42.	South.	3.	North End, 180m Level.	Msv. Cpy + Po.

TLS.3-43.	South.	3.	North end, 180m Level.	(Not Sectioned).
TLS.1-44.	South.	1.	South End. 180m Level.	Cpy Stringers.
TLS.3-45.	South.	3.	North End, 210m Level.	Banded Py + Sphal.
TLS.3-46.	South.	3.	North End. 210m Level.	Msv. Cpy + Po.
TLS.1-47.	South.	1.	South End, 210m Level.	Cpy Stringers.
TLS.1-48.	South.	1.	South End, 210m Level.	Cpy Stringers.
TLS.1-49.	South.	1.	South End, 210m Level.	Msv. Sphal.
TLS.1-50.	South.	1	South End, 210m Level.	Msv. Cpy + Po.
TLS.1-51.	South.	1.	North End, 210m Level.	Msv. Cpy + Po.
TLS.1-52.	South.	1.	North End, 210m Level.	Msv. Py.
TLS.1-53.	South.	1.	North End, 210m Level.	Msv. Py.
TLS.2-54.	South.	2.	North End, 210m Level.	Banded Py + Sphal.
TLS.2-55.	South.	2.	South End, 210m Level.	Banded Py + Sphal.
TLS.3-56.	South.	3.	South End, 130m Level.	Cpy Stringers.
TLS.3-57.	South.	3.	Centre, 130m Level.	Msv. Sphal.
TLS.3-58.	South.	3.	Centre, 130m Level.	Diss. Py + Cpy.
TLS.3-59.	South.	3.	Centre, 130m Level.	Cpy Stringers.
TLS.3-60.	South.	3.	Centre/North, 130m Level.	Msv. Sphal.
TLS.3-61.	South.	3.	Centre/North, 130m Level.	Cpy Stringers.
TLN.2-62.	North.	2.	South End, 200m Level.	Sheared Cpy + Sphal.
TLN.2-63.	North.	2.	South End, 200m Level.	Sheared Cpy + Sphal.
TLS.5-64.	South.	5.	Centre, 215m Level.	Msv. Sphal.
TLS.2-65.	South.	2.	North End, 210m Level.	Cpy Stringers.
TLS.1-66.	South.	1.	South End, 210m Level.	Banded Py + Sphal.
TLS.1-67.	South.	1.	Centre, 210m Level.	Diss. Py + Cpy.
TLS.1-68.	South.	1.	Centre, 210m Level.	Msv. Cpy + Po.
TLS.2-69.	South.	2.	Centre, 130m Level.	Msv. Py.
TLS.2-70.	South.	2.	Centre, 130m Level.	Banded Py + Sphal.
TLN.1-71.	North.	1.	Centre, 110m Level.	Cpy Stringers.
TLN.1-72.	North.	1.	Centre, 110m Level.	Msv. Sphal.
TLN.1-73.	North.	1.	Centre, 110m Level.	Vein Qtz + Cpy.
TLN.2-74.	North.	2.	Centre, 245m Level.	Msv. Sphal.
TLN.2-75.	North.	2.	Centre, 245m Level.	Mixed/Banded Cpy + Sphal.
TLN.2-76.	North.	2.	Centre, 245m Level.	Msv. Cpy + Po.
TLN.2-77.	North.	2.	North End, 245m Level.	(Not Sectioned).
TLN.2-78.	North.	2.	North End, 245m Level.	Mixed/Banded Cpy + Sphal.
TLN.2-79.	North.	2.	Centre/North, 245m Level.	Mixed/Banded Cpy + Sphal.
TLN.2-80.	North.	2.	South End, 245m Level.	Cpy Stringers.
TLN.2-81.	North.	2.	South End, 245m Level.	Sheared Cpy + Sphal.
TLN.2-82.	North.	2.	Centre/North, 245m Level.	Vein Qtz + Cpy.
TLN.2-83.	North.	2.	Centre/North, 245m Level.	Msv. Cpy + Po.
TLS.5-83A.	South.	5.	Sec 12+00E, 210m Level.	Msv. Py.
TLS.5-84.	South.	5.	Sec 12+00E, 210m Level.	Banded Py + Sphal.
TLS.5-85.	South.	5.	Sec 11+90E, 210m Level.	Msv. Sphal.
TLS.5-86.	South.	5.	Sec 11+90E, 210m Level.	Banded Py + Sphal.
TLN.1-87.	North.	1.	Centre/South, 105m Level.	Msv. Sphal.
TLN.1-88.	North.	1.	Centre/South, 105m Level.	Banded Py + Sphal.
TLN.1-89.	North.	1.	Centre/South, 105m Level.	Cpy Stringers.
TLN.1-90.	North.	1.	Centre/South, 105m Level.	Cpy Stringers.
TLN.2-91.	North.	2.	Centre, 240m Level.	Mixed/Banded Cpy + Sphal.
TLN.2-92.	North.	2.	Centre, 240m Level.	Sheared Cpy + Sphal.
TLS.2-93.	South.	2.	North End, 80m Level.	Banded Py + Sphal.
TLS.2-94.	South.	2.	Centre, 80m Level.	Banded Py + Sphal.
TLN.2-95.	North.	2.	South End, 255m Level.	Msv. Sphal.

TLN.2-96.	North.	2.	South End, 255m Level.	Sheared Cpy + Sphal.
TLN.1-97.	North.	1.	Centre, 80m Level.	Banded Py + Sphal.
TLN.1-98.	North.	1.	Centre, 80m Level.	Diss. Py + Cpy.
TLS.1-99.	South.	1.	North End, 125m Level.	Banded Py + Sphal.
TLS.1-100.	South.	1.	North End, 125m Level.	Banded Py + Sphal.
TLS.1-101.	South.	1.	North End, 125m Level.	Banded Py + Sphal.
TLS.5-102.	South.	5.	Sec 11+81E, 205m Level.	Banded Py + Sphal.
TLS.5-103.	South.	5.	Sec 11+81E, 205m Level.	Msv. Sphal.
TLS.5-104.	South.	5.	Sec 11+81E, 205m Level.	Banded Py + Sphal.
TLS.5-105.	South.	5.	Sec 12+02E, 205m Level.	Banded Py + Sphal.
TLS.5-106.	South.	5.	Sec 12+02E, 205m Level.	Msv. Py.
TLS.5-107.	South.	5.	Sec 12+02E, 205m Level.	Banded Py + Sphal.
TLS.5-108.	South.	5.	Sec 11+75E, 205m Level.	Banded Py + Sphal.
TLS.5-109.	South.	5.	Sec 11+75E, 205m Level.	Banded Py + Sphal.
TLS.5-110.	South.	5.	Sec 11+80E, 205m Level.	Banded Py + Sphal.
TLS.5-111.	South.	5.	Sec 12+10E, 205m Level.	Banded Py + Sphal.
TLN.2-112.	North.	2.	Sec 11+00E, 425m Level.	Sheared Cpy + Sphal.
TLN.2-113.	North.	2.	Sec 11+00E, 425m Level.	Sheared Cpy + Sphal.
TLN.2-114.	North.	2.	Sec 11+00E, 425m Level.	Mixed/Banded Cpy + Sphal.